



HAL
open science

Long-term regulation of colorectal cancer cells under mechanical stress

Malèke Mouelhi

► **To cite this version:**

Malèke Mouelhi. Long-term regulation of colorectal cancer cells under mechanical stress. Biological Physics [physics.bio-ph]. Université Claude Bernard - Lyon I, 2023. English. NNT : 2023LYO10110 . tel-04390112

HAL Id: tel-04390112

<https://theses.hal.science/tel-04390112v1>

Submitted on 12 Jan 2024

HAL is a multi-disciplinary open access archive for the deposit and dissemination of scientific research documents, whether they are published or not. The documents may come from teaching and research institutions in France or abroad, or from public or private research centers.

L'archive ouverte pluridisciplinaire **HAL**, est destinée au dépôt et à la diffusion de documents scientifiques de niveau recherche, publiés ou non, émanant des établissements d'enseignement et de recherche français ou étrangers, des laboratoires publics ou privés.



THESE de DOCTORAT DE L'UNIVERSITE CLAUDE BERNARD LYON 1

Discipline : Biophysique

Soutenue publiquement 07/07/2023, par :
Malèke Mouelhi

Long-term regulation of colorectal cancer cells under mechanical stress

Devant le jury composé de :

Dr. Claire WILHELM

Directrice de Recherche, CNRS Paris

Rapporteure

Pr. Sylvain GABRIELE

Professeur associé, Université de Mons - Belgique

Rapporteur

Dr. Emmanuèle HELFER

Directrice de Recherche, CNRS Marseille

Examinatrice

Dr. Véronique MAGUER-SATTA

Directrice de Recherche, CNRS Lyon

Présidente du jury

Dr. Olivier MEURETTE

Maître de Conférences, Université Lyon 1

Examineur

Dr. Giovanni CAPPELLO

Directeur de Recherche, CNRS Grenoble

Examineur

Dr. Charlotte RIVIERE

Maître de Conférences, Université Lyon 1

Directrice de thèse

Dr. Sylvain MONNIER

Maître de Conférences, Université Lyon 1

Co-directeur de thèse

Dr. Morgan DELARUE

Chargé de Recherche, CNRS Toulouse

Invité

Acknowledgments

J'aimerais tout d'abord remercier mes rapporteurs Claire Wilhelm et Sylvain Gabriele d'avoir accepté ce rôle. Je tiens à remercier également les autres membres du jury Emmanuèle Helfer, Véronique Maguer-Satta, Olivier Meurette, Giovanni Cappello d'avoir accepté d'évaluer mon travail. Merci aussi à Morgan Delarue d'avoir accepté d'être membre invité de mon jury.

Merci à mes directeurs de thèse Charlotte et Sylvain, vous qui m'avez connu dès la 2^e année de médecine. Merci de m'avoir donné le goût à l'interdisciplinarité et à la biophysique, merci de m'avoir accepté en thèse, merci pour ces quatre belles années, pleine de confiance et d'estime. Merci pour votre accompagnement sans faille et votre continuelle bienveillance. J'ai appris tellement à vos côtés et peut-être que cela marquera le début d'une fructueuse collaboration scientifique, qui sait ?

J'aimerai aussi remercier Jean-Louis Bessereau pour son soutien et son suivi depuis la 2^e année de médecine dans ce double cursus passionnant, merci d'avoir démocratiser et ouvert les portes des doubles cursus Médecine/Science à Lyon. Merci également à l'École de l'Inserm-Liliane Bettencourt et à ses directeurs Eric Clauser et Boris Barbour et merci au doyen Gilles Rode de la Faculté de Médecine Lyon Est de nous donner les moyens de réaliser nos projets.

Je souhaiterais également remercier Matthieu Piel pour les nombreuses discussions et échanges sur mon projet de thèse toujours extrêmement pertinents.

Merci à nos nombreux collaborateurs, du CRCL tout d'abord : Mathieu Gabut, Coraline Isaac, Cédric Chaveroux, Cédric Duret et à Julie Pannequin de l'IGF.

Je remercie également les membres de mon comité de suivi de thèse Loic Vanel, Anne-Laure Biance et Fabien Montel qui m'ont vu évoluer au fil des années.

Merci à tous les membres de l'équipe biophysique Jean-Paul Rieu, Hélène Delanoe-Ayari, Thomas Dehoux, Olivier Cochet-Escartin, Maroun Abi-Ghanem, Lorraine Montel, Stéphane Joly. Sans oublier l'équipe Liquide et Interface ! Je tiens à remercier en particulier Catherine, Anne-Laure, Cécile, Marie, Jean, Agnès, Gilles, Remy, Sylvain D. Merci pour ces discussions animées, merci pour votre écoute et votre bienveillance, et merci pour les déjeuners en infiltrée chez les permanents !

Merci Matthieu pour ton soutien inconditionnel, ton écoute, ta patience, tu me pousses chaque jour à donner le meilleur de moi-même ! Et j'espère qu'un jour tu croiras en toi comme tu crois en moi !

Merci aux post-doctorants, doctorants et stagiaires, actuels ou passés qui ont croisé ma route : Audrey, Antony, Saba, Alexis C, Guqi, Alexis V, Justin, Clément, Akash, Victor, Ong, Dolachai,

Yedhir, Camille, Julie, Manon, Fred, Guillaume, Martin, Hugo, Nasser, Tommasso, Valentin, Kaabir, Gaëtan N, Gaëtan J, Marie, Alexis S, Samuel, Joaquim, Lucie, Bastien, Antoine, Morgane, Malaury, Pauline...

Estelle, j'aurai aimé que nos chemins se soient croisés plus tôt mais je suis heureuse d'avoir pu apprendre à te connaître, tu es une personne extraordinaire, ne doute jamais de toi, je suis sûre que l'avenir te réservera de belles choses !

Spécial remerciement pour les membres du meilleur bureau de l'ILM (n'en déplaise à certains !) : Aymeric et Lucie, je suis tellement contente de vous avoir rencontrés et de l'amitié qui en découle, merci pour les fous rires, votre bonne humeur, les partages de gâteaux, viennoiseries et autres gourmandises ! (Et merci pour tous les ragots !). Aymeric, toi qui étais là quasi-toute ma thèse, merci pour toutes les discussions, les weekends et les soirées à se tenir compagnie. Courage pour cette fin de thèse, tu vas y arriver ! Et Lucie, ce n'est que le début alors profite à fond de cette aventure car elle s'achève plus vite que l'on ne pense. Je souhaite également la bienvenue à Adèle dans ce magnifique bureau, dommage que l'on n'ait pas eu la chance de beaucoup se côtoyer..

Une très grande pensée pour Grégoire, avec qui j'ai commencé ma thèse. Qui aurait pu deviner que ce mardi 1^{er} octobre 2019 marquera le début d'une belle amitié.

Une pensée également pour mes plus fidèles amies sur qui je peux toujours compter, dans les durs moments comme dans les bons ! Merci à Sara, Salma et Jérôme, merci à Kako, Lila, Dodo, Titi, Aicha, Inès, Sybille <3

Enfin, je tenais à remercier toute ma famille pour leur soutien et amour inconsidérable. Papa, Yasser, Alaâ, Hénia et Asma. Et plus particulièrement, Maman et Inès qui me supporte quotidiennement. Inès merci de m'aider à sortir de ma zone de confort, merci de m'accompagner et de m'aider au quotidien. Maman, toi qui m'a encouragé à me dépasser, viser l'excellence mais surtout à apprécier ce que je fais, je te remercie pour ton aide et ton soutien infailible, merci de croire en moi et de me pousser dans mes rêves les plus fous, sans toi je n'y serai jamais arrivée, je t'aime fort.

Résumé

La manière dont les cellules cancéreuses interagissent avec leur environnement *in situ* a des implications majeures sur la compréhension de la physiopathologie tumorale et la réponse aux traitements. En effet, le microenvironnement tumoral influence fortement le devenir tumoral et notamment une sous population de cellules particulières, possédant des propriétés souches (appelés cellules souches cancéreuses) qui sont extrêmement plastiques. Ces cellules sont supposées actuellement être en grande partie responsables de la progression tumorale, la résistance aux traitements et des rechutes. Cependant, au cours de l'évolution tumorale, les propriétés physiques du microenvironnement tumoral sont également fortement modifiées par rapport aux tissus sains environnants. Les cellules cancéreuses subissent donc des variations majeures des forces physiques qu'elles supportent avec notamment la rigidification de la matrice extracellulaire et la prolifération dans un espace confiné. Il est donc important de comprendre comment cet environnement les impacte afin de mieux cibler les stratégies thérapeutiques. Pour démêler les nombreux facteurs qui influent sur la structure, la mécanique et la fonction des tissus et cellules tumorales, l'équipe a développé de nombreux microsystemes en hydrogel afin de reproduire de façon standardisée *in vitro* l'environnement mécanique que rencontre la tumeur *in vivo*. C'est dans ce cadre que mon projet de recherche s'évertue à comprendre comment l'environnement tumoral, d'un point de vue mécanique, influe sur le devenir cellulaire cancéreux à long terme. Pour cela, je combine deux approches complémentaires : une déformation mécanique est imposée soit en 2D en confinant des cellules cancéreuses isolées, soit en 3D en comprimant de façon isotrope des sphéroïdes tumoraux.

Dans un premier temps, j'ai pu mettre en évidence, sur une lignée de cancer colorectal, des modifications structurales au niveau du noyau, régulées de manière temporelle sur plusieurs jours. Contrairement à ce qui se passe pour un confinement à court terme, j'ai mis en évidence pour la première fois une régulation nucléaire globale lors d'un confinement prolongé, avec une diminution du volume nucléaire en 24h, et une réinitialisation de la forme nucléaire. De manière surprenante, cette régulation n'est pas liée à un ralentissement de la croissance au cours de la progression dans le cycle cellulaire mais se produit lors de la division cellulaire confinée. De plus, ces changements nucléaires sont conservés lors de la génération cellulaire suivante permettant au noyau d'atteindre une homéostasie. Ces résultats pourraient changer la donne pour ce qui est de comprendre comment les paramètres physiques du tissu influencent la croissance et la division des cellules puisque le rôle clé de la division dans l'adaptation des cellules cancéreuses à des contraintes mécaniques prolongées n'a jusqu'alors jamais été montré.

Afin de mieux caractériser l'impact des contraintes mécaniques sur le devenir tumoral, il était encore nécessaire de complexifier le modèle et d'intégrer le microenvironnement. De ce fait, en plus de ce travail fondamental sur les cellules isolées, le deuxième enjeu de ma thèse a été de reproduire *in vitro*, sur un tissu modèle 3D (sphéroïdes tumoraux), les contraintes auxquelles sont soumises les tumeurs *in vivo*. En combinant un contrôle de l'environnement physique et un contrôle du contenu du milieu de culture, j'ai pu soumettre des sphéroïdes en croissance à un stress mécanique et métabolique combiné. J'ai, d'abord, pu montrer le rôle primordial de l'environnement nutritif tumoral dans la plasticité et le destin cellulaire tout en mettant en évidence l'apparition d'une population de cellules souches cancéreuses sous contrainte mécanique. Mes résultats ouvrent ainsi de nouvelles questions sur l'interaction entre l'environnement nutritif et mécanique, influençant tous deux le phénotype et l'expression génique des sphéroïdes colorectaux.

Tous ces changements ne sont pas sans conséquences et pourraient expliquer en partie l'échec des thérapies actuelles à apporter une guérison complète au plus grand nombre de patients victimes de cancers.

Mots clés : cancer colorectal ; mécanobiologie du cancer ; microenvironnement ; microsysteme en hydrogel ; cellules souches cancéreuses ; régulation à long terme.

Abstract

How cancer cells interact with their environment *in situ* has major implications for understanding tumor pathophysiology and response to therapy. Indeed, the tumor microenvironment strongly influences the tumor fate and more particularly a specific subpopulation of tumor cells that are recovering properties of stem cells, called cancer stem-like cells, which are extremely plastic. These cells are assumed to be largely responsible for tumor progression, treatment resistance and relapse. However, during tumor progression, the physical properties of the tumor microenvironment are also strongly modified compared to the surrounding healthy tissue. Therefore, cancer cells undergo major variations in the physical forces they withstand, including rigidification of the extracellular matrix and proliferation in a confined space. Thus, it is important to understand how this environment impacts them to better target therapeutic strategies. To disentangle the many factors that influence the structure, mechanics and function of tumor tissues and cells, our team has developed numerous hydrogel-based microsystems to reproduce in a standardized way the mechanical environment that the tumor undergoes *in vivo*. It is within this framework that my research project aims at understanding how the tumor environment, from a mechanical point of view, influences the long-term cancer cell fate. To do so, I combine two complementary approaches: mechanical deformation is imposed either in 2D by confining isolated cancer cells, or in 3D by isotropically compressing tumor spheroids.

Firstly, I was able to demonstrate, in a colorectal cancer cell line, structural changes in the nucleus, regulated temporally over several days. Contrary to what happens during short-term confinement, I have shown for the first time a global nuclear regulation during prolonged uniaxial confinement, with a decrease of the nuclear volume in 24 hours, and a reset of the nuclear shape. Surprisingly, this regulation is not related to a reduced growth during cell cycle progression but occurs during confined cell division. Moreover, these nuclear changes are preserved during the next cell generation allowing the nucleus to reach homeostasis. These results may change the understanding of how physical parameters of the tissue influence cell growth and division since the key role of division in the adaptation of cancer cells to prolonged mechanical stress has never been shown before.

To better characterize the impact of mechanical stress on tumor fate, it was still necessary to make the model more complex and to integrate the microenvironment. Therefore, in addition to this fundamental work on isolated cells, the second challenge of my thesis was to reproduce *in vitro*, on a 3D model tissue (tumor spheroids), the constraints to which tumors are subjected *in vivo*. By combining a control of the physical and nutritive environment, I was able to subject growing spheroids to a combined mechanical and metabolic stress. I was able to show the important role of the tumor nutrient environment in cell plasticity and fate while demonstrating the appearance of a cancer stem cell population under mechanical stress. My results open new questions on the interaction between the nutrient and mechanical environment, both influencing the phenotype and gene expression of colorectal spheroids.

All these changes are not without consequences and could explain in part the failure of current therapies to bring a complete cure to the largest number of cancer patients.

Keywords: *colorectal cancer; cancer mechanobiology; microenvironment; hydrogel microsystem; cancer stem cells; long-term regulation.*

Forward

PhD director: Dr. Charlotte Rivière

Co-director: Dr. Sylvain Monnier

PhD thesis: from 1/10/2019 to 30/09/2023

Context of the thesis:

I am a French medical student engaged in a research joint course at the French institution "Ecole de l'inserm – Liliane Bettencourt", which allows health students to get an early scientific formation into research. Thanks to this MD-PhD program, after three years of medicine and a Master 2 in Cell Physics, I started a PhD in the field of cancer mechanobiology.

My PhD was carried out at the Institute of Light and Matter (ILM) of Lyon, Université Claude Bernard Lyon 1 in the Biophysics Team.

It was founded by a Grant of the French government (Ministry of Higher Education and Research) for the first three years and by the ARC Foundation for my 4th year, attributed by the doctoral school "Matériaux" (University of Lyon).



PUBLICATIONS:

Mouelhi M, Saffon A, Delanoe-Ayari H, Monnier M, Rivière C: **Mitosis down-regulates nuclear volume and resets nuclear envelope folding of cancer cells under prolonged confinement.**
Submitted, 2023.

Mouelhi M, Bastien E, Joly S, Jardiné G, Duret C, Chaveroux C, Rivière C, Monnier S: **3D compression drives colorectal cancer cells toward stem-like phenotype independently of metabolic stress.**
In preparation, 2023.

Guqi Y, Monnier S, Mouelhi M, Dehoux T: **Probing molecular crowding in compressed tissues with Brillouin light scattering.**
PNAS 2021, <https://doi.org/10.1073/pnas.2113614119> [Appendix 2].

Table of Content

ACKNOWLEDGMENTS	3
RÉSUMÉ	5
ABSTRACT	7
FORWARD	9
TABLE OF CONTENT	11
ABBREVIATIONS AND ACRONYMS	15
LIST OF FIGURES	16
LIST OF TABLES	17
CHAPTER 1 – GENERAL INTRODUCTION	19
<i>Motivation</i>	21
1. <i>Cancer generality</i>	22
2. <i>Cancer cell plasticity</i>	23
2.1. Tumor heterogeneity	23
2.2. Cancer Stem Cells (CSCs)	25
2.3. At the origin of drug resistance and therapy relapse?	27
3. <i>Tumor microenvironment (TME)</i>	28
3.1. Metabolic environment	30
3.2. Non-malignant cellular components	31
3.3. Contribution of the extracellular matrix	33
3.4. Reproducing <i>in vitro</i> the complex TME	35
4. <i>Mechanical constraints on tumor tissues</i>	37
4.1. Physical properties of the tumor microenvironment	37
4.2. <i>In vitro</i> models to reproduce mechanical stress	40
4.3. Mechanosensitive signaling pathways	41
5. <i>Mechanical properties of cancer cells</i>	45
5.1. Plasma membrane and cytoskeleton	45
5.2. Specificity of the nucleus	47
5.3. Pathological context	52
5.4. <i>In vitro</i> models	55
6. <i>Colorectal cancer specificity</i>	57
6.1. Colorectal cancer subtypes characterization	58
6.2. Colorectal cancer stem cells	59
6.3. Specificity of the microenvironment	60
6.4. Specificity of the nucleus	61
<i>Objectives of the PhD</i>	63
<i>References</i>	64
CHAPTER 2 – LONG-TERM IMPACT OF UNIAXIAL CONFINEMENT	85
MITOSIS DOWN-REGULATES NUCLEAR VOLUME AND RESETS NUCLEAR ENVELOPE FOLDING OF CANCER CELLS UNDER PROLONGED CONFINEMENT	87
<i>Abstract</i>	87
<i>Introduction</i>	88
<i>Results</i>	88
Multi-height soft confiner	88
Long-term nuclear volume regulation	89
Long-term regulation of nuclear tension	90
Cell cycle progression does not explain long-term nuclear adaptation	91

Long-term nuclear adaptation occurs during confined mitosis	92
Adaptation of nucleus phenotype and volume is contractility-dependent	93
Cells regulate their apparent nuclear surface during mitosis	93
<i>Figures</i>	94
<i>Discussion</i>	104
Strong confinement increases nuclear envelope tension and growth	104
Mitosis plays a key role in nuclear adaptation to confinement and alleviation of nuclear envelope tension	104
The critical role of actomyosin contractility in the regulation of lamina tension and nuclear volume	105
Regulation of nuclear repair mechanism associated with lamina folding and nuclear volume loss	105
<i>Conclusion and outlooks</i>	106
Outlook in the context of cancer	106
Potential implications for drug resistance of cancer cells	107
<i>Material and methods</i>	107
Cell culture	107
Drug treatments	107
Multi-height micro-milled mold fabrication	108
Microfabrication-based confinement of cell populations	108
Agarose molding	108
Immunostaining	109
Confocal fluorescence microscopy	109
Epifluorescence imaging	109
Live-cell imaging	109
Quantitative image analysis	109
Statistics and reproducibility of experiments	110
Supplementary Material 1 – Geometrical model	111
<i>References</i>	112
<i>Acknowledgment</i>	115
<i>Author contribution</i>	115
<i>Supplementary Figures</i>	116
<i>Supplementary Movies</i>	125

CHAPTER 3 – LONG-TERM IMPACT OF 3D ISOTROPIC COMPRESSION 127

3D COMPRESSION DRIVES COLORECTAL CANCER CELLS TOWARD STEM-LIKE PHENOTYPE INDEPENDENTLY OF METABOLIC STRESS 129

<i>Abstract</i>	129
<i>Introduction</i>	130
<i>Results</i>	131
Nutritive culture conditions are crucial for cell identity and highlight cancer cells plasticity	131
Glutamine starvation induces metabolic stress	136
Mechanical stress does not induce metabolic stress	139
Isotropic compression triggers dedifferentiation of colorectal cancer cells	141
Supplementary Figures	143
<i>Discussion and perspectives</i>	147
Microenvironment affects cellular plasticity	147
Putative molecular signaling pathways involved in this CSC-driven plasticity	148
Mechanical stress may increase cancer cell drug resistance and tumor relapse	149
Tumors are affected by several types of mechanical constraints	149
<i>Conclusion</i>	150
<i>Material and methods</i>	151
Cell culture	151
Multicellular tumor spheroids	152
Agarose microwells microfabrication	152
Dextran osmotic compression	154
Confocal fluorescence microscopy	154
Live-cell imaging	154
RTqPCR	155
Quantitative image analysis	155

Statistics and reproducibility of experiments	156
References	157
CHAPTER 4 – GENERAL DISCUSSION AND PERSPECTIVES.....	163
<i>Long-term cancer cell nuclear adaptation to imposed deformation</i>	<i>165</i>
In depth-understanding of the mechanisms and molecular pathway(s) involved in such nuclear adaptation.....	165
In depth-analysis of the consequences of such nuclear adaptation for cancer relapse and resistance to treatment	171
<i>Cancer cell identity change under long-term mechanical constraints</i>	<i>172</i>
References	174
GENERAL CONCLUSION	177
GLOSSARY	179
APPENDICES	181
<i>Appendix 1: Table summarizing the different types of experimental methods to apply mechanical constraints on cells</i>	<i>183</i>
References	185
Appendix 2.....	189

Abbreviations and acronyms

AFM: Atomic Force Microscopy	LINC: Linker of Nucleoskeleton and Cytoskeleton Complex
APTS: Amino-propyl-tri(ethoxy)silane	MCTS: Multicellular Tumor Spheroid
CAF: Cancer-Associated Fibroblast	MSI: Microsatellite Instability
CIN: Chromosomal Instability	MSS: Microsatellite Stability
CRC: Colorectal Cancer	NE: Nuclear Envelope
CSC: Cancer Stem Cell	NPC: Nuclear Pore Complex
DMEM: Dulbecco's Modified Eagle's Medium	ONM: Outer Nuclear Membrane
ECM: Extracellular Matrix	PDMS: PolyDiMéthylSiloxane
EMT: Epithelial-to-mesenchymal transition	PEG: Polyethylene glycol
ER: Endoplasmic Reticulum	PFA: Paraformaldehyde
FAK: Focal Adhesion Kinase	PG: Proteoglycan
FBS: Fetal Bovine Serum	PI3K: Phosphatidylinositol-3 kinases
FGF: Fibroblast Growth Factor	pMLC: Phospho-Myosin Light Chain
GAG: Glycosaminoglycan	qRT-PCR: quantitative Reverse Transcriptase – Polymerase Chain Reaction
GFP: Green Fluorescent Protein	TAM: Tumor-Associated Macrophage
HGPS: Hutchinson - Gilford progeria syndrome	TGF- β : Transforming growth factor β
HIF-1/2: Hypoxia Inducible Factor $\frac{1}{2}$	TME: Tumor Microenvironment
IF: Immunostaining Fluorescence	VEGF: Vascular Endothelial Growth Factor
IFP: Interstitial Fluid Pressure	YAP: Yes-Associated protein
INM: Inner Nuclear Membrane	

List of Figures

CHAPTER 1

FIGURE 1: HALLMARKS OF CANCER.	23
FIGURE 2: TUMORAL HETEROGENEITY.	24
FIGURE 3: MODELS OF TUMOR GROWTH.	25
FIGURE 4: CSCs RESISTANCE TO THERAPIES	28
FIGURE 5: COMPLEXITY OF THE TUMOR MICROENVIRONMENT.	29
FIGURE 6: OVERVIEW OF DIFFERENT 3D IN VITRO MODELS.	35
FIGURE 7: REPRESENTATION OF SIMILARITIES BETWEEN MULTICELLULAR TUMOR SPHEROID MODEL AND TUMOR.	36
FIGURE 8: PHYSICAL CONSTRAINT INFLUENCES TUMOR PROGRESSION.	38
FIGURE 9: MEASUREMENTS OF TUMORAL IN SITU FORCES.	40
FIGURE 10: METHODS OF MECHANICAL CONSTRAINS APPLICATION IN 3D OVERVIEW.	41
FIGURE 11: MOLECULAR MECHANOSIGNALING PATHWAYS	44
FIGURE 12: INCREASED TENSION IMPACTS SEVERAL SIGNALING PATHWAYS MODIFYING CELLULAR RESPONSES.	45
FIGURE 13: DIAGRAM DEPICTING THE WHOLE MECHANOSIGNALING CHAIN.	46
FIGURE 14: NUCLEAR ARCHITECTURE.	48
FIGURE 15: NUCLEAR RESPONSE TO MECHANICAL CUES.	50
FIGURE 16: NUCLEAR MECHANOTRANSDUCTION.	52
FIGURE 17: NUCLEAR ENVELOPE RUPTURE AND REPAIR MECHANISM.	53
FIGURE 18: HISTOPATHOLOGICAL IMAGES OF IN VIVO DEFORMED NUCLEI.	55
FIGURE 19: OVERVIEW OF THE DIFFERENT CELLULAR CONFINEMENT SET UPS IN 2D.	57
FIGURE 20: RECAPITULATIONS OF CRC MAIN MUTATIONS.	59
FIGURE 21: SIMPLIFIED DIAGRAM OF MICROENVIRONMENTAL CHANGES DURING COLORECTAL CANCER PROGRESSION.	61
FIGURE 22: NUCLEAR ENVELOPE PROTEOMIC ANALYSIS OF SEVERAL CRC CELL LINES.	62

CHAPTER 2

FIGURE 23: NUCLEAR VOLUME IS REGULATED ACCORDING TO THE LEVEL OF CONFINEMENT.	95
FIGURE 24: REGULATION OF NUCLEAR TENSION.	97
FIGURE 25: GLOBAL PHENOTYPIC REGULATION OF THE NUCLEUS OCCURS THROUGH MITOSIS.	99
FIGURE 26: CONTRACTILITY IS ESSENTIAL FOR NUCLEAR REGULATION.	101
FIGURE 27: NUCLEAR TOTAL SURFACE DETERMINES THE FINAL NUCLEAR VOLUME.	103
FIGURE 28: SUPPLEMENTARY FIG. 1	117
FIGURE 29: SUPPLEMENTARY FIG. 2	119
FIGURE 30: SUPPLEMENTARY FIG. 3	121
FIGURE 31: SUPPLEMENTARY FIG. 4	123
FIGURE 32: SUPPLEMENTARY FIG. 5	125

CHAPTER 3

FIGURE 33: EXPERIMENTAL OUTLOOK AND TIMELINE.	132
FIGURE 34: M11 MEDIUM MODULATES HT29 COLORECTAL SPHEROIDS BY RESETTING A NEW CELLULAR IDENTITY.	133
FIGURE 35: M11 MEDIUM HAS SIMILAR EFFECT ON 2D MONOLAYER.	134
FIGURE 36: M11 MEDIUM FAVORS SPHEROIDS FORMATION IN SINGLE CELL ASSAY.	135
FIGURE 37: SHORT- AND LONG-TERM IMPACT OF GLUTAMINE STARVATION ON 3D SPHEROIDS.	138
FIGURE 38: MECHANICAL PRESSURE DOES NOT INDUCE METABOLIC STRESS.	140
FIGURE 39: MECHANICAL COMPRESSION INCREASES STEMNESS MARKER INDEPENDENTLY OF GLUTAMINE STARVATION.	142
FIGURE 40: ISOTROPIC COMPRESSION DEDIFFERENTIATE HT29 TUMOR SPHEROIDS.	143
FIGURE 41: NO CUMULATIVE EFFECT OF METABOLIC STRESS AND MECHANICS ON NANOG EXPRESSION.	144
FIGURE 42: 3D SPATIAL LOCALIZATION OF NANOG PROTEIN WITHIN TUMOR SPHEROIDS.	145
FIGURE 43: M11 EFFECT ON HYPOXIA AND STRESS METABOLIC GENES.	146
FIGURE 44: 300 μ M DIAMETER "U" SHAPED MICROWELLS MOLD.	153

CHAPTER 4

FIGURE 45: REPRESENTATIVE IMAGES OF STAINED YAP IN HT-29 CELLS UNDER CONFINEMENT.	166
FIGURE 46: NUCLEAR AREA ADAPTATION IS ALTERED UNDER CONTRACTILITY LINKED DRUGS.	167
FIGURE 47: REPRESENTATIVE IMAGES OF STAINED VIMENTIN IN HT-29 CELLS UNDER DIFFERENT LEVELS OF CONFINEMENT.	168
FIGURE 48: NUCLEI DISPLACEMENT DURING MITOSIS.	169
FIGURE 49: HCT-116 CELL LINES NUCLEAR READOUTS UNDER STRONG CONFINEMENT.	171

List of Tables

CHAPTER 3

TABLE 1: DETAILED MEDIUM COMPOSITION.....	151
TABLE 2: QPCR PRIMERS.....	155

Chapter 1

General Introduction

*« Le commencement de toutes les sciences, c'est
l'étonnement de ce que les choses sont ce qu'elles sont »*

Aristote

Content

MOTIVATION	21
1. CANCER GENERALITY	22
2. CANCER CELL PLASTICITY	23
2.1. TUMOR HETEROGENEITY	23
2.2. CANCER STEM CELLS (CSCs).....	25
2.3. AT THE ORIGIN OF DRUG RESISTANCE AND THERAPY RELAPSE?	27
3. TUMOR MICROENVIRONMENT (TME).....	28
3.1. METABOLIC ENVIRONMENT.....	30
3.2. NON-MALIGNANT CELLULAR COMPONENTS	31
3.3. CONTRIBUTION OF THE EXTRACELLULAR MATRIX	33
3.4. REPRODUCING <i>IN VITRO</i> THE COMPLEX TME	35
4. MECHANICAL CONSTRAINTS ON TUMOR TISSUES.....	37
4.1. PHYSICAL PROPERTIES OF THE TUMOR MICROENVIRONMENT	37
4.2. <i>IN VITRO</i> MODELS TO REPRODUCE MECHANICAL STRESS	40
4.3. MECHANOSENSITIVE SIGNALING PATHWAYS	41
5. MECHANICAL PROPERTIES OF CANCER CELLS.....	45
5.1. PLASMA MEMBRANE AND CYTOSKELETON	45
5.2. SPECIFICITY OF THE NUCLEUS.....	47
5.3. PATHOLOGICAL CONTEXT	52
5.4. <i>IN VITRO</i> MODELS.....	55
6. COLORECTAL CANCER SPECIFICITY.....	57
6.1. COLORECTAL CANCER SUBTYPES CHARACTERIZATION.....	58
6.2. COLORECTAL CANCER STEM CELLS	59
6.3. SPECIFICITY OF THE MICROENVIRONMENT	60
6.4. SPECIFICITY OF THE NUCLEUS.....	61
OBJECTIVES OF THE PHD	63
REFERENCES	64

Motivation

Cancer is an extremely complex pathology, which despite intense research is still one of the major causes of death in the world. This raises important public health challenges mainly due to post-treatment relapse and metastases.

However, it is now well established that cancer progression and metastasis depend on the bidirectional interaction between cancer cells and their environment. The tumor microenvironment is a composite and dynamic structure with vascular vessels, immune infiltrates, fibroblasts, and an extracellular matrix. The evolution of this microenvironment associated with tumor development induces modifications of the biochemical signals perceived by the cells but also changes in the mechanical properties that influence the behavior of the cancer cells. This participates in the progression of the tumor and its drug resistance which is a major issue in fighting against cancer relapse. Cancer cells are thus subjected to different types of mechanical stresses, all of which have different implications and impacts depending on the tumor stage. These may include extracellular matrix (ECM) remodeling, compressive stresses on the solid tumor, or shear stresses during metastatic cell escape. The crosstalk between the cancer cells and their physical environment has raised attention the last decades, and studies have shown the increase in therapeutic resistance under mechanical constraints, to the extent that alleviating mechanical stress is now envisioned as an interesting therapeutic strategy. Although the increasing consideration of the mechanical properties in the tumor environment, several questions remain unanswered. How the long-term mechanical constraints affect tumor progression? Can cancer cells adapt to such prolonged stresses? If so, through which mechanisms? How physical stress alters cancer identity? And can it promote cancer growth?

The influence of long-term mechanical constraints on cancer cells has long been under investigated due to the lack of tools allowing proper culture conditions and mimicking the ones found *in vivo*. Studying the long-term co-evolution of the cancer cells with their physical and cellular environment is crucial for the understanding of fundamental mechanisms behind drug resistance and cancer relapse, as well as the development of new efficient therapies.

1. Cancer generality

Cancer is a generic term for a broad group of diseases altering any part of the body. It is the leading cause of death worldwide with nearly 10 million deaths in 2020 and an incidence of more than 19 million worldwide according to the World Health Organization and the International Agency for Research on Cancer (IARC) (Ferlay et al., 2021). The main cause of death from cancer is due to metastasis. Therefore, it is a major public health issue that needs a better understanding of the arising causes and the underlying biological mechanisms of this complex pathology. One simplistic explanation is the transformation of normal cells into malignant cells in a multistage process that generally progress from a pre-cancerous lesion to a malignant tumor. These changes are usually described as the results of the interaction of a person's genetic factors and external agents such as physical carcinogens (UV or radiations), chemical carcinogens (such as tobacco or alcohol) and biological carcinogens such as infection by cancer inducer viruses. However, this explanation is too naive and cancer is a dynamic disease involving changes in genetic, epigenetic, surrounding tumor microenvironment in terms of molecular, cellular, biochemical and biophysical features. In this context, more than 20 years ago, Hanahan and Weinberg published the hallmarks of cancer, which are six cancer capabilities, shared by most of human cancer. These hallmarks include sustaining proliferative signaling, evading growth suppressors, resisting cell death, enabling replicative immortality, inducing angiogenesis, and activating invasion and metastasis (Hanahan and Weinberg, 2000). Due to conceptual progress in the field, tumor biology can no longer be understood simply by enumerating the traits of the cancer cells but instead must encompass the contributions of the "tumor microenvironment" to tumorigenesis. Therefore, since then, other hallmarks and enabling characteristics have emerged: reprogramming of energy metabolism, evading immune destruction, phenotypic plasticity, non-mutational epigenetic reprogramming, polymorphic microbiome and senescent cells (Hanahan, 2022; Hanahan and Weinberg, 2011) (Figure 1). The evolution of cancer hallmark over time testifies the fail to address cancer complexity as a list of rationalized characteristics and traits and the need to consider cancer as a complex, heterogenous and multifactorial entity.

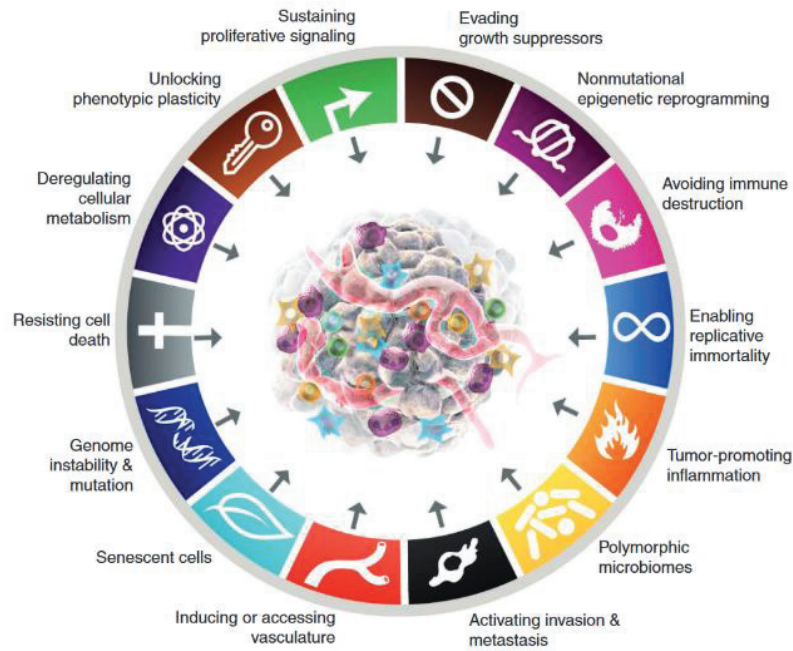


Figure 1: Hallmarks of cancer.

Fourteen conceptual characteristics associated with development and progression of human cancers, from (Hanahan, 2022).

2. Cancer cell plasticity

2.1. Tumor heterogeneity

Patient therapeutic relapse and drug resistance can be explained by the important heterogeneity within and across patients' cancers. Cancer heterogeneity can be divided into two categories: inter- and intra-tumoral, Figure 2 (LeSavage et al., 2021). Inter-tumoral heterogeneity describes population-level variations between patient with the same histological type. This heterogeneity is due to patient specific factors such as germline genetic variations, differences in somatic mutation profile or different environmental factors. Inter-tumoral heterogeneity can also arise from altered tumor cell origin, stage of diagnosis, treatment status and patient systemic health. The intra-tumoral heterogeneity refers to both spatiotemporal cellular and extracellular diversity within a given patient's cancer including primary tumor and metastatic sites. Spatial heterogeneity ensues a non-uniform distribution of genetically distinct tumor cell subclones within a disease site (Figure 2). Whereas temporal heterogeneity refers to molecular and/or cellular variation of a tumor over time, either as a natural progression of the tumor or as a consequence of exposure to selective pressures created by treatments (Dagogo-Jack and Shaw, 2018). The distinct cancer cells subpopulations at the origin of this heterogeneity display divergent genetic and transcriptomic profiles, epigenetic signatures, metabolic rates, cellular phenotypes, and morphologies that directly

influence cancer progression and drug resistance. Genomic and transcriptomic instability facilitate cancer's ability to dynamically select, harbor and amplify distinct malignant subpopulation at the origin of tumor heterogeneity. However, not only cancer cells subclones contribute to this tumor heterogeneity but the whole tumoral stroma, that is dynamically evolving during tumor course, as well. Indeed, the altered ECM, the soluble factors and the presence of non-malignant cells, such as fibroblasts, immune cells or endothelial cells, grandly contributes to this biological diversity and influences neoplastic cell phenotype through complex signaling (LeSavage et al., 2021; ND et al., 2013). Moreover, intra-tumoral heterogeneity might results in the presence and differentiation of cancer stem-like cells into diverse tumorigenic progeny even if it remains unclear what fraction of cancers follow the stem-cell model (Meacham and Morrison, 2013). It is now clearer that tumor heterogeneity explains some low clinical outcomes due to intrinsic and acquired therapeutic resistance. Therefore, taking into account those multifactorial heterogeneities is essential for the advances of personalized cancer therapy.

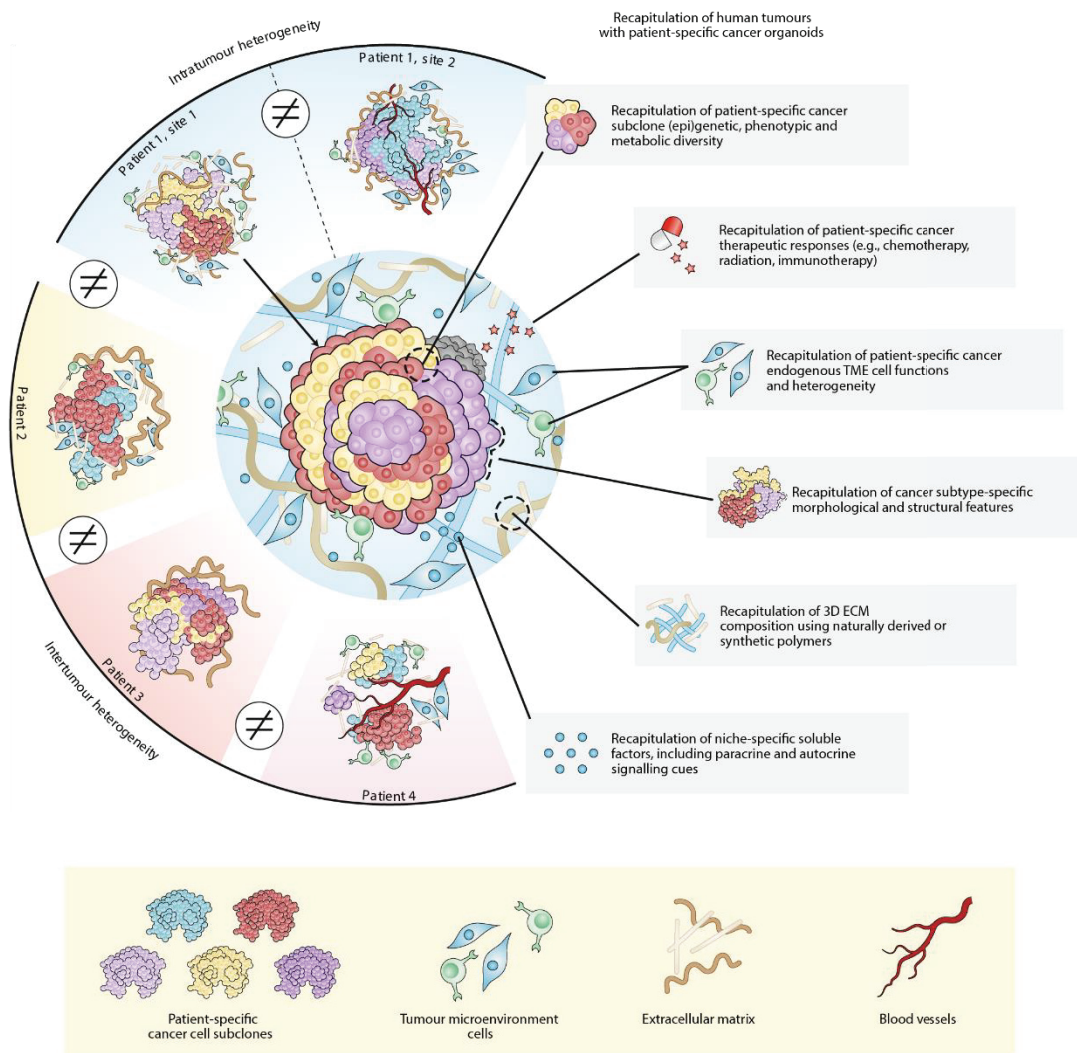


Figure 2: Tumoral heterogeneity.

Each patient's tumor has a unique cellular, molecular and environmental characteristics contributing to the important heterogeneity within and across tumors. (LeSavage et al., 2021)

2.2. Cancer Stem Cells (CSCs)

Cancer Stem Cells (CSCs) are functionally defined as cells with self-renewal, pluripotency, and tumor initiation capabilities after *in vivo* transplantation (Nassar and Blanpain, 2016). These cells, firstly described in teratocarcinoma (Kleinsmith and Pierce, 1964), can give rise to cancer cells composing the bulk of tumor, therefore reproducing the initial tumor heterogeneity. Two hypotheses have been proposed to describe their origin: clonal evolution and cancer stem cell models (Visvader and Lindeman, 2012). Clonal evolution is defined as a non-hierarchical model predicting that the sequential accumulation of mutations in tumor cells leads to a tumor cell with a selective advantage that promotes the emergence of a dominant clone. All tumor cells derived from this clone have similar tumorigenic capacity until they acquire additional mutations that may alter their proliferative or invasive capabilities. In contrast, the CSC hypothesis is defined as a hierarchical model that predicts that mutations affecting a stem or progenitor cell would confer new tumor-initiating capabilities (Figure 3). The resulting CSCs would thus have retained their ability to renew and differentiate while being able to initiate heterogeneous tumors.

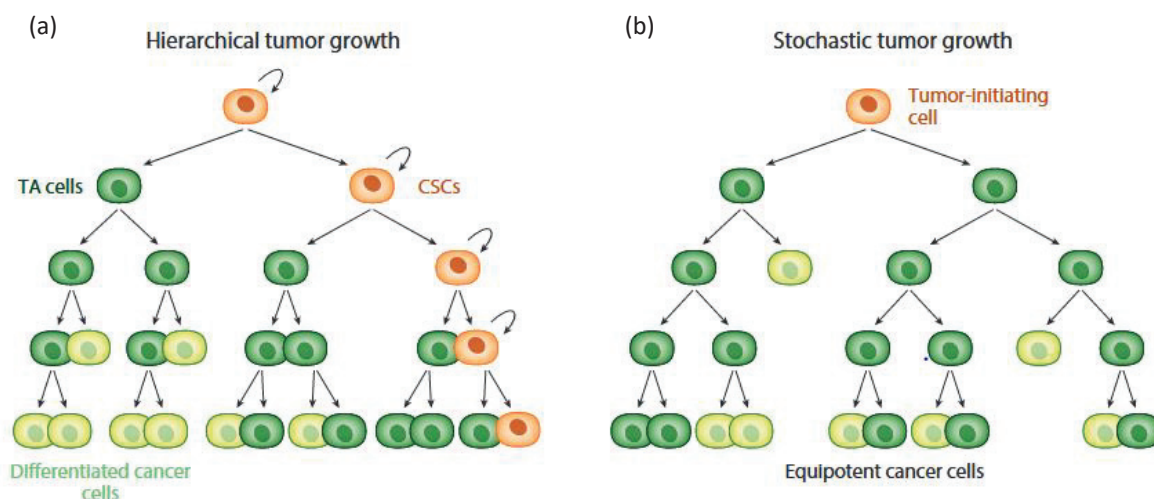


Figure 3: Models of tumor growth.

(a) Cancer stem cell model, where only the CSCs subpopulation present self-renewal and pluripotency properties. **(b)** Clonal evolution model, where all cancer cells are equipotent and can either self-renew or differentiate. TA: Transient Amplifying, from (Nassar and Blanpain, 2016).

Although demonstrated in 1994 in acute myeloid leukemia (Lapidot et al., 1994) and, since, well-established in the field of hematology, the concept of cancer stem cells has more recently been translated to a range of solid tumors, including breast (Al-Hajj et al., 2003), colon (Dalerba et al., 2007), prostate (Collins et al., 2005) and primary brain tumors (Singh et al., 2003) (Visvader, 2011). The current controversy about this model stems from the fact that (i) multiple definitions are used (tumor of origin, cell initiating tumor, and CSC) in the context of different

solid or liquid tumors, and (ii) these cell populations have been widely described by the markers they express. Indeed, the study of cancer stem cells is challenging due to the difficulty of their isolation and characterization. Many efforts were first made to isolate them from membrane molecular markers related to their stem properties, among them CD133 (a cell transmembrane glycoprotein involved in the regulation of stemness and associated with cancer recurrence), CD44 (a cell surface glycoprotein involved in malignant progression), EpCAM (an epithelial cell adhesion molecule involved in Wnt Pathway) (Nagare et al., 2016). However, their expression is generally tissue-dependent and despite an increasing number of studies, the use of these molecular markers is not sufficient to identify a CSC even in a specific tissue. This leads researchers to combine several types of markers (Munro et al., 2018). As demonstrated by the pioneer work of Yamanaka (Takahashi and Yamanaka, 2006) and Thompson (Yu et al., 2007), a core of pluripotent transcription factors is crucial for the transformation of mature somatic cells into a stem cell state. These factors such as Oct4, Sox2, Nanog, Klf4 are overexpressed in many CSC of solid tumors and could help refine the panels of biomarkers for the identification of CSC (Munro et al., 2018). Nevertheless, an emerging consensus suggests that a "cellular state" with some degree of plasticity may better define CSCs rather than a molecular phenotype (Zipori, 2004). Indeed, the presence of CSC with heterogeneous molecular portraits within the same tumor (Dieter et al., 2011) show that the expression of molecular markers reflects the state of that population at a given time and that CSC would rather refer to a dynamic cellular state. This description may also explain the difficulty in characterizing and identifying specific markers for these rare cell populations.

Moreover, the origin of CSCs remains a complicated question; the analogy with healthy stem cells suggests that they are the result of the alteration of stem cells into cancer cells, but they also seem to be able to originate from more mature cells (Chaffer and Weinberg, 2015) through a process of dedifferentiation. Even if the phenotypic switch from a CSC to a non-CSC state has been largely portrayed as a unidirectional process, a growing body of data has shown that cancer cells and CSCs are capable of significant plasticity regulated by multiple factors, which would allow them to adapt to their environment (Batlle and Clevers, 2017; ND et al., 2013). These findings demonstrate that non-stem cells and non-CSCs can be forced in an oncogene-dependent manner into a CSC-like state with poorly tumorigenic capacity but a highly pluripotent potential (ND et al., 2013). This dedifferentiation process can occur through the co-opting by cancer cells of an embryonic developmental program: the epithelial-to-mesenchymal transition (EMT) (Mani et al., 2008). EMT corresponds to the cellular process happening when epithelial cells lose adhesion with their neighbors to adopt a mesenchymal morphology allowing them to migrate over long distances (Nassar and Blanpain, 2016). In the context of cancer, the EMT process enhances cancer's invasiveness, and metastatic potential and has been found at the invasive fronts of several cancer types (Spaderna et al., 2006; Thiery

et al., 2009) correlating with poor prognosis (Polyak and Weinberg, 2009). EMT is controlled by a combination of cell-intrinsic properties – such as a cell epigenetic profile – together with stimuli from the tumor microenvironment, signaling pathways, transcription factors, and even micro-RNAs. This dedifferentiation process is also associated with the loss of epithelial markers (vimentin, N-cadherin, etc) and the acquisition of stemness ones (c-Myc, Nanog, Oct4, etc).

2.3. At the origin of drug resistance and therapy relapse?

An important feature of CSC is their capacity to regenerate the entire tumor heterogeneity and therefore, maintaining tumor propagation. They are also suspected to massively contribute to therapy resistance and cancer relapse. Indeed, according to Nassar and Blanpain (Nassar and Blanpain, 2016), these cells can either be intrinsically resistant to conventional therapy, thus, persisting after treatment, or becoming resistant under the selective pressure of therapy (Figure 4). The intrinsic resistance character of CSC may be due to their ability to resist DNA-damage induced cell death (Beck and Blanpain, 2013). It has been demonstrated in breast cancer, that CSC exposed to radiation therapy contains lower levels of reactive oxygen species (ROS) – which is a metabolic stress reaction that induces DNA damage – in the contrary of non-CSC (Diehn et al., 2009). Besides, some CSC can express high levels of multidrug resistance as ALDH, found in many CSC, mediates therapy resistance through metabolism and detoxification of chemotherapeutic agents and the activation of the pro-survival PI3K/Akt and MAPK/ERK pathways. The tumor microenvironment (TME) also contributes to CSC drug resistance. Indeed, it has been shown in colorectal cancer, that TGF- β signaling in CSC increases their resistance to cisplatin chemotherapy. Moreover, chemotherapy activates cancer-associated fibroblasts (CAF) secretion of interleukins IL-17A that stimulates CSC self-renewal and tumor growth (Lotti et al., 2013).

The cancerous plasticity phenomenon questions the models and the recent hierarchy of cancer cells but has important clinical consequences. Indeed, the fact that non-CSC can switch to a CSC state suggests that CSCs can be created de novo at different stages of tumorigenesis, and that the pool of CSCs within a tumor may be continually renewing and/or expanding (ND et al., 2013). Thus, an important consideration is the notion that therapies promoting CSC differentiation toward a non-stem state may fail, in the same way as therapies aiming at eradicating CSC if non-CSC cells can recreate the pool of CSC. Therefore, it is crucial to better understand the regulation of the CSC/non-CSC equilibrium and the factors contributing to shifting such equilibrium. Finally, a proposition could be to target the TME to counteract this dedifferentiation and future cancer relapse.

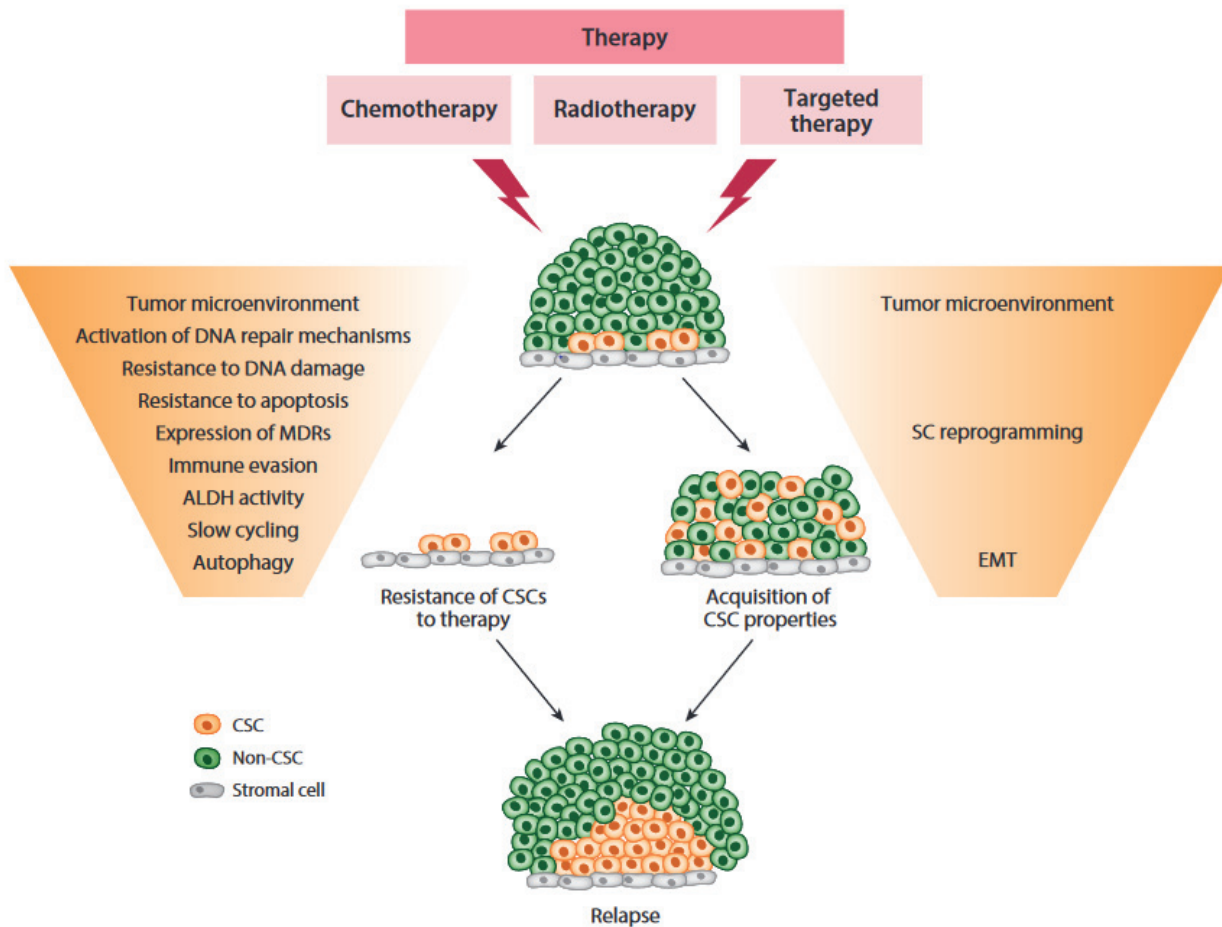


Figure 4: CSCs resistance to therapies

Multiple intrinsic and extrinsic mechanisms inducing CSCs resistance to therapies.

ALDH: aldehyde dehydrogenase; MDRs: multidrug resistance proteins.

From (Nassar and Blanpain, 2016).

3. Tumor microenvironment (TME)

In physiological conditions, there is a dynamic equilibrium between cells and the components of their environment both interacting with each other. When a cancerous process occurs, this equilibrium is perturbed. This altered tumor microenvironment (TME), also called stroma, plays a crucial role in the development and progression of the tumor. The TME is composed of an extracellular matrix (ECM), a heterogeneous population of cells – including immune cells, endothelial cells, cancer-associated fibroblast, mesenchymal and epithelial cells, etc –, a disorganized vascular network, and some immune molecules. The dialog between the tumor and its surrounding cells is either direct or through soluble factors such as cytokines, chemokines, or growth factors. Thus, the TME is continuously evolving and dynamically regulating cancer progression, influencing the therapeutic outcome, therefore multiple

therapies directed to various components of the TME have been developed in recent years (Bejarano et al., 2021). Besides, during cancer dissemination, cells are confronted to very distinct niches and are, thus, subjected to evolve in different environmental conditions.

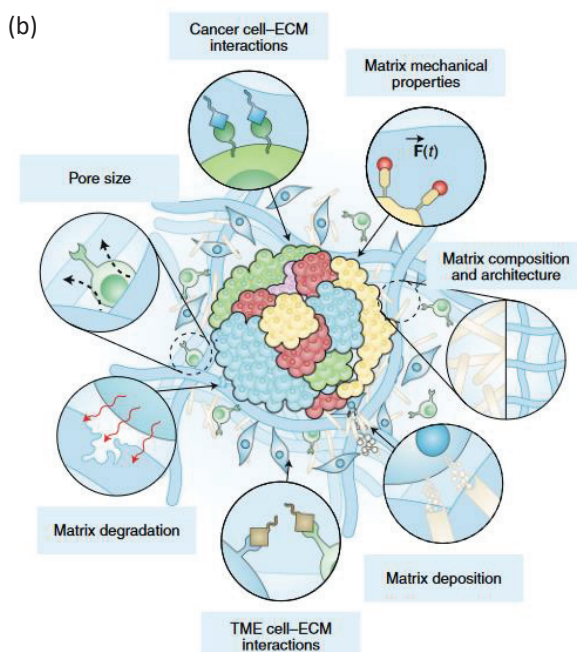
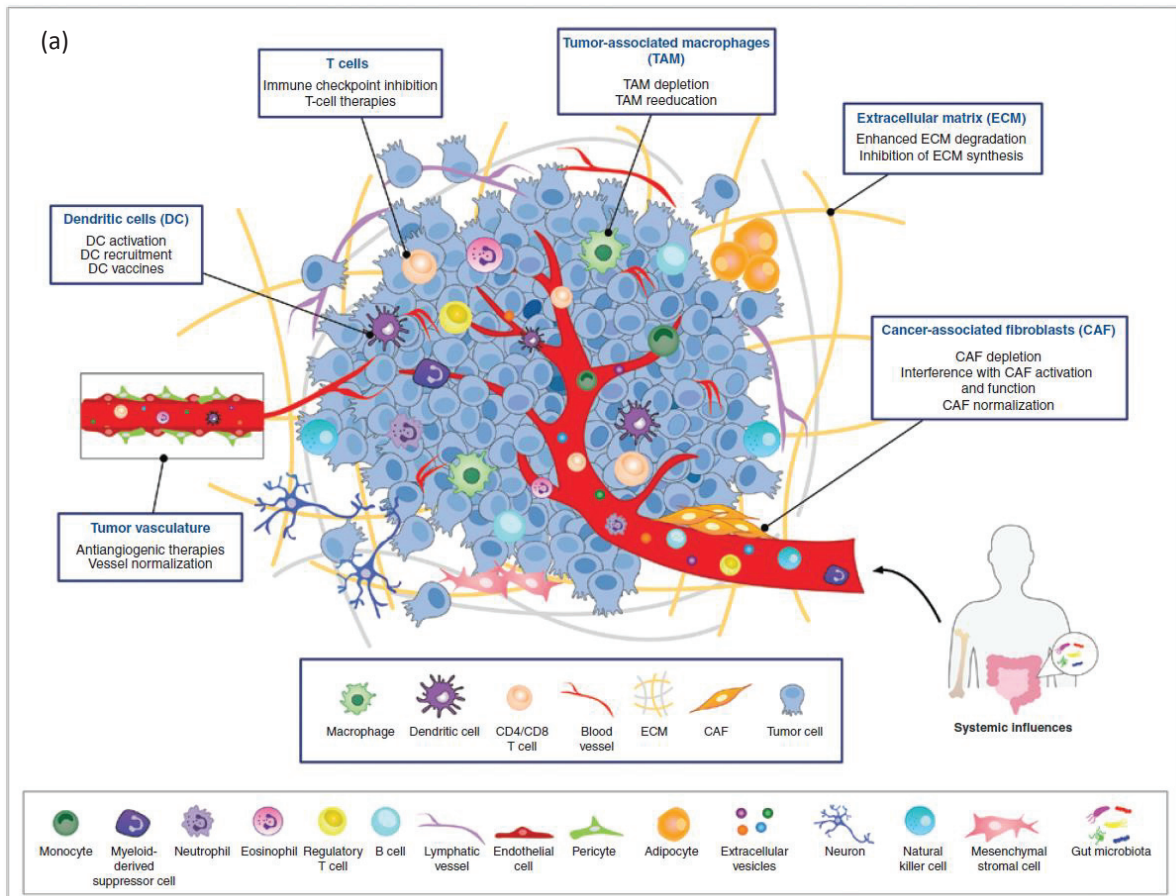


Figure 5: Complexity of the tumor microenvironment.

(a) The tumor microenvironment is composed of diverse cell types including immune cells (lymphocytes, TAM, dendritic cell) and stromal cells (CAFs, tissue-specific cells), a new vasculature and a remodeled ECM, as well as many secreted factors, from (Bejarano et al., 2021). (b) The several biochemical and mechanical interactions of cancer cells with the ECM, from (LeSavage et al., 2021).

3.1. Metabolic environment

During tumor progression, cancer cells must adapt to a variety of changes within their TME: from physical constraints to metabolic stress and immune surveillance. Indeed, within a tumor, an important temporal and spatial metabolic heterogeneity exists (Birsoy et al., 2014). This is due to the disorganized intratumoral vasculature (Figure 5) as nutrient and oxygen access are proportional to vascular access. When the metabolic resources are finite, this can lead to nutrient depletion and accumulation of metabolic waste (Pavlova et al., 2022). However, to produce biomass to maintain growth in such deprived conditions, cancer cells need to reprogram their metabolism (Choi and Park, 2018). To counteract these metabolic challenges, cancer cells not only import nutrients from the surrounding TME but refocuses their metabolism to reuse the metabolic waste product to support their biosynthesis and their energy status (Cairns et al., 2011). Nutrient competition within the tumoral stroma has a pro-tumorigenic role as it impairs effective antitumor immunity (Lyssiotis and Kimmelman, 2017). Moreover, metabolite intermediates not only serve as a substrate for energy and biomass production but also act as signaling modulators by regulating gene and protein expression and influencing the behavior of non-malignant cells present in the TME (Figure 5) which in turn promotes tumor expansion (Pavlova et al., 2022).

Nutrient

Glucose and glutamine are the two most important nutrients used by cancer cells for their proliferation and growth. Therefore, to sustain their needs during tumor progression, cancer cells have to reprogram their metabolic pathways. The best characterized metabolic change of cancer cells is the Warburg effect which concerns glucose metabolism that produces energy. Cancer cells shift their ATP production through oxidative phosphorylation to ATP generation through glycolysis, even under normal oxygen concentrations (Warburg, 1956). This effect is regulated by many metabolic or oncogenic-induced factors such as the PI3K, hypoxia-inducible factor (HIF), p53 and MYC pathways. Thus, unlike normal cells, many tumoral cells use aerobic glycolysis to convert incoming glucose to lactate rather than metabolizing it in the mitochondria through oxidative phosphorylation (Semenza et al., 2001; Warburg, 1956). This increase in lactate acidifies the TME and influences how the immune system recognizes and responds to the tumor, partially contributing to immune escape (Lyssiotis and Kimmelman, 2017).

As for glutamine, despite being a non-essential amino acid, its catabolism provides an essential source of carbon and nitrogen for cancer cell proliferation (Choi and Park, 2018; Nguyen and Durán, 2018; Windmueller and Spaeth, 1974). For this reason, most cancer cells are dependent on glutamine for their survival and were called “glutamine addicted” (Eagle, 1955). Thus, glutamine intracellular signaling promotes hallmarks of malignancies by assisting proliferation, impeding cell death, and sustaining invasion and metastasis. Indeed, it has been shown that a

subpopulation of breast cancer cells has gained the ability to grow in a deprived glutamine environment and display aggressiveness markers such as reduced anchoring growth, enhanced expression of mesenchymal markers and therapeutic resistance (Hensley et al., 2013; Singh et al., 2012). It is unknown whether glutamine prevents the development of aggressive markers or if glutamine starvation selects a particular subpopulation with aggressive characteristics. However, it has been shown in human pluripotent stem cells that glutamine signaling is essential for differentiation and cell fate determination (Lu et al., 2022, 2019).

In addition to the call for energy, or the need for macromolecular building block, cancer cell metabolic adaptation also requires the maintenance of a redox balance (Pavlova et al., 2022). For that, cells require a source of either reducing power such as NADPH and NADH (electron donors), or oxidative power such as NAD⁺ which are crucial for several enzymatic reactions in biosynthesis. Moreover, NADPH is also an antioxidant and contributes to the defense against reactive oxygen species (ROS) that are produced during rapid proliferation (Cairns et al., 2011).

Oxygen

In addition to nutrients, insufficient tissue coverage and abnormal characteristics of tumor vasculature limit gas exchange and create regions of hypoxia. Several studies have demonstrated the role of hypoxia in promoting tumor survival and progression by changing tumor metabolism, angiogenesis, invasion, and drug resistance (Pan et al., 2017). Hypoxia also contributes to tumor heterogeneity by stimulating CSC properties (Nassar and Blanpain, 2016). Highly hypoxic TME has been correlated to poor clinical prognosis (Bristow and Hill, 2008; McIntyre and Harris, 2015) as the sensitivity to radiation, conventional chemotherapy and targeted therapy are affected under hypoxia. Moreover, several molecular pathways affecting cell metabolism are altered under hypoxia. Indeed, hypoxia regulates gene expression through the transcriptional factors HIF-1 α and HIF-2 α (Hypoxia Induced Factors) that can bind to the promoter of many genes (Cairns et al., 2011; Pan et al., 2017). This hypoxic response increases glycolytic activity and decreases mitochondrial respiration leading to even more lactate deposition in the TME (Lyssiotis and Kimmelman, 2017; Yoo et al., 2020). Of note, the *in vitro* culture conditions in which both oxygen and nutrients are always in excess contributed to mask the nature and importance of metabolic restriction in cancer.

3.2. Non-malignant cellular components

Vascular and lymphatic networks

Similarly to every organ, both primary tumors and metastatic cancers rely on blood vessels for their supply in nutrients and oxygen, as well as for their removal of carbon dioxide and metabolic waste to sustain their growth. For that, tumors can develop different strategies for vascularization: formation of new blood vessels through angiogenesis, using the pre-existing

vessels via co-option vascularization (Bejarano et al., 2021; Wang et al., 2017) or via vascular mimicry by transdifferentiating cancer cells to endothelial cells (Qian et al., 2016). Of note, to survive the hypoxic TME, primary tumor cells adjust to low oxygen setting and induce a molecular switch thanks to the Hypoxia-Induced Factor (HIF) favoring angiogenesis (Semenza, 2009). Besides, the resulting tumor vasculature is often uncontrolled, tortuous and heterogeneous. Numerous growth factors were described as regulators of angiogenesis such as platelet-derived growth factor (PDGF), fibroblast growth factor (FGF) and transforming growth factor α (TGF α). However, vascular endothelial growth factor (VEGF) is considered as the main angiogenic molecule in malignancy and is secreted by both tumor cells (mainly) and stromal cells within the TME (Wu and Dai, 2017).

Moreover, in the context of cancer, the primary role of lymphatic vessels to remove interstitial fluid and tissue immunosurveillance is impaired. Indeed, tumor cells can co-opt lymphatic vasculature for cancer dissemination in the whole body (Bejarano et al., 2021; Randolph et al., 2017). It has been shown that local tumor invasion correlated with excellent lymphatic vessel density (Shields et al., 2004; Wang et al., 2017).

Immune and inflammatory cells

A growing body of data has shown that both the innate immune system (composed of macrophages, neutrophils, dendritic cells, and natural-killer cells) and adaptive immune cells including lymphocytes T and B contribute to tumor progression (Hinshaw and Shevde, 2019).

Tumor-associated macrophages (TAM) are one of the most important innate immune cells in the TME (Figure 5), they are generally associated with poor clinical outcomes (Cassetta and Pollard, 2018; DeNardo and Ruffell, 2019) due to their role in chemotherapy resistance showed both *in vitro* and *in vivo* (Baghban et al., 2020). According to their polarization status, macrophages can be categorized into M1 or M2 subtypes. In cancer, TAMs are heterogeneous, and several studies have highlighted the tumoricidal role of M1 TAM, and the tumorigenic role of M2 TAM (Wu and Dai, 2017). The established pro-tumoral role of TAM includes production of migration-stimulating factors, promoting angiogenic switch and facilitating cancer cell immune evasion (Xiao and Yu, 2021). M1 and M2 TAMs are plastic and reversible and the TME plays a crucial role in regulating their functional polarization (Sica et al., 2008; Wu and Dai, 2017). Thus, the reciprocal interaction between cancer cells and infiltrating or resident macrophage is primordial for the tumor's immune fate.

Cancer-associated fibroblast

Cancer-associated fibroblasts (CAF) are the most abundant cells in the tumoral stroma (Figure 5). Their presence is known to facilitate tumorigenesis in various physicochemical ways by promoting cancer cell proliferation, tumoral migration, angiogenesis, therapeutic resistance

and immune escape or even synthesizing and remodeling the ECM (Chen and Song, 2019; Kalluri, 2016). CAFs are mainly derived from resident fibroblasts that are recruited and activated within the stroma thanks to many soluble factors and cytokine such as TGF- β , FGF2, and PDGF, but can also originate from mesenchymal cells, adipose cells of cancer epithelial cells after EMT (Wu and Dai, 2017). The TME regroups a functional and molecular heterogeneity of CAF. The myofibroblastic subtype, mainly originated from TGF- β induced differentiation, induces synthesis and secretion of ECM and the release of matrix proteinases resulting in ECM remodeling, serving to guide the structures that direct metastasis migration (Labernadie et al., 2017; Pan et al., 2017; Xiao and Yu, 2021). Additionally, the non-myofibroblastic subtype of CAF secrete cytokines such as various growth factors (VEGF, PDGF, etc) stimulating tumor growth, angiogenesis and contributing to drug resistance.

3.3. Contribution of the extracellular matrix

As described above, the TME is a complex system consisting of an ECM, many types of cells, interstitial fluid and soluble factors that control the complex interaction between cancer cells and their environment (Figure 5b). The ECM is the major component of the stroma and plays a crucial role in the proliferation, differentiation and maintenance of tissue (Mohan et al., 2020). ECM is mainly composed of water, proteins and polysaccharides and has specific biophysical and mechanical properties. Among the matrix constituents, collagen is the most abundant even if its composition and structure vary according to the tissue. During cancer progression, the ECM serves as a pathological scaffold leading to aberrant signaling and to changes in its composition, becoming disorganized, thus promoting cellular transformation and metastasis escape (Le et al., 2020).

Collagens

Collagens are the most abundant proteins in mammals as they represent 30% of the total protein mass. They are the scaffold of the ECM and the main source of its structural stiffness. The heterogeneity of the collagen superfamily is due to translational and post-transcriptional modifications leading to an important functional diversity. Fibrillary collagen such as type I, II and III are the main responsible for the mechanical properties of the ECM in terms of stiffness and structure (Doyle et al., 2015). As the tumor progresses, abnormal remodeling of collagens occurs which in turn leads to its excessive accumulation, altered proportion and change in architecture (Kim et al., 2021). Thus, collagens can be modified by cancer cells to regulate their *in situ* neoplasia, invasion and dissemination (Xu et al., 2019). Type I collagen is found to be increased in tumor tissues compared to healthy ones, especially for colorectal cancer (Kim et al., 2021; Kirkland, 2009; Zou et al., 2013). Moreover, studies have shown that type I collagen promotes tumor growth via the activation of PI3K/AKT/Snail signaling and, therefore, promotes EMT (Wu et al., 2019). Loss of differentiation has also been shown as type I collagen

downregulates E-cadherin and β -catenin for the benefit of stem cell markers such as CD133 (Kirkland, 2009).

Proteoglycans

Proteoglycans (PG) are composite molecules constituted with a core protein covalently linked to glycosaminoglycans chains (GAGs). GAGs are polysaccharides chains and are thought to provide lubrication and structural integrity to the cells in the intestine ECM (Meran et al., 2017). Major GAGs are heparan sulfate, chondroitin sulfate, hyaluronic acid and keratan sulfate. It has been shown, in the intestine tissues, that heparan sulfate-based PGs promote intestinal regeneration by modulating Wnt/ β -catenin signaling pathway (Meran et al., 2017). More generally, PGs maintain ECM structure by organizing collagen fiber deposition, and are related to cancer development. As they can bind to growth factors, cytokines and other ECM molecules, PGs also play an important role in modulating downstream cell signaling (Nallanthighal et al., 2019). Each malignant tumor has a unique PG profile, which is closely related to its biological behavior and differentiation (Kim et al., 2021).

Glycoproteins (Fibronectin and laminins)

Glycoproteins make the ECM a cohesive network of molecules by linking cells together with structural components such as fibulin, fibrillin, laminin, or fibronectin. Glycoproteins can bind to integrins, non-integrin receptors, growth factors, and other ECM components to activate downstream signaling pathways and activate EMT, self-renewal, promoting the emergence of CSC subpopulation (Nallanthighal et al., 2019).

Fibronectin is a major adhesive ECM glycoprotein. This glycoprotein, found in a wide range of tissues, forms a fibrillary supramolecular assembly within the ECM and binds to many ECM proteins such as collagens, GAGs, and several transmembrane proteins suggesting its multifunctional role in the ECM (Meran et al., 2017). Fibronectins have a unique motif called arginine-glycine-aspartate (RGD) allowing them to bind to integrins. Those molecular bonds regulate the formation and organization of the focal adhesions, thus, directing cell migration and setting the cell's mechanical state by activation of the actin cytoskeleton notably (Kim et al., 2021).

Laminins are multimeric basement membrane proteins and a major constituent of the intestinal crypt basement participating in the establishment of epithelial cell polarity (Teller and Beaulieu, 2001). Moreover, laminins are involved in a wide range of pathological phenomena such as tumor angiogenesis, cell infiltration and cancer metastasis (Gordon-Weeks and Yuzhalin, 2020; Qin et al., 2017).

3.4. Reproducing *in vitro* the complex TME

Classical 2D culture systems are widely used for fundamental research, therapeutic efficacy analysis, or pathology modeling. However, even if they have allowed pioneer works, they present important limitations as they do not recapitulate the complexity of the architecture, nor the chemical and physical environment found *in vivo*. Therefore, 3D culture models have emerged as interesting alternatives between 2D cell culture and animal models, Figure 6 (Heinrich et al., 2021; Pampaloni et al., 2007).

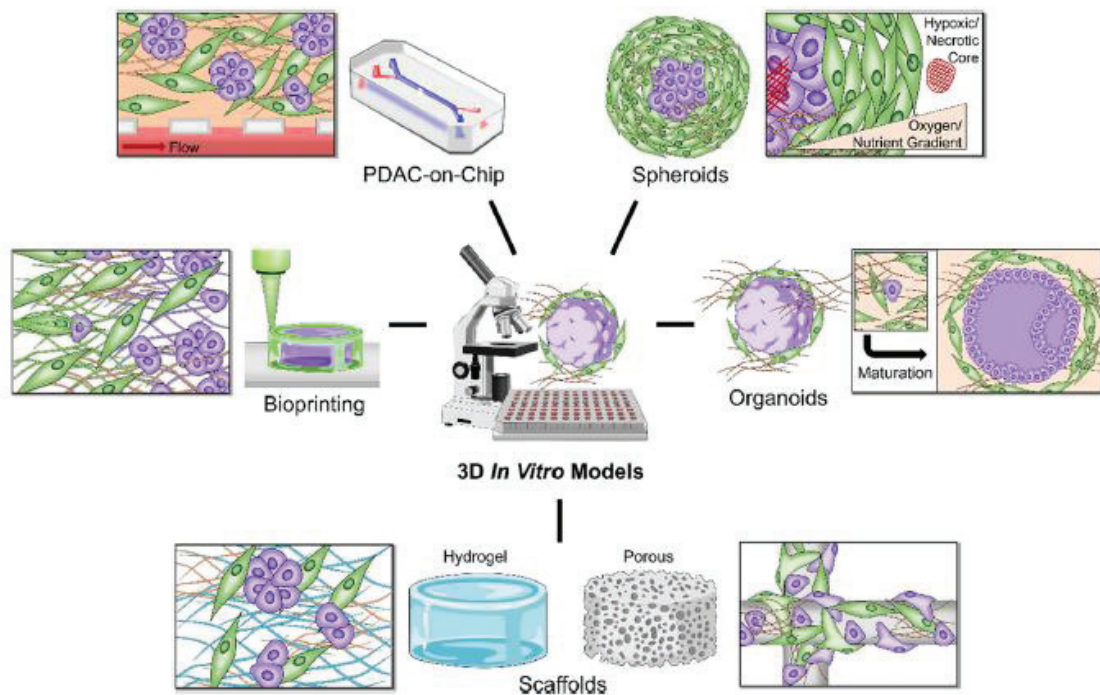


Figure 6: Overview of different 3D *in vitro* models.
From (Heinrich et al., 2021).

In my PhD, I used the multicellular spheroid model. It is one of the most used models for the study of non-vascularized solid tumors as it remains relatively simple and allows the reproduction of the cellular 3D organization of micro-tumors. Indeed, these dense self-assembled 3D constructs tend to form a spherical shape after self-aggregation and accurately recapitulate tumor features including cellular heterogeneity, cell-cell, and cell-ECM interactions, and a tumor morphology composed of different cell layers (Figure 6) (Pampaloni et al., 2007; Rodrigues et al., 2021). Thus, they also present physiopathological characteristics encountered *in vivo* such as the establishment of a gradient of nutrients, oxygen and pH (Figure 7), activating cell signaling pathways and the resulting gene expression patterns. This physiochemical gradient generally induces the formation of three concentric zones on a spheroid – an anoxic core in the center containing necrotic cells, for large spheroids (minimum

500 μm diameter), a middle hypoxic zone that has a low concentration of oxygen and nutrients, and an outer zone containing highly proliferative cells, Figure 7 (Millard et al., 2017; Nath and Devi, 2016; Rodrigues et al., 2021). Moreover, multicellular tumor spheroids can eventually model the difficulty of penetration of therapeutic molecules. Although more time-consuming and expensive than 2D cell culture, spheroids are increasingly used, and more complex structures are arising that allow co-culture with stromal or immune cells or combining other methods such as 3D bioprinting technologies, microfluidics, and scaffold-based platforms to generate more physiologically representative tumor models.

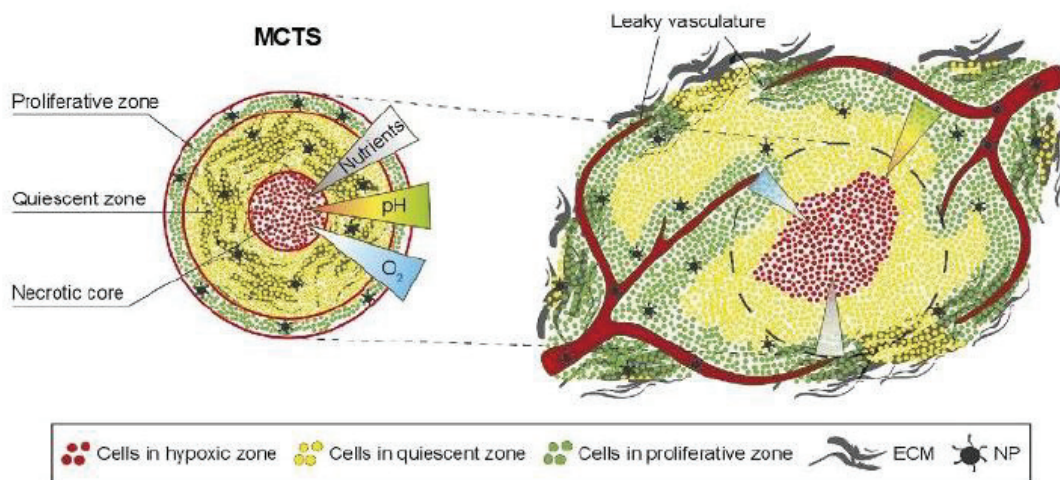


Figure 7: Representation of similarities between MultiCellular Tumor Spheroid model and tumor.
From (Millard et al., 2017).

In scaffold-based systems, multicellular tumor spheroids can be cultured within biomaterials, including decellularized native tissues, or in 3D scaffolds based on ceramics, synthetic – such as polyethylene glycol (PEG), and coated with peptide or fibrinogen to promote cell adhesion – and/or natural polymers including collagen, alginate, chitosan (Figure 6) (Rodrigues et al., 2021). Those systems should provide an appropriate environment for cell adhesion, proliferation, differentiation, and migration to allow the generation of *in vitro* tumor models that closely recapitulate essential cell-ECM interactions (Ferreira et al., 2020). Hydrogel-based scaffolds are widely used due to their ability to modulate their mechanical properties to closely mimic the tumor ECM.

Novel *in vitro* techniques like 3D bioprinting have emerged creating even more complex scaffolds with a more precise architecture and composition (Figure 6) (Langer et al., 2019). This novel approach allows the control of the spatial distribution of cells and facilitates cancer cell patterning as it enables the incorporation of cancer cells into a composite environment made of tumor, stromal cells and ECM where interaction and organization of the tissue can be studied (Asghar et al., 2015).

Another way to mimic the biophysical and chemical condition of the TME *in vitro* is the use of microfluidic chips. The goal of microfluidics is to build platforms that can model the pathophysiological functions of tissues and organs. These chips, also called organ-on-chip devices consist of a network of microfluidic channels allowing a continuous perfused cell culture and thus, enhancing control of nutrient transport and chemical gradients (Figure 6) (LeSavage et al., 2021). Organ-on-chip or tumor-on-chip in the context of cancer enables the standardization of complex systems designed with precise control of the mechanical forces applied, the orientation of tissue interfaces, and the types and localization of cells (Mollica et al., 2019).

4. Mechanical constraints on tumor tissues

The evolution of this microenvironment associated with tumor development induces changes in biochemical signals perceived by the cells but also changes in mechanical properties that influence the behavior of cancer cells, participating in tumor progression and therapy resistance (Madl and Heilshorn, 2018). Indeed, tumors are more rigid and generate and withstand mechanical stresses that can reach up to several kPa (Jain et al., 2014). These cancer cells are, thus, subjected to different types of mechanical stresses that all have different implications and impacts depending on the tumor stage (Holle et al., 2016). These may include ECM remodeling, compressive stresses on the solid tumor, proliferation of cells in a confined environment (Nia et al., 2017), elevation of interstitial fluid pressure (Libutti et al., 2018) or shear stresses during metastatic cell escape (Figure 8a) (Butcher et al., 2009).

4.1. Physical properties of the tumor microenvironment

The first interesting element concerns the change in ECM mechanics that has multiple effects on tumor tissue. As detailed in the sections above, during tumorigenesis ECM undergo massive remodeling which results in an increased amount of collagen proteins, a more important crosslinking, and a complete reorganization of matrix fibers. Therefore, the physical architecture and mechanical properties due to the density, the porosity, the size and the orientation of fibers are altered resulting in an increase of ECM stiffness (Kalli and Stylianopoulos, 2018; Nallanthighal et al., 2019). Beyond a simple static support, the ECM also influences cancer cell's fate and regulates cell interactions and gene expression through a process called mechanotransduction (Discher et al., 2005). However, the mechanical stress on cells varies according to their position in the tissue. Indeed, it has been shown on breast MCF10A tumor spheroids that cell and nuclear volumes vary between the core and the periphery of the spheroids due to the gradient of intratumoral stress and supracellular fluid flow between these two regions (Han et al., 2019), suggesting an interesting contribution of

local confinements on tumor cellular heterogeneity (Almagro et al., 2022). This variation influences their proliferation, migration, branching, stem cell phenotype and cancer cell survival and invasiveness. An increase in environmental mechanical stress reduces their proliferation rate (Delarue et al., 2014b; Helmlinger et al., 1997), induces apoptosis (Cheng et al., 2009) and enhances their invasive and metastatic potential (Almagro et al., 2022; Ingber, 2005; Kalli et al., 2018; Kumar and Weaver, 2009; Nelson et al., 2005; Tse et al., 2012).

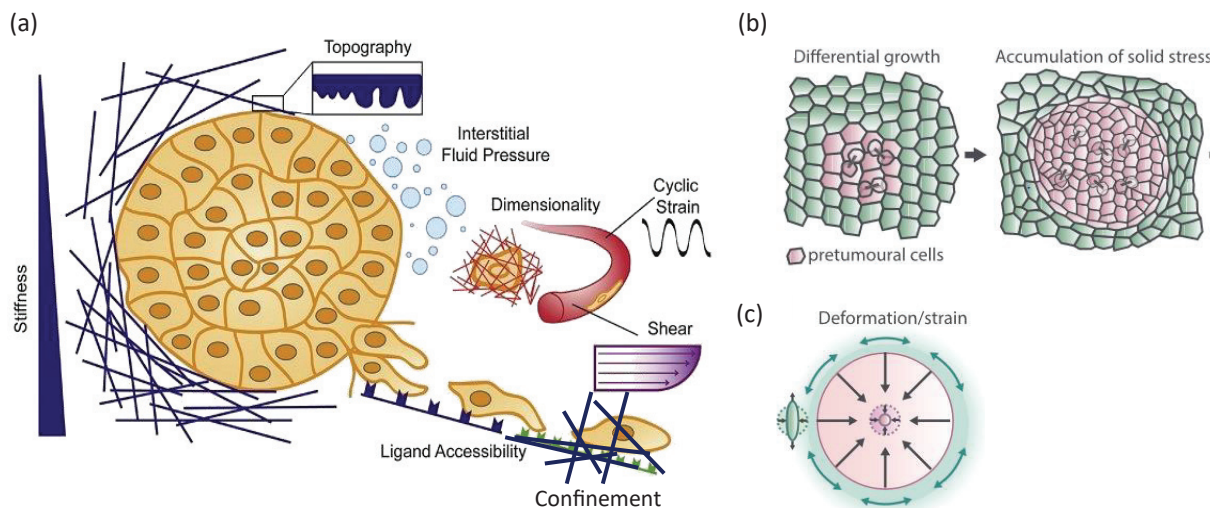


Figure 8: Physical constraint influences tumor progression.

(a) Physical characteristics of the TME that influence tumor development, adapted from (Holle et al., 2016).

(b) Tissue deformation due to the over-proliferation of cancer cells resulting in an accumulated solid stress.

(c) The internal tumor mass (purple) is compressed while the periphery is rather stretched (green). Central cells are compressed isotropically while cells at the periphery are stretched tangentially to the tumor. Middle slice representation of a 3D tumor mass. (b-c) from (Levayer, 2019).

The solid mechanics of tumors

Three main types of mechanical stresses influence tumor evolution at the tissue level: i) the externally applied stress on the tumor by the host tissues, ii) the growth-induced stress, which is the accumulated stress within the tumor due to the proliferation of cells in a confined environment, and iii) the swelling stress due to increased swelling of the hyaluronic acid tissue component (Voutouri and Stylianopoulos, 2018). These stresses are regrouped in the term “solid stress” (Figure 8b) as they are due to the solid phase of the tumor and exclude fluid mechanics such as interstitial fluid pressure (IFP). During tumor progression, the evolution of the mechanical properties of both the tumor and the host tissue – in terms of stiffness/elastic modulus –, the density of stromal cells in the TME – that are able to modulate ECM composition and organization –, strongly determine the level of solid stress (Stylianopoulos et al., 2018).

Relationship between the tumor and the mechanical properties of the host tissue

The generation of solid stress during tumor progression depends on the resistance from the host tissue. Indeed, if the tumor is softer than the host tissue it would be hard for the tumor to grow. On the contrary, if the tumor is stiffer than the host tissue, as it grows it would displace the surrounding tissue, which in turn would resist tumor expansion (Nia et al., 2017; Stylianopoulos et al., 2013). Besides, the stiffer the surrounding tissue is, the higher the stress in the tumor becomes. This internal tumor stress is compressive in all directions whereas near the interface between the tumor and normal tissue, the stress is compressive in the radial direction and tensile in the circumferential direction (Figure 8b-c) (Kalli and Stylianopoulos, 2018; Levayer, 2019; Northcott et al., 2018; Voutouri et al., 2014). Thus, mechanical interactions with the host tissue strongly affect the tumor's state of stress.

Previous studies estimated tumor internal stresses by physically cutting excised tumors (Figure 9c-d) and then, introducing the resulting tissue deformation parameters in their mathematical models (Nia et al., 2017, p. 201; Stylianopoulos et al., 2012; Voutouri et al., 2014). More recently, elastic microbeads have allowed the characterization of the mechanical effect of compression on the propagation of isotropic stresses within a tumor spheroid (Figure 9b) (Dolega et al., 2017) and oil droplets have allowed the observation of cell-generated stresses *in situ* via quantifying spatiotemporal changes in endogenous cell-generated stresses within growing spheroids (Lucio et al., 2017), Figure 9a.

The fluid mechanics of tumors

Solid stress can also affect tumor development by indirectly compressing intratumor blood and lymphatic vessels (Aragona et al., 2013; Jain et al., 2014). On top of that, increased vascular permeability and impaired lymphatic drainage result in hypoperfused tumors – leading to a drop in microvessels pressure – and a drastic elevation of the interstitial fluid pressure (Jain et al., 2014; Stylianopoulos et al., 2013).

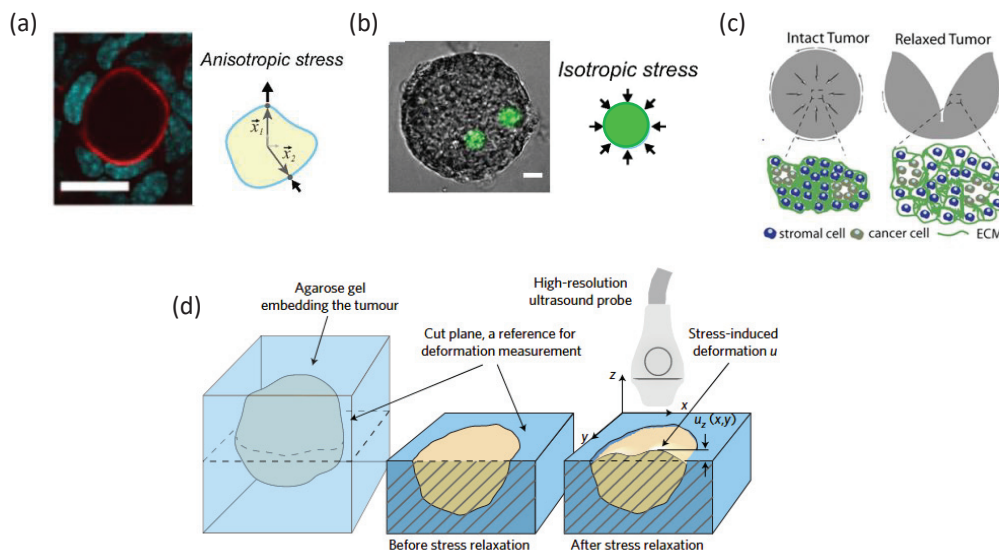


Figure 9: Measurements of tumoral in situ forces.

(a) Anisotropic stress measured by cell-sized oil droplet with the mean curvature map of the droplet's surface, from (Lucio et al., 2017). (b) Isotropic stress measured by fluorescent elastic microbeads, with a bright field image at the equatorial plane of a tumor spheroid, from (Dolega et al., 2017). (c) Schematic of the released growth stress-induced after excision of a tumor mass, from (Stylianopoulos et al., 2012). (d) Study of the released stress of the embedded and cut tumor and analysis of its geometry with high-resolution ultrasound, from (Nia et al., 2017).

4.2. *In vitro* models to reproduce mechanical stress

In 3D models, the effect of ECM stiffness is extensively studied in the context of tumor progression. For that, 3D tumor spheroids are included in gels made of collagen, Matrigel, or a homemade combination of matrix proteins (Ferreira et al., 2020; Rodrigues et al., 2021). Variation of the ECM stiffness – usually increased to reproduce *in vivo* physiopathology – is made by changing proteins density or the degree of the crosslinking of the matrix allowing researchers to study the mechanical downstream impact of ECM-originating mechanical cues (Khavari et al., 2016). However, the impact of applied stress on tumor development remains poorly understood. For that, several experimental set-ups were developed in the past two decades to mimic solid stress during tumor growth (Kalli and Stylianopoulos, 2018). The oldest technique consists of growing tumor spheroids in a confined environment leading to the development of isotropic solid stress (Figure 10b). For that, Helmlinger et al., have grown colon adenocarcinoma spheroids embedded within an agarose gel and have estimated the accumulated solid stress during tumor expansion (between 6-16kPa) (Helmlinger et al., 1997). Other studies estimated this solid stress in the context of breast, pancreatic and brain tumors, that varies from 0.2 to 20 kPa). These differences are explained by the tumor model and the experimental procedure used in each study such as the concentration of the surrounding

polymer gel, impacting its rheology. Despite these differences, they all demonstrated the inhibition of tumor growth under an increased compressive stress (Cheng et al., 2009; Delarue et al., 2014b; Helmlinger et al., 1997; Prunet, 2020; Roose et al., 2003). The application of an isotropic compressive stress can also be performed using Dextran polymers (Figure 10a). Dextran is a long-chain polymer incorporated in the culture medium that induces a global osmo-mechanical pressure applied to the surface of spheroids. It has been recently shown that dextran mainly compresses the intercellular spaces allowing to measure the bulk modulus (Delarue et al., 2014b, 2014a; Dolega et al., 2021; Montel et al., 2012). Another microfluidic-based, developed technique consists of the encapsulation of spheroids inside elastic and size-controlled microcapsules (Figure 10c) (Alessandri et al., 2013) that allows the measurements of the resistance of growing spheroids. Moreover, polydimethylsiloxane polymer (PDMS) devices can be used to restrict spheroids growth within walls (Figure 10d) (Desmaison et al., 2013) or a cage (Figure 10e) (Meriem et al., 2023).

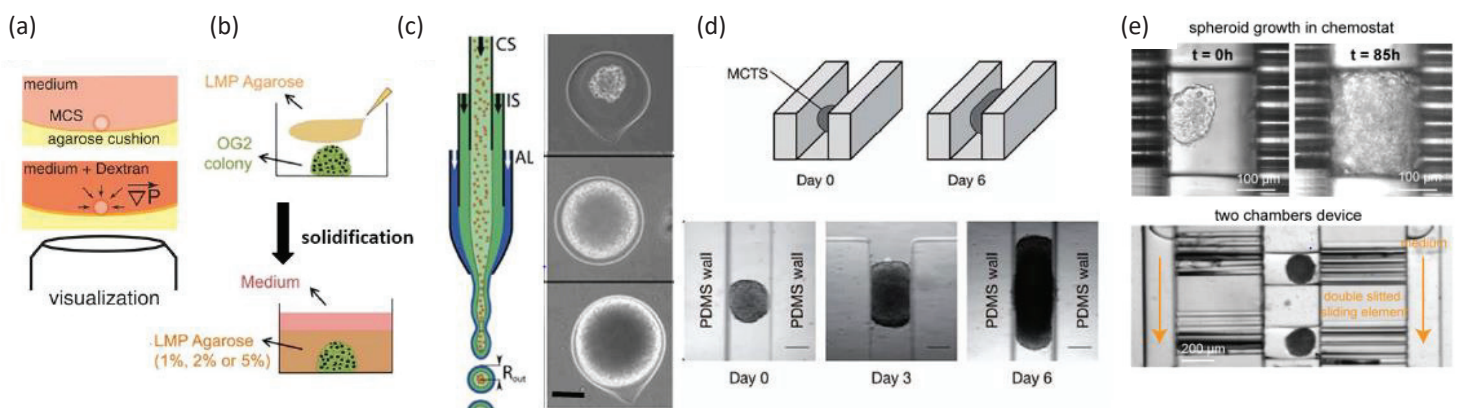


Figure 10: Methods of mechanical constrains application in 3D overview.

(a) Dextran osmo-mechanical compression, from (Rizzuti et al., 2020). **(b)** Inclusion in agarose gel, from (Du et al., 2019). **(c)** Growth and compression in elastic capsule, from (Alessandri et al., 2013). **(d-e)** Growth in a restrained PDMS environment, either by walls (Desmaison et al., 2013) or by a cage (Meriem et al., 2023).

4.3. Mechanosensitive signaling pathways

The mechanotransduction phenomenon is the process of converting a mechanical signal into a biochemical one resulting in a cellular response (Jalouk and Lammerding, 2009). Cells can sense and translate these external mechanical cues into signaling that influences gene expression and in turn impact cell structure and behavior (Vogel and Sheetz, 2006). Various elements are described as factors in the transmission of mechanical signals (Mendez and Janmey, 2012). Starting from the ability of cells to probe the physical features of the

microenvironment through integrins to the transduction at the molecular level thanks to transcriptional factors.

YAP/TAZ and the Hippo pathway

YAP transcription factor and its co-factor TAZ have been identified as the main mechanotransducers and are involved in various cellular settings (Figure 11a). Their regulation is impacted by a broad range of mechanical inputs such as shear stress, tensile forces, or matrix stiffness (Elosegui-Artola et al., 2017) and therefore their role is critical in several human malignancies with aberrant cell mechanics such as atherosclerosis, fibrosis, pulmonary hypertension, inflammation, muscular dystrophy and cancer (Panciera et al., 2017). A growing body of data demonstrated that YAP/TAZ are crucial for cancer initiation or growth in several solid tumors like breast or colorectal cancer. Indeed, their activation instructs malignant properties including cancer stem cells properties, unrestrained proliferation, cell survival, chemoresistance and metastasis (Cordenonsi et al., 2011; Panciera et al., 2017; Zanconato et al., 2016). YAP/TAZ activity is normally restricted by the Hippo signaling pathway through phosphorylation and sequestration in the cytosol (Figure 11b). Therefore, changes in the mechanical properties of the TME – including aberrant tissue organization, accumulation of stromal cells, increased compression forces and interstitial pressure as well as ECM remodeling – overrules the YAP-inhibition induced by the Hippo pathway (Totaro et al., 2018). Noteworthy, despite their activation in numerous cancers, no activating mutations of YAP/TAZ nor at Hippo signaling were found in human cancers (Panciera et al., 2017; Zanconato et al., 2016).

β -catenin and Wnt signaling pathway

Besides their previously described roles, YAP/TAZ are also biochemical and transcriptional mediators of Wnt signaling and, therefore, promote cell proliferation and tumorigenesis (Diamantopoulou et al., 2017; Llado et al., 2015; Oudhoff et al., 2016). Indeed, activation of YAP/TAZ, induced by mechanical cues or Hippo inactivation can lead to β -catenin nuclear localization (Imajo et al., 2015; Nowell et al., 2016). When the Wnt pathway is “inactivated” YAP/TAZ and β -catenin are incorporated into the destruction complex for them to be sequestered in the cytoplasm and/or degraded (Figure 11c). However, when Wnt signaling is “activated”, disassembly of this complex abolishes both β -catenin and YAP/TAZ cytosolic inhibition, triggering their nuclear accumulation and subsequent activation of targeted genes (Figure 11c) (Azzolin et al., 2014, 2012; Totaro et al., 2018). This highlights the mechanical interplay between YAP/TAZ transcription factors and β -catenin and the complexity of molecular signaling in the context of cancer. Wnt is a paramount intracellular signaling pathway regulating cell function and cell fate transition in both physiological and pathological contexts including cancer (Fernández-Sánchez et al., 2015). Increasing amounts of its effector β -catenin contribute to the formation of cell-cell adhesions leading to cellular differentiation and mesenchymal to epithelial transitions. Its regulation by mechanical cues implicates several

mechanosensitive pathways including cell-ECM interactions, TGF- β and Notch signaling (Totaro et al., 2017).

Piezo mechanosensory channels

Stretch-activated ion channels are others cell membrane mechanosensors. These very well conserved proteins are included in the plasma membrane and can undergo a change of conformation in response to an applied force. A change in membrane curvature, an increase in membrane tension, or forces exerted from the substrate or from the underlying cytoskeleton network result in channel opening and ions exchange between the intracellular and extracellular compartments (De Belly et al., 2022). This is the case for the well-known PIEZO1 channel, which discovery led to a Nobel Prize¹ (Coste et al., 2010). The mechanical stretching of this channel leads to Ca²⁺ influx regulating various cellular behavior. Indeed, studies have shown the role of PIEZO1 mechanosensing in neuron development (Segel et al., 2019), in cell fate and aging (He et al., 2018), in cancer (Chen et al., 2018), in cell division (David et al., 2023) and even in confined migration (Srivastava et al., 2020).

PI3k/AKT pathway and ERK activity

PI3K/AKT signaling is another pathway important for stem cell function. It is directly regulated by cell-substrate mechanical input (Rivière et al., 2007) and mediated by focal adhesion kinase (FAK) (Figure 12) (Broders-Bondon et al., 2018). An increase in tissues stiffness, as encounter in cancer, intensifies PI3K-FAK mediated signaling leading to enhanced cell migratory capacity (Wu et al., 2019). The major mediator of this mechanical signaling is PiP₃ (phosphatidylinositol 3,4,5-trisphosphate) which is the result of the phosphorylation of PiP₂ (phosphatidylinositol 4,5-bisphosphate) by the phosphoinositide-3 kinase (PI3K) leading to downstream activation of AKT/mTOR (De Belly et al., 2022). This signaling axis modulates primary cellular functions such as protein synthesis, cell survival (Vara et al., 2004) but is also involved in the regulation of cell size giving a mechanistic link to cell cycle progression under confinement (Delarue et al., 2014b; Nam et al., 2019).

Integrin/FAK activity is also associated with ERK activation (Farahani et al., 2021) and contribute to cell hyperproliferation and increase motility in cancer context (Figure 12) (Broders-Bondon et al., 2018; Provenzano et al., 2009). In physiological context, ERK signaling determines cell fate transitions under specific mechanical input such as shear stresses in differentiating alveolar and osteogenic cells (Li et al., 2018; Liu et al., 2010). Pluripotent stem cells fate is also regulated by ERK signaling through stretching forces and decrease in membrane tension (De Belly et al., 2021; Verstreken et al., 2019).

¹ <https://www.nobelprize.org/prizes/medicine/2021/advanced-information/>

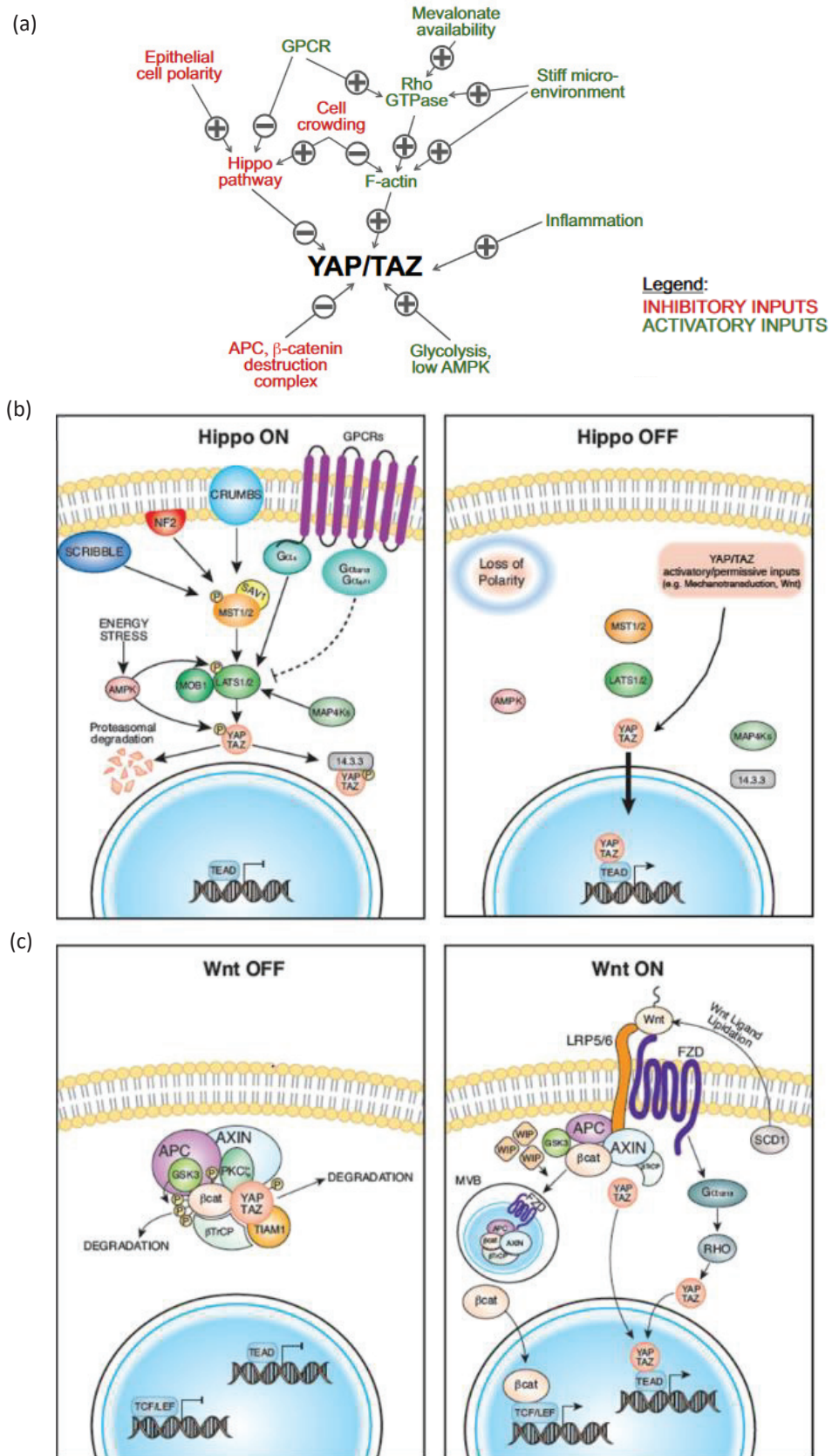


Figure 11: Molecular mechanosignaling pathways
 (a) Inputs regulating YAP/TAZ activity in cancer cells, from (Zanconato et al., 2016). (b-c) Simplified diagram of the activated or inactivated Hippo (b) or Wnt pathway (c), from (Totaro et al., 2018).

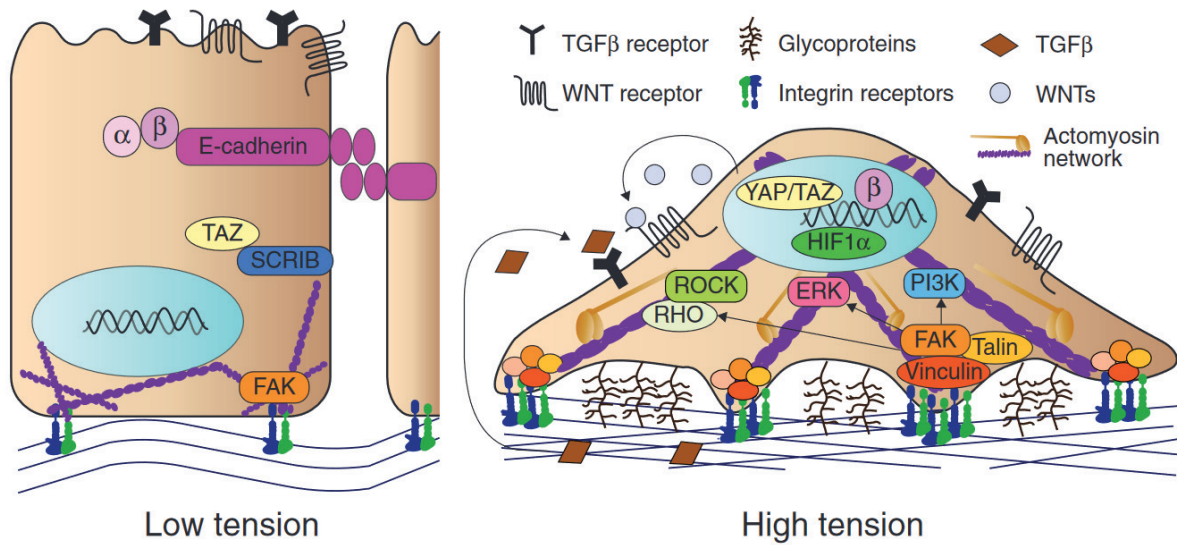


Figure 12: Increased tension impacts several signaling pathways modifying cellular responses.
 From (Northey et al., 2017).

5. Mechanical properties of cancer cells

Cancer-isolated cells are subjected to numerous constraints during metastasis when they are escaping and migrating away from the main tumor. They will invade the bloodstream and experience shear forces due to blood flow, or transient confinement when they migrate through a dense ECM or even a constant applied stress within a highly fibrotic tissue (Figure 5, Figure 8a).

5.1. Plasma membrane and cytoskeleton

Cells sense and respond to the various mechanical cues of their environment through mechanotransduction. Indeed, mechanical stimuli activate numerous mechanosensors at the cell surface leading to intracellular signaling to trigger a biological response. Plasma membrane is the first key step in this chain of transduction. It is constituted of a lipid bilayer whose composition and structure define its physical properties (De Belly et al., 2022). The tension of the plasma membrane is influenced by the level of packing/ordering of its lipids as well as the different transmembrane and membrane-connected proteins (Sitarska and Diz-Muñoz, 2020). Those proteins are part of cell adhesion and mechanosensory complexes that can be divided in four groups (Figure 13). First, we can cite the cell-cell adhesion complex mediated by cadherin-catenin junctions. High cell-cell adhesions can lead to an accumulation of β -catenin activating Wnt signaling and regulating cell fate by differentiation of human pluripotent stem cells for example. Substrate mechanosensing can also control cell fate through traction forces mediated by integrins (Lampi and Reinhart-King, 2018). Integrins are transmembrane proteins

connecting the extracellular matrix with cell cytoskeleton by focal adhesion complex and adaptor proteins including paxillin, talin or vinculin (Kechagia et al., 2019). This cell-ECM adhesion serves as a bidirectional mechanical link between the cell and its environment and are part of the molecular clutch dynamics (Elosegui-Artola et al., 2018).

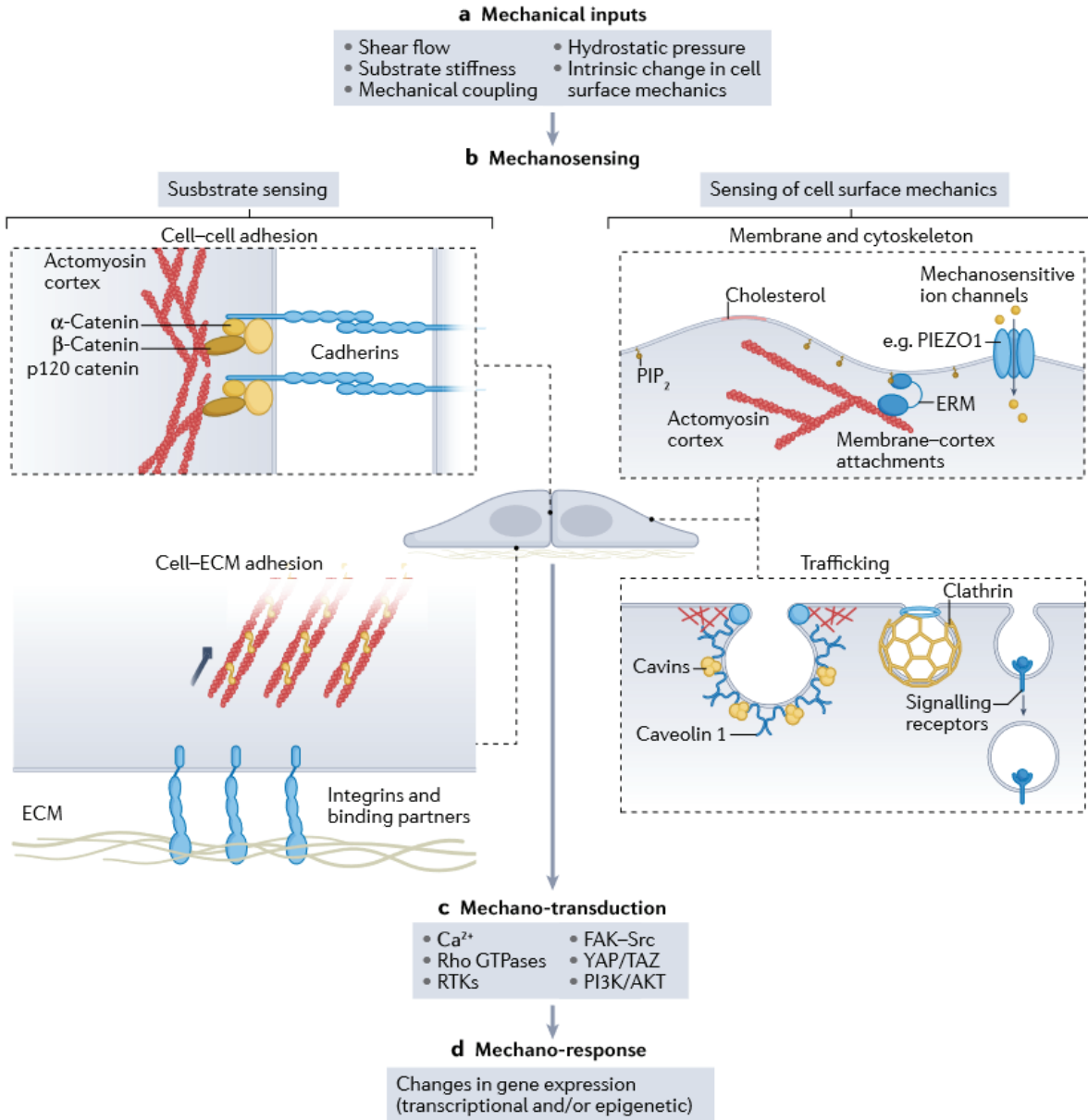


Figure 13: Diagram depicting the whole mechanosignaling chain.

Cells sense several mechanical stimuli from the environment (a), thanks to cell surface mechanosensors (b) to induce intracellular signaling response through mechanosensitive pathways (c) leading to a downstream biological response (d). From (De Belly et al., 2022).

Another key regulator of cell surface mechanics is the underlying actin cortex. Actin is a major component of the cytoskeleton originating at focal adhesions and polymerized into contractile bundles of actin filaments and myosin motors called stress fibers and are involved in substrate stiffness sensing (Lee and Kumar, 2016; Shivashankar, 2011). Moreover, actin is highly connected to other cytoskeleton filaments such as microtubules – that can provide structural integrity to the cell body (Brangwynne et al., 2006) – and intermediate filaments (Herrmann et al., 2007; Shivashankar, 2011). A large body of data demonstrates the crucial role of the cytoskeleton in transmitting various signal and offering a protective shell to the cell nucleus as well as regulating nuclear volume (Patteson et al., 2019; Stewart et al., 2007).

5.2. Specificity of the nucleus

5.2.1. Nuclear architecture

The nucleus is the largest cellular organelle and is separated from the cytoplasm by the nuclear envelope (NE) whose function is to compartmentalize the genome and regulate access to DNA. In eukaryotes, the nuclear envelope consists of two lipid bilayers: the outer nuclear membrane (ONM) and the inner nuclear membrane (INM) that merge at the nuclear pore complexes (NPC), that allow bidirectional transport (Figure 14). The ONM is continuous with the endoplasmic reticulum (ER) and at the INM is assembled a complex of proteins called the nuclear lamina. The main components of this meshwork are the type V intermediate filament proteins called nuclear lamins. In mammalian cells, these lamins are divided into two types based on their structure: the B-type lamins (lamin B1 and lamin B2) and the A-type lamins (lamin A and its splicing variant lamin C) (Vahabikashi et al., 2022). The density of these lamin filaments can be irregular across the INM surface but act as a nucleoskeletal network that anchors to the INM, NPC and peripheral heterochromatin (Figure 14) (Turgay et al., 2017). Indeed, the nucleus surrounds a highly organized genome which is essential for the regulation of gene expression and repression. The poorly compacted and transcriptionally active euchromatin is located more toward the center of the nucleus, whereas the highly condensed and transcriptionally repressed heterochromatin is attached to the nuclear lamina – also known as lamina associated domains – thanks to emerin proteins (Figure 14) thus, allowing lamins to have a critical function in gene expression and cell cycle regulation (Gruenbaum and Foisner, 2015). The NE is also connected to the cell cytoplasm and the cell surface by the Linker of Nucleoskeleton and Cytoskeleton (LINC) complex (Lammerding et al., 2022). This complex is composed of transmembrane proteins such as Nesprin and Sun proteins that constitute a physical link between the nucleoplasm and the cytoplasm.

Together, the three components of the NE: the membranes, the lamin filaments and NPC establish a barrier between the nucleoplasm and the cytoplasm and have an impact on the nuclear mechanics and rigidity.

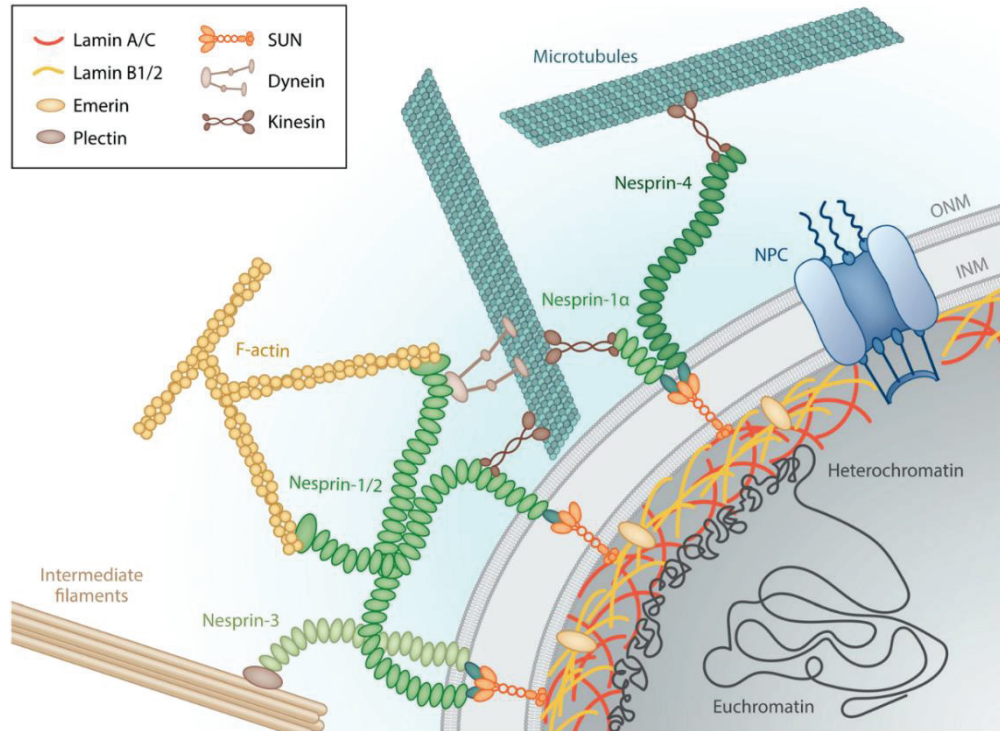


Figure 14: Nuclear architecture.
From (Vahabikashi et al., 2022).

5.2.2. Nuclear mechanics

The nuclear envelope and especially the lamin proteins are not only important structural components of nuclear shape and architecture but also nuclear mechanical integrity (Buxboim et al., 2017; Gruenbaum and Foisner, 2015). Indeed, cells depleted with lamin A and/or C present irregularly shaped nuclei, critically reduced nuclear stiffness and increased nuclear fragility (De Vos et al., 2011; Lammerding et al., 2006, 2004; Stephens et al., 2019). Conversely, cells that overexpress lamin A have a stiffer nucleus and a more important resistance to deformation. Evidence shows that both lamin A and C contribute to nuclear stiffness whereas lamin B1 contributes to nuclear integrity but not stiffness (Lammerding et al., 2006; Swift et al., 2013). Another study showed that B-type lamin convey elastic properties to the nucleus envelope whereas nuclear viscosity is specified by A-type lamins (Wintner et al., 2020). These functional differences between lamin A and B can be due to the more important presence of lamin A in the nucleoplasm and the capacity of A-type lamin to form a thicker meshwork (~ 15 nm) than B-type (~ 7 nm) (Goldberg et al., 2008). Moreover, it has been shown that nuclear lamina can act as a “shock-absorber” when the nucleus is subjected to small deformation and

tensile forces (Dahl et al., 2004; Friedl et al., 2011). Indeed, the intermediate filament meshwork of lamin regulates nuclear rigidity and respond dynamically to mechanical tension by changing its molecular composition and conformation (Figure 15) (Swift et al., 2013). Also, the ratio between A- and B-type lamins varies between cell types and tissues affecting nuclear mechanical stability and gives insights into the particular constraints that nuclei face in their microenvironment (Buxboim et al., 2017; Kalukula et al., 2022; Patil and Sengupta, 2021).

These findings are consistent with Dickinson et al, (Dickinson et al., 2022) who demonstrated that the nuclear shape is dynamic and can be affected by forces from the cytoskeleton during migration and cell spreading, although nuclei are usually considered as stiff and viscous (Dahl et al., 2005). Indeed, several studies have demonstrated that the nucleus behaves as a viscoelastic material with an elastic shell, the NE – defined by an instantaneous and reversible deformation – and a viscous core, the chromatin – exhibiting flow and can undergo irreversible deformation when subjected to forces (Kalukula et al., 2022; Lomakin et al., 2020; Srivastava et al., 2021).

Besides these structural proteins, chromatin itself has distinct mechanical properties and changes in its structure and assembly impact nuclear deformability. It has been shown in embryonic stem cells that poorly condensed euchromatin is relatively soft but after differentiation and condensation of chromatin due to a more restrictive transcriptional state, nuclear stiffness is sixth time increased (Pajerowski et al., 2007). Thus, chromatin also contributes to the overall nuclear stiffness and could be impacted by external forces (Figure 15) (Nava et al., 2020; Stephens et al., 2017). Of note, the lipid nuclear membranes play a minor role in nuclear rigidity and offer little resistance to nuclear deformation (Friedl et al., 2011; Rowat et al., 2008).

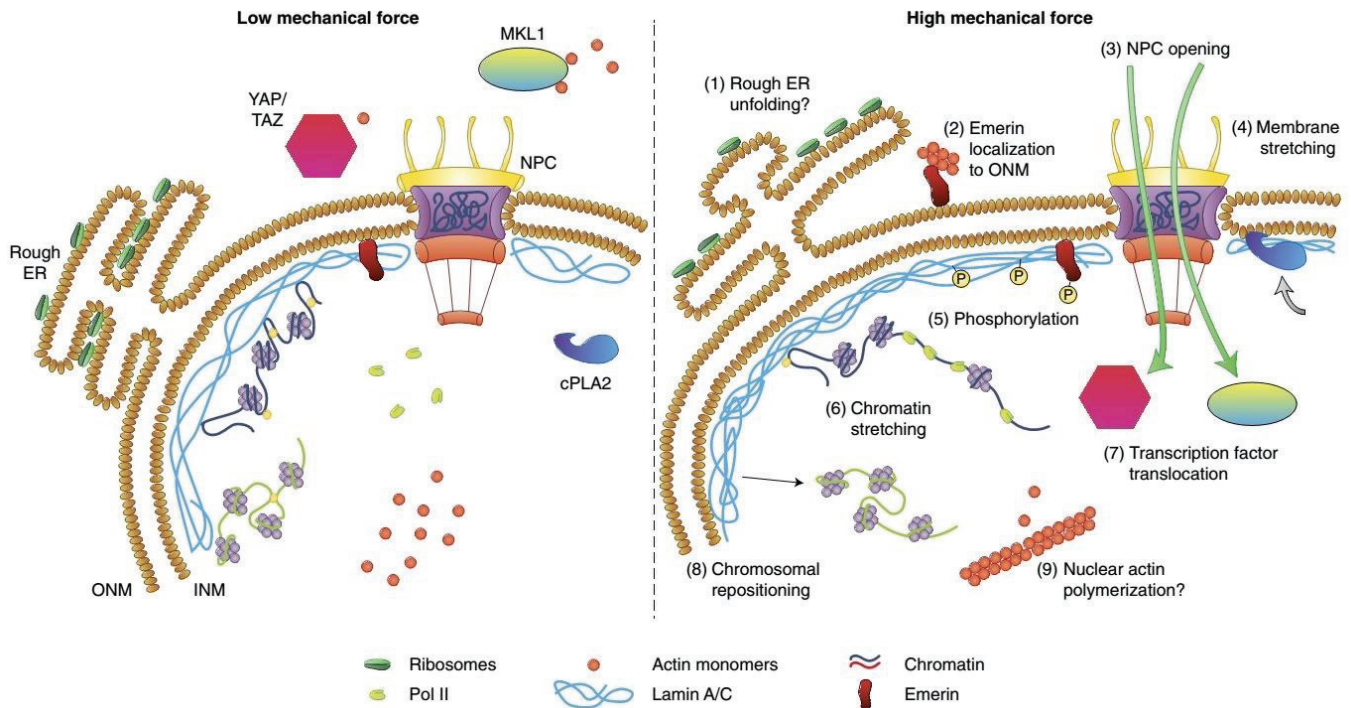


Figure 15: Nuclear response to mechanical cues.

Under high mechanical force, the nuclear membrane stretches altering the conformation of the ER, the NPC, impacting chromatin organization and actin polymerization and in turn modulation downstream signaling, from (Kirby and Lammerding, 2018).

5.2.3. Nuclear mechanotransduction

It is now well known that the nucleus plays an important role in the cellular perception of mechanical stimuli and is capable of orchestrating key cellular functions in response to mechanical forces or deformations (Figure 16a). Thus, the nucleus can adapt to its physical and mechanical environment and changes its morphology or the expression of certain genes accordingly (Figure 16b) (Long and Lammerding, 2021). Similar to the cellular plasma membrane, the NE is subjected to important tensile or compressive forces either from the cytoskeleton or directly from the external environment (Aureille et al., 2017; Maniotis et al., 1997; Wang et al., 2009). To that extent, LINC complexes allow the transmission of forces and mechanical cues between the two cellular compartments with, on one side, the cytoskeleton and, on the other side, a network of lamins which in turn regulate chromatin organization and genes (Figure 15) (Bouzid et al., 2019; Vahabikashi et al., 2022; Wong et al., 2021). By mechanically linking the nucleus to the cell membrane through cytoplasmic actomyosin, microtubule and intermediate filament, the LINC complex plays a significant role in regulating nuclear shape, positioning and movement. Forces are, then, transmitted to the nuclear interior and applied to heterochromatin via nuclear lamina and may results in chromatin deformation and opening (such as H3K9me3 or H3K27me3 demethylation (Sun et al., 2020)), promoting

transcription of mechanosensitive genes (Figure 16b) (Amar et al., 2021; Lammerding et al., 2022).

The NE can undergo more or less important deformations, whose extent depends mainly on the amount of membrane reservoir available and the mechanical properties of the surrounding cytoskeletal structures (Diz-Muñoz et al., 2013; Lomakin et al., 2020). This will lead to an increase in nuclear membrane tension triggering a stretch-mediated calcium entry and the recruitment of the cytosolic phospholipase A2 (cPLA2). Activation of this enzyme will activate lipid hormone pathways such as the eicosanoid cascade leading to several downstream responses such as cortical actomyosin contractility and increased cell migratory capacity by modulating cell morphology to escape from confinement (Lomakin et al., 2020; Venturini et al., 2020), thus providing a novel nuclear mechanotransduction mechanism (Shen et al., 2022). Besides, NPC are also mechanosensitive and respond to elevated nuclear membrane tension by increasing their pore diameter (Figure 15), and thus modulating nucleo-cytoplasmic transport (Elosegui-Artola et al., 2017), permitting nucleo-cytoplasmic trafficking in a force-dependent manner (Andreu et al., 2022; Matsuda and Mofrad, 2022).

Therefore, nucleo-cytoplasmic transport of important transcription and epigenetic regulators can be altered upon nuclear deformation. For example, subcellular localization of mechanosensitive transcription factors, such as MRTF and YAP – that respond to changes in cellular contractility and actomyosin organization – can be modulated by nuclear deformation which has essential roles in regulating several biological processes (Bertillot et al., 2022; Dupont and Wickström, 2022).

Importantly, most of the nuclear mechanotransduction changes detailed in this section result from downstream effects of molecular signaling pathways initiated from the cell surface or directly in the cytoplasm that were described in sections 4.3 and 5.1.

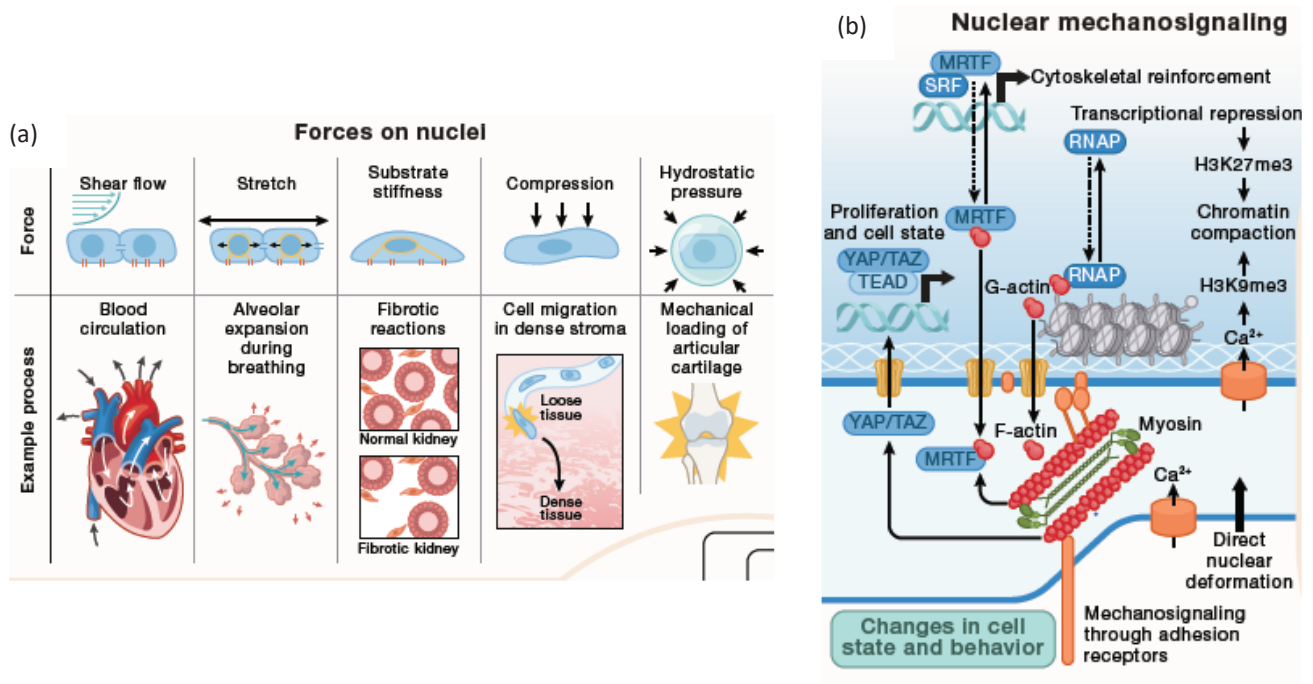


Figure 16: Nuclear mechanotransduction.

(a) Types of forces acting on nuclei and their biological examples. (b) Overview of nuclear mechanosignaling and its impact on gene expression, from (Bertillot et al., 2022).

5.3. Pathological context

5.3.1. Consequences of nuclear deformation: NE blebbing & rupture

The nucleus is constantly subjected to forces, during cell adhesion on different substrate stiffness, during confined migration for metastatic escape or immune surveillance, during developmental processes at cell polarization or when a cell is squeezed in a fibrosis event. The consequences of the previously described nuclei deformations can be of various severity: from a morphology change to a nuclear instability leading to a rupture of the NE integrity, depending on the type, the duration and the degree of the deformation. Upon large deformations, a dissociation between the double lipidic membrane and the lamina meshwork occurs, leading to a nuclear bleb. These blebs, first described a century ago by Ramon y Cajal in 1918, are round protrusions of nucleoplasm and inflate due to the increasing intranuclear pressure (Figure 17). However, at the opposite of plasma membrane blebs, these particular blebs do not retract. If substantial physical stress resulting from compressive or tensile forces continues to be applied, a lamina gap is formed at the base of the bleb leading to the extrusion of chromatin through the hole and forming a chromatin herniation (Hatch, 2018). The mechanical fragility engendered by nuclear blebs leads inevitably to NE rupture. NE rupture is a transient phenomenon followed by a rapid nuclear membrane repair (few minutes, (De Vos et al., 2011; Vargas et al., 2012)) mechanism based on the recruitment of specific proteins at the site of the rupture including the endosomal sorting complex required for transport ESCRT-III machinery

(Figure 17) (Chen et al., 2018; Denais et al., 2016; Le Berre et al., 2012; Raab et al., 2016). BAF cytoplasmic proteins accumulate at the rupture site leading the ESCRT-III complex to reseal the gap and recruiting lamin A/C to contribute to the restoration of the envelope integrity (Halfmann et al., 2019; Young et al., 2020). Nuclear envelope rupture results in loss of nucleus compartmentalization and mislocalization of nuclear proteins and exposure of chromosomal DNA to the cytoplasm leading to the activation of the pro-inflammatory cGAS–STING DNA-sensing pathway. cGAS detection of chromosomal DNA serves a crucial role in innate immune sensing of nuclear membrane rupture (Denais et al., 2016; Maclejewski and Hatch, 2020; Raab et al., 2016).

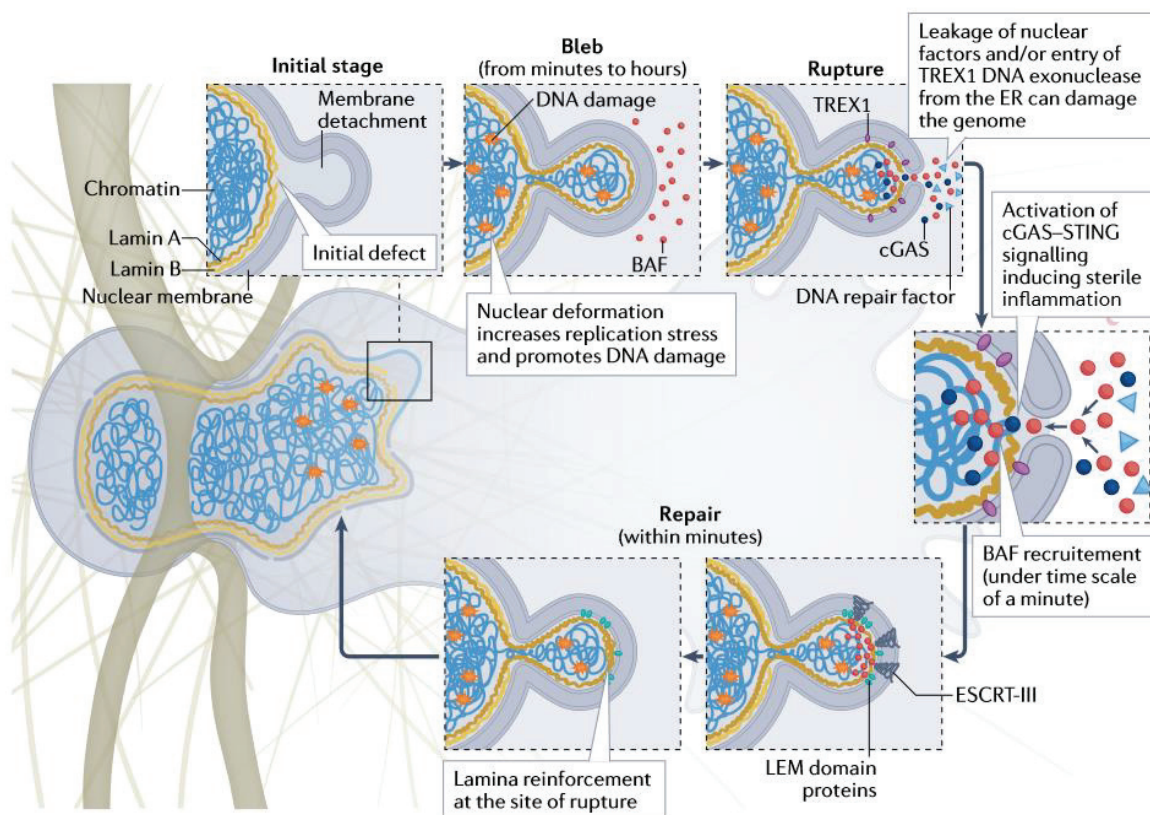


Figure 17: Nuclear envelope rupture and repair mechanism.

Migration through tight spaces or external confinement can lead to nuclear blebbing, rupturing and repairing, from (Kalukula et al., 2022).

Another consequence of soaring nuclear deformation or NE rupture is compromised genomic integrity. Indeed, some basic nuclear processes such as DNA transcription or replication or chromosomal rearrangement could be perturbed and lead to aneuploidy and/or DNA damage (Hatch, 2018). Recent studies have shown that this DNA damage following NE rupture is mediated by the ER-associated exonuclease TREX1 (Nader et al., 2021) or by loss of the DNA repair factors into the cytosol (Irianto et al., 2017; Pfeifer et al., 2018). Nuclear deformation-

induced DNA damages can also be triggered without NE rupture by an increase in replication stress mainly in S/G2 phases of the cell cycle (Shah et al., 2020).

These NE ruptures can also occur without mechanical inputs but with loss of lamin A/C or B (De Vos et al., 2011) or mutated lamins (Goldman et al., 2004; Muchir et al., 2004) or with peripheral disrupted heterochromatin (Kalukula et al., 2022; Stephens et al., 2019).

However, an increase in nucleus surface tension does not always lead to the formation of nuclear protrusions and NE ruptures. Indeed, it has been shown that NE has some reservoir in the form of large lamina invaginations that can unfold under mechanical deformation before increasing its surface tension or stretching the NE (Le Berre et al., 2012; Lomakin et al., 2020; Venturini et al., 2020). Thus, the lamin network is tension sensitive and its underlying response is crucial for NE integrity (Cho et al., 2019). Besides, the NE unfolding should be followed by the decompaction of the underlying heterochromatin.

Recently, it has been shown, that cytoplasmic vimentin intermediate filaments can mechanically protect nucleus integrity avoiding NE rupture by forming a protective cage around it when cells are migrating through tight spaces (Patteson et al., 2019; Stephens et al., 2017).

5.3.2. Environmental or mutational causes

Several diseases involve alteration of the mechanical environment of the cell or impaired ability to respond to mechanical stress. This is mainly due to abnormalities in nuclear structure and chromatin organization which are found in pathological contexts such as premature aging, cancer and metastatic potential. Mutations and variants of gene encoding for NE components such as Nesprins, Emerins and SuNs proteins but also Lamins are called envelopathies or laminopathies when it concerns only lamin genes (Kalukula et al., 2022; Somech et al., 2005). These mutations impair nuclei' mechanical properties leading to nuclear fragility in stressed tissues like muscle or cardiac tissue. Mutations of LMNA gene (coding for A-type lamins) are involved in several rare genetic disorders such as congenital cardiomyopathy (Hershberger et al., 2013), various types of muscular dystrophy (Bonne et al., 1999) and Hutchinson–Gilford progeria syndrome (HGPS) (De Sandre-Giovannoli et al., 2003; Goldman et al., 2004). They all present nuclear instability, a more deformable nuclei and an altered nuclear shape. Patient with HGPS present highly globulated and irregularly shaped nuclei (Uhler and Shivashankar, 2018). Some dystrophies such as Emery-Dreifuss muscular dystrophies – due to a mutation of the emerin, EMD coding gene – have also flawed LINC complexes that may perturb mechanotransduction pathways (Maurer and Lammerding, 2019; Vahabikashi et al., 2022). Moreover, solid tumors also display a wide range of nuclear aberrant shapes and mechanics. These abnormalities can be due to dysregulated lamin levels, chromosomal rearrangements or a stiffer stroma surrounding the tumor (Figure 18). Importantly, nuclear fragility is

associated with poor patient prognosis and in turn leads to increased frequency of DNA damage and cell death (Gruenbaum and Foisner, 2015).

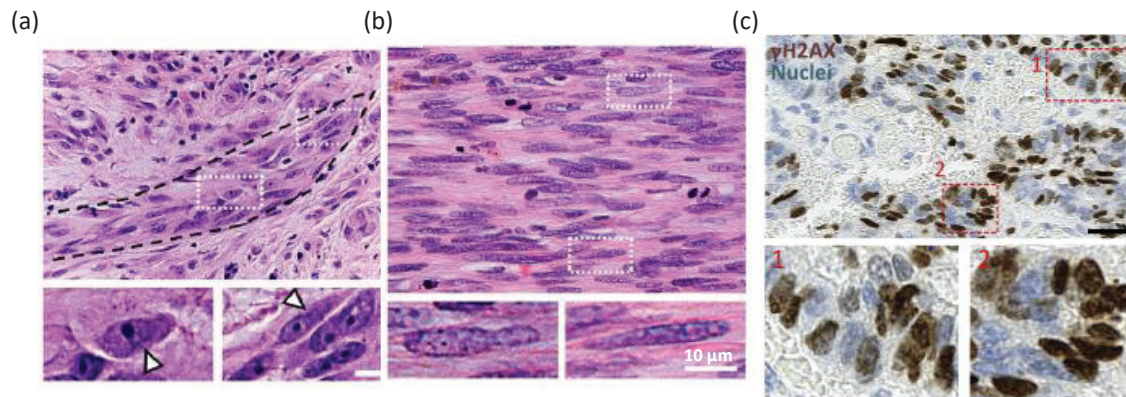


Figure 18: Histopathological images of in vivo deformed nuclei.

IHC images of invasive fronts of human melanoma (a), fibrosarcoma (b) and colorectal cancer (c), showing shaped, elongated and partially deformed nuclei, from (Friedl et al., 2011; Nader et al., 2021)

5.4. *In vitro* models

Multiple techniques have been developed to reproduce the mechanical constraints that isolated cancer cells undergo when escaping from the main tumor to induce metastasis. Among these techniques, two main categories emerge: transient confinement during cell migration or constant cell squeezing.

5.4.1. Confined migration

Confined cell migration set-ups mimic cancer cells passage through vascular endothelium to reach blood circulation. For this purpose, microchannels (Holle et al., 2019; Terenna et al., 2008; Vargas et al., 2016), narrow channels with constrictions (Figure 19b) (Raab et al., 2016), narrow pillars (Figure 19a) (Davidson et al., 2014; Denais et al., 2016; Shah et al., 2020) and even transwell plates with pores of defined size (Figure 19c) (Fanfone et al., 2022; Pfeifer et al., 2018; Xia et al., 2019) have been designed to induce cellular deformations. Those PDMS-based microfluidic chips are easy to set up and allow high throughput experiments. Although PDMS is a highly used material in the field of mechanobiology, it does not allow biomimetic experimental conditions. Indeed, it is impermeable to small molecules which can lead to rapid conditioning of the culture medium (decrease of available nutrients and increase of secreted factors) if no perfusion system is added (Le Berre et al., 2014). Moreover, although the integration of a perfusion system, hydrophobic molecules still massively absorb at its surface, and thus complicating the drug assays experiments (Toepke and Beebe, 2006; van Meer et al., 2017). Several studies focus on confined cell migration within 3D matrices allowing a more

complex and representative environment (Wolf et al., 2013). Noteworthy, with such systems, the applied mechanical constraint is temporary and spatially localized. Such confinement affects mainly the cell nucleus due to the lower deformability and the higher stiffness of the nucleus compared to the rest of the cell.

5.4.2. Cell compression devices

Cell compression experiments have the advantage of allowing the application of a uniaxial stress or a deformation on the entire cell body in a stable manner in time (from minutes to days according to the system). First, we can cite the PDMS piston developed by Matthieu Piel's team, which allowed a pioneer work in the field of mechanobiology (Figure 19d) (Le Berre et al., 2012; Liu et al., 2015). This system, compatible with high-resolution microscopy allows the precise confinement of cells thanks to a network of PDMS pillars but does not offer the possibility of a medium reservoir allowing a continuous nutrient supply. Other set-ups were then developed, based on the same PDMS pillars network but offering a perfusable system (Figure 19e) (Demou, 2010; Kittur et al., 2014). To these systems, an agarose "cushion" has been added, and the application of constraints is controlled by a piston or a weight (Figure 19g) (Tse et al., 2012). More recently, an agarose-based confiner system was developed by Audrey Prunet, a former PhD student of the biophysics team at the ILM, allowing the study of cellular response to confinement up to several days (Prunet et al., 2020). This system, now transfer to Idylle², is stable and presents a medium reservoir on top with an open access to the tank for medium renewal (Figure 19f). It is also compatible with timelapse microscopy, *in situ* immunostaining as well as molecular analysis such as western blot. Cell squeezing can also be performed using Atomic Force Microscopy (AFM) allowing a fine spatial and force magnitude control. A flat cantilever allows a uniform uniaxial cell confinement as used in (Lomakin et al., 2020). However, a medium curved or a high curved cantilever favor a localized squeezing (e.g. only on the nucleus, Figure 19h) (Xia et al., 2018).

² <https://www.idylle-labs.com/agarsqueezer-by-softconfiner>

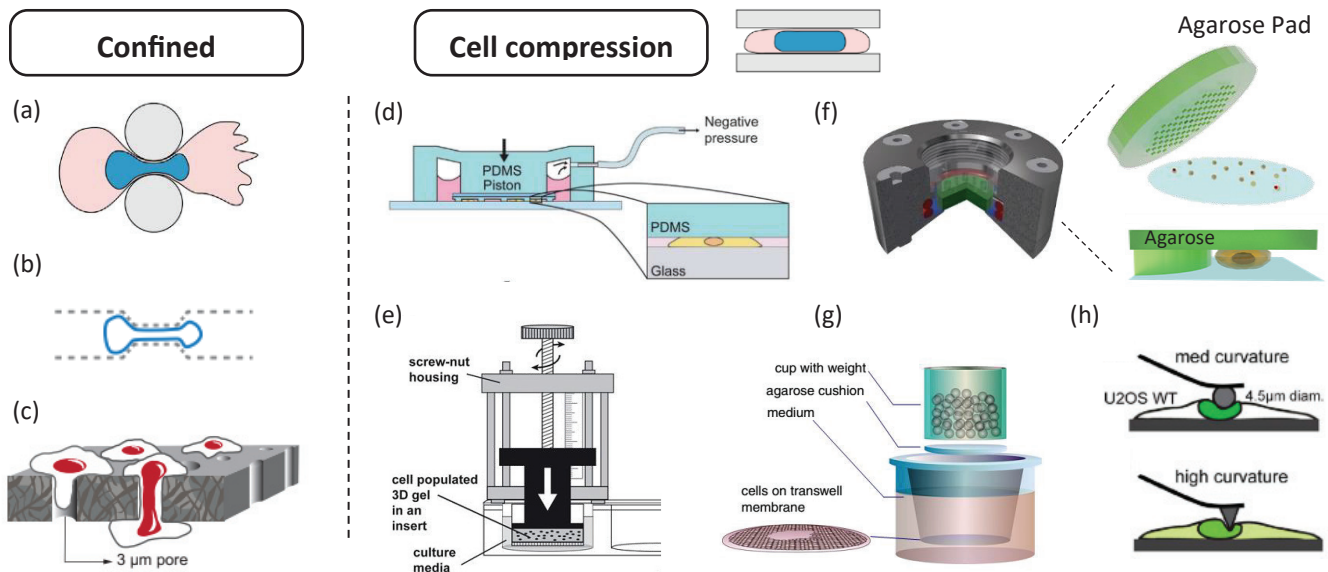


Figure 19: Overview of the different cellular confinement set ups in 2D.

(a) Confined migration through narrow pillars, from (Shah et al., 2020). (b) Confined migration through narrow channels presenting a constriction, from (Raab et al., 2016). (c) Confinement by migration through small pores, from (Fanfone et al., 2022). (d) Uniaxial confinement thanks to PDMS piston, from (Le Berre et al., 2012). (e) Another type of PDMS piston, from (Demou, 2010). (f) Soft confiner, from (Prunet et al., 2020). (g) Agarose “cushion”, from (Tse et al., 2012). (h) AFM cantilever compression, from (Xia et al., 2018).

6. Colorectal cancer specificity

Colorectal cancer (CRC), or cancer of the large bowel, is a generic term regrouping cancer of the colon, the rectosigmoid junction and the rectum. CRC is the third most common cancer worldwide with almost 2 million cases diagnosed in 2020 according to the World Health Organization and the second most common cause of cancer death, leading to almost 1 million deaths per year. It is the 3rd most common cancer in men and the 2nd most common cancer in women. These numbers are expected to continue increasing, as the International Agency for Research on Cancer (IARC) estimates an increase of incidence by 56% between 2020 and 2040 to more than 3 million new cases per year. The estimated increase in mortality is even larger, by 69%, intriguingly most of the increase is expected to occur in high Human Development Index countries. CRC cancer is a diverse disease whose outcome largely depends on location, histological and molecular subtypes as well as the stage at diagnosis (IARC, 2019).

6.1. Colorectal cancer subtypes characterization

Classification of CRC is traditionally performed according to the histological subtypes as defined by WHO (Board, 2019) and specific staging systems such as the Duke's classification. The most common subtype is adenocarcinoma which accounts for 85% of CRC cases worldwide. Molecular characterizations are increasingly important and two major pathways are known in the development of CRC: the chromosomal instability (CIN) pathway and the microsatellite instability (MSI) pathway (Bogaert and Prenen, 2014; Fleming et al., 2012). CIN is characterized by DNA aneuploidy and different mutations in different proto-oncogenes such as K-RAS or APC and tumor suppressor genes such as p53 (Figure 20a). The MSI pathway defines the status of genomic instability due to a deficient DNA mismatch repair system (De Smedt et al., 2015). Moreover, it has been shown that MSI tumors have a better prognosis than MSS tumors due to the higher level of neoantigens and a more robust immunoeediting, making MSI tumors good candidates for checkpoint blockade immunotherapy (Xiao and Freeman, 2015). The molecular status of several human CRC cell lines commonly used in cancerology research is recapitulated in Figure 20b. The HT-29 cell line is a colorectal adenocarcinoma with an epithelial morphology presenting MSS status with APC, BRAF, and p53 genes mutations. This cell line was used in my PhD work and is well identified in the literature (Chang et al., 2015; Durinikova et al., 2018; Fogh et al., 1977; Gheytauchi et al., 2021; Manhas et al., 2016; Wang et al., 2016; Zhang et al., 2017; Zoetemelk et al., 2019).

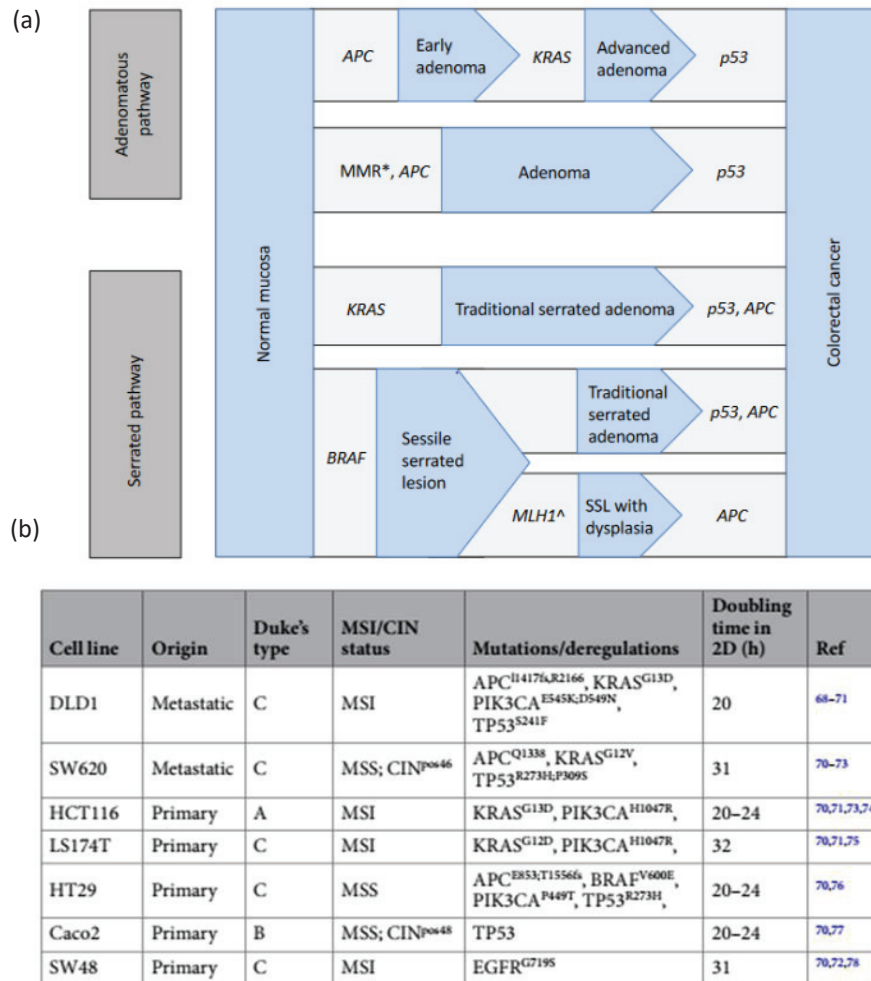


Figure 20: Recapitulations of CRC main mutations.

(a) Simplified diagram of colorectal cancer pathways. From (IARC, 2019). (b) Panel of CRC cell lines used in culture. MSI: microsatellite instability; MSS: microsatellite stability; CIN: chromosomal instability pathway. From (Zoetemelk et al., 2019).

6.2. Colorectal cancer stem cells

As described in the section 2.2, CSCs are a subpopulation of tumor cells that presents characteristics of self-renewal and a potential for multi-directional differentiation. Colorectal CSC working model was first validated via a group of surface markers after functional transplantation assays (Dalerba et al., 2007). Surface markers such as EpCAM (a cell adhesion molecule involved in Wnt Pathway), CD44 (Lee et al., 2017) (a cell surface glycoprotein involved in malignant progression) and CD133 (Kazama et al., 2018; Mirzaei et al., 2016; Todaro et al., 2010) (a cell transmembrane glycoprotein involved in the regulation of stemness and associated with cancer recurrence) have been extensively studied over the past two decades in colorectal cancer (Dalerba et al., 2007; Pan et al., 2017; Zhou et al., 2017). In addition, other more universal CSC pluripotent markers including Nanog, Oct4, Sox2, c-Myc, and KLF4 have been studied in CRC (Angius et al., 2021; Munro et al., 2018; Zhou et al., 2017). We can also

cite Lgr5 intestinal stemness marker that has been shown to increase in colorectal malignancies both in human and murine tumors (Beumer and Clevers, 2016; Chen et al., 2014; He et al., 2014; Shimokawa et al., 2017). Several studies have shown that colorectal cancer cells with stem-like properties present higher levels of stemness markers Oct4 and Sox2 as well as tumor sphere forming ability (both *in vitro* and *in vivo*), confirming the importance of phenotypic markers and their biological role in stemness function (Dotse and Bian, 2016; Li et al., 2012; Shaheen et al., 2016; Wahab et al., 2017; Zhi et al., 2015).

A growing body of data suggests that the heterogeneous nature of CRC is related to CSCs (Angius et al., 2021). The emergence of these neoplastic cells with stemness behaviors might be due to the transdifferentiation of colorectal cancer epithelial cells. Indeed, APC mutations – present in 90% of CRC – provoke abnormalities in key mediators of the WNT pathway. Due to a wrong activation of the WNT signaling that promotes stemness and inappropriate stabilization of β -catenin, colorectal cells could undergo EMT (Angius et al., 2021; Vermeulen et al., 2010). Evidence of EMT in CRC has been demonstrated by the increased expression of stemness factors such as Snail, Lgr5, CD133, CD44, and EpCAM. Besides, it has been shown that, in CRC, TGF- β induces EMT markers – like Twist1 and N-cadherin – and upregulates pluripotent transcription markers such as Oct4, Sox2, Nanog and Klf4 (Zhou et al., 2017).

6.3. Specificity of the microenvironment

Altered microenvironment and tissue mechanics are a hallmark of cancer and impact tumor development and progression. Indeed, the dysregulated ECM production in CRC and the modified physical properties of the TME contributes to patient prognosis. During CRC tumorigenesis, ECM undergoes a complete change in terms of composition, structure and amount (Figure 21) compared to healthy colorectal tissues (Karlsson and Nyström, 2022). The expression of collagen I is increased with tumor stage (Li et al., 2020) and the architecture of collagen fibers reorganizes within the ECM, becoming irregular and promoting cancer cell proliferation both *in vitro* and *in vivo* (Li et al., 2020) and cancer cell migration (Brauchle et al., 2018). Besides, in areas of high collagen deposition, colorectal stroma stiffness can increase up to four-fold higher than in normal tissue (Brauchle et al., 2018; Zanotelli et al., 2020). Patients presenting an increase expression of collagen I have significantly lower survival rates compared to patients with low expression (Brauchle et al., 2018). The collagen network deposition grandly contributes to tumor stiffening and is thought to be involved in the malignant transformation of tissue and the migration of colorectal tumors. Moreover, studies have demonstrated that CRC is seven times stiffer than colon normal tissue (from 0.9kPa to 7.5kPa; (Zanotelli et al., 2020)). According to (Phipps et al., 2005), this change in elastic modulus seems to correlate with clinical factors such as the size of the tumor, the vascular invasion, and poorly differentiated clusters. Such aberrations in the colorectal TME perturb

tissue homeostasis and can provide the perfect conditions to induce cancer stem cells (Kim et al., 2021; Pan et al., 2017). Moreover, a study demonstrated the role of TAMs-inducing EMT program to enhance CRC invasion, migration, and metastasis in human CRC samples and *in vitro* co-culture (Baghban et al., 2020). Of note, Bejarano et al., (Bejarano et al., 2021) highlighted the importance of gut microbiome in the context of colorectal TME to influence CRC. All these findings demonstrate the highly modified colorectal TME during tumorigenesis.

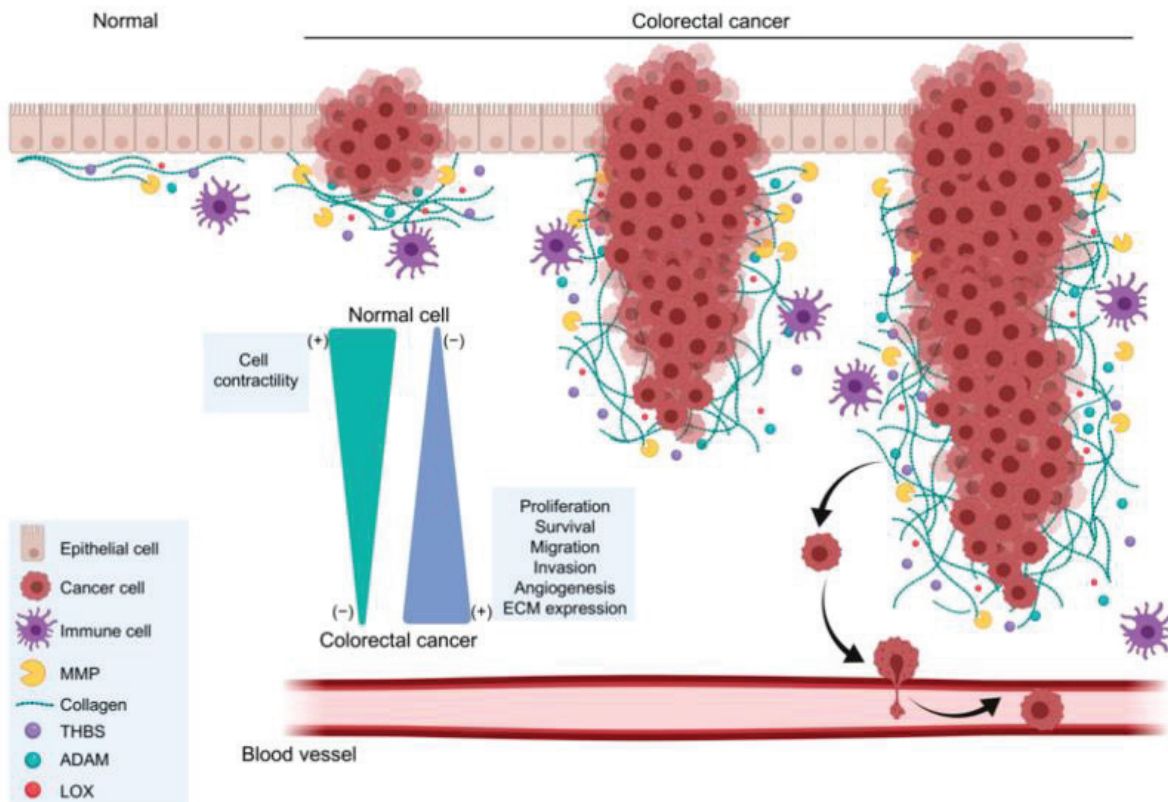


Figure 21: Simplified diagram of microenvironmental changes during colorectal cancer progression. THBS: Thrombospondin; ADAM: A disintegrin and metalloproteinase; LOX: Lysyl oxidase. From (Kim et al., 2021).

6.4. Specificity of the nucleus

The structural composition of CRC nuclei has an impact on tumor invasiveness and patient prognosis. Especially, it has been shown that A-type lamins increase the risk of death and are implicated in tumor progression (Willis et al., 2008) as lamin A participates in activating the expression of E-cadherin, involved in the EMT which in turn increases tumor invasiveness. Moreover, lamin B2 expression is downregulated in colorectal cancer cell lines presenting CIN mutations compared to cell lines exhibiting MSI (Figure 22) (Kuga et al., 2014). Kuga et al also demonstrated that lamin B2 is essential for mitotic spindle formation suggesting that lamin B2 is crucial for maintaining chromosome integrity. Thus, those results highlight that the major

cause of chromosomal instability pathway is chromosome missegregation caused by the absence of lamin B2 in forming proper bipolar spindle during cell division. Similarly as the other CIN colorectal cell lines, the HT-29 cell line presents very poor levels of lamin B2 and only a low level of lamin B1.

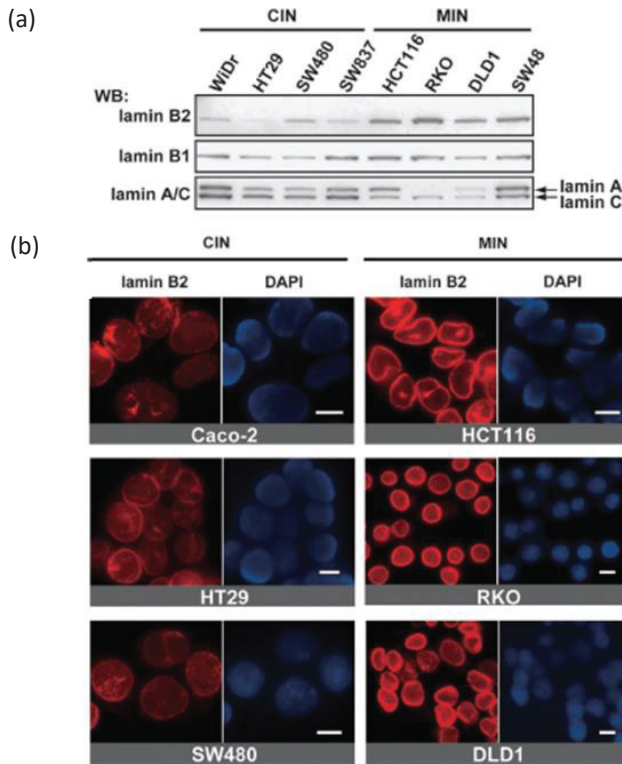


Figure 22: Nuclear envelope proteomic analysis of several CRC cell lines.

(a) Western blot analysis of several types of lamins from different CIN and MIN cell lines.

(b) Immunostaining images of Lamin B2 and DAPI from different CIN and MIN cell lines

From (Kuga et al., 2014).

Objectives of the PhD

Throughout this first introductory chapter, we have seen the crucial role of physical changes in the tumor microenvironment on tumor development and progression at different scales. Therefore, the biophysics team research topics particularly focus on the coupling between mechanics and biology for cells or tissues including the mechano-genetic regulation, the tissue-level rheological properties and even the development of culture and analysis platforms called organ-on-chips. To disentangle the many factors that influence the structure, mechanics and function of tumor tissues and cells, our team has developed numerous micro-fluidic hydrogel systems to reproduce in a standardized way the mechanical environment that the tumor undergoes *in vivo*.

It is within this framework that my research project aims at understanding how the tumor environment, from a mechanical point of view, influences the long-term cancer cell fate. To do so, my experimental PhD was divided into two complementary approaches and focused on colorectal cancer.

The first part consists of **studying the effect of uniaxial prolonged confinement in 2D, on isolated cancer cells**. Taking advantage of a new hydrogel-based microsystem that has been developed by a former PhD student on the team, I could perform a precisely controlled cell confinement for several days while overcoming the barrier of medium turnover. This system allowed me to perform highly original experiments of real-time microscopy and *in situ* immunolabeling to study the cancer cell nucleus adaptation over long term confinement (several days). The results obtained in this part led to an article, presented in Chapter 2, and submitted for publication. Additional preliminary data that goes beyond the scope of the paper are also discussed in the Chapter 4.

The second challenge of my PhD was **to understand the impact of isotropic compression on 3D tumor spheroids on cancer cells identity**. To this end, I used an agarose-based microwells technique, developed in the team to standardize and increase tumor spheroid production while controlling growth conditions and performed isotropic mechanical compressions. This axis initiated a collaborative project with the team of Cédric Chaveroux from the CRCL in Lyon and the team of Julie Pannequin from the IGF in Montpellier who have the biological expertise on the metabolic impact and on colorectal cancer stem cells, respectively. It is in this multidisciplinary framework that I have studied the impact of mechanical stress/metabolic stress coupling in 3D on colorectal cancer tumor spheroids with high throughput. By combining biological and physical quantitative measurement, I have shown that both mechano-osmotic pressure and nutrient-deficient conditions reduce spheroid growth while promoting a stem state in a non-nutritive dependent manner. The obtained results are detailed in Chapter 3 in a scientific paper format in preparation for submission.

During my PhD, I obtained very interesting results on both types of approach using experimental protocols and automated analysis tools that I developed, to gain in efficiency and to increase the reproducibility.

References

- Alessandri, K., Sarangi, B.R., Gurchenkov, V.V., Sinha, B., Kießling, T.R., Fetler, L., Rico, F., Scheuring, S., Lamaze, C., Simon, A., Geraldo, S., Vignjevic, D., Doméjean, H., Rolland, L., Funfak, A., Bibette, J., Bremond, N., Nassoy, P., 2013. Cellular capsules as a tool for multicellular spheroid production and for investigating the mechanics of tumor progression in vitro. *Proc. Natl. Acad. Sci. U. S. A.* 110, 14843–8. <https://doi.org/10.1073/pnas.1309482110>
- Al-Hajj, M., Wicha, M.S., Benito-Hernandez, A., Morrison, S.J., Clarke, M.F., 2003. Prospective identification of tumorigenic breast cancer cells. *Proc. Natl. Acad. Sci.* 100, 3983–3988. <https://doi.org/10.1073/pnas.0530291100>
- Almagro, J., Messal, H.A., Elosegui-artola, A., Rheenen, J.V., Behrens, A., 2022. Tissue architecture in tumor initiation and progression. *Trends Cancer* xx, 1–12. <https://doi.org/10.1016/j.trecan.2022.02.007>
- Amar, K., Wei, F., Chen, J., Wang, N., 2021. Effects of forces on chromatin. *APL Bioeng.* 5, 041503. <https://doi.org/10.1063/5.0065302>
- Andreu, I., Granero-Moya, I., Chahare, N.R., Clein, K., Molina-Jordán, M., Beedle, A.E.M., Elosegui-Artola, A., Abenza, J.F., Rossetti, L., Trepát, X., Raveh, B., Roca-Cusachs, P., 2022. Mechanical force application to the nucleus regulates nucleocytoplasmic transport. *Nat. Cell Biol.* 24, 896–905. <https://doi.org/10.1038/s41556-022-00927-7>
- Angius, A., Scanu, A.M., Arru, C., Muroli, M.R., Rallo, V., Deiana, G., Ninniri, M.C., Carru, C., Porcu, A., Pira, G., Uva, P., Cossu-Rocca, P., De Miglio, M.R., 2021. Portrait of Cancer Stem Cells on Colorectal Cancer: Molecular Biomarkers, Signaling Pathways and miRNAome. *Int. J. Mol. Sci.* 22, 1603. <https://doi.org/10.3390/ijms22041603>
- Aragona, M., Panciera, T., Manfrin, A., Giullitti, S., Michielin, F., Elvassore, N., Dupont, S., Piccolo, S., 2013. A mechanical checkpoint controls multicellular growth through YAP/TAZ regulation by actin-processing factors. *Cell* 154, 1047–1059. <https://doi.org/10.1016/j.cell.2013.07.042>
- Asghar, W., El Assal, R., Shafiee, H., Pitteri, S., Paulmurugan, R., Demirci, U., 2015. Engineering cancer microenvironments for in vitro 3-D tumor models. *Mater. Today* 18, 539–553. <https://doi.org/10.1016/j.mattod.2015.05.002>
- Aureille, J., Belaadi, N., Guilluy, C., 2017. Mechanotransduction via the nuclear envelope: a distant reflection of the cell surface. *Curr. Opin. Cell Biol.* 44, 59–67. <https://doi.org/10.1016/j.ceb.2016.10.003>
- Azzolin, L., Panciera, T., Soligo, S., Enzo, E., Bicciato, S., Dupont, S., Bresolin, S., Frasson, C., Basso, G., Guzzardo, V., Fassina, A., Cordenonsi, M., Piccolo, S., 2014. YAP/TAZ incorporation in the β -catenin destruction complex orchestrates the Wnt response. *Cell* 158, 157–170. <https://doi.org/10.1016/j.cell.2014.06.013>
- Azzolin, L., Zanconato, F., Bresolin, S., Forcato, M., Basso, G., Bicciato, S., Cordenonsi, M., Piccolo, S., 2012. Role of TAZ as mediator of Wnt signaling. *Cell* 151, 1443–1456. <https://doi.org/10.1016/j.cell.2012.11.027>
- Baghban, R., Roshangar, L., Jahanban-Esfahlan, R., Seidi, K., Ebrahimi-Kalan, A., Jaymand, M., Kolahian, S., Javaheri, T., Zare, P., 2020. Tumor microenvironment complexity and therapeutic

- implications at a glance. *Cell Commun. Signal.* 18, 59. <https://doi.org/10.1186/s12964-020-0530-4>
- Batlle, E., Clevers, H., 2017. Cancer stem cells revisited. *Nat. Med.* 23, 1124–1134. <https://doi.org/10.1038/nm.4409>
- Beck, B., Blanpain, C., 2013. Unravelling cancer stem cell potential. *Nat. Rev. Cancer* 13, 727–738. <https://doi.org/10.1038/nrc3597>
- Bejarano, L., Jordão, M.J.C., Joyce, J.A., 2021. Therapeutic Targeting of the Tumor Microenvironment. *Cancer Discov.* 11, 933–959. <https://doi.org/10.1158/2159-8290.CD-20-1808>
- Bertillot, F., Miroshnikova, Y.A., Wickström, S.A., 2022. SnapShot: Mechanotransduction in the nucleus. *Cell* 185, 3638-3638.e1. <https://doi.org/10.1016/j.cell.2022.08.017>
- Beumer, J., Clevers, H., 2016. Regulation and plasticity of intestinal stem cells during homeostasis and regeneration. *Development* 143, 3639–3649. <https://doi.org/10.1242/dev.133132>
- Birsoy, K., Possemato, R., Lorbeer, F.K., Bayraktar, E.C., Thiru, P., Yucel, B., Wang, T., Chen, W.W., Clish, C.B., Sabatini, D.M., 2014. Metabolic determinants of cancer cell sensitivity to glucose limitation and biguanides. *Nature* 508, 108–112. <https://doi.org/10.1038/nature13110>
- Board, W.C. of T.E., 2019. Digestive System Tumours.
- Bogaert, J., Prenen, H., 2014. Molecular genetics of colorectal cancer. *Ann. Gastroenterol.* 27, 9–14.
- Bonne, G., Barletta, M.R.D., Varnous, S., Bécane, H.-M., Hammouda, E.-H., Merlini, L., Muntoni, F., Greenberg, C.R., Gary, F., Urtizberea, J.-A., Duboc, D., Fardeau, M., Toniolo, D., Schwartz, K., 1999. Mutations in the gene encoding lamin A/C cause autosomal dominant Emery-Dreifuss muscular dystrophy. *Nat. Genet.* 21, 285–288. <https://doi.org/10.1038/6799>
- Bouزيد, T., Kim, E., Riehl, B.D., Esfahani, A.M., Rosenbohm, J., Yang, R., Duan, B., Lim, J.Y., 2019. The LINC complex, mechanotransduction, and mesenchymal stem cell function and fate. *J. Biol. Eng.* 13, 68. <https://doi.org/10.1186/s13036-019-0197-9>
- Brangwynne, C.P., MacKintosh, F.C., Kumar, S., Geisse, N.A., Talbot, J., Mahadevan, L., Parker, K.K., Ingber, D.E., Weitz, D.A., 2006. Microtubules can bear enhanced compressive loads in living cells because of lateral reinforcement. *J. Cell Biol.* 173, 733–741. <https://doi.org/10.1083/jcb.200601060>
- Brauchle, E., Kasper, J., Daum, R., Schierbaum, N., Falch, C., Kirschniak, A., Schäffer, T.E., Schenke-Layland, K., 2018. Biomechanical and biomolecular characterization of extracellular matrix structures in human colon carcinomas. *Matrix Biol. J. Int. Soc. Matrix Biol.* 68–69, 180–193. <https://doi.org/10.1016/j.matbio.2018.03.016>
- Bristow, R.G., Hill, R.P., 2008. Hypoxia, DNA repair and genetic instability. *Nat. Rev. Cancer* 8, 180–192. <https://doi.org/10.1038/nrc2344>
- Brodere-Bondon, F., Ho-Bouldoires, T.H.N., Fernandez-Sanchez, M.E., Farge, E., 2018. Mechanotransduction in tumor progression: The dark side of the force. *J. Cell Biol.* 217. <https://doi.org/10.1083/jcb.201701039>
- Butcher, D.T., Alliston, T., Weaver, V.M., 2009. A tense situation: Forcing tumour progression. *Nat. Rev. Cancer* 9, 108–122. <https://doi.org/10.1038/nrc2544>
- Buxboim, A., Irianto, J., Swift, J., Athirasala, A., Shin, J.W., Rehfeldt, F., Discher, D.E., 2017. Coordinated increase of nuclear tension and lamin-A with matrix stiffness outcompetes lamin-B receptor

- that favors soft tissue phenotypes. *Mol. Biol. Cell* 28, 3333–3348. <https://doi.org/10.1091/mbc.E17-06-0393>
- Cairns, R.A., Harris, I.S., Mak, T.W., 2011. Regulation of cancer cell metabolism. *Nat. Rev. Cancer* 11, 85–95. <https://doi.org/10.1038/nrc2981>
- Cassetta, L., Pollard, J.W., 2018. Targeting macrophages: therapeutic approaches in cancer. *Nat. Rev. Drug Discov.* 17, 887–904. <https://doi.org/10.1038/nrd.2018.169>
- Chaffer, C.L., Weinberg, R.A., 2015. How does multistep tumorigenesis really proceed? *Cancer Discov.* 5, 22–24. <https://doi.org/10.1158/2159-8290.CD-14-0788>
- Chang, T.C., Yeh, C.T., Adebayo, B.O., Lin, Y.C., Deng, L., Rao, Y.K., Huang, C.C., Lee, W.H., Wu, A.T.H., Hsiao, M., Wu, C.H., Wang, L.S., Tzeng, Y.M., 2015. 4-Acetylanthroquinol B inhibits colorectal cancer tumorigenesis and suppresses cancer stem-like phenotype. *Toxicol. Appl. Pharmacol.* 288, 258–268. <https://doi.org/10.1016/j.taap.2015.07.025>
- Chen, X., Song, E., 2019. Turning foes to friends: targeting cancer-associated fibroblasts. *Nat. Rev. Drug Discov.* 18, 99–115. <https://doi.org/10.1038/s41573-018-0004-1>
- Chen, X., Wanggou, S., Bodalía, A., Zhu, M., Dong, W., Fan, J.J., Yin, W.C., Min, H.K., Hu, M., Draghici, D., Dou, W., Li, F., Coutinho, F.J., Whetstone, H., Kushida, M.M., Dirks, P.B., Song, Y., Hui, C. chung, Sun, Y., Wang, L.Y., Li, X., Huang, X., 2018. A Feedforward Mechanism Mediated by Mechanosensitive Ion Channel PIEZO1 and Tissue Mechanics Promotes Glioma Aggression. *Neuron* 100, 799-815.e7. <https://doi.org/10.1016/j.neuron.2018.09.046>
- Chen, X., Wei, B., Han, X., Zheng, Z., Huang, J., Liu, J., Huang, Y., Wei, H., 2014. LGR5 is required for the maintenance of spheroid-derived colon cancer stem cells. *Int. J. Mol. Med.* 34, 35–42. <https://doi.org/10.3892/ijmm.2014.1752>
- Cheng, G., Tse, J., Jain, R.K., Munn, L.L., 2009. Micro-Environmental Mechanical Stress Controls Tumor Spheroid Size and Morphology by Suppressing Proliferation and Inducing Apoptosis in Cancer Cells. *PLOS ONE* 4, e4632. <https://doi.org/10.1371/journal.pone.0004632>
- Cho, S., Vashisth, M., Abbas, A., Majkut, S., Vogel, K., Xia, Y., Ivanovska, I.L., Irianto, J., Tewari, M., Zhu, K., Tichy, E.D., Mourkioti, F., Tang, H.-Y., Greenberg, R.A., Prosser, B.L., Discher, D.E., 2019. Mechanosensing by the Lamina Protects against Nuclear Rupture, DNA Damage, and Cell-Cycle Arrest. *Dev. Cell* 49, 920-935.e5. <https://doi.org/10.1016/j.devcel.2019.04.020>
- Choi, Y.-K., Park, K.-G., 2018. Targeting Glutamine Metabolism for Cancer Treatment. *Biomol. Ther.* 26, 19–28. <https://doi.org/10.4062/biomolther.2017.178>
- Collins, A.T., Berry, P.A., Hyde, C., Stower, M.J., Maitland, N.J., 2005. Prospective Identification of Tumorigenic Prostate Cancer Stem Cells. *Cancer Res.* 65, 10946–10951. <https://doi.org/10.1158/0008-5472.CAN-05-2018>
- Cordenonsi, M., Zanconato, F., Azzolin, L., Forcato, M., Rosato, A., Frasson, C., Inui, M., Montagner, M., Parenti, A.R., Poletti, A., Daidone, M.G., Dupont, S., Basso, G., Bicciato, S., Piccolo, S., 2011. The Hippo Transducer TAZ Confers Cancer Stem Cell-Related Traits on Breast Cancer Cells. *Cell* 147, 759–772. <https://doi.org/10.1016/j.cell.2011.09.048>
- Coste, B., Mathur, J., Schmidt, M., Earley, T.J., Ranade, S., Petrus, M.J., Dubin, A.E., Patapoutian, A., 2010. Piezo1 and Piezo2 Are Essential Components of Distinct Mechanically Activated Cation Channels. *Science* 330, 55–60. <https://doi.org/10.1126/science.1193270>

- Dagogo-Jack, I., Shaw, A.T., 2018. Tumour heterogeneity and resistance to cancer therapies. *Nat. Rev. Clin. Oncol.* 15, 81–94. <https://doi.org/10.1038/nrclinonc.2017.166>
- Dahl, K.N., Engler, A.J., Pajerowski, J.D., Discher, D.E., 2005. Power-law rheology of isolated nuclei with deformation mapping of nuclear substructures. *Biophys. J.* 89, 2855–2864. <https://doi.org/10.1529/biophysj.105.062554>
- Dahl, K.N., Kahn, S.M., Wilson, K.L., Discher, D.E., 2004. The nuclear envelope lamina network has elasticity and a compressibility limit suggestive of a molecular shock absorber. *J. Cell Sci.* 117, 4779–4786. <https://doi.org/10.1242/jcs.01357>
- Dalerba, P., Dylla, S.J., Park, I.-K., Liu, R., Wang, X., Cho, R.W., Hoey, T., Gurney, A., Huang, E.H., Simeone, D.M., Shelton, A.A., Parmiani, G., Castelli, C., Clarke, M.F., 2007. Phenotypic characterization of human colorectal cancer stem cells. *Proc. Natl. Acad. Sci. U. S. A.* 104, 10158–10163. <https://doi.org/10.1073/pnas.0703478104>
- David, L., Martinez, L., Xi, Q., Kooshesh, K.A., Zhang, Y., Shah, J.V., Maas, R.L., Wu, H., 2023. Piezo mechanosensory channels regulate centrosome integrity and mitotic entry. *Proc. Natl. Acad. Sci.* 120, e2213846120. <https://doi.org/10.1073/pnas.2213846120>
- Davidson, P.M., Denais, C., Bakshi, M.C., Lammerding, J., 2014. Nuclear deformability constitutes a rate-limiting step during cell migration in 3-D environments. *Cell. Mol. Bioeng.* 7, 293–306. <https://doi.org/10.1007/s12195-014-0342-y>
- De Belly, H., Paluch, E.K., Chalut, K.J., 2022. Interplay between mechanics and signalling in regulating cell fate. *Nat. Rev. Mol. Cell Biol.* 23, 465–480. <https://doi.org/10.1038/s41580-022-00472-z>
- De Belly, H., Stubb, A., Yanagida, A., Labouesse, C., Jones, P.H., Paluch, E.K., Chalut, K.J., 2021. Membrane Tension Gates ERK-Mediated Regulation of Pluripotent Cell Fate. *Cell Stem Cell* 28, 273-284.e6. <https://doi.org/10.1016/j.stem.2020.10.018>
- De Sandre-Giovannoli, A., Bernard, R., Cau, P., Navarro, C., Amiel, J., Boccaccio, I., Lyonnet, S., Stewart, C.L., Munnich, A., Le Merrer, M., Lévy, N., 2003. Lamin A Truncation in Hutchinson-Gilford Progeria. *Science* 300, 2055–2055. <https://doi.org/10.1126/science.1084125>
- De Smedt, L., Lemahieu, J., Palmans, S., Govaere, O., Tousseyn, T., Van Cutsem, E., Prenen, H., Tejpar, S., Spaepen, M., Matthijs, G., Decaestecker, C., Moles Lopez, X., Demetter, P., Salmon, I., Sagaert, X., 2015. Microsatellite instable vs stable colon carcinomas: analysis of tumour heterogeneity, inflammation and angiogenesis. *Br. J. Cancer* 113, 500–509. <https://doi.org/10.1038/bjc.2015.213>
- De Vos, W.H., Houben, F., Kamps, M., Malhas, A., Verheyen, F., Cox, J., Manders, E.M.M., Verstraeten, V.L.R.M., van Steensel, M.A.M., Marcelis, C.L.M., van den Wijngaard, A., Vaux, D.J., Ramaekers, F.C.S., Broers, J.L.V., 2011. Repetitive disruptions of the nuclear envelope invoke temporary loss of cellular compartmentalization in laminopathies. *Hum. Mol. Genet.* 20, 4175–4186. <https://doi.org/10.1093/hmg/ddr344>
- Delarue, M., Joanny, J.-F., Jülicher, F., Prost, J., 2014a. Stress distributions and cell flows in a growing cell aggregate. *Interface Focus* 4, 20140033. <https://doi.org/10.1098/rsfs.2014.0033>
- Delarue, M., Montel, F., Vignjevic, D., Prost, J., Joanny, J.F., Cappello, G., 2014b. Compressive stress inhibits proliferation in tumor spheroids through a volume limitation. *Biophys. J.* 107, 1821–1828. <https://doi.org/10.1016/j.bpj.2014.08.031>

- Demou, Z.N., 2010. Gene Expression Profiles in 3D Tumor Analogs Indicate Compressive Strain Differentially Enhances Metastatic Potential. *Ann. Biomed. Eng.* 38, 3509–3520. <https://doi.org/10.1007/s10439-010-0097-0>
- Denais, C.M., Gilbert, R.M., Isermann, P., McGregor, A.L., Te Lindert, M., Weigel, B., Davidson, P.M., Friedl, P., Wolf, K., Lammerding, J., 2016. Nuclear envelope rupture and repair during cancer cell migration. *Science* 352, 353–358. <https://doi.org/10.1126/science.aad7297>
- DeNardo, D.G., Ruffell, B., 2019. Macrophages as regulators of tumor immunity and immunotherapy. *Nat. Rev. Immunol.* 19, 369–382. <https://doi.org/10.1038/s41577-019-0127-6>
- Desmaison, A., Frongia, C., Grenier, K., Ducommun, B., Lobjois, V., 2013. Mechanical Stress Impairs Mitosis Progression in Multi-Cellular Tumor Spheroids. *PLOS ONE* 8, e80447. <https://doi.org/10.1371/journal.pone.0080447>
- Diamantopoulou, Z., White, G., Fadlullah, M.Z.H., Dreger, M., Pickering, K., Maltas, J., Ashton, G., MacLeod, R., Baillie, G.S., Kouskoff, V., Lacaud, G., Murray, G.I., Sansom, O.J., Hurlstone, A.F.L., Malliri, A., 2017. TIAM1 Antagonizes TAZ/YAP Both in the Destruction Complex in the Cytoplasm and in the Nucleus to Inhibit Invasion of Intestinal Epithelial Cells. *Cancer Cell* 31, 621–634.e6. <https://doi.org/10.1016/j.ccell.2017.03.007>
- Dickinson, R.B., Katiyar, A., Dubell, C.R., Lele, T.P., 2022. Viscous shaping of the compliant cell nucleus. *APL Bioeng.* 6, 010901. <https://doi.org/10.1063/5.0071652>
- Diehn, M., Cho, R.W., Lobo, N.A., Kalisky, T., Dorie, M.J., Kulp, A.N., Qian, D., Lam, J.S., Ailles, L.E., Wong, M., Joshua, B., Kaplan, M.J., Wapnir, I., Dirbas, F., Somlo, G., Garberoglio, C., Paz, B., Shen, J., Lau, S.K., Quake, S.R., Brown, J.M., Weissman, I.L., Clarke, M.F., 2009. Association of Reactive Oxygen Species Levels and Radioresistance in Cancer Stem Cells. *Nature* 458, 780–783. <https://doi.org/10.1038/nature07733>
- Dieter, S.M., Ball, C.R., Hoffmann, C.M., Nowrouzi, A., Herbst, F., Zavidij, O., Abel, U., Arens, A., Weichert, W., Brand, K., Koch, M., Weitz, J., Schmidt, M., Von Kalle, C., Glimm, H., 2011. Distinct types of tumor-initiating cells form human colon cancer tumors and metastases. *Cell Stem Cell* 9, 357–365. <https://doi.org/10.1016/j.stem.2011.08.010>
- Discher, D.E., Janmey, P., Wang, Y.-L., 2005. Tissue cells feel and respond to the stiffness of their substrate. *Science* 310, 1139–43. <https://doi.org/10.1126/science.1116995>
- Diz-Muñoz, A., Fletcher, D.A., Weiner, O.D., 2013. Use the force: membrane tension as an organizer of cell shape and motility. *Trends Cell Biol.* 23, 47–53. <https://doi.org/10.1016/j.tcb.2012.09.006>
- Dolega, M.E., Delarue, M., Ingremeau, F., Prost, J., Delon, A., Cappello, G., 2017. Cell-like pressure sensors reveal increase of mechanical stress towards the core of multicellular spheroids under compression. *Nat. Commun.* 8, 1–9. <https://doi.org/10.1038/ncomms14056>
- Dolega, M.E., Monnier, S., Brunel, B., Joanny, J.F., Recho, P., Cappello, G., 2021. Extra-cellular matrix in multicellular aggregates acts as a pressure sensor controlling cell proliferation and motility. *eLife* 10. <https://doi.org/10.7554/ELIFE.63258>
- Dotse, E., Bian, Y., 2016. Isolation of colorectal cancer stem-like cells. *Cytotechnology* 68, 609–619. <https://doi.org/10.1007/s10616-014-9806-0>

- Doyle, A.D., Carvajal, N., Jin, A., Matsumoto, K., Yamada, K.M., 2015. Local 3D matrix microenvironment regulates cell migration through spatiotemporal dynamics of contractility-dependent adhesions. *Nat. Commun.* 6, 8720. <https://doi.org/10.1038/ncomms9720>
- Dupont, S., Wickström, S.A., 2022. Mechanical regulation of chromatin and transcription. *Nat. Rev. Genet.* 23, 624–643. <https://doi.org/10.1038/s41576-022-00493-6>
- Durinikova, E., Kozovska, Z., Poturnajova, M., Plava, J., Cierna, Z., Babelova, A., Bohovic, R., Schmidtova, S., Tomas, M., Kucerova, L., Matuskova, M., 2018. ALDH1A3 upregulation and spontaneous metastasis formation is associated with acquired chemoresistance in colorectal cancer cells. *BMC Cancer* 18, 1–15. <https://doi.org/10.1186/s12885-018-4758-y>
- Eagle, H., 1955. Nutrition Needs of Mammalian Cells in Tissue Culture. *Science* 122, 501–504. <https://doi.org/10.1126/science.122.3168.501>
- Elosegui-Artola, A., Andreu, I., Beedle, A.E.M., Lezamiz, A., Uroz, M., Kosmalska, A.J., Oria, R., Kechagia, J.Z., Rico-Lastres, P., Le Roux, A.L., Shanahan, C.M., Trepas, X., Navajas, D., Garcia-Manyes, S., Roca-Cusachs, P., 2017. Force Triggers YAP Nuclear Entry by Regulating Transport across Nuclear Pores. *Cell* 171, 1397–1410.e14. <https://doi.org/10.1016/j.cell.2017.10.008>
- Elosegui-Artola, A., Trepas, X., Roca-Cusachs, P., 2018. Control of Mechanotransduction by Molecular Clutch Dynamics. *Trends Cell Biol.* 28, 356–367. <https://doi.org/10.1016/j.tcb.2018.01.008>
- Fanfone, D., Wu, Z., Mammi, J., Berthenet, K., Neves, D., Weber, K., Halaburkova, A., Virard, F., Bunel, F., Jamard, C., Hernandez-Vargas, H., Tait, S.W., Hennino, A., Ichim, G., 2022. Confined migration promotes cancer metastasis through resistance to anoikis and increased invasiveness. *eLife* 11, e73150. <https://doi.org/10.7554/eLife.73150>
- Farahani, P.E., Lemke, S.B., Dine, E., Uribe, G., Toettcher, J.E., Nelson, C.M., 2021. Substratum stiffness regulates Erk signaling dynamics through receptor-level control. *Cell Rep.* 37. <https://doi.org/10.1016/j.celrep.2021.110181>
- Ferlay, J., Colombet, M., Soerjomataram, I., Parkin, D.M., Piñeros, M., Znaor, A., Bray, F., 2021. Cancer statistics for the year 2020: An overview. *Int. J. Cancer* 149, 778–789. <https://doi.org/10.1002/ijc.33588>
- Fernández-Sánchez, M.E., Barbier, S., Whitehead, J., Béalle, G., Michel, A., Latorre-Ossa, H., Rey, C., Fouassier, L., Claperon, A., Brullé, L., Girard, E., Servant, N., Rio-Frio, T., Marie, H., Lesieur, S., Housset, C., Gennisson, J.-L., Tanter, M., Ménager, C., Fre, S., Robine, S., Farge, E., 2015. Mechanical induction of the tumorigenic β -catenin pathway by tumour growth pressure. *Nature* 523, 92–95. <https://doi.org/10.1038/nature14329>
- Ferreira, L.P., Gaspar, V.M., Mano, J.F., 2020. Decellularized Extracellular Matrix for Bioengineering Physiometric 3D in Vitro Tumor Models. *Trends Biotechnol.* 38, 1397–1414. <https://doi.org/10.1016/j.tibtech.2020.04.006>
- Fleming, M., Ravula, S., Tatishchev, S.F., Wang, H.L., 2012. Colorectal carcinoma: Pathologic aspects. *J. Gastrointest. Oncol.* 3, 153–173. <https://doi.org/10.3978/j.issn.2078-6891.2012.030>
- Fogh, J., Fogh, J.M., Orfeo, T., 1977. One Hundred and Twenty-Seven Cultured Human Tumor Cell Lines Producing Tumors in Nude Mice²³. *JNCI J. Natl. Cancer Inst.* 59, 221–226. <https://doi.org/10.1093/jnci/59.1.221>

- Friedl, P., Wolf, K., Lammerding, J., 2011. Nuclear mechanics during cell migration. *Curr. Opin. Cell Biol.* 23, 55–64. <https://doi.org/10.1016/j.ceb.2010.10.015>
- Gheytanchi, E., Naseri, M., Karimi-Busheri, F., Atyabi, F., Mirsharif, E.S., Bozorgmehr, M., Ghods, R., Madjd, Z., 2021. Morphological and molecular characteristics of spheroid formation in HT-29 and Caco-2 colorectal cancer cell lines. *Cancer Cell Int.* 21, 1–16. <https://doi.org/10.1186/s12935-021-01898-9>
- Goldberg, M.W., Huttenlauch, I., Hutchison, C.J., Stick, R., 2008. Filaments made from A- and B-type lamins differ in structure and organization. *J. Cell Sci.* 121, 215–225. <https://doi.org/10.1242/jcs.022020>
- Goldman, R.D., Shumaker, D.K., Erdos, M.R., Eriksson, M., Goldman, A.E., Gordon, L.B., Gruenbaum, Y., Khuon, S., Mendez, M., Varga, R., Collins, F.S., 2004. Accumulation of mutant lamin A causes progressive changes in nuclear architecture in Hutchinson–Gilford progeria syndrome. *Proc. Natl. Acad. Sci.* 101, 8963–8968. <https://doi.org/10.1073/pnas.0402943101>
- Gordon-Weeks, A., Yuzhalin, A.E., 2020. Cancer Extracellular Matrix Proteins Regulate Tumour Immunity. *Cancers* 12, 3331. <https://doi.org/10.3390/cancers12113331>
- Gruenbaum, Y., Foisner, R., 2015. Lamins: Nuclear Intermediate Filament Proteins with Fundamental Functions in Nuclear Mechanics and Genome Regulation. *Annu. Rev. Biochem.* 84, 131–164. <https://doi.org/10.1146/annurev-biochem-060614-034115>
- Halfmann, C.T., Sears, R.M., Katiyar, A., Busselman, B.W., Aman, L.K., Zhang, Q., O’Bryan, C.S., Angelini, T.E., Lele, T.P., Roux, K.J., 2019. Repair of nuclear ruptures requires barrier-to-autointegration factor. *J. Cell Biol.* 218, 2136–2149. <https://doi.org/10.1083/jcb.201901116>
- Han, Y.L., Pegoraro, A.F., Li, H., Li, K., Yuan, Y., Xu, G., Gu, Z., Sun, J., Hao, Y., Gupta, S.K., Li, Y., Tang, W., Kang, H., Teng, L., Fredberg, J.J., Guo, M., 2019. Cell swelling, softening and invasion in a three-dimensional breast cancer model. *Nat. Phys.* <https://doi.org/10.1038/s41567-019-0680-8>
- Hanahan, D., 2022. Hallmarks of Cancer: New Dimensions. *Cancer Discov.* 12, 31–46. <https://doi.org/10.1158/2159-8290.CD-21-1059>
- Hanahan, D., Weinberg, R.A., 2011. Hallmarks of Cancer: The Next Generation. *Cell* 144, 646–674. <https://doi.org/10.1016/j.cell.2011.02.013>
- Hanahan, D., Weinberg, R.A., 2000. The Hallmarks of Cancer. *Cell* 100, 57–70. [https://doi.org/10.1016/S0092-8674\(00\)81683-9](https://doi.org/10.1016/S0092-8674(00)81683-9)
- Hatch, E.M., 2018. Nuclear envelope rupture: little holes, big openings. <https://doi.org/10.1016/j.ceb.2018.02.001>
- He, L., Si, G., Huang, J., Samuel, A.D.T., Perrimon, N., 2018. Mechanical regulation of stem-cell differentiation by the stretch-activated Piezo channel. *Nature* 555, 103–106. <https://doi.org/10.1038/nature25744>
- He, S., Zhou, H., Zhu, X., Hu, S., Fei, M., Wan, D., Gu, W., Yang, X., Shi, D., Zhou, Jian, Zhou, Jin, Zhu, Z., Wang, L., Li, D., Zhang, Y., 2014. Expression of Lgr5, a marker of intestinal stem cells, in colorectal cancer and its clinicopathological significance. *Biomed. Pharmacother.* 68, 507–513. <https://doi.org/10.1016/j.biopha.2014.03.016>

- Heinrich, M.A., Mostafa, A.M.R.H., Morton, J.P., Hawinkels, L.J.A.C., Prakash, J., 2021. Translating complexity and heterogeneity of pancreatic tumor: 3D in vitro to in vivo models. *Adv. Drug Deliv. Rev.* 174, 265–293. <https://doi.org/10.1016/j.addr.2021.04.018>
- Helmlinger, G., Netti, P.A., Lichtenbeld, H.C., Melder, R.J., Jain, R.K., 1997. Solid stress inhibits the growth of multicellular tumor spheroids. *Nat. Biotechnol.* 15, 778–783. <https://doi.org/10.1038/nbt0897-778>
- Hensley, C.T., Wasti, A.T., DeBerardinis, R.J., 2013. Glutamine and cancer: cell biology, physiology, and clinical opportunities. *J. Clin. Invest.* 123, 3678–3684. <https://doi.org/10.1172/JCI69600>
- Herrmann, H., Bär, H., Kreplak, L., Strelkov, S.V., Aebi, U., 2007. Intermediate filaments: from cell architecture to nanomechanics. *Nat. Rev. Mol. Cell Biol.* 8, 562–573. <https://doi.org/10.1038/nrm2197>
- Hershberger, R.E., Hedges, D.J., Morales, A., 2013. Dilated cardiomyopathy: the complexity of a diverse genetic architecture. *Nat. Rev. Cardiol.* 10, 531–547. <https://doi.org/10.1038/nrcardio.2013.105>
- Hinshaw, D.C., Shevde, L.A., 2019. The Tumor Microenvironment Innately Modulates Cancer Progression. *Cancer Res.* 79, 4557–4566. <https://doi.org/10.1158/0008-5472.CAN-18-3962>
- Holle, A.W., Govindan Kutty Devi, N., Clar, K., Fan, A., Saif, T., Kemkemer, R., Spatz, J.P., 2019. Cancer Cells Invade Confined Microchannels via a Self-Directed Mesenchymal-to-Amoeboid Transition. *Nano Lett.* 19, 2280–2290. <https://doi.org/10.1021/acs.nanolett.8b04720>
- Holle, A.W., Young, J.L., Spatz, J.P., 2016. In vitro cancer cell–ECM interactions inform in vivo cancer treatment. *Adv. Drug Deliv. Rev., Extracellular Matrix (ECM) and ECM-like materials: Therapeutic Tools and Targets in Cancer Treatment* 97, 270–279. <https://doi.org/10.1016/j.addr.2015.10.007>
- IARC, 2019. Colorectal Cancer Screening.
- Imajo, M., Ebisuya, M., Nishida, E., 2015. Dual role of YAP and TAZ in renewal of the intestinal epithelium. *Nat. Cell Biol.* 17, 7–19. <https://doi.org/10.1038/ncb3084>
- Ingber, D.E., 2005. Mechanical control of tissue growth: function follows form. *Proc. Natl. Acad. Sci. U. S. A.* 102, 11571–2. <https://doi.org/10.1073/pnas.0505939102>
- Irianto, J., Xia, Y., Pfeifer, C.R., Athirasala, A., Ji, J., Alvey, C., Tewari, M., Bennett, R.R., Harding, S.M., Liu, A.J., Greenberg, R.A., Discher, D.E., 2017. DNA Damage Follows Repair Factor Depletion and Portends Genome Variation in Cancer Cells after Pore Migration. *Curr. Biol.* 27, 210–223. <https://doi.org/10.1016/j.cub.2016.11.049>
- Jaalouk, D.E., Lammerding, J., 2009. Mechanotransduction gone awry. *Nat. Rev. Mol. Cell Biol.* 10, 63–73. <https://doi.org/10.1038/nrm2597>
- Jain, R.K., Martin, J.D., Stylianopoulos, T., 2014. The role of mechanical forces in tumor growth and therapy. *Annu. Rev. Biomed. Eng.* 16, 321–46. <https://doi.org/10.1146/annurev-bioeng-071813-105259>
- Kalli, M., Papageorgis, P., Gkretsi, V., Stylianopoulos, T., 2018. Solid Stress Facilitates Fibroblasts Activation to Promote Pancreatic Cancer Cell Migration. *Ann. Biomed. Eng.* 46, 657–669. <https://doi.org/10.1007/s10439-018-1997-7>

- Kalli, M., Stylianopoulos, T., 2018. Defining the Role of Solid Stress and Matrix Stiffness in Cancer Cell Proliferation and Metastasis. *Front. Oncol.* 8. <https://doi.org/10.3389/fonc.2018.00055>
- Kalluri, R., 2016. The biology and function of fibroblasts in cancer. *Nat. Rev. Cancer* 16, 582–598. <https://doi.org/10.1038/nrc.2016.73>
- Kalukula, Y., Stephens, A.D., Lammerding, J., Gabriele, S., 2022. Mechanics and functional consequences of nuclear deformations. *Nat. Rev. Mol. Cell Biol.* 23, 583–602. <https://doi.org/10.1038/s41580-022-00480-z>
- Karlsson, S., Nyström, H., 2022. The extracellular matrix in colorectal cancer and its metastatic settling – Alterations and biological implications. *Crit. Rev. Oncol. Hematol.* 175, 103712. <https://doi.org/10.1016/j.critrevonc.2022.103712>
- Kazama, S., Kishikawa, J., Kiyomatsu, T., Kawai, K., Nozawa, H., Ishihara, S., Watanabe, T., 2018. Expression of the stem cell marker CD133 is related to tumor development in colorectal carcinogenesis. *Asian J. Surg.* 41, 274–278. <https://doi.org/10.1016/j.asjsur.2016.12.002>
- Kechagia, J.Z., Ivaska, J., Roca-Cusachs, P., 2019. Integrins as biomechanical sensors of the microenvironment. *Nat. Rev. Mol. Cell Biol.* 20, 457–473. <https://doi.org/10.1038/s41580-019-0134-2>
- Khavari, A., Nydén, M., Weitz, D.A., Ehrlicher, A.J., 2016. Composite alginate gels for tunable cellular microenvironment mechanics. *Sci. Rep.* 6, 30854. <https://doi.org/10.1038/srep30854>
- Kim, M.-S., Ha, S.-E., Wu, M., Zogg, H., Ronkon, C.F., Lee, M.-Y., Ro, S., 2021. Extracellular Matrix Biomarkers in Colorectal Cancer. *Int. J. Mol. Sci.* 22, 9185. <https://doi.org/10.3390/ijms22179185>
- Kirkland, S.C., 2009. Type I collagen inhibits differentiation and promotes a stem cell-like phenotype in human colorectal carcinoma cells. *Br. J. Cancer* 101, 320–326. <https://doi.org/10.1038/sj.bjc.6605143>
- Kittur, H., Weaver, W., Di Carlo, D., 2014. Well-plate mechanical confinement platform for studies of mechanical mutagenesis. *Biomed. Microdevices* 16, 439–447. <https://doi.org/10.1007/s10544-014-9846-4>
- Kleinsmith, L.J., Pierce, G.B., 1964. MULTIPOTENTIALITY OF SINGLE EMBRYONAL CARCINOMA CELLS. *Cancer Res.* 24, 1544–1551.
- Kuga, T., Nie, H., Kazami, T., Satoh, M., Matsushita, K., Nomura, F., Maeshima, K., Nakayama, Y., Tomonaga, T., 2014. Lamin B2 prevents chromosome instability by ensuring proper mitotic chromosome segregation. *Oncogenesis* 3, e94. <https://doi.org/10.1038/oncsis.2014.6>
- Kumar, S., Weaver, V.M., 2009. Mechanics, malignancy, and metastasis: the force journey of a tumor cell. *Cancer Metastasis Rev.* 28, 113–27. <https://doi.org/10.1007/s10555-008-9173-4>
- Labernadie, A., Kato, T., Brugués, A., Serra-Picamal, X., Derzsi, S., Arwert, E., Weston, A., González-Tarragó, V., Elosegui-Artola, A., Albertazzi, L., Alcaraz, J., Roca-Cusachs, P., Sahai, E., Trepac, X., 2017. A mechanically active heterotypic E-cadherin/N-cadherin adhesion enables fibroblasts to drive cancer cell invasion. *Nat. Cell Biol.* 19, 224–237. <https://doi.org/10.1038/ncb3478>
- Lammerding, J., Engler, A.J., Kamm, R., 2022. Mechanobiology of the cell nucleus. *APL Bioeng.* 6, 040401. <https://doi.org/10.1063/5.0135299>

- Lammerding, J., Fong, L.G., Ji, J.Y., Reue, K., Stewart, C.L., Young, S.G., Lee, R.T., 2006. Lamins A and C but not lamin B1 regulate nuclear mechanics. *J. Biol. Chem.* 281, 25768–25780. <https://doi.org/10.1074/jbc.M513511200>
- Lammerding, J., Schulze, P.C., Takahashi, T., Kozlov, S., Sullivan, T., Kamm, R.D., Stewart, C.L., Lee, R.T., 2004. Lamin A/C deficiency causes defective nuclear mechanics and mechanotransduction. *J. Clin. Invest.* 113, 370–378. <https://doi.org/10.1172/JCI200419670>
- Lampi, M.C., Reinhart-King, C.A., 2018. Targeting extracellular matrix stiffness to attenuate disease: From molecular mechanisms to clinical trials. *Sci. Transl. Med.* 10, eaao0475. <https://doi.org/10.1126/scitranslmed.aa0475>
- Langer, E.M., Allen-Petersen, B.L., King, S.M., Kendsersky, N.D., Turnidge, M.A., Kuziel, G.M., Riggers, R., Samatham, R., Amery, T.S., Jacques, S.L., Sheppard, B.C., Korkola, J.E., Muschler, J.L., Thibault, G., Chang, Y.H., Gray, J.W., Presnell, S.C., Nguyen, D.G., Sears, R.C., 2019. Modeling Tumor Phenotypes In Vitro with Three-Dimensional Bioprinting. *Cell Rep.* 26, 608–623.e6. <https://doi.org/10.1016/j.celrep.2018.12.090>
- Lapidot, T., Sirard, C., Vormoor, J., Murdoch, B., Hoang, T., Caceres-Cortes, J., Minden, M., Paterson, B., Caligiuri, M.A., Dick, J.E., 1994. A cell initiating human acute myeloid leukaemia after transplantation into SCID mice. *Nature* 367, 645–648. <https://doi.org/10.1038/367645a0>
- Le Berre, M., Aubertin, J., Piel, M., 2012. Fine control of nuclear confinement identifies a threshold deformation leading to lamina rupture and induction of specific genes. *Integr. Biol. U. K.* 4, 1406–1414. <https://doi.org/10.1039/c2ib20056b>
- Le Berre, M., Zlotek-Zlotkiewicz, E., Bonazzi, D., Lautenschlaeger, F., Piel, M., 2014. Chapter 14 - Methods for Two-Dimensional Cell Confinement, in: Piel, M., Théry, M. (Eds.), *Methods in Cell Biology, Micropatterning in Cell Biology Part C*. Academic Press, pp. 213–229. <https://doi.org/10.1016/B978-0-12-800281-0.00014-2>
- Le, C.C., Bennisroune, A., Langlois, B., Salesse, S., Boulagnon-Rombi, C., Morjani, H., Dedieu, S., Appert-Collin, A., 2020. Functional Interplay Between Collagen Network and Cell Behavior Within Tumor Microenvironment in Colorectal Cancer. *Front. Oncol.* 10, 527. <https://doi.org/10.3389/fonc.2020.00527>
- Lee, S., Kumar, S., 2016. Actomyosin stress fiber mechanosensing in 2D and 3D. *F1000Research* 5, F1000 Faculty Rev-2261. <https://doi.org/10.12688/f1000research.8800.1>
- Lee, S.Y., Kim, K.A., Kim, C.H., Kim, Y.J., Lee, J.-H., Kim, H.R., 2017. CD44-shRNA recombinant adenovirus inhibits cell proliferation, invasion, and migration, and promotes apoptosis in HCT116 colon cancer cells. *Int. J. Oncol.* 50, 329–336. <https://doi.org/10.3892/ijo.2016.3801>
- LeSavage, B.L., Suhar, R.A., Broguiere, N., Lutolf, M.P., Heilshorn, S.C., 2021. Next-generation cancer organoids. *Nat. Mater.* <https://doi.org/10.1038/s41563-021-01057-5>
- Levayer, R., 2019. Solid stress, competition for space and cancer: The opposing roles of mechanical cell competition in tumour initiation and growth. *Semin. Cancer Biol.* 0–1. <https://doi.org/10.1016/j.semcancer.2019.05.004>
- Li, Jiao, Wang, Z., Chu, Q., Jiang, K., Li, Juan, Tang, N., 2018. The Strength of Mechanical Forces Determines the Differentiation of Alveolar Epithelial Cells. *Dev. Cell* 44, 297–312.e5. <https://doi.org/10.1016/j.devcel.2018.01.008>

- Li, Y., Xiao, B., Tu, S., Wang, Y., Zhang, X., 2012. Cultivation and identification of colon cancer stem cell-derived spheres from the Colo205 cell line. *Braz. J. Med. Biol. Res.* 45, 197–204. <https://doi.org/10.1590/S0100-879X2012007500015>
- Li, Z.-L., Wang, Z.-J., Wei, G.-H., Yang, Y., Wang, X.-W., 2020. Changes in extracellular matrix in different stages of colorectal cancer and their effects on proliferation of cancer cells. *World J. Gastrointest. Oncol.* 12, 267–275. <https://doi.org/10.4251/wjgo.v12.i3.267>
- Libutti, S.K., Tamarkin, L., Nilubol, N., 2018. Targeting the invincible barrier for drug delivery in solid cancers: interstitial fluid pressure. *Oncotarget* 9, 35723–35725. <https://doi.org/10.18632/oncotarget.26267>
- Liu, L., Yuan, W., Wang, J., 2010. Mechanisms for osteogenic differentiation of human mesenchymal stem cells induced by fluid shear stress. *Biomech. Model. Mechanobiol.* 9, 659–670. <https://doi.org/10.1007/s10237-010-0206-x>
- Liu, Y.J., Le Berre, M., Lautenschlaeger, F., Maiuri, P., Callan-Jones, A., Heuzé, M., Takaki, T., Voituriez, R., Piel, M., 2015. Confinement and low adhesion induce fast amoeboid migration of slow mesenchymal cells. *Cell* 160, 659–672. <https://doi.org/10.1016/j.cell.2015.01.007>
- Llado, V., Nakanishi, Y., Duran, A., Reina-Campos, M., Shelton, P.M., Linares, J.F., Yajima, T., Campos, A., Aza-Blanc, P., Leitges, M., Diaz-Meco, M.T., Moscat, J., 2015. Repression of Intestinal Stem Cell Function and Tumorigenesis through Direct Phosphorylation of β -Catenin and Yap by PKC ζ . *Cell Rep.* 10, 740–754. <https://doi.org/10.1016/j.celrep.2015.01.007>
- Lomakin, A.J., Cattin, C.J., Garcia-Arcos, J.M., Zhitnyak, I.Y., Driscoll, M.K., Welf, E.S., Petrie, R.J., Lennon-Duménil, A.M., Müller, D.J., 2020. The nucleus acts as a ruler tailoring cell responses to spatial constraints 2894. <https://doi.org/10.1101/863514>
- Long, J.T., Lammerding, J., 2021. Nuclear Deformation Lets Cells Gauge Their Physical Confinement. *Dev. Cell* 56, 156–158. <https://doi.org/10.1016/j.devcel.2021.01.002>
- Lotti, F., Jarrar, A.M., Pai, R.K., Hitomi, M., Lathia, J., Mace, A., Gantt, G.A., Sukhdeo, K., DeVecchio, J., Vasanji, A., Leahy, P., Hjelmeland, A.B., Kalady, M.F., Rich, J.N., 2013. Chemotherapy activates cancer-associated fibroblasts to maintain colorectal cancer-initiating cells by IL-17A. *J. Exp. Med.* 210, 2851–2872. <https://doi.org/10.1084/jem.20131195>
- Lu, V., Dahan, P., Ahsan, F.M., Patananan, A.N., Roy, I.J., Torres, A., Nguyen, R.M.T., Huang, D., Braas, D., Teitell, M.A., 2019. Mitochondrial metabolism and glutamine are essential for mesoderm differentiation of human pluripotent stem cells. *Cell Res.* 29, 596–598. <https://doi.org/10.1038/s41422-019-0191-2>
- Lu, V., Roy, I.J., Torres, A., Joly, J.H., Ahsan, F.M., Graham, N.A., Teitell, M.A., 2022. Glutamine-dependent signaling controls pluripotent stem cell fate. *Dev. Cell* 57, 610–623.e8. <https://doi.org/10.1016/j.devcel.2022.02.003>
- Lucio, A.A., Mongera, A., Shelton, E., Chen, R., Doyle, A.M., Campàs, O., 2017. Spatiotemporal variation of endogenous cell-generated stresses within 3D multicellular spheroids. *Sci. Rep.* 7. <https://doi.org/10.1038/s41598-017-12363-x>
- Lyssiotis, C.A., Kimmelman, A.C., 2017. Metabolic Interactions in the Tumor Microenvironment. *Trends Cell Biol., Special Issue: Cell Communication* 27, 863–875. <https://doi.org/10.1016/j.tcb.2017.06.003>

- Maclejowski, J., Hatch, E.M., 2020. Nuclear Membrane Rupture and Its Consequences. *Annu. Rev. Cell Dev. Biol.* 36, 85–114. <https://doi.org/10.1146/annurev-cellbio-020520-120627>
- Madl, C.M., Heilshorn, S.C., 2018. Engineering Hydrogel Microenvironments to Recapitulate the Stem Cell Niche. *Annu. Rev. Biomed. Eng.* 20, 21–47. <https://doi.org/10.1146/annurev-bioeng-062117-120954>
- Manhas, J., Bhattacharya, A., Agrawal, S.K., Gupta, B., Das, P., Deo, S.V.S., Pal, S., Sen, S., 2016. Characterization of cancer stem cells from different grades of human colorectal cancer. *Tumour Biol. J. Int. Soc. Oncodevelopmental Biol. Med.* 37, 14069–14081. <https://doi.org/10.1007/s13277-016-5232-6>
- Mani, S.A., Guo, W., Liao, M.-J., Eaton, E.N., Ayyanan, A., Zhou, A.Y., Brooks, M., Reinhard, F., Zhang, C.C., Shipitsin, M., Campbell, L.L., Polyak, K., Brisken, C., Yang, J., Weinberg, R.A., 2008. The epithelial-mesenchymal transition generates cells with properties of stem cells. *Cell* 133, 704–715. <https://doi.org/10.1016/j.cell.2008.03.027>
- Maniotis, A.J., Chen, C.S., Ingber, D.E., 1997. Demonstration of mechanical connections between integrins, cytoskeletal filaments, and nucleoplasm that stabilize nuclear structure. *Proc. Natl. Acad. Sci.* 94, 849–854. <https://doi.org/10.1073/pnas.94.3.849>
- Matsuda, A., Mofrad, M.R.K., 2022. On the nuclear pore complex and its emerging role in cellular mechanotransduction. *APL Bioeng.* 6, 011504. <https://doi.org/10.1063/5.0080480>
- Maurer, M., Lammerding, J., 2019. The Driving Force: Nuclear Mechanotransduction in Cellular Function, Fate, and Disease. *Annu. Rev. Biomed. Eng.* 21, 443–468. <https://doi.org/10.1146/annurev-bioeng-060418-052139>
- McIntyre, A., Harris, A.L., 2015. Metabolic and hypoxic adaptation to anti-angiogenic therapy: a target for induced essentiality. *EMBO Mol. Med.* 7, 368–379. <https://doi.org/10.15252/emmm.201404271>
- Meacham, C.E., Morrison, S.J., 2013. Tumour heterogeneity and cancer cell plasticity. *Nature* 501, 328–337. <https://doi.org/10.1038/nature12624>
- Mendez, M.G., Janmey, P.A., 2012. Transcription factor regulation by mechanical stress. *Int. J. Biochem. Cell Biol.* 44, 728–732. <https://doi.org/10.1016/j.biocel.2012.02.003>
- Meran, L., Baulies, A., Li, V.S.W., 2017. Intestinal Stem Cell Niche: The Extracellular Matrix and Cellular Components. *Stem Cells Int.* 2017, e7970385. <https://doi.org/10.1155/2017/7970385>
- Meriem, Z.B., Mateo, T., Faccini, J., Denais, C., Dusfour-Castan, R., Guynet, C., Merle, T., Suzanne, M., Di-Luoffo, M., Guillermet-Guibert, J., Alric, B., Landiech, S., Malaquin, L., Mesnilgrete, F., Laborde, A., Mazenq, L., Courson, R., Delarue, M., 2023. An easy-to-use microfluidic mechano-chemostat for tissues and organisms reveals that confined growth is accompanied with increased macromolecular crowding. <https://doi.org/10.1101/2023.03.29.534752>
- Millard, M., Yakavets, I., Zorin, V., Kulmukhamedova, A., Marchal, S., Bezdetsnaya, L., 2017. Drug delivery to solid tumors: the predictive value of the multicellular tumor spheroid model for nanomedicine screening. *Int. J. Nanomedicine* 12, 7993–8007. <https://doi.org/10.2147/IJN.S146927>
- Mirzaei, H., Salehi, H., Sahebkar, A., Avan, A., Jaafari, M.R., Namdar, A., Rezaei, A., Mirzaei, H.R., 2016. Deciphering biological characteristics of tumorigenic subpopulations in human colorectal

- cancer reveals cellular plasticity. *J. Res. Med. Sci.* 21, 64. <https://doi.org/10.4103/1735-1995.187355>
- Mohan, V., Das, A., Sagi, I., 2020. Emerging roles of ECM remodeling processes in cancer. *Semin. Cancer Biol.*, Translating Extracellular Matrix 62, 192–200. <https://doi.org/10.1016/j.semcancer.2019.09.004>
- Mollica, P.A., Booth-Creech, E.N., Reid, J.A., Zamponi, M., Sullivan, S.M., Palmer, X.-L., Sachs, P.C., Bruno, R.D., 2019. 3D bioprinted mammary organoids and tumoroids in human mammary derived ECM hydrogels. *Acta Biomater.*, Biomaterials for Cell Manufacturing and Tissue Biofabrication 95, 201–213. <https://doi.org/10.1016/j.actbio.2019.06.017>
- Montel, F., Delarue, M., Elgeti, J., Vignjevic, D., Cappello, G., Prost, J., 2012. Isotropic stress reduces cell proliferation in tumor spheroids. *New J. Phys.* 14, 055008. <https://doi.org/10.1088/1367-2630/14/5/055008>
- Muchir, A., Medioni, J., Laluc, M., Massart, C., Arimura, T., Kooi, A.J.V.D., Desguerre, I., Mayer, M., Ferrer, X., Briault, S., Hirano, M., Worman, H.J., Mallet, A., Wehnert, M., Schwartz, K., Bonne, G., 2004. Nuclear envelope alterations in fibroblasts from patients with muscular dystrophy, cardiomyopathy, and partial lipodystrophy carrying lamin A/C gene mutations. *Muscle Nerve* 30, 444–450. <https://doi.org/10.1002/mus.20122>
- Munro, M.J., Wickremesekera, S.K., Peng, L., Tan, S.T., Itinteang, T., 2018. Cancer stem cells in colorectal cancer: a review. *J. Clin. Pathol.* 71, 110–116. <https://doi.org/10.1136/jclinpath-2017-204739>
- Nader, G.P. de F., Agüera-Gonzalez, S., Routet, F., Gratia, M., Maurin, M., Cancila, V., Cadart, C., Palamidessi, A., Ramos, R.N., San Roman, M., Gentili, M., Yamada, A., Williard, A., Lodillinsky, C., Lagoutte, E., Villard, C., Viovy, J.-L., Tripodo, C., Galon, J., Scita, G., Manel, N., Chavrier, P., Piel, M., 2021. Compromised nuclear envelope integrity drives TREX1-dependent DNA damage and tumor cell invasion. *Cell* 1–17. <https://doi.org/10.1016/j.cell.2021.08.035>
- Nagare, R.P., Sneha, S., Priya, S.K., Ganesan, T.S., 2016. Cancer Stem Cells – Are Surface Markers Alone Sufficient? *Curr. Stem Cell Res. Ther.* 12, 37–44.
- Nallanthighal, S., Heiserman, J.P., Cheon, D.-J., 2019. The Role of the Extracellular Matrix in Cancer Stemness. *Front. Cell Dev. Biol.* 7.
- Nam, S., Gupta, V.K., Lee, H., Lee, J.Y., Wisdom, K.M., Varma, S., Flaum, E.M., Davis, C., West, R.B., Chaudhuri, O., 2019. Cell cycle progression in confining microenvironments is regulated by a growth-responsive TRPV4-PI3K/Akt-p27Kip1 signaling axis. *Sci. Adv.* 5, eaaw6171. <https://doi.org/10.1126/sciadv.aaw6171>
- Nassar, D., Blanpain, C., 2016. Cancer Stem Cells: Basic Concepts and Therapeutic Implications. *Annu. Rev. Pathol.* 11, 47–76. <https://doi.org/10.1146/annurev-pathol-012615-044438>
- Nath, S., Devi, G.R., 2016. Three-dimensional culture systems in cancer research: Focus on tumor spheroid model. *Pharmacol. Ther.* 163, 94–108. <https://doi.org/10.1016/j.pharmthera.2016.03.013>
- Nava, M.M., Miroshnikova, Y.A., Biggs, L.C., Whitefield, D.B., Metge, F., Boucas, J., Vihinen, H., Jokitalo, E., Li, X., García Arcos, J.M., Hoffmann, B., Merkel, R., Niessen, C.M., Dahl, K.N., Wickström,

- S.A., 2020. Heterochromatin-Driven Nuclear Softening Protects the Genome against Mechanical Stress-Induced Damage. *Cell* 1–18. <https://doi.org/10.1016/j.cell.2020.03.052>
- ND, M., RA, W., CL, C., 2013. Cell plasticity and heterogeneity in cancer. *Clin. Chem.* 59, 168–179. <https://doi.org/10.1373/CLINCHEM.2012.184655>
- Nelson, C.M., Jean, R.P., Tan, J.L., Liu, W.F., Sniadecki, N.J., Spector, A.A., Chen, C.S., 2005. Emergent patterns of growth controlled by multicellular form and mechanics. *Proc. Natl. Acad. Sci. U. S. A.* 102, 11594–9. <https://doi.org/10.1073/pnas.0502575102>
- Nguyen, T.-L., Durán, R.V., 2018. Glutamine metabolism in cancer therapy. *Cancer Drug Resist.* <https://doi.org/10.20517/cdr.2018.08>
- Nia, H.T., Liu, H., Seano, G., Datta, M., Jones, D., Rahbari, N., Incio, J., Chauhan, V.P., Jung, K., Martin, J.D., Askoxylakis, V., Padera, T.P., Fukumura, D., Boucher, Y., Hornicek, F.J., Grodzinsky, A.J., Baish, J.W., Munn, L.L., Jain, R.K., 2017. Solid stress and elastic energy as measures of tumour mechanopathology. *Nat. Biomed. Eng.* 1, 1–11. <https://doi.org/10.1038/s41551-016-0004>
- Northcott, J.M., Dean, I.S., Mouw, J.K., Weaver, V.M., 2018. Feeling Stress: The Mechanics of Cancer Progression and Aggression. *Front. Cell Dev. Biol.* 6. <https://doi.org/10.3389/fcell.2018.00017>
- Northey, J.J., Przybyla, L., Weaver, V.M., 2017. Tissue Force Programs Cell Fate and Tumor Aggression. *Cancer Discov.* 7, 1224–1237. <https://doi.org/10.1158/2159-8290.CD-16-0733>
- Nowell, C.S., Odermatt, P.D., Azzolin, L., Hohnel, S., Wagner, E.F., Fantner, G.E., Lutolf, M.P., Barrandon, Y., Piccolo, S., Radtke, F., 2016. Chronic inflammation imposes aberrant cell fate in regenerating epithelia through mechanotransduction. *Nat. Cell Biol.* 18, 168–180. <https://doi.org/10.1038/ncb3290>
- Oudhoff, M.J., Braam, M.J.S., Freeman, S.A., Wong, D., Rattray, D.G., Wang, J., Antignano, F., Snyder, K., Refaeli, I., Hughes, M.R., McNagny, K.M., Gold, M.R., Arrowsmith, C.H., Sato, T., Rossi, F.M.V., Tatlock, J.H., Owen, D.R., Brown, P.J., Zaph, C., 2016. SETD7 Controls Intestinal Regeneration and Tumorigenesis by Regulating Wnt/ β -Catenin and Hippo/YAP Signaling. *Dev. Cell* 37, 47–57. <https://doi.org/10.1016/j.devcel.2016.03.002>
- Pajeroski, J.D., Dahl, K.N., Zhong, F.L., Sammak, P.J., Discher, D.E., 2007. Physical plasticity of the nucleus in stem cell differentiation. *Proc. Natl. Acad. Sci.* 104, 15619–15624. <https://doi.org/10.1073/pnas.0702576104>
- Pampaloni, F., Reynaud, E.G., Stelzer, E.H.K., 2007. The third dimension bridges the gap between cell culture and live tissue. *Nat. Rev. Mol. Cell Biol.* 8, 839–845. <https://doi.org/10.1038/nrm2236>
- Pan, T., Xu, J., Zhu, Y., 2017. Self-renewal molecular mechanisms of colorectal cancer stem cells. *Int. J. Mol. Med.* 39, 9–20. <https://doi.org/10.3892/ijmm.2016.2815>
- Panciera, T., Azzolin, L., Cordenonsi, M., Piccolo, S., 2017. Mechanobiology of YAP and TAZ in physiology and disease. *Nat. Rev. Mol. Cell Biol.* 18, 758–770. <https://doi.org/10.1038/nrm.2017.87>
- Patil, S., Sengupta, K., 2021. Role of A- and B-type lamins in nuclear structure–function relationships. *Biol. Cell* 113, 295–310. <https://doi.org/10.1111/boc.202000160>
- Patteson, A.E., Vahabikashi, A., Pogoda, K., Adam, S.A., Mandal, K., Kittisopikul, M., Sivagurunathan, S., Goldman, A., Goldman, R.D., Janmey, P.A., 2019. Vimentin protects cells against nuclear rupture and DNA damage during migration. <https://doi.org/10.1083/jcb.201902046>

- Pavlova, N.N., Zhu, J., Thompson, C.B., 2022. The hallmarks of cancer metabolism: Still emerging. *Cell Metab.* 34, 355–377. <https://doi.org/10.1016/j.cmet.2022.01.007>
- Pfeifer, C.R., Xia, Y., Zhu, K., Liu, D., Irianto, J., Morales García, V.M., Santiago Millán, L.M., Niese, B., Harding, S., Deviri, D., Greenberg, R.A., Discher, D.E., 2018. Constricted migration increases DNA damage and independently represses cell cycle. *Mol. Biol. Cell* 29, 1948–1962. <https://doi.org/10.1091/mbc.E18-02-0079>
- Phipps, S., Yang, T.H.J., Habib, F.K., Reuben, R.L., McNeill, S.A., 2005. Measurement of tissue mechanical characteristics to distinguish between benign and malignant prostatic disease. *Urology* 66, 447–450. <https://doi.org/10.1016/j.urology.2005.03.017>
- Polyak, K., Weinberg, R.A., 2009. Transitions between epithelial and mesenchymal states: acquisition of malignant and stem cell traits. *Nat. Rev. Cancer* 9, 265–273. <https://doi.org/10.1038/nrc2620>
- Provenzano, P.P., Inman, D.R., Eliceiri, K.W., Keely, P.J., 2009. Matrix density-induced mechanoregulation of breast cell phenotype, signaling and gene expression through a FAK–ERK linkage. *Oncogene* 28, 4326–4343. <https://doi.org/10.1038/onc.2009.299>
- Prunet, A., 2020. Développement de système pour l'étude de l'impact des contraintes mécaniques sur le comportement de cellules cancéreuses (phdthesis). Université de Lyon.
- Prunet, A., Lefort, S., Delanoë-Ayari, H., Laperrousaz, B., Simon, G., Barentin, C., Saci, S., Argoul, F., Guyot, B., Rieu, J.P., Gobert, S., Maguer-Satta, V., Rivière, C., 2020. A new agarose-based microsystem to investigate cell response to prolonged confinement. *Lab. Chip* 20, 4016–4030. <https://doi.org/10.1039/d0lc00732c>
- Qian, C.-N., Tan, M.-H., Yang, J.-P., Cao, Y., 2016. Revisiting tumor angiogenesis: vessel co-option, vessel remodeling, and cancer cell-derived vasculature formation. *Chin. J. Cancer* 35, 10. <https://doi.org/10.1186/s40880-015-0070-2>
- Qin, Y., Rodin, S., Simonson, O.E., Hollande, F., 2017. Laminins and cancer stem cells: Partners in crime? *Semin. Cancer Biol.*, Novel molecular adaptation in cancer treatment and diagnostics 45, 3–12. <https://doi.org/10.1016/j.semcancer.2016.07.004>
- Raab, M., Gentili, M., De Belly, H., Thiam, H.R., Vargas, P., Jimenez, A.J., Lautenschlaeger, F., Voituriez, R., Lennon-Duménil, A.M., Manel, N., Piel, M., 2016. ESCRT III repairs nuclear envelope ruptures during cell migration to limit DNA damage and cell death. *Science* 352, 359–362. <https://doi.org/10.1126/science.aad7611>
- Randolph, G.J., Ivanov, S., Zinselmeyer, B.H., Scallan, J.P., 2017. The Lymphatic System: Integral Roles in Immunity. *Annu. Rev. Immunol.* 35, 31–52. <https://doi.org/10.1146/annurev-immunol-041015-055354>
- Rivière, C., Marion, S., Guillén, N., Bacri, J.-C., Gazeau, F., Wilhelm, C., 2007. Signaling through the phosphatidylinositol 3-kinase regulates mechanotaxis induced by local low magnetic forces in *Entamoeba histolytica*. *J. Biomech.* 40, 64–77. <https://doi.org/10.1016/j.jbiomech.2005.11.012>
- Rodrigues, J., Heinrich, M.A., Teixeira, L.M., Prakash, J., 2021. 3D In Vitro Model (R)evolution: Unveiling Tumor–Stroma Interactions. *Trends Cancer* 7, 249–264. <https://doi.org/10.1016/j.trecan.2020.10.009>

- Roose, T., Netti, P.A., Munn, L.L., Boucher, Y., Jain, R.K., 2003. Solid stress generated by spheroid growth estimated using a linear poroelasticity model☆. *Microvasc. Res.* 66, 204–212. [https://doi.org/10.1016/S0026-2862\(03\)00057-8](https://doi.org/10.1016/S0026-2862(03)00057-8)
- Rowat, A.C., Lammerding, J., Herrmann, H., Aebi, U., 2008. Towards an integrated understanding of the structure and mechanics of the cell nucleus. *BioEssays* 30, 226–236. <https://doi.org/10.1002/bies.20720>
- Segel, M., Neumann, B., Hill, M.F.E., Weber, I.P., Viscomi, C., Zhao, C., Young, A., Agle, C.C., Thompson, A.J., Gonzalez, G.A., Sharma, A., Holmqvist, S., Rowitch, D.H., Franze, K., Franklin, R.J.M., Chalut, K.J., 2019. Niche stiffness underlies the ageing of central nervous system progenitor cells. *Nature* 573, 130–134. <https://doi.org/10.1038/s41586-019-1484-9>
- Semenza, G.L., 2009. Regulation of cancer cell metabolism by hypoxia-inducible factor 1. *Semin. Cancer Biol., The Warburg Effect: The Re-discovery of the Importance of Aerobic Glycolysis in Tumor Cells* 19, 12–16. <https://doi.org/10.1016/j.semcancer.2008.11.009>
- Semenza, G.L., Artemov, D., Bedi, A., Bhujwala, Z., Chiles, K., Feldser, D., Laughner, E., Ravi, R., Simons, J., Taghavi, P., Zhong, H., 2001. “The metabolism of tumours”: 70 years later. *Novartis Found. Symp.* 240, 251–260; discussion 260–264.
- Shah, P., Hobson, C.M., Cheng, S., Colville, M.J., Paszek, M.J., Superfine, R., Lammerding, J., 2020. Nuclear Deformation Causes DNA Damage by Increasing Replication Stress. *Curr. Biol.* 1–13. <https://doi.org/10.1016/j.cub.2020.11.037>
- Shaheen, S., Ahmed, M., Lorenzi, F., Nateri, A.S., 2016. Spheroid-Formation (Colonsphere) Assay for in Vitro Assessment and Expansion of Stem Cells in Colon Cancer. *Stem Cell Rev. Rep.* 12, 492–499. <https://doi.org/10.1007/s12015-016-9664-6>
- Shen, Z., Lengyel, M., Niethammer, P., 2022. The yellow brick road to nuclear membrane mechanotransduction. *APL Bioeng.* 6, 021501. <https://doi.org/10.1063/5.0080371>
- Shields, J.D., Borsetti, M., Rigby, H., Harper, S.J., Mortimer, P.S., Levick, J.R., Orlando, A., Bates, D.O., 2004. Lymphatic density and metastatic spread in human malignant melanoma. *Br. J. Cancer* 90, 693–700. <https://doi.org/10.1038/sj.bjc.6601571>
- Shimokawa, M., Ohta, Y., Nishikori, S., Matano, M., Takano, A., Fujii, M., Date, S., Sugimoto, S., Kanai, T., Sato, T., 2017. Visualization and targeting of LGR5 + human colon cancer stem cells. *Nature* 545, 187–192. <https://doi.org/10.1038/nature22081>
- Shivashankar, G.V., 2011. Mechanosignaling to the Cell Nucleus and Gene Regulation. *Annu. Rev. Biophys.* 40, 361–378. <https://doi.org/10.1146/annurev-biophys-042910-155319>
- Sica, A., Larghi, P., Mancino, A., Rubino, L., Porta, C., Totaro, M.G., Rimoldi, M., Biswas, S.K., Allavena, P., Mantovani, A., 2008. Macrophage polarization in tumour progression. *Semin. Cancer Biol., The Role of the Microenvironment in Tumor Biology* 18, 349–355. <https://doi.org/10.1016/j.semcancer.2008.03.004>
- Singh, B., Tai, K., Madan, S., Raythatha, M.R., Cady, A.M., Braunlin, M., Irving, L.R., Bajaj, A., Lucci, A., 2012. Selection of Metastatic Breast Cancer Cells Based on Adaptability of Their Metabolic State. *PLOS ONE* 7, e36510. <https://doi.org/10.1371/journal.pone.0036510>
- Singh, S.K., Clarke, I.D., Terasaki, M., Bonn, V.E., Hawkins, C., Squire, J., Dirks, P.B., 2003. Identification of a cancer stem cell in human brain tumors. *Cancer Res.* 63, 5821–5828.

- Sitarska, E., Diz-Muñoz, A., 2020. Pay attention to membrane tension: Mechanobiology of the cell surface. *Curr. Opin. Cell Biol., Cell Dynamics* 66, 11–18. <https://doi.org/10.1016/j.ceb.2020.04.001>
- Somech, R., Shaklai, S., Amariglio, N., Rechavi, G., Simon, A.J., 2005. Nuclear Envelopathies—Raising the Nuclear Veil. *Pediatr. Res.* 57, 8–15. <https://doi.org/10.1203/01.PDR.0000159566.54287.6C>
- Spaderna, S., Schmalhofer, O., Hlubek, F., Berx, G., Eger, A., Merkel, S., Jung, A., Kirchner, T., Brabletz, T., 2006. A Transient, EMT-Linked Loss of Basement Membranes Indicates Metastasis and Poor Survival in Colorectal Cancer. *Gastroenterology* 131, 830–840. <https://doi.org/10.1053/j.gastro.2006.06.016>
- Srivastava, N., Nader, G.P. de F., Williard, A., Rollin, R., Cuvelier, D., Lomakin, A., Piel, M., 2021. Nuclear fragility, blaming the blebs. *Curr. Opin. Cell Biol., Cell Nucleus* 70, 100–108. <https://doi.org/10.1016/j.ceb.2021.01.007>
- Srivastava, N., Traynor, D., Piel, M., Kabla, A.J., Kay, R.R., 2020. Pressure sensing through Piezo channels controls whether cells migrate with blebs or pseudopods. *Proc. Natl. Acad. Sci.* 117, 2506–2512. <https://doi.org/10.1073/pnas.1905730117>
- Stephens, A.D., Banigan, E.J., Adam, S.A., Goldman, R.D., Marko, J.F., 2017. Chromatin and lamin a determine two different mechanical response regimes of the cell nucleus. *Mol. Biol. Cell* 28, 1984–1996. <https://doi.org/10.1091/mbc.E16-09-0653>
- Stephens, A.D., Liu, P.Z., Kandula, V., Chen, H., Almassalha, L.M., Herman, C., Backman, V., O’Halloran, T., Adam, S.A., Goldman, R.D., Banigan, E.J., Marko, J.F., 2019. Physicochemical mechanotransduction alters nuclear shape and mechanics via heterochromatin formation. *Mol. Biol. Cell* 30, 2320–2330. <https://doi.org/10.1091/mbc.E19-05-0286>
- Stewart, C.L., Roux, K.J., Burke, B., 2007. Blurring the Boundary: The Nuclear Envelope Extends Its Reach. *Science* 318, 1408–1412. <https://doi.org/10.1126/science.1142034>
- Stylianopoulos, T., Martin, J.D., Chauhan, V.P., Jain, S.R., Diop-Frimpong, B., Bardeesy, N., Smith, B.L., Ferrone, C.R., Hornicek, F.J., Boucher, Y., Munn, L.L., Jain, R.K., 2012. Causes, consequences, and remedies for growth-induced solid stress in murine and human tumors. *Proc. Natl. Acad. Sci. U. S. A.* 109, 15101–8. <https://doi.org/10.1073/pnas.1213353109>
- Stylianopoulos, T., Martin, J.D., Snuderl, M., Mpekris, F., Jain, S.R., Jain, R.K., 2013. Coevolution of solid stress and interstitial fluid pressure in tumors during progression: implications for vascular collapse. *Cancer Res.* 73, 3833–41. <https://doi.org/10.1158/0008-5472.CAN-12-4521>
- Stylianopoulos, T., Munn, L.L., Jain, R.K., 2018. Reengineering the Physical Microenvironment of Tumors to Improve Drug Delivery and Efficacy: From Mathematical Modeling to Bench to Bedside. *Trends Cancer* 4, 292–319. <https://doi.org/10.1016/j.trecan.2018.02.005>
- Sun, J., Chen, J., Mohagheghian, E., Wang, N., 2020. Force-induced gene up-regulation does not follow the weak power law but depends on H3K9 demethylation. *Sci. Adv.* 6, eaay9095. <https://doi.org/10.1126/sciadv.aay9095>
- Swift, J., Ivanovska, I.L., Buxboim, A., Harada, T., Dingal, P.C.D.P., Pinter, J., Pajerowski, J.D., Spinler, K.R., Shin, J.-W., Tewari, M., Rehfeldt, F., Speicher, D.W., Discher, D.E., 2013. Nuclear Lamin-A

- Scales with Tissue Stiffness and Enhances Matrix-Directed Differentiation. *Science* 341, 1240104. <https://doi.org/10.1126/science.1240104>
- Takahashi, K., Yamanaka, S., 2006. Induction of Pluripotent Stem Cells from Mouse Embryonic and Adult Fibroblast Cultures by Defined Factors. *Cell* 126, 663–676. <https://doi.org/10.1016/j.cell.2006.07.024>
- Teller, I.C., Beaulieu, J.F., 2001. Interactions between laminin and epithelial cells in intestinal health and disease. *Expert Rev. Mol. Med.* 3, 1–18. <https://doi.org/10.1017/S1462399401003623>
- Terenna, C.R., Makushok, T., Velve-Casquillas, G., Baigl, D., Chen, Y., Bornens, M., Paoletti, A., Piel, M., Tran, P.T., 2008. Physical mechanisms redirecting cell polarity and cell shape. *Curr. Biol.* CB 18, 1748. <https://doi.org/10.1016/j.cub.2008.09.047>
- Thiery, J.P., Acloque, H., Huang, R.Y.J., Nieto, M.A., 2009. Epithelial-Mesenchymal Transitions in Development and Disease. *Cell* 139, 871–890. <https://doi.org/10.1016/j.cell.2009.11.007>
- Todaro, M., Francipane, M.G., Medema, J.P., Stassi, G., 2010. Colon Cancer Stem Cells: Promise of Targeted Therapy. *Gastroenterology* 138, 2151–2162. <https://doi.org/10.1053/j.gastro.2009.12.063>
- Toepke, M.W., Beebe, D.J., 2006. PDMS absorption of small molecules and consequences in microfluidic applications. *Lab. Chip* 6, 1484–1486. <https://doi.org/10.1039/B612140C>
- Totaro, A., Castellan, M., Battilana, G., Zanconato, F., Azzolin, L., Giulitti, S., Cordenonsi, M., Piccolo, S., 2017. YAP/TAZ link cell mechanics to Notch signalling to control epidermal stem cell fate. *Nat. Commun.* 8, 15206. <https://doi.org/10.1038/ncomms15206>
- Totaro, A., Panciera, T., Piccolo, S., 2018. YAP/TAZ upstream signals and downstream responses. *Nat. Cell Biol.* 20, 888–899. <https://doi.org/10.1038/s41556-018-0142-z>
- Tse, J.M., Cheng, G., Tyrrell, J.A., Wilcox-Adelman, S.A., Boucher, Y., Jain, R.K., Munn, L.L., 2012. Mechanical compression drives cancer cells toward invasive phenotype. *Proc. Natl. Acad. Sci.* 109, 911–916. <https://doi.org/10.1073/pnas.1118910109>
- Turgay, Y., Eibauer, M., Goldman, A.E., Shimi, T., Khayat, M., Ben-Harush, K., Dubrovsky-Gaupp, A., Sapra, K.T., Goldman, R.D., Medalia, O., 2017. The molecular architecture of lamins in somatic cells. *Nature* 543, 261–264. <https://doi.org/10.1038/nature21382>
- Uhler, C., Shivashankar, G.V., 2018. Nuclear Mechanopathology and Cancer Diagnosis. *Trends Cancer* 4, 320–331. <https://doi.org/10.1016/j.trecan.2018.02.009>
- Vahabikashi, A., Adam, S.A., Medalia, O., Goldman, R.D., 2022. Nuclear lamins: Structure and function in mechanobiology. *APL Bioeng.* 6, 011503. <https://doi.org/10.1063/5.0082656>
- van Meer, B.J., de Vries, H., Firth, K.S.A., van Weerd, J., Tertoolen, L.G.J., Karperien, H.B.J., Jonkheijm, P., Denning, C., IJzerman, A.P., Mummery, C.L., 2017. Small molecule absorption by PDMS in the context of drug response bioassays. *Biochem. Biophys. Res. Commun.* 482, 323–328. <https://doi.org/10.1016/j.bbrc.2016.11.062>
- Vara, J.Á.F., Casado, E., de Castro, J., Cejas, P., Belda-Iniesta, C., González-Barón, M., 2004. PI3K/Akt signalling pathway and cancer. *Cancer Treat. Rev.* 30, 193–204. <https://doi.org/10.1016/j.ctrv.2003.07.007>

- Vargas, J.D., Hatch, E.M., Anderson, D.J., Hetzer, M.W., 2012. Transient nuclear envelope rupturing during interphase in human cancer cells. *Nucleus* 3, 88–100. <https://doi.org/10.4161/nucl.18954>
- Vargas, P., Chabaud, M., Thiam, H.-R., Lankar, D., Piel, M., Lennon-Dumenil, A.-M., 2016. Study of dendritic cell migration using micro-fabrication. *J. Immunol. Methods* 432, 30–34. <https://doi.org/10.1016/j.jim.2015.12.005>
- Venturini, V., Pezzano, F., Castro, F.C., Häkkinen, H.M., Jiménez-Delgado, S., Colomer-Rosell, M., Marro, M., Tolosa-Ramon, Q., Paz-López, S., Valverde, M.A., Weghuber, J., Loza-Alvarez, P., Krieg, M., Wieser, S., Ruprecht, V., 2020. The nucleus measures shape changes for cellular proprioception to control dynamic cell behavior. *Science* 370. <https://doi.org/10.1126/science.aba2644>
- Vermeulen, L., De Sousa E Melo, F., van der Heijden, M., Cameron, K., de Jong, J.H., Borovski, T., Tuynman, J.B., Todaro, M., Merz, C., Rodermond, H., Sprick, M.R., Kemper, K., Richel, D.J., Stassi, G., Medema, J.P., 2010. Wnt activity defines colon cancer stem cells and is regulated by the microenvironment. *Nat. Cell Biol.* 12, 468–476. <https://doi.org/10.1038/ncb2048>
- Verstreken, C.M., Labouesse, C., Agle, C.C., Chalut, K.J., 2019. Embryonic stem cells become mechanoresponsive upon exit from ground state of pluripotency. *Open Biol.* 9, 180203. <https://doi.org/10.1098/rsob.180203>
- Visvader, J.E., 2011. Cells of origin in cancer. *Nature* 469, 314–322. <https://doi.org/10.1038/nature09781>
- Visvader, J.E., Lindeman, G.J., 2012. Cancer stem cells: current status and evolving complexities. *Cell Stem Cell* 10, 717–28. <https://doi.org/10.1016/j.stem.2012.05.007>
- Vogel, V., Sheetz, M., 2006. Local force and geometry sensing regulate cell functions. *Nat. Rev. Mol. Cell Biol.* 7, 265–275. <https://doi.org/10.1038/nrm1890>
- Voutouri, C., Mpekris, F., Papageorgis, P., Odysseos, A.D., Stylianopoulos, T., 2014. Role of constitutive behavior and tumor-host mechanical interactions in the state of stress and growth of solid tumors. *PLoS ONE* 9. <https://doi.org/10.1371/journal.pone.0104717>
- Voutouri, C., Stylianopoulos, T., 2018. Accumulation of mechanical forces in tumors is related to hyaluronan content and tissue stiffness. *PLoS ONE* 13. <https://doi.org/10.1371/journal.pone.0193801>
- Wahab, S.M.R., Islam, F., Gopalan, V., Lam, A.K.-Y., 2017. The Identifications and Clinical Implications of Cancer Stem Cells in Colorectal Cancer. *Clin. Colorectal Cancer* 16, 93–102. <https://doi.org/10.1016/j.clcc.2017.01.011>
- Wang, M., Zhao, J., Zhang, L., Wei, F., Lian, Y., Wu, Y., Gong, Z., Zhang, S., Zhou, J., Cao, K., Li, X., Xiong, W., Li, G., Zeng, Z., Guo, C., 2017. Role of tumor microenvironment in tumorigenesis. *J. Cancer* 8, 761–773. <https://doi.org/10.7150/jca.17648>
- Wang, N., Tytell, J.D., Ingber, D.E., 2009. Mechanotransduction at a distance: mechanically coupling the extracellular matrix with the nucleus. *Nat. Rev. Mol. Cell Biol.* 10, 75–82. <https://doi.org/10.1038/nrm2594>
- Wang, R., Wei, J., Zhang, S., Wu, X., Guo, J., Liu, M., Du, K., Xu, J., Peng, L., Lv, Z., You, W., Xiong, Y., Fu, Z., 2016. Peroxiredoxin 2 is essential for maintaining cancer stem cell-like phenotype through

- activation of Hedgehog signaling pathway in colon cancer. *Oncotarget* 7, 86816–86828. <https://doi.org/10.18632/oncotarget.13559>
- Warburg, O., 1956. On the Origin of Cancer Cells. *Science* 123, 309–314. <https://doi.org/10.1126/science.123.3191.309>
- Willis, N.D., Cox, T.R., Rahman-Casañs, S.F., Smits, K., Przyborski, S.A., van den Brandt, P., van Engeland, M., Weijnenberg, M., Wilson, R.G., de Bruïne, A., Hutchison, C.J., 2008. Lamin A/C is a risk biomarker in colorectal cancer. *PloS One* 3, e2988. <https://doi.org/10.1371/journal.pone.0002988>
- Windmueller, H.G., Spaeth, A.E., 1974. Uptake and Metabolism of Plasma Glutamine by the Small Intestine. *J. Biol. Chem.* 249, 5070–5079. [https://doi.org/10.1016/S0021-9258\(19\)42329-6](https://doi.org/10.1016/S0021-9258(19)42329-6)
- Wintner, O., Hirsch-Attas, N., Schlossberg, M., Brofman, F., Friedman, R., Kupervaser, M., Kitsberg, D., Buxboim, A., 2020. A Unified Linear Viscoelastic Model of the Cell Nucleus Defines the Mechanical Contributions of Lamins and Chromatin. *Adv. Sci.* 7, 1901222. <https://doi.org/10.1002/advs.201901222>
- Wolf, K., te Lindert, M., Krause, M., Alexander, S., te Riet, J., Willis, A.L., Hoffman, R.M., Figdor, C.G., Weiss, S.J., Friedl, P., 2013. Physical limits of cell migration: Control by ECM space and nuclear deformation and tuning by proteolysis and traction force. *J. Cell Biol.* 201, 1069–1084. <https://doi.org/10.1083/jcb.201210152>
- Wong, X., Loo, T.-H., Stewart, C.L., 2021. LINC complex regulation of genome organization and function. *Curr. Opin. Genet. Dev., Genome Architecture and Expression* 67, 130–141. <https://doi.org/10.1016/j.gde.2020.12.007>
- Wu, T., Dai, Y., 2017. Tumor microenvironment and therapeutic response. *Cancer Lett., New developments on Targeted Cancer Therapy* 387, 61–68. <https://doi.org/10.1016/j.canlet.2016.01.043>
- Wu, X., Cai, J., Zuo, Z., Li, J., 2019. Collagen facilitates the colorectal cancer stemness and metastasis through an integrin/PI3K/AKT/Snail signaling pathway. *Biomed. Pharmacother.* 114, 108708. <https://doi.org/10.1016/j.biopha.2019.108708>
- Xia, Y., Ivanovska, I.L., Zhu, K., Smith, L., Irianto, J., Pfeifer, C.R., Alvey, C.M., Ji, J., Liu, D., Cho, S., Bennett, R.R., Liu, A.J., Greenberg, R.A., Discher, D.E., 2018. Nuclear rupture at sites of high curvature compromises retention of DNA repair factors. *J. Cell Biol.* 217, 3796–3808. <https://doi.org/10.1083/jcb.201711161>
- Xia, Y., Pfeifer, C.R., Zhu, K., Irianto, J., Liu, D., Pannell, K., Chen, E.J., Dooling, L.J., Tobin, M.P., Wang, M., Ivanovska, I.L., Smith, L.R., Greenberg, R.A., Discher, D.E., 2019. Rescue of DNA damage after constricted migration reveals a mechano-regulated threshold for cell cycle. *J. Cell Biol.* 218, 2542–2563. <https://doi.org/10.1083/JCB.201811100>
- Xiao, Y., Freeman, G.J., 2015. The Microsatellite Instable (MSI) Subset of Colorectal Cancer is a particularly good candidate for checkpoint blockade immunotherapy. *Cancer Discov.* 5, 16–18. <https://doi.org/10.1158/2159-8290.CD-14-1397>
- Xiao, Y., Yu, D., 2021. Tumor microenvironment as a therapeutic target in cancer. *Pharmacol. Ther.* 221, 107753. <https://doi.org/10.1016/j.pharmthera.2020.107753>

- Xu, S., Xu, H., Wang, W., Li, S., Li, H., Li, T., Zhang, W., Yu, X., Liu, L., 2019. The role of collagen in cancer: from bench to bedside. *J. Transl. Med.* 17, 309. <https://doi.org/10.1186/s12967-019-2058-1>
- Yoo, H.C., Yu, Y.C., Sung, Y., Han, J.M., 2020. Glutamine reliance in cell metabolism. *Exp. Mol. Med.* 52, 1496–1516. <https://doi.org/10.1038/s12276-020-00504-8>
- Young, A.M., Gunn, A.L., Hatch, E.M., 2020. BAF facilitates interphase nuclear membrane repair through recruitment of nuclear transmembrane proteins. *Mol. Biol. Cell* 31, 1551–1560. <https://doi.org/10.1091/mbc.E20-01-0009>
- Yu, J., Vodyanik, M.A., Smuga-Otto, K., Antosiewicz-Bourget, J., Frane, J.L., Tian, S., Nie, J., Jonsdottir, G.A., Ruotti, V., Stewart, R., Slukvin, I.I., Thomson, J.A., 2007. Induced Pluripotent Stem Cell Lines Derived from Human Somatic Cells. *Science* 318, 1917–1920. <https://doi.org/10.1126/science.1151526>
- Zanconato, F., Cordenonsi, M., Piccolo, S., 2016. YAP/TAZ at the Roots of Cancer. *Cancer Cell* 29, 783–803. <https://doi.org/10.1016/j.ccell.2016.05.005>
- Zanotelli, M.R., Chada, N.C., Johnson, C.A., Reinhart-King, C.A., 2020. The Physical Microenvironment of Tumors: Characterization and Clinical Impact. *Biophys. Rev. Lett.* 15, 51–82. <https://doi.org/10.1142/S1793048020300029>
- Zhang, F., Sun, H., Zhang, S., Yang, X., Zhang, G., Su, T., 2017. Overexpression of PER3 inhibits self-renewal capability and chemoresistance of colorectal cancer stem-like cells via inhibition of notch and β -catenin signaling. *Oncol. Res.* 25, 709–719. <https://doi.org/10.3727/096504016X14772331883976>
- Zhi, Y., Mou, Z., Chen, J., He, Y., Dong, H., Fu, X., Wu, Y., 2015. B7H1 Expression and Epithelial-To-Mesenchymal Transition Phenotypes on Colorectal Cancer Stem-Like Cells. *PLOS ONE* 10, e0135528. <https://doi.org/10.1371/journal.pone.0135528>
- Zhou, Y., Xia, L., Wang, H., Oyang, L., Su, M., Liu, Q., Lin, J., Tan, S., Tian, Y., Liao, Q., Cao, D., 2017. Cancer stem cells in progression of colorectal cancer. *Oncotarget* 9, 33403–33415. <https://doi.org/10.18632/oncotarget.23607>
- Zipori, D., 2004. The nature of stem cells: State rather than entity. *Nat. Rev. Genet.* 5, 873–878. <https://doi.org/10.1038/nrg1475>
- Zoetemelk, M., Rausch, M., Colin, D.J., Dormond, O., Nowak-Sliwinska, P., 2019. Short-term 3D culture systems of various complexity for treatment optimization of colorectal carcinoma. *Sci. Rep.* 9, 7103. <https://doi.org/10.1038/s41598-019-42836-0>
- Zou, X., Feng, B., Dong, T., Yan, G., Tan, B., Shen, H., Huang, A., Zhang, X., Zhang, M., Yang, P., Zheng, M., Zhang, Y., 2013. Up-regulation of type I collagen during tumorigenesis of colorectal cancer revealed by quantitative proteomic analysis. *J. Proteomics* 94, 473–485. <https://doi.org/10.1016/j.jprot.2013.10.020>

Chapter 2

Long-term impact of uniaxial confinement

« Chaque bonne réalisation, grande ou petite, connaît ses périodes de corvées et de triomphes ; un début, un combat et une victoire »

Gandhi

Content

ABSTRACT	87
INTRODUCTION	88
RESULTS	88
MULTI-HEIGHT SOFT CONFINER	88
LONG-TERM NUCLEAR VOLUME REGULATION	89
LONG-TERM REGULATION OF NUCLEAR TENSION	90
CELL CYCLE PROGRESSION DOES NOT EXPLAIN LONG-TERM NUCLEAR ADAPTATION	91
LONG-TERM NUCLEAR ADAPTATION OCCURS DURING CONFINED MITOSIS	92
ADAPTATION OF NUCLEUS PHENOTYPE AND VOLUME IS CONTRACTILITY-DEPENDENT	93
CELLS REGULATE THEIR APPARENT NUCLEAR SURFACE DURING MITOSIS	93
FIGURES	94
DISCUSSION	104
STRONG CONFINEMENT INCREASES NUCLEAR ENVELOPE TENSION AND GROWTH	104
MITOSIS PLAYS A KEY ROLE IN NUCLEAR ADAPTATION TO CONFINEMENT AND ALLEVIATION OF NUCLEAR ENVELOPE TENSION	104
THE CRITICAL ROLE OF ACTOMYOSIN CONTRACTILITY IN THE REGULATION OF LAMINA TENSION AND NUCLEAR VOLUME 105	
REGULATION OF NUCLEAR REPAIR MECHANISM ASSOCIATED WITH LAMINA FOLDING AND NUCLEAR VOLUME LOSS	105
CONCLUSION AND OUTLOOKS	106
OUTLOOK IN THE CONTEXT OF CANCER	106
POTENTIAL IMPLICATIONS FOR DRUG RESISTANCE OF CANCER CELLS	107
MATERIAL AND METHODS	107
CELL CULTURE	107
DRUG TREATMENTS	107
MULTI-HEIGHT MICRO-MILLED MOLD FABRICATION	108
MICROFABRICATION-BASED CONFINEMENT OF CELL POPULATIONS	108
AGAROSE MOLDING	108
IMMUNOSTAINING	109
CONFOCAL FLUORESCENCE MICROSCOPY	109
EPIFLUORESCENCE IMAGING	109
LIVE-CELL IMAGING	109
QUANTITATIVE IMAGE ANALYSIS	109
STATISTICS AND REPRODUCIBILITY OF EXPERIMENTS	110
SUPPLEMENTARY MATERIAL 1 – GEOMETRICAL MODEL	111
REFERENCES	112
ACKNOWLEDGMENT	115
AUTHOR CONTRIBUTION	115
SUPPLEMENTARY FIGURES	116
SUPPLEMENTARY MOVIES	125

Mitosis down-regulates nuclear volume and resets nuclear envelope folding of cancer cells under prolonged confinement

Malèke Mouelhi^{1*}, Alexis Saffon¹, Hélène Delanoë-Ayari¹, Sylvain Monnier^{1+*}, Charlotte Rivière^{1,2,3+*}

¹ *Univ Lyon, Université Claude Bernard Lyon 1, CNRS, Institut Lumière Matière, UMR 5306, 69622, Villeurbanne, France*

² *Institut Universitaire de France (IUF), France*

³ *Institut Convergence PLAsCAN, Centre de Cancérologie de Lyon, INSERM U1052-CNRS UMR5286, Univ Lyon, Université Claude Bernard Lyon 1, Centre Léon Bérard, Lyon, France*

⁺Senior author contributed equally to this work

^{*}Corresponding authors

Abstract

During their life, mammalian cells are subjected to numerous mechanical constraints, especially in pathological contexts such as cancer. Most studies on cell confinement focus on short periods, and little is still known about cell adaptation to prolonged squeezing, over several cell divisions. Using a hydrogel-based confinement system, we reveal the unsuspected role of mitosis in long-term adaptation to prolonged uniaxial confinement, in a contractility-dependent manner. To adapt to the level of confinement and to alleviate the imposed mechanical stress, nuclei are reaching a new homeostatic state following the first confined cell division: cells down-regulate their nuclear volume, together with a reset of their nuclear envelope folding. A simple geometric model suggests that this new nuclear volume is triggered by the apparent surface of the nuclear envelope.

Our findings have important implications for the fundamental understanding of nuclear regulation under mechanical constraints and are critical to better comprehend cancer cells plasticity.

Introduction

Cancer is a leading cause of death worldwide, despite continual progress in therapeutic strategies and in our understanding of cancer cell biology. The role of mechanics in cancer cell response has raised attention over the last decades¹⁻⁴, and alleviating mechanical stress is now envisioned as an interesting therapeutic strategy^{5,6}. Deformed nuclei within tumors has been reported *in vivo*^{7,8}, though consequences on cell fate remain unknown. Pioneer works have identified an alteration of cell mitosis under such confined situations^{9,10}, with modified cell cycle progression and division¹¹, the presence of multi-daughter events, daughter cells of unequal size, and induction of cell death¹². Conversely, it has been shown that flattening is required for the G1-S transition¹³, as well as the G2-M transition¹⁴. The role of the nucleus as a mechanosensor is now clearly recognized^{15,16}, with a mechanism of nuclear repair¹⁷ and rescue of DNA damage¹⁸. Upon squeezing, the nucleus shortly unfolds its inner lamin envelope, activating the cytosolic phospholipase A2 (cPLA2)-Arachidonic acid (AA) pathway¹⁵, as well as myosin II contractility and switches towards a motile phenotype¹⁶. Nuclear blebs and chromatin herniation can also occur, leading to transient events of nuclear rupture and repair^{17,19}. However, all these studies analyzed the short-term nuclear adaptation (within minutes to a few hours), and cancer cells adaptation to a prolonged imposed deformation (over several days) remains unexplored, specifically how such deformation affects cell cycle progression.

We have recently developed an agarose-based soft-confiner, ideal to analyze the proliferation of squeezed cells for several days²⁰. Here, based on the compatibility of this assay with *in-situ* immunostaining and time-lapse analysis, we explored how the nucleus responds to an imposed deformation for several days in a colorectal cancer cell model (HT-29). As expected, within a short timeframe, an unfolding of the nuclear envelope and the appearance of nuclear blebs were observed. Under prolonged confinement, we evidenced for the first time a global nuclear adaptation, with a decrease in nuclear volume within 24 h, and a readjustment of nuclear shape, namely the disappearance of blebs and refolding of the nuclear envelope. Surprisingly, all these changes were triggered by mitosis in a contractility-dependent manner and were conserved by the next daughter's generation, setting a new state of homeostasis.

Results

Multi-height soft confiner

Cells were confined using the agarose-based confiner previously published²⁰. In this system, a 2% agarose pad presenting an array of pillars with a height smaller than that of the cell enabled precise cell squeezing. All experiments were performed using agarose exhibiting a stiffness of 150 kPa²⁰. In this stiffness range, it is not possible for cells to deform the confining agarose gel. The method originally published by Prunet et al.²⁰ relied on standard photolithography

processes to create the wafers needed for agarose molding, and could only confine cells at a single height per system. We have now upgraded this soft confiner by implementing the possibility to submit a cell population to multiple confinements simultaneously. For that, we developed a multi-height micro-milled mold (Figure 1a), allowing us to control the height of the pillars with a micron resolution. We can confine cells at four different heights within the same system, with a central control zone included, where no confinement was imposed. Each pillar with a given shape corresponds to a specific height: 9 μm (the highest pillar with the least confinement), 7 μm (intermediate confinement), 5 μm (strong confinement) and 3 μm (the strongest confinement) (Figure 1b-c). This multi-height mold was reproducible over time, as illustrated in Figure 1d, where the heights of stained cells/nuclei measured at 2 h and 24 h were almost identical. Moreover, cells were properly and homogeneously confined within each zone, and displayed the following average heights: $15 \pm 0.13 \mu\text{m}$ for control condition, $8.7 \pm 0.45 \mu\text{m}$ (slight confinement), $6.9 \pm 0.16 \mu\text{m}$ (intermediate confinement, twice the cell size), $5.1 \pm 0.13 \mu\text{m}$ (strong confinement), to $3.7 \pm 0.25 \mu\text{m}$ (very strong confinement, below a fourth of the original cell size) (Figure 1d-e). These cellular heights corresponded to a decrease in nuclear height from $10 \pm 0.10 \mu\text{m}$ (control condition) to $5.9 \pm 0.08 \mu\text{m}$ (slight confinement), $4.9 \pm 0.10 \mu\text{m}$ (intermediate confinement), $3.9 \pm 0.04 \mu\text{m}$ (strong confinement), $2.9 \pm 0.08 \mu\text{m}$ (very strong confinement) (Figure 1d-e).

Hence, by modifying the soft confiner we previously designed, we obtained a user-friendly, robust, and time-saving system to visualize and analyze the long-term effect of four levels of cell confinement on cancer cell morphology and biology.

Long-term nuclear volume regulation

Having optimized the confinement system, we then investigated how long-term confinement affects cell nuclei. We first computed the nuclear deformation for each level of confinement (Figure 1f) and obtained a nuclear deformation along the z-direction (ϵ_{Nz}) of $41 \pm 3\%$ for slightly confined cells, $52 \pm 0.5\%$ for an intermediate confinement, $60 \pm 1\%$ and $70 \pm 2\%$ for strong and very strong levels of confinement, respectively (Figure 1f). These deformations are associated with changes in nuclear projected-area and nuclear volume. At 2 h of confinement, the nuclear-projected area increased with the level of confinement (Figure 1e-g), while the volume of each nucleus, computed by approximating the shape of the nucleus to a cylinder (See schematic representation in Figure 1g), remained constant for all imposed deformations (Figure 1h, squares). Intriguingly, at 24 h of confinement, the nuclear-projected area of confined cells decreased towards that of the control condition (Figure 1g, triangles). This decrease in nuclear-projected area corresponds to a proportional decrease in nuclear volume after 24 h of confinement (Figure 1 h, triangles), with a nuclear volume loss from $20 \pm 6.4 \%$ (for slight confinement), $25 \pm 7.3 \%$ (for intermediate confinement), $39 \pm 8\%$ (for strong confinement) to $34 \pm 15\%$ (for very strong confinement, Supplementary Fig. 1a). Interestingly,

this loss in nuclear volume was inversely proportional to nuclear deformation ϵ_{Nz} (Figure 1h, dotted line).

In addition, the distance between the cell membrane and the nuclear envelope was significantly reduced with confinement (Figure 1d, Supplementary Fig. 1c) and accompanied by the re-localization of the contractility machinery (Phosphorylated Myosin Light Chain (p-MLC) staining) from above the nucleus to the lateral plane indicating a cortex rearrangement (Supplementary Fig. 1d).

Moreover, at 2 h of cell confinement, DNA damages appeared as evidenced by an increase in the number of γ H2AX foci (marker of double-strand breaks, Supplementary Fig. 1e-f) per cells. This confinement-induced DNA damages was repaired at 24 h, as the number of foci per cells in confined conditions was identical to that of unconfined ones (Supplementary Fig. 1e-f).

Long-term regulation of nuclear tension

Under the strongest levels of confinement (60% and 70% nuclear deformation), we observed nuclear protrusions at 2 h (Figure 1e, strong-very strong confinement panel and Figure 2a), which participated in the increase in nuclear-projected area, though not entirely as the increase remained significantly different even if protrusions were dismissed to compute the projected area (Supplementary Fig. 1b). As observed, the nuclear volume remains constant for short timescales (2 h), but due to the applied confinement and geometrical considerations, the nuclear envelope (NE) unfolds, its tension increases²¹, which can lead to nuclear protrusions²²⁻²⁴. Nuclear protrusions are dynamic structures whose membrane can rupture – visualized by leakage of NLS-RFP dye to the cytoplasm (Supplementary Fig 2a, arrows) – and repair¹⁷.

The proportion of nuclei displaying protrusions (indiscriminately called blebs in the rest of the manuscript for simplicity), as well as dividing, apoptotic and normal nuclei was quantified according to their morphology (Figure 2a, insets). Under slight confinement (41 % nuclear deformation), blebbing nuclei represented only 4.2 ± 4.7 % of all nuclei (Figure 2b). However, the proportion of these nuclei gradually increased with the degree of confinement and represented 37.7 ± 6.7 % and 63.4 ± 11.8 % of all nuclei for 60% and 70% of nuclear deformation, respectively (Figure 2b). Strikingly, at 24 h of confinement, those proportions dropped to less than 10 %, which was reflected by an increase in normal nuclei proportions (Figure 2c-d). The number of blebs per cell and the size of those blebs were also drastically reduced at 24 h under strong confinement (Supplementary Fig. 2b-e). This change in nuclear phenotype at 24 h is in accordance with the reduction in nuclear volume and the refolding of the nuclear envelope. Nuclear envelope folding was quantified from lamin A/C immunostained images with the positive area defined as the excess area of the lamina envelope compared to the nuclear area (See methods and schematic representation in Figure 2f). In control

conditions, the nuclear envelope was folded, reaching similar levels at 2h ($56 \pm 1.5\%$) and 24h ($57 \pm 2\%$) (Figure 2e-f). Under a strong level of confinement (60% nuclear deformation), a complete unfolding of the nuclear envelope was observed at 2 h, evidenced by a radical decrease of the positive area (Figure 2e-f, down to $20 \pm 1 \%$). Strikingly, at 24 h, a refolding of lamin A/C was observed (Figure 2e), with an increase in the positive area ($34 \pm 1 \%$) (Figure 2e-f).

Thus, not only was nuclear volume regulated at 24 h of confinement but also nuclear blebbing, and nuclear envelope folding, suggesting either a relaxation of the nuclear envelope tension, either an inability of cells with blebs to divide. All these changes (volume decrease, blebs disappearance, nuclear envelope refolding) are referred as global “nuclear adaptation” in the rest of the manuscript.

In addition, we noticed a constant proportion of dividing cells at 24 h of confinement below 60% of nuclear deformation, albeit a slight increase at 70% nuclear deformation (Figure 2c-d). This increase in dividing nuclei was most likely due to an increase in the duration of mitosis (Supplementary Fig. 3a), already described by Lancaster et al. ¹⁰.

Cell cycle progression does not explain long-term nuclear adaptation

We next performed experiments to narrow the range of potential mechanisms involved in this long-term nuclear adaptation. To this end, we conducted time-lapse experiments on live cells by confining HT-29 expressing the FUCCI fluorescent cell cycle reporter system over 3 to 4 days (Figure 3a). We first, hypothesized that an alteration of cell cycle progression could explain the loss of nuclear volume observed under prolonged confinement. It was reported that mechanically confined cell, without having the possibility to round up for division, results in stressed cell division with delayed mitosis, multi-daughter mitosis events, unevenly sized daughter cells and induction of cell death^{9,10}. We confirmed this experimentally and saw a gradual increase in abnormal divisions with the level of confinement, from none for control conditions to $40 \pm 4\%$ for very strong confinement (Supplementary Fig. 3b, Supplementary Movie 1). In addition, for mother cells, while the duration of the first mitosis was similar for control and slight confinement (Supplementary Fig. 3a, respectively $1,8 \pm 0,1$ h and $1,6 \pm 0,1$ h), it doubled for cells under strong confinement ($3,5 \pm 0,4$ h), and considerably increased up to $9,2 \pm 0,8$ h for very strong confinement, reaching up to 20h in some cases (Supplementary Fig. 3a). The time spent in G2 for mother cells also increased for cells under very strong confinement (Supplementary Fig. 3c) and led to a larger increase in volume during this S-G2-phase (Supplementary Fig. 3d), with no significant increase in volume detected before the G2-phase (Supplementary Fig. 3e).

We then focused on the cell cycle taking place after a first confined division. Surprisingly, for the daughter cells, we found that confinement did not significantly change the duration of the

whole cell cycle (Figure 3b) and neither that of its subpart (G1, S-G2 Supplementary Fig. 3f). Indeed, the entire cell cycle for daughter cells lasted 27 ± 7 h under slight confinement, $23 \text{ h} \pm 4$ under strong confinement compared to 22 ± 5 h under no confinement (Figure 3b). Similarly, relative nuclear growth (change in volume normalized by their initial volume) remained unchanged under confinement during the entire cell cycle (Figure 3c), and during its subpart (Supplementary Fig. 3g). Likewise, nuclear growth rates of confined cells were similar regardless of the level of confinement (Figure 3d), with no significant difference in its subpart (Supplementary Fig. 3h). These results suggest that long-term nuclear volume regulation of daughter cells cannot be explained by changes during cell cycle progression nor growth rate.

Long-term nuclear adaptation occurs during confined mitosis

We then focused on changes of nuclear volume during confined mitosis. A reasonable assumption is that the nuclear volume is conserved throughout mitosis, so that the volume of the sum of the two daughter cells after division is equal to the volume of their mother cell. Intriguingly, nuclei were smaller after the first division under confinement (Figure 3e-f), with a volume ratio decreasing gradually with increasing nuclear deformation, similarly to the one observed at 24 h on fixed samples (Figure 1h, 3f and Supplementary Figure 3i for the fit). The loss of volume during mitosis reached up to $60 \pm 15\%$ for the strongest confinement (Figure 3f). The fact that we obtain the same proportionality on both fixed (Figure 1h) and live (Figure 3f) experiments confirm the robustness of our results concerning such nuclear size regulation. On the contrary, during the second division under confinement, we observed no volume loss (Figure 3f, generation 2). Hence, the nuclear volume seems to have reached homeostasis after the first confined division and does not shrink further during a second confined division. Therefore, mitosis appears to be the main checkpoint in the observed long-term adaptation of nuclear volume.

This prompted us to investigate whether mitosis could also play a role in the loss of nuclear blebs. Using time-lapse experiments, we quantified the nuclear blebs before and after confined divisions (Figure 3g-h). Before mitosis, the mean number of blebs per cell was 1 ± 0.3 for cells under strong confinement (Figure 3h, 60% nuclear deformation), and reached 3 ± 2.2 for very strong confinement (Figure 3h, 70% nuclear deformation). However, immediately after mitosis, the mean number of blebs per cell was close to 0 for both strong and very strong confinement (Figure 3g-h, Supplementary Movie 2). In addition, we observed no blebs before the second mitosis (Figure 3h). We can thus conclude that the loss of nuclear blebs is essentially due to cells undergoing mitosis, suggesting that nuclear volume and nuclear envelope tension are tightly coupled, and supporting the hypothesis that mitosis is a key regulator of nuclear envelope tension.

Adaptation of nucleus phenotype and volume is contractility-dependent

Acto-myosin contractility is a well-known transducer of stress to the nucleus, inducing deformation and blebbing²². Conversely, it has been shown recently that nuclear tension and blebbing increase cell contractility^{15,16}. Therefore, to gain further insights into the mechanisms involved in this global nuclear adaptation, we inhibited cell contractility using Blebbistatin, a pharmacological inhibitor of myosin II. The addition of Blebbistatin immediately after confining cells, impeded nuclear volume regulation, as evidenced at 24 h under very strong confinement (Figure 4a-b). Of note, while at 2 h under very strong confinement (70% nuclear deformation) the number of nuclear blebs drastically increased with or without the addition of Blebbistatin (Figure 4c, 2 h), very few blebs had disappeared at 24h with Blebbistatin (Figure 4c, 24 h and Supplementary Fig. 4d). Similarly, inhibiting contractility before applying the confinement (Blebbistatin added 1h before confinement) also prevented the regulation of nuclear volume and blebs (Supplementary Fig. 4 a-c).

Cells regulate their apparent nuclear surface during mitosis

From our data, we calculated the apparent surface of confined nuclei S_{app} (See Supp. Mat 1), which corresponds to the surface of a cylinder. As expected, the apparent surface passively increases after 2 h under confinement, while it seemed to remain constant at 24h (Figure 5a). Moreover, this constant apparent surface was similar for non-confined cells. This strongly suggests that the apparent surface is the key parameter regulated during prolonged confinement.

To test whether it is the total surface of nuclear envelope that determines the nuclear volume, we estimated the surface for unfolded nuclear envelope conditions after 2 h under confinement S_0 (See Supp. Mat. 1). From S_{app} (apparent surface) and S_0 (total surface, obtained in the unfolded nuclear envelope condition) we computed the expected nuclear volumes in confined conditions (Figure 5b) and found that the volumes calculated using S_{app} were in good agreement with the experimental volumes measured after 24 h under confinement (Figure 5c). Collectively, these geometrical arguments strongly suggest that the nuclear volume is not limited by the total surface of the nuclear envelope available, but rather actively set by the apparent surface that remains constant under different geometrical constraints.

Figures

Figure 1

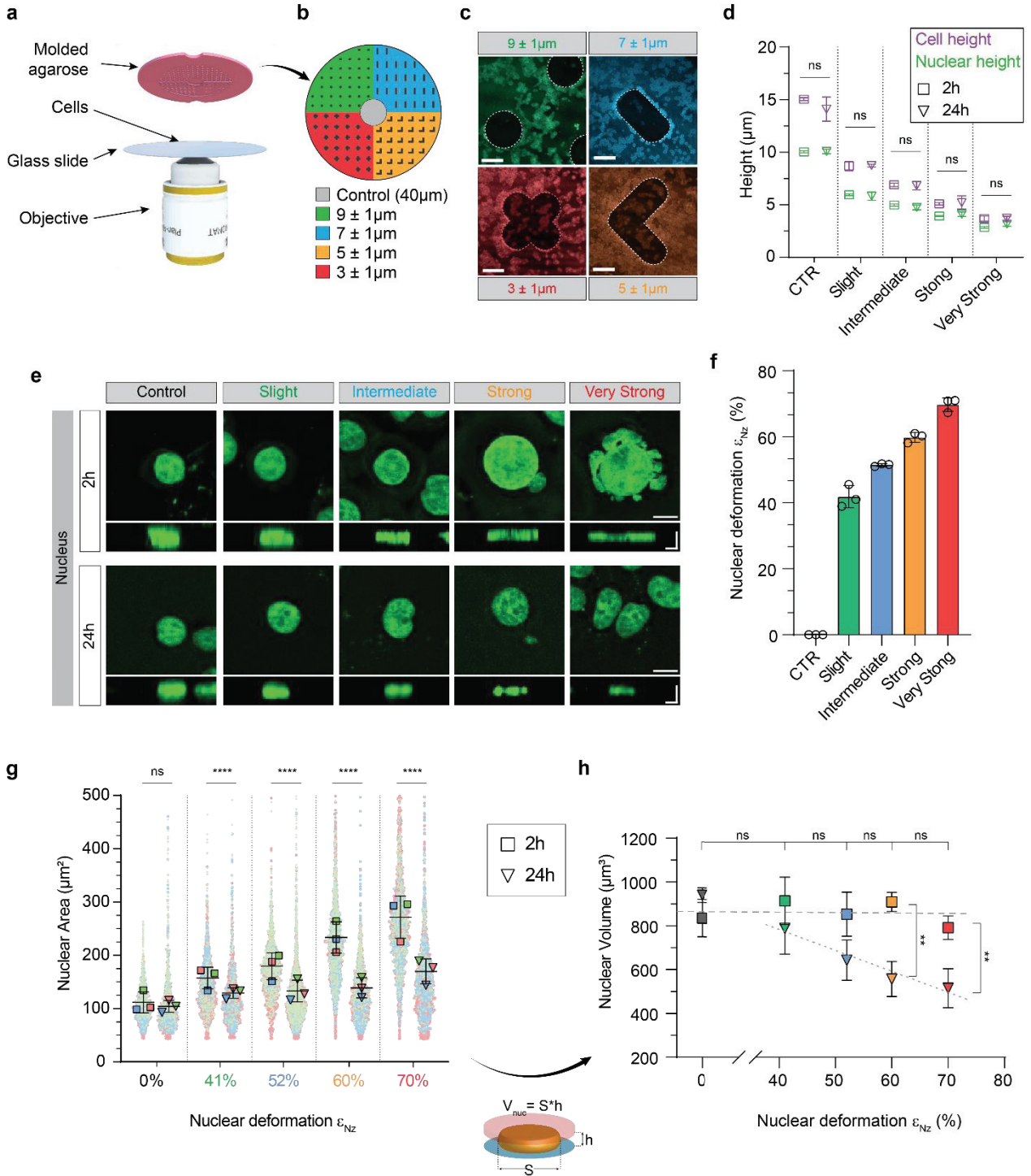


Figure 23: Nuclear volume is regulated according to the level of confinement.

(a) 3D representation of confinement principle showing the molded agarose pad. **(b)** Schematic diagram of the multi-height pad with the theoretical heights of each pillar. **(c)** Confocal images of cells and the shaped pillar of each confined zone. *Scale bar = 250 μm .* **(d)** Quantification of cells and nuclear height by z-stack confocal imaging, under each confined zone. *N = 3 experiments with n = 30 cells; Mann-Whitney test.* **(e)** Representative confocal images of nuclei stained with NucGreen in XY (*Scale bar = 10 μm*) and its orthogonal view (*Scale bar = 5 μm*) at 2 h and 24 h under each level of confinement. **(f)** Nuclear deformation in percent for each degree of confinement defined as $\varepsilon_{NZ} = \left(\frac{h_{nuc}^{ctr} - h_{nuc}}{h_{nuc}^{ctr}} \right) \times 100$. **(g)** SuperPlot quantifying the projected nuclear area. In each condition, the 3 colors represent 3 distinct experiments with their respective individuals and average value represented by small and large dots respectively. *N = 3 experiments with n > 5,000 cells/experiments; Welch's test. Welch's ANOVA test was also performed between each confined condition at 24 h and was not significant.* **(h)** Nuclear volume quantification. *N = 3 experiments with n > 5,000 cells/experiments; Welch's test. Ordinary one-way ANOVA was carried out between each confinement condition at 2 h and was not significant.*

Figure 2

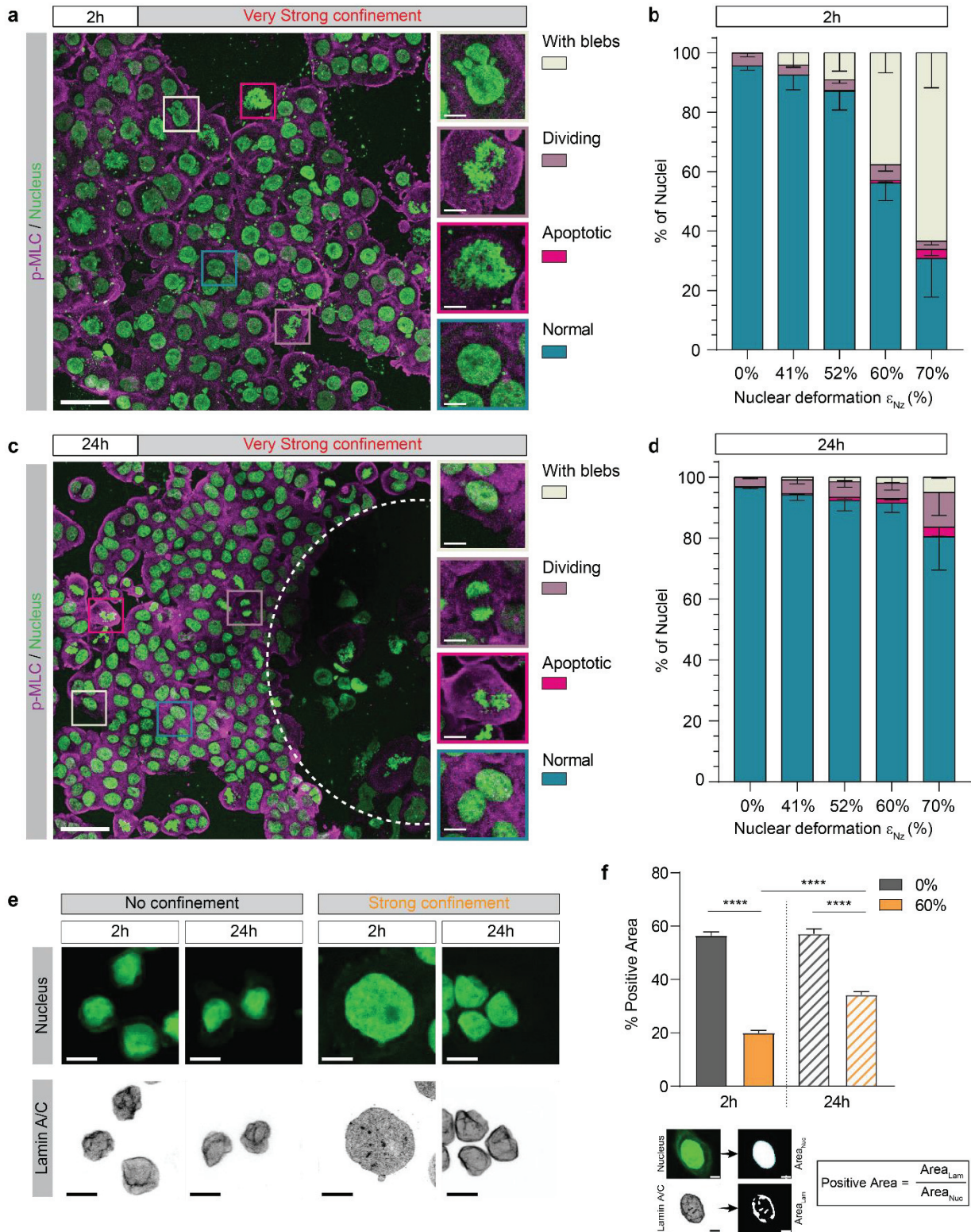


Figure 24: Regulation of nuclear tension.

(a, c) Max projection confocal images of stained nuclei and pMLC at 2 h and 24 h, respectively, scale bar = 50 μm . Cropped nuclei correspond to nuclei with blebs, dividing and apoptotic cells and normal nuclei, at 2 h **(a)** and 24 h **(c)**, scale bar = 10 μm . **(b, d)** Percentage of HT-29 cells presenting nuclear blebs, dividing, apoptotic cells, or normal nuclei in control condition or under confinement, at 2 h **(b)** and 24 h **(d)**. $N = 3$ experiments with $n > 5,000$ cells/experiments. **(e)** Representative confocal images (max intensity projection) of stained nuclei and lamin A/C without confinement (control) or under 60% nuclear deformation (strong confinement) at 2 h and 24 h. Scale bar = 10 μm . **(f)** Quantification of the positive area of the nuclear envelope (lamin A/C) which represents the folded nuclear envelope. $N = 3$ experiments with $n > 30$ cells/experiments; mean \pm SEM; Mann-Whitney test.

Figure 3

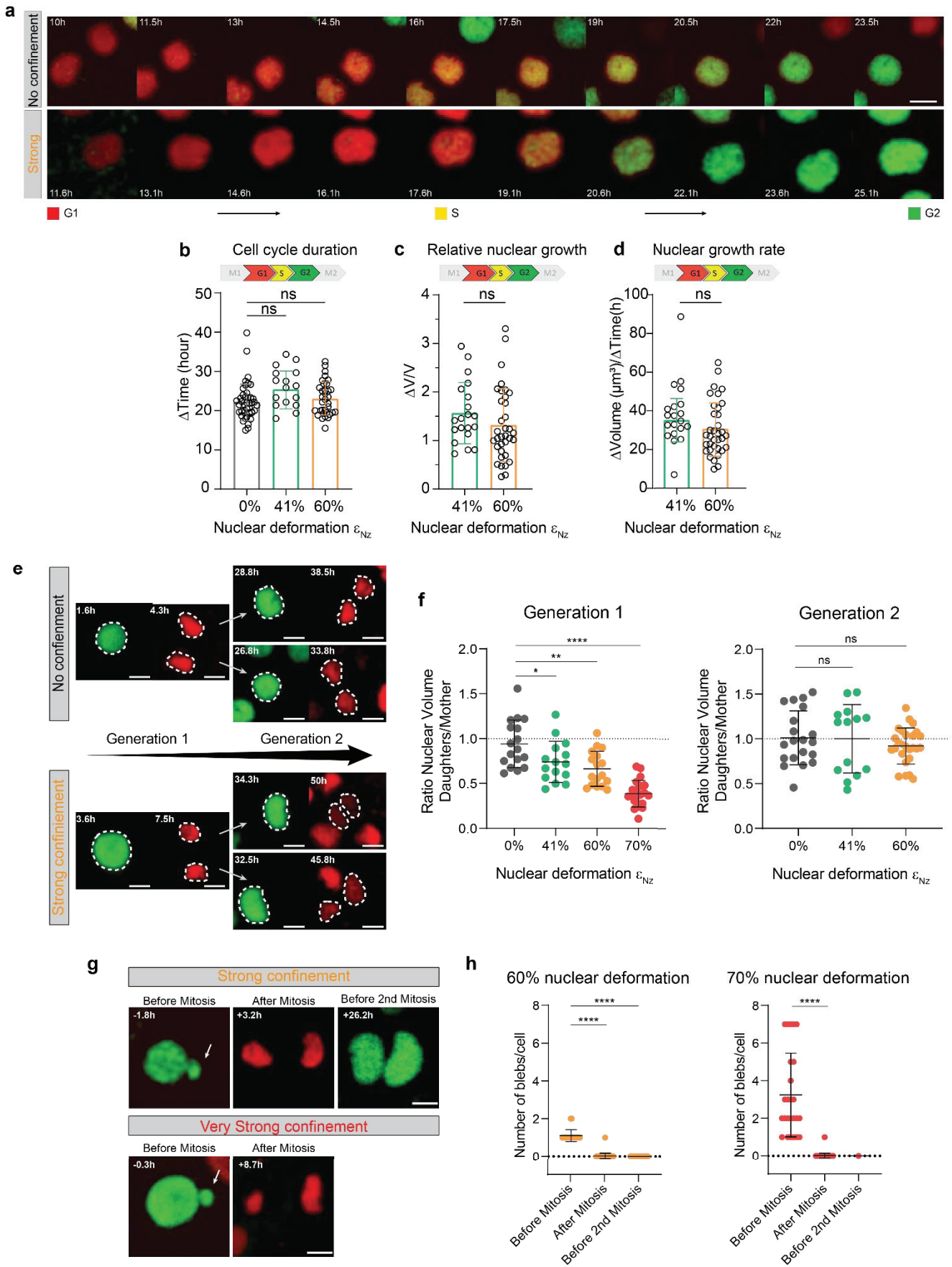


Figure 25: Global phenotypic regulation of the nucleus occurs through mitosis.

(a) Time-lapse images of HT-29 nuclei expressing the FUCCI fluorescent cell cycle reporter, without confinement (control) or under strong confinement (60% nuclear deformation). *Scale bar = 10 μm .* **(b, c, d)** Quantification of the duration **(b)**, the relative nuclear growth **(c)** and the nuclear growth rate **(d)** of HT-29-Fucci cells under several levels of confinement during an entire cell cycle after the first cell division. *N = 2 experiments with $n > 200$ cells, Mann-Whitney test for (b, c), and unpaired t-test for (d).* **(e)** Representative images of nuclei at the end of the G2 phase (just before mitosis) and its respective daughter nuclei just after mitosis (beginning of G1 phase), following two consecutive divisions, for control and strong confinement conditions. *Scale bar = 10 μm .* **(f)** Quantification of the size of daughter nuclei over their respective mother following two consecutive divisions, under several levels of confinement. *N = 2 experiments with $n = 130$ cells, unpaired t-test.* **(g)** Sequential images of a blebbing nucleus under strong or very strong confinement before and after mitosis, NEB is set here as a reference time $t = 0$ h. *Scale bar = 10 μm .* **(h)** Quantification of the number of blebs before and after mitosis under strong and very strong confinement. *N = 3 experiments with $n = 167$ cells, Mann-Whitney test.*

Figure 4

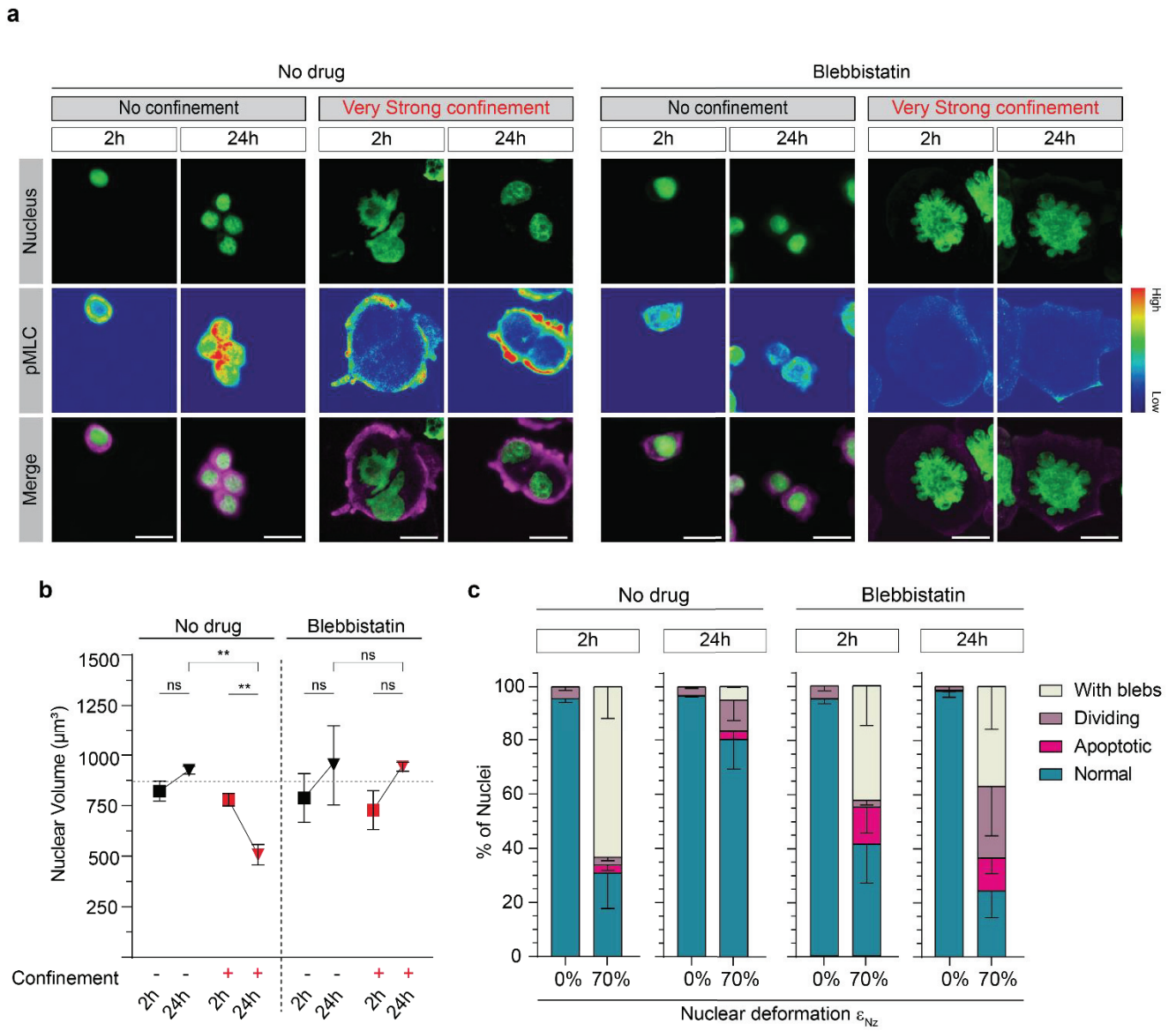


Figure 26: Contractility is essential for nuclear regulation.

(a) Representative images of stained nuclei and phospho-Myosin Light Chain either with or without Blebbistatin at 2 h and 24 h, without confinement or under very strong confinement. *Scale bar = 20 μ m.* **(b)** Quantification of nuclear volume at 2 h and 24 h with or without Blebbistatin, without confinement or under very strong confinement. *N = 3 experiments with n=9,818 cells, mean \pm SEM, unpaired t-test (for no drug conditions) or Mann-Whitney test (for Blebbistatin conditions).* **(c)** Quantification of nuclei with blebs, dividing, apoptotic, or normal without confinement or under very strong confinement at 2 h and 24 h, with no drug or with Blebbistatin. *N = 3 experiments with n = 9,818 cells.*

Figure 5

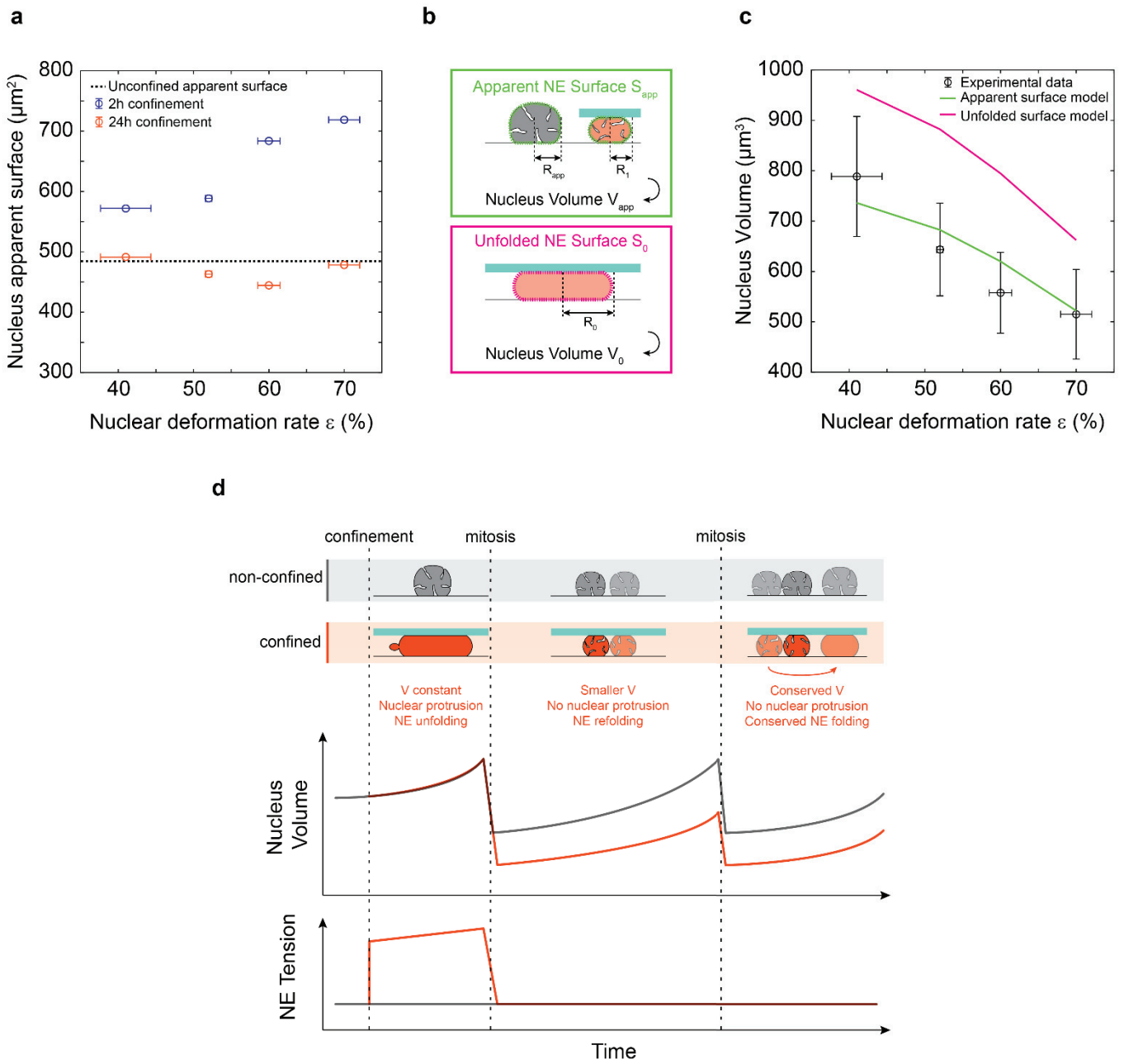


Figure 27: Nuclear total surface determines the final nuclear volume.

(a) Nuclear apparent surface as a function of the deformation ε_{NZ} at 2 h and 24 h under confinement. The dashed line shows the apparent surface measured for unconfined cells. **(b)** Schematic representation of the geometric model, showing the apparent nuclear envelope surface S_{app} and the unfolded nuclear envelope surface S_0 . **(c)** Calculations of nuclear volume using the apparent surface (green) and the total surface (pink). The total surface is obtained from the tensed nuclear envelope measured under intermediate confinement at 2 h. Experimental values are shown in black. **(d)** Diagram summarizing the results showing that under confinement before mitosis, the nuclear envelope is tensed and tension increases as evidenced by the nuclear blebs. Tension is then released during the first mitosis as the nuclear volume is lower at mitosis exit. Low initial tension is restored, nuclear-envelope folds appear again but not blebs.

Discussion

Deciphering how the nucleus reacts to long-term confinement is of primary importance in the context of cancer progression and response to treatment^{25,26}. Using an imposed deformation, we show that the nucleus is regulating both its volume and its structure (blebs, lamin A/C folding) within 24 h. We evidenced that this regulation is mediated by mitosis: nuclei then reach a new state of homeostasis, with no further adaptation observed in the next generations. This regulation is an active process requiring the contractility machinery. In addition, a simple model supports the idea that the total nuclear surface is key in setting the nucleus size and consequently alleviating nuclear envelope tension (see Figure 5d for a schematic representation).

Strong confinement increases nuclear envelope tension and growth

Taking advantage of the compatibility of our soft-confiner system with time-lapse microscopy, we were able to follow the same cells for several cell divisions and observed different steps of adaptation to various levels of confinement. The first step takes place before the first division of confined cells. Within the first hours of confinement, only highly confined cells display an increase in nuclear growth rate (Supplementary Fig. 3c-d), in accordance with the nuclear envelope tension threshold observed for HeLa cells¹⁵. This increase in growth rate might be due to an increase in nuclear import following a rise in nuclear envelope tension and uncoupled nuclear and cytoplasmic volumes as proposed by Pennacchio et al.²⁷⁻²⁹. This bias in nuclear shuttling can generate an increase in nuclear osmotic pressure and account for the blebbing observed during the first hours under confinement (Figure 2a-b)^{8,30}. This increase in growth rate is also accompanied by a lengthening of the G2 phase (Supplementary Fig. 3c). Conversely, slighter levels of confinement did not impact cell cycle progression (Supplementary Fig. 3c-e), suggesting that the flattening required for the G1 to S transition observed for HeLa cells¹³ should be sufficient to fully extend the nuclear envelope or might be cell type dependent.

Mitosis plays a key role in nuclear adaptation to confinement and alleviation of nuclear envelope tension

The key step in nuclear adaptation to confinement is clearly cell mitosis. We clearly show that the regulation of nuclear volume observed at 24 h of confinement largely originated from volumetric changes at division exit (Figures 1h and 3f). Confined mitosis can be prolonged due to defects in spindle assembly¹⁰ or leads to asymmetric or multi-daughter division⁹, but so far such shrinking of the nucleus during division has never been observed to our knowledge. More strikingly, no more shrinking was observed for the second division under confinement (Figure

3f). This important observation points out toward a true adaptation to confinement: once adapted, there is no further volume decrease.

So far, however, the mechanisms involved remain elusive. Using a mechanistic approach, we showed that the apparent nuclear surface is the parameter conserved over a long time and therefore during cell division (Figure 5). By regulating the apparent surface of their nucleus, cells can adjust their nuclear envelope tension to a homeostatic level. Indeed, mitosis also plays a pivotal role in relaxing the nuclear envelope tension generated by confinement as nuclear blebs disappeared completely after the first mitosis (Figure 3h), while nuclear envelope folds reappeared in confined conditions at 24 h (Figure 2e-f).

Of note, we also observed a population of abnormal divisions (multi-daughter cells, cells blocked in mitosis), as already reported for HeLa cells^{9,10}. In the future, it could also be of interest to analyze how this abnormal subpopulation regulates (or not) its nuclei.

The critical role of actomyosin contractility in the regulation of lamina tension and nuclear volume

The nuclear adaptation we evidenced was lost by blocking contractility via Blebbistatin treatment. This result is in accordance with the fact that abnormal actomyosin contractility is associated with changes in cell division, such as defects in spindle positioning^{10,31}, failed mitosis, and the appearance of polynucleated cells^{9,10}. During cell division, actomyosin contractility participates in cleavage furrow formation³². Here, our results suggest that contractility is required to set nuclear volume and nuclear envelope folding, mostly during nuclear envelope reformation at the end of mitosis.

Regulation of nuclear repair mechanism associated with lamina folding and nuclear volume loss

Consistent with previous studies^{33,34}, we also evidenced an increase in DNA-damage at 2 h of confinement (Supplementary Fig. 1e-f). Such an increase in DNA-damage could lead to chromosomal instability and mutations^{35,36}. However, very interestingly, in addition to lamina refolding and nuclear volume loss, we also observed a decrease in DNA damage at 24 h of confinement (disappearance of most γ -H2AX foci, Supplementary Fig. 1e-f). This is in accordance with the reported role of lamin in the DNA damage repair pathway³⁷ and a lower nuclear envelope tension associated with bleb disappearance. Such repair mechanisms have also been reported in other confinement situations¹⁸, as well as in response to other stresses like radiotherapy³⁸. As such repair mechanism is highly correlated with cell-cycle re-entry¹⁸, this is again consistent with a key role for mitosis in such DNA-damage regulation in response to nuclear deformation.

Growing evidence also indicates a role for lamins in the regulation of transcription³⁹, replication, and genome stability⁴⁰. It will be very interesting to further investigate the effect on transcription activity, protein synthesis, as well as chromatin condensation.

Conclusion and outlooks

Here, under prolonged cancer cell squeezing, we experimentally highlighted the critical role of mitosis in the regulation of nuclear envelope lamina folding, nuclear blebs, and nuclear volume. Using simple geometric assumptions, we show that homeostasis of nuclear volume is set by the apparent surface of the nuclear envelope.

This study calls for in-depth analysis of the molecular pathways at play, as well as for deciphering the consequences that such regulation could have in the context of cancer and resistance to therapies. We anticipate the role of calcium as well as cPLA2, both of which were recently reported to be involved in nuclear deformation sensing¹⁵. The nuclear to cytoplasmic ratio, which is constant within a given population, is most likely to be impacted by the confinement and changes in nuclear envelope tension^{27,41,42}, and might be at play in the regulation we describe herein. The import/export regulated by the nuclear pore complex is also a putative important player²⁸. Lastly, we identified a clear change in lamin unfolding/refolding during this nuclear adaptation: lamins and lamin-associated proteins are known regulators of nuclear size⁴² and should therefore be further investigated, especially in the context of cancer.

Noteworthy, as already mentioned, the agarose gel used herein exhibit a stiffness of 150 kPa²⁰, which is too rigid for the cell to deform the gel. It would be interesting in the future to analyze cell response using softer gels (in the kPa range). Indeed, if the cells are able to deform the gel, the nuclear regulation highlighted in this study could be completely different. In Lancaster et al.¹⁰, when the mitotic cells were able to deform the gel, they divide normally.

Outlook in the context of cancer

Abnormal nuclei shape⁴³, together with alterations in the expression of lamin A and lamin B is a hallmark for the prognosis of many tumors²⁵, including colorectal cancer⁴⁴. Low lamin A/C is associated with a decrease in stiffness, irregular shape, and larger nuclei deformation⁴⁵ as well as increased metastatic capacities⁴⁶. Noteworthy, the HT-29 cell line used in this study presents the p53 mutation⁴⁷, has no lamin B2, and low lamin B1 level⁴⁸. Loss of lamin B1 leads to nuclear blebs, while it has been reported that nuclear envelope rupture is dependent on p53⁴⁹. To gain further insight into the role of lamins and p53 mutations in nuclear regulation we evidenced in this study, it would be interesting to analyze nuclear adaption in response to prolonged confinement in other cancer cell lines of different origins, as well as in colorectal

cancer cell lines of higher grades, with no p53 mutation and/or exhibiting different levels of lamins expression.

Potential implications for drug resistance of cancer cells

The regulation of nuclear size identified in this study could have important consequences on resistance to classical chemotherapeutic treatment targeting proliferation. In addition, emerging pharmaceutical compounds specifically targeting nuclei size are currently under investigation (Nuclear Size Rectifiers⁵⁰). Deciphering the molecular pathways involved in such nuclear regulation and more specifically the inner nuclear membrane re-assembly post-mitosis^{51,52} could pave the way towards novel therapeutic strategies. Finally, our soft confiner is an ideal tool for identifying cancer drug targets as it allows users to test several conditions simultaneously.

Material and methods

Cell culture

HT-29 wild type colorectal adenocarcinoma cells were purchased from the ATCC (HT29 HTB-38). A stable cell line expressing NLS-mKate2 was established using the lentiviral vector IncuCyte® nuclight orange ($\lambda_{ex}=555\text{nm}$, $\lambda_{em}=584\text{nm}$): the cells were selected using puromycin according to the manufacturer protocol. The stable HT29 expressing Fucci (Cdt1-RFP and hGeminin-GFP) cell line was a gift from Dr. Toufic Renno's team (CRCL, Lyon, France).

All cells were cultured in Dulbecco's modified Eagle's medium (DMEM - Glutamax, Gibco™) supplemented with 10% heat-inactivated fetal bovine serum (FBS; PanBiotech™), 100 units/100µg penicillin/streptomycin (Gibco™). Routinely, all HT-29 cell lines were grown in T-25 cell culture flasks and kept at 37°C and under 5% CO₂. Culture medium was changed regularly, and cell passage was carried out at 70% confluency. Cell lines were tested for Mycoplasma every 6 months and the tests were negative.

Drug treatments

The following pharmacological inhibitors and chemical compounds were used: Blebbistatin (Tocris™) at a final 100 µM concentration.

To inhibit cell contractility before confinement, we added 500µL of medium with 100µM blebbistatin 1h prior confinement.

To inhibit cell's contractility after confinement, 500 µL of medium solution with 200 µM of Blebbistatin was added following the confinement (to reach a final concentration within the confiner of 100 µM). Initial rinsing after confinement was also made with medium containing Blebbistatin at 100 µM.

Multi-height micro-milled mold fabrication

The height of the micropillars (from 9 μm to 3 μm) determines the level of spatial confinement of cells. The array presents regularly distributed pillars (distance between each pillar of 800 μm) with specific shapes according to their height: the “o” shape for 9 μm ; the “-” shape for 7 μm ; the “L” shape for 5 μm ; the “+” shape for 3 μm . The field of pillars is surrounded by a solid band of 3.5 mm to stabilize the structure, and two external notches to enable the proper positioning during molding. The pillars were drawn using Autodesk software and the mold was created using the CNC Mini-Mill/GX on brass.

Microfabrication-based confinement of cell populations

Cell confinement was performed using the agarose-based soft cell confiner methods previously described²⁰ and now available as Agarsqueezer (<https://www.idylle-labs.com/agarsqueezer-by-softconfiner>). All cell lines were seeded in the systems overnight before confinement on glass coverslips previously coated with fibronectin 50 $\mu\text{g}/\text{mL}$ (Sigma-Aldrich™) (1h incubation in the system at room temperature and washed 3 times with PBS). All the cell lines were seeded at the same intermediate cell density level: 500 μL of a cell solution at 180,000cells/mL.

Agarose molding

Based on the procedure described in Prunet et al.²⁰, molding was adapted to obtain accurate agarose-replicates from the newly developed multi-height brass mold. First, a solution of agarose diluted in distilled water (2% (w/v)) was prepared by autoclaving at 120 °C for 10 min, or 30s microwave (1000 W). All the following steps were performed under a sterile culture hood, and the polycarbonate (PC) holder was UV sterilized before use (20 min on each side under 24W, 365 nm). 400 μL of the prepared agarose solution was deposited in the prewarmed PC holder (placed on a hot plate at 75°C) and was left at room temperature for 5 min to let it gel. Then, 500 μL of the prepared agarose solution was deposited on the prewarmed micro-milled brass mold (on the same hot plate temperature) with the PC holder and placed under the press (Supplementary Fig. 5). The press generates a uniform pressure and ensures the contact between the PC holder and the mold, to ensure proper molding and resolute pillars. After 30 min under press at room temperature, the PC holder was gently removed from the brass mold. Evenly distributed holes were drilled into the gel using a 20G and 16G puncher and through holes present on the PC holder. In total, five 16G holes and four 20G holes were done. The molded agarose gel was then placed in sterile PBS and sterilized under UV light (20 min on each side). The molded agarose can be stored in its PC holder at 4°C in PBS until further use. It was replaced either by culture medium or by drug treatment and incubated at 37 °C at least 12h before the confinement experiment.

Immunostaining

During confinement, cells were fixed *in situ* with paraformaldehyde (PFA): cell culture medium was removed, and cells were washed twice with PBS. 4% PFA (Electron Microscopy Sciences™) was added and incubated for 40 min at RT. After incubation, samples were rinsed with PBS - 3% BSA (Sigma-Aldrich™) (3x20min). The agarose gel is then removed and cells were permeabilized using 0.5% Triton X-100 (Acros Organics™) for 10 min at RT. After blocking with PBS - 3% BSA (3*5min) to inhibit non-specific binding of antibodies, cells were incubated overnight at 4°C with primary antibodies diluted in PBS - 2% BSA - 0.1% Triton X-100. After 3x5min washes with PBS, samples were incubated with secondary antibodies for 2 h at RT. The primary antibodies used were: p-MLC (Cell signaling™ at 1/50); LaminA/C (Santa Cruz Biotechnology™ at 1/100), γ H2Ax (Santa Cruz Biotechnology™ at 1/200). NucGreen™ Dead 488 (Invitrogen™, 1 drop per 3 ml in PBS); Alexa 647 Phalloidin (Invitrogen™ at 1/500); Alexa 555 Phalloidin (Invitrogen™ at 1/500) were also used. The secondary antibodies used were: Anti-Mouse 647 (Invitrogen™ at 1/500); anti-rabbit 647 (Invitrogen™ at 1/500), anti-mouse 555 (Invitrogen™ at 1/500). Coverslips were then mounted using 2 drops of Fluoroshield™ (Sigma-Aldrich™) and varnish-sealed after overnight hardening at room temperature.

Confocal fluorescence microscopy

Fixed samples were visualized using a Leica SP5 confocal microscope with a 20x Dry objective (NA = 0.65), a 40x oil immersion (NA = 1.25), a 40x Dry (NA = 0.95) or a 63x oil immersion (NA = 1.25) objectives. Images were collected in sequential mode using averaging at a resolution of 1024x1024. Z-stacks of cells were acquired to precisely measure the height of confinement and nuclear volumes ($dz = 0.2 \mu\text{m}$ or $0.5 \mu\text{m}$ for each stack).

Epifluorescence imaging

Fixed samples were also visualized using an inverted microscope Leica DMI8 using epifluorescence microscopy with a 40x dry objective (NA = 0.55).

Live-cell imaging

Cells were observed with an inverted microscope Leica DMI8 using epifluorescence imaging. Timelapse imaging was performed for 2 to 5 days in a controlled environment (CO_2 , temperature, and humidity), using a 20x dry objective (NA = 0.65). A motorized x-y stage enabled the concomitant recording of up to 20 regions for each system every 10 min.

Quantitative image analysis

Cell height, nuclear area, and volume were assessed with a homemade routine workflow using both ImageJ/Fiji and MATLAB® software. First, after applying a gaussian blur on nuclei-stained images, nuclei were automatically detected either using the stardist Fiji plugin⁵³ or

using the Otsu's threshold detection directly in Matlab[®]. Mask and labeled images obtained were exported in Matlab[®] to perform automated morphological analyses on individual pre-labeled nuclei. The Z-plot profile of ImageJ/Fiji was used on orthogonal views of both nuclei and phalloidin staining to obtain nuclear and cell heights, respectively. Codes are available upon request.

For the nuclear area, at least four different areas were imaged and analysed per conditions.

DNA compaction was determined by measuring the fluorescence intensity levels of NucGreen –a DNA intercalant – on an inverted epifluorescence microscope (Leica DMI8), and normalized by the height of nuclei.

Proportion analysis of nuclear blebs both in live and fixed experiments was conducted using the cell counter plugin of ImageJ/Fiji. To further characterize the nuclear blebbing phenotype, labeled images of nuclei and their blebs were obtained using the stardist Fiji plugin⁵³ (blebs are automatically extracted from the main nuclei using stardist) We filtered the core nucleus and their blebs based on their respective area. If the area of an object was below 100 μm^2 for confined conditions, it was considered to be a bleb.

DNA damage analysis was automatically performed using the Find Maxima tool within each nucleus in ImageJ/Fiji.

The percentage of **positive nuclear envelope area** corresponds to the excess area of the lamina envelope compared to the nuclear area. This parameter was derived from methods used in^{15,54}. The nuclear envelope-positive area was assessed by thresholding the maximum intensity projection images of lamin A/C staining obtained by confocal microscopy (x63 objective NA 1.25, Leica SP5) and merging them with nuclei masks. This allowed us to study the laminas within the nucleus and provided information on the proportion of area with laminas within the nucleus (positive area).

Live movies were analyzed manually by using either MTrackJ, or manual tracking and ROI manager tool in ImageJ/Fiji plugin. Thus, we could measure nuclear areas over time in each phase of the cell cycle and the corresponding duration of those phases.

For each experiment, at least three different areas within each confined zone of the confiner were analyzed.

Statistics and reproducibility of experiments

Statistical data were expressed as mean \pm standard deviation unless mentioned otherwise. Sample size (n) and the number of repetitions (N) are specified in the text of the paper or figure legends. The statistical significance between experimental conditions was determined using a two-tailed unpaired t-test, Welch's test, Mann-Whitney test, or ANOVA after

confirming that the data met appropriate assumptions (normality distribution, homogeneous variance, and independent sampling). All data were analyzed with GraphPad Prism 8.0. (San Diego, CA, USA). **** P < 0.0001, *** P < 0.001, ** P < 0.01, * P < 0.05.

Supplementary Material 1 – Geometrical model

Confined nuclei can be modeled as a cylinder. Thus, their surfaces were calculated using the following equations.

$$2\pi R_1 h + 2\pi R_1^2 = S_{app} \quad (\text{Equation 1})$$

With R_1 , the diameter of the nucleus, h , its height, and S_{app} , its apparent surface.

R_1 , the radius of this cylinder can then be extracted:

$$R_1^2 + R_1 h - \frac{S_{app}}{2\pi} = 0 \quad (2)$$

With a positive solution:

$$R_1 = \frac{-h + \sqrt{\Delta}}{2} \quad (4)$$

To compute the nuclear-envelope surface to add during division, we first calculated the surface of the mother cell using equation 1 and then its volume. Using the obtained volume and equation 1 for two cells, we finally computed the surface of the two daughter cells. For non-confined cells, we used a similar approach with spheres rather than cylinders.

References

1. Butcher, D. T., Alliston, T. & Weaver, V. M. A tense situation: forcing tumour progression. *Nat. Rev. Cancer* **9**, 108–22 (2009).
2. Helmlinger, G., Netti, P. A., Lichtenbeld, H. C., Melder, R. J. & Jain, R. K. Solid stress inhibits the growth of multicellular tumor spheroids. *Nat. Biotechnol.* **15**, 778–783 (1997).
3. Jain, R. K., Martin, J. D. & Stylianopoulos, T. The role of mechanical forces in tumor growth and therapy. *Annu. Rev. Biomed. Eng.* **16**, 321–46 (2014).
4. Mohammadi, H. & Sahai, E. Mechanisms and impact of altered tumour mechanics. *Nat. Cell Biol.* **20**, 766–774 (2018).
5. Sheridan, C. Pancreatic cancer provides testbed for first mechanotherapeutics. *Nat. Biotechnol.* **37**, 829–831 (2019).
6. Mpekris, F. *et al.* Combining microenvironment normalization strategies to improve cancer immunotherapy. *Proc. Natl. Acad. Sci.* **117**, 3728–3737 (2020).
7. Friedl, P., Wolf, K. & Lammerding, J. Nuclear mechanics during cell migration. *Curr. Opin. Cell Biol.* **23**, 55–64 (2011).
8. Nader, G. P. de F. *et al.* Compromised nuclear envelope integrity drives TREX1-dependent DNA damage and tumor cell invasion. *Cell* **184**, 5230-5246.e22 (2021).
9. Tse, H. T. K., Weaver, W. M. C. & Carlo, D. Increased asymmetric and multi-daughter cell division in mechanically confined microenvironments. *PLoS ONE* **7**, 1–8 (2012).
10. Lancaster, O. M. *et al.* Mitotic Rounding Alters Cell Geometry to Ensure Efficient Bipolar Spindle Formation. *Dev. Cell* **25**, 270–283 (2013).
11. Moriarty, R. A. & Stroka, K. M. Physical confinement alters sarcoma cell cycle progression and division. *Cell Cycle* **17**, 2360–2373 (2018).
12. Gupta, V. K. & Chaudhuri, O. Mechanical regulation of cell-cycle progression and division. *Trends Cell Biol.* **32**, 773–785 (2022).
13. Aureille, J. *et al.* Nuclear envelope deformation controls cell cycle progression in response to mechanical force. *EMBO Rep.* **20**, 1–11 (2019).
14. Dantas, M., Oliveira, A., Aguiar, P., Maiato, H. & Ferreira, J. G. Nuclear tension controls mitotic entry by regulating cyclin B1 nuclear translocation. *J. Cell Biol.* **221**, e202205051 (2022).
15. Lomakin, A. J. *et al.* The nucleus acts as a ruler tailoring cell responses to spatial constraints. *Science* **370**, eaba2894 (2020).
16. Venturini, V. *et al.* The nucleus measures shape changes for cellular proprioception to control dynamic cell behavior. *Science* **370**, eaba2644 (2020).
17. Raab, M. *et al.* ESCRT III repairs nuclear envelope ruptures during cell migration to limit DNA damage and cell death. *Science* **352**, 359–362 (2016).

18. Xia, Y. *et al.* Rescue of DNA damage after constricted migration reveals a mechano-regulated threshold for cell cycle. *J. Cell Biol.* **218**, 2542–2563 (2019).
19. Srivastava, N. *et al.* Nuclear fragility, blaming the blebs. *Curr. Opin. Cell Biol.* **70**, 100–108 (2021).
20. Prunet, A. *et al.* A new agarose-based microsystem to investigate cell response to prolonged confinement. *Lab. Chip* **20**, 4016–4030 (2020).
21. Charras, G. T., Coughlin, M., Mitchison, T. J. & Mahadevan, L. Life and Times of a Cellular Bleb. *Biophys. J.* **94**, 1836–1853 (2008).
22. Maclejewski, J. & Hatch, E. M. Nuclear Membrane Rupture and Its Consequences. *Annu. Rev. Cell Dev. Biol.* **36**, 85–114 (2020).
23. Le Berre, M., Aubertin, J. & Piel, M. Fine control of nuclear confinement identifies a threshold deformation leading to lamina rupture and induction of specific genes. *Integr. Biol. U. K.* **4**, 1406–1414 (2012).
24. Vargas, J. D., Hatch, E. M., Anderson, D. J. & Hetzer, M. W. Transient nuclear envelope rupturing during interphase in human cancer cells. *Nucl. Austin Tex* **3**, 88–100 (2012).
25. Chow, K.-H., Factor, R. E. & Ullman, K. S. The nuclear envelope environment and its cancer connections. *Nat. Rev. Cancer* **12**, 196–209 (2012).
26. Stylianopoulos, T., Munn, L. L. & Jain, R. K. Reengineering the Physical Microenvironment of Tumors to Improve Drug Delivery and Efficacy: From Mathematical Modeling to Bench to Bedside. *Trends Cancer* **4**, 292–319 (2018).
27. Pennacchio, F. A. *et al.* Force-biased nuclear import sets nuclear-cytoplasmic volumetric coupling by osmosis. 2022.06.07.494975 Preprint at <https://doi.org/10.1101/2022.06.07.494975> (2022).
28. Andreu, I. *et al.* Mechanical force application to the nucleus regulates nucleocytoplasmic transport. *Nat. Cell Biol.* **24**, 896–905 (2022).
29. Elosgui-Artola, A. *et al.* Force Triggers YAP Nuclear Entry by Regulating Transport across Nuclear Pores. *Cell* **171**, 1397-1410.e14 (2017).
30. Mistriotis, P. *et al.* Confinement hinders motility by inducing RhoA-mediated nuclear influx, volume expansion, and blebbing. *J. Cell Biol.* **218**, 4093–4111 (2019).
31. Rosenblatt, J., Cramer, L. P., Baum, B. & McGee, K. M. Myosin II-Dependent Cortical Movement Is Required for Centrosome Separation and Positioning during Mitotic Spindle Assembly. *Cell* **117**, 361–372 (2004).
32. Straight, A. F. *et al.* Dissecting Temporal and Spatial Control of Cytokinesis with a Myosin II Inhibitor. *Science* **299**, 1743–1747 (2003).
33. Shah, P. *et al.* Nuclear Deformation Causes DNA Damage by Increasing Replication Stress. *Curr. Biol.* **31**, 753-765.e6 (2021).
34. Pfeifer, C. R. *et al.* Constricted migration increases DNA damage and independently represses cell cycle. *Mol. Biol. Cell* **29**, 1948–1962 (2018).

35. Shah, P., Wolf, K. & Lammerding, J. Bursting the Bubble – Nuclear Envelope Rupture as a Path to Genomic Instability? *Trends Cell Biol.* **27**, 546–555 (2017).
36. Uhler, C. & Shivashankar, G. V. Regulation of genome organization and gene expression by nuclear mechanotransduction. *Nat. Rev. Mol. Cell Biol.* **18**, 717–727 (2017).
37. Gonzalez-Suarez, I. *et al.* Novel roles for A-type lamins in telomere biology and the DNA damage response pathway. *EMBO J.* **28**, 2414–2427 (2009).
38. Huang, R.-X. & Zhou, P.-K. DNA damage response signaling pathways and targets for radiotherapy sensitization in cancer. *Signal Transduct. Target. Ther.* **5**, 1–27 (2020).
39. Mattout-Drubezki, A. & Gruenbaum, Y. Dynamic interactions of nuclear lamina proteins with chromatin and transcriptional machinery. *Cell. Mol. Life Sci. CMLS* **60**, 2053–2063 (2003).
40. Patil, S. & Sengupta, K. Role of A- and B-type lamins in nuclear structure–function relationships. *Biol. Cell* **113**, 295–310 (2021).
41. Rollin, R., Joanny, J.-F. & Sens, P. Cell size scaling laws: a unified theory. *BioRxiv* 20220801502021 1–20 (2022).
42. Jevtić, P. & Levy, D. L. Mechanisms of Nuclear Size Regulation in Model Systems and Cancer. in *Cancer Biology and the Nuclear Envelope* (eds. Schirmer, E. C. & de las Heras, J. I.) vol. 773 537–569 (Springer New York, 2014).
43. de Las Heras, J. I. & Schirmer, E. C. The nuclear envelope and cancer: a diagnostic perspective and historical overview. *Adv. Exp. Med. Biol.* **773**, 5–26 (2014).
44. Willis, N. D. *et al.* Lamin A/C is a risk biomarker in colorectal cancer. *PloS One* **3**, e2988 (2008).
45. Friedl, P., Wolf, K. & Lammerding, J. Nuclear mechanics during cell migration. *Curr. Opin. Cell Biol.* **23**, 55–64 (2011).
46. Bell, E. S. *et al.* Low lamin A levels enhance confined cell migration and metastatic capacity in breast cancer. *Oncogene* **41**, 4211–4230 (2022).
47. Zoetemelk, M., Rausch, M., Colin, D. J., Dormond, O. & Nowak-Sliwinska, P. Short-term 3D culture systems of various complexity for treatment optimization of colorectal carcinoma. *Sci. Rep.* **9**, 7103 (2019).
48. Kuga, T. *et al.* Lamin B2 prevents chromosome instability by ensuring proper mitotic chromosome segregation. *Oncogenesis* **3**, e94 (2014).
49. Yang, Z., Maciejowski, J. & de Lange, T. Nuclear Envelope Rupture Is Enhanced by Loss of p53 or Rb. *Mol. Cancer Res.* **15**, 1579–1586 (2017).
50. Schirmer, E. C., Latonen, L. & Tollis, S. Nuclear size rectification: A potential new therapeutic approach to reduce metastasis in cancer. *Front. Cell Dev. Biol.* **10**, 1022723 (2022).
51. Gorjánác, M. Nuclear assembly as a target for anti-cancer therapies. *Nucl. Austin Tex* **5**, 47–55 (2014).

52. Rose, M., Burgess, J. T., O'Byrne, K., Richard, D. J. & Bolderson, E. The role of inner nuclear membrane proteins in tumourigenesis and as potential targets for cancer therapy. *Cancer Metastasis Rev.* **41**, 953–963 (2022).
53. Schmidt, U., Weigert, M., Broaddus, C. & Myers, G. Cell Detection with Star-Convex Polygons. in *Medical Image Computing and Computer Assisted Intervention – MICCAI 2018* (eds. Frangi, A. F., Schnabel, J. A., Davatzikos, C., Alberola-López, C. & Fichtinger, G.) 265–273 (Springer International Publishing, 2018). doi:10.1007/978-3-030-00934-2_30.
54. Purushothaman, D. *et al.* The transcription factor PREP1(PKNOX1) regulates nuclear stiffness, the expression of LINC complex proteins and mechanotransduction. *Commun. Biol.* **5**, 1–14 (2022).

Acknowledgment

This work was supported by ANR Institut Convergence Plascan, the Institut Universitaire de France (IUF) and the ARC for part of M. Mouelhi salary. The authors would like to acknowledge C. Chaveroux, Marie Piecyk, C. Duret (CRCL) and S. Joly for the transfection and selection of HT-29-FUCCI cell line, R. Fulcrand for the preparation of 5- μm wafer molds, M. Mercury for the microscope holder and the press. G. Jardiné for his help to compute nuclear volume of control cells, B. Manship for English editing of the manuscript, as well as M. Piel for fruitful discussions of our results and careful reading of the manuscript.

Author contribution

S.M. and C.R. contributed equally to this work. S.M and C.R. supervised the project. M.M., S.M. and C.R. designed the research. M.M., A.S. performed the experiments. M.M., H.A. performed the modeling. M.M., A.S., S.M. and C.R. analyzed the data. M.M., S.M. and C.R. wrote the manuscript. All authors helped to edit the manuscript.

Supplementary Figures

Supplementary Figure 1

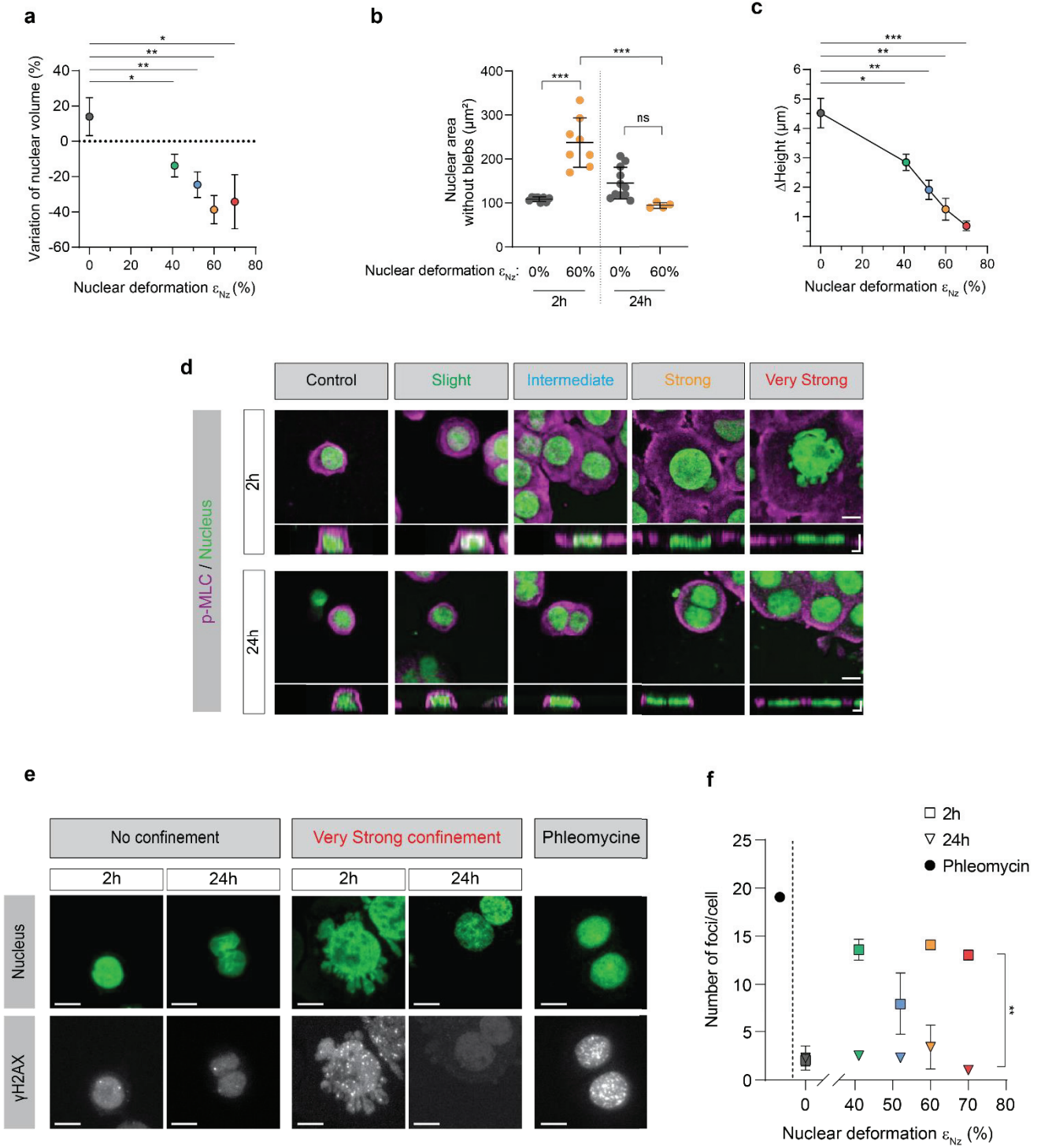


Figure 28: Supplementary Fig. 1

(a) Variation of nuclear volume between 2 h and 24 h according to the nuclear deformation (which correspond to the height of the confinement). *N = 3 experiments with $n > 5,000$ cells/experiment, unpaired t-test.* **(b)** Scatter plot of nuclear area without the blebs at 2 h and 24 h without confinement or under strong confinement. *N = 3 experiments with $n = 31$ cells, unpaired t-test.* **(c)** The difference in height between the nucleus and its cell membrane under increasing nuclear deformation. *N = 3 experiments with $n > 5,000$ cells/experiment.* **(d)** Representative images of stained nuclei and p-MLC in XY (scale bar = 10 μm) and its orthogonal view under increasing confinement (scale bar = 5 μm). **(e)** Representative images of nuclei and DNA damage, shown by stained γH2AX foci. Phleomycin is a drug that induces DNA damage used here as a positive control. *Scale bar = 10 μm .* **(f)** Quantification of the number of foci/cell, representative of the DNA damages according to an increase in nuclear deformation. *N = 2 experiments with $n > 2000$; mean \pm SEM; unpaired t-test. Ordinary one-way ANOVA was also performed on all 24 h confinement conditions and was no significant.*

Supplementary Figure 2

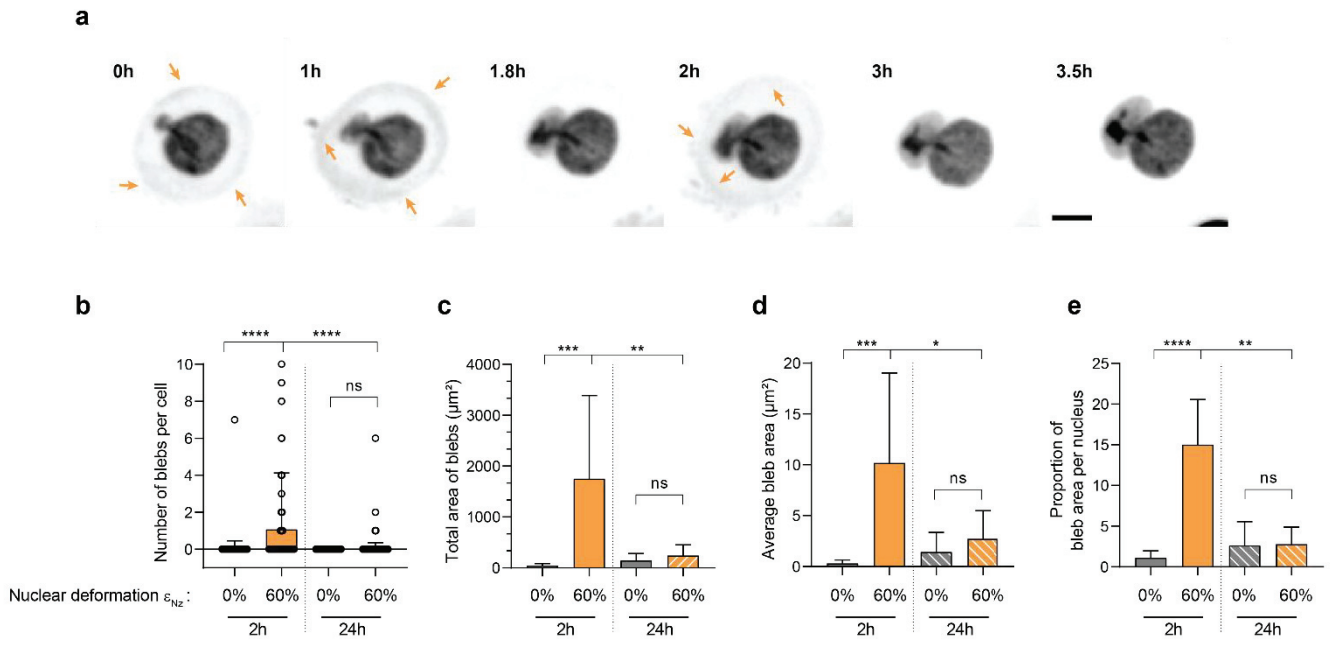


Figure 29: Supplementary Fig. 2

(a) Sequential images of HT-29 cell expressing NLS-mKate2 under strong confinement. Arrows show NLS-mKate2 dye leakage within the cytoplasm indicating nuclear membrane rupture. *Scale bar = 10 μm .* **(b)** Bar chart of the number of blebs per cell according to the nuclear deformation (0% or 60%) at 2 h or 24 h of confinement. *$N = 3$ experiments with $n = 1,376$ cells, unpaired t -test.* **(c)** Quantification of the total area of blebs without confinement or under strong confinement (60% nuclear deformation) between 2 h and 24 h. *$N = 3$ experiments with $n = 36$, Mann-Whitney test.* **(d)** Quantification of the average area of blebs without confinement or under high confinement (60% nuclear deformation) between 2 h and 24 h. *$N = 3$ experiments with $n = 36$, Mann-Whitney test.* **(e)** Proportion (in percentage) of bleb area per nucleus without confinement or under high confinement (60% nuclear deformation) between 2 h and 24 h. *$N = 3$ experiments with $n = 1,376$ cells, Kolmogorov-Smirnov test.*

Supplementary Figure 3

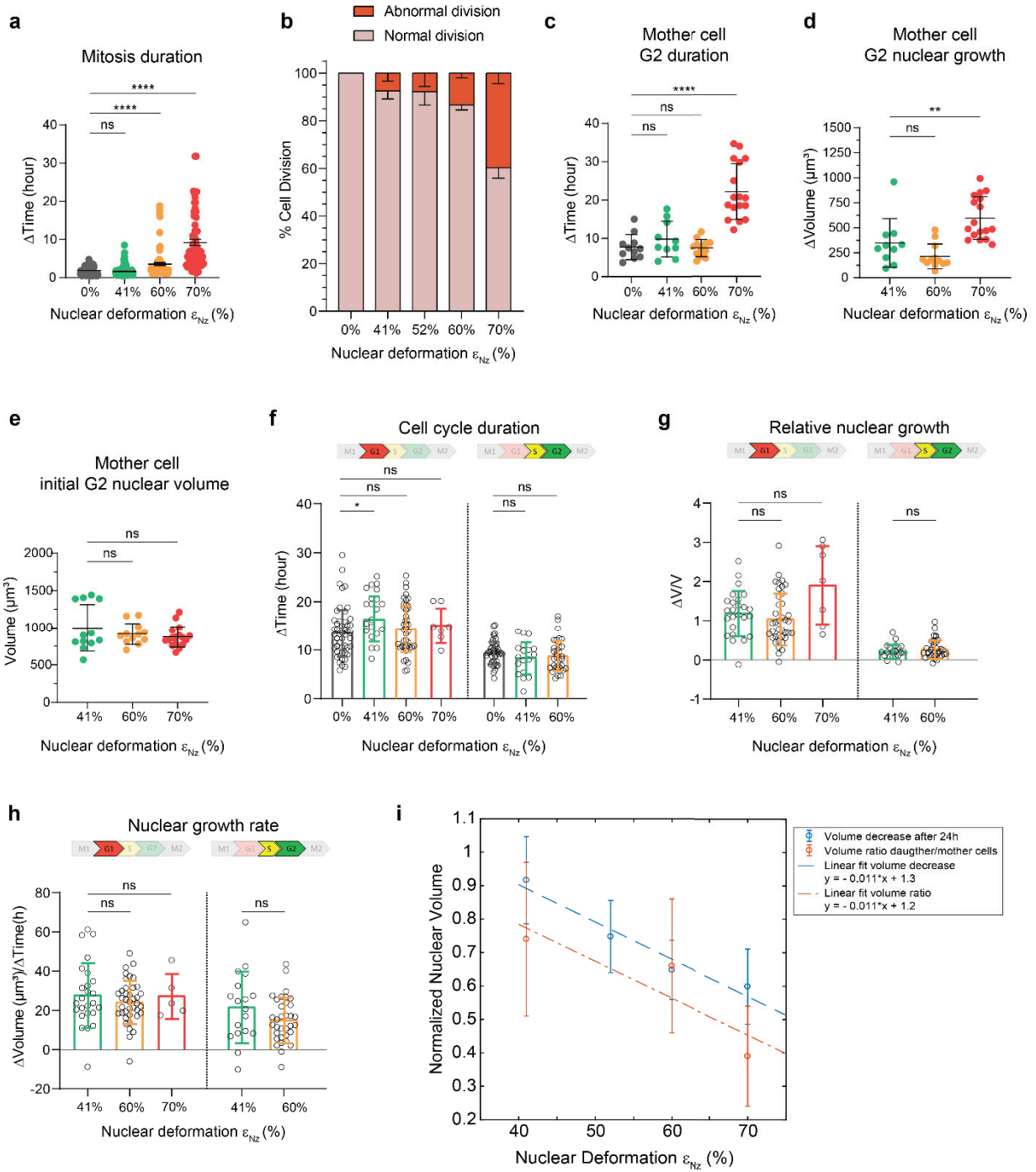


Figure 30: Supplementary Fig. 3

(a) Scatter plot of mitosis duration under confinement. $N = 3$ experiments with $n = 398$ cells; mean \pm SEM, Mann-Whitney test. **(b)** Percentage of normal or abnormal (multi-daughter cells and unevenly sized daughter cells) cell division under increasing confinement. $N = 2$ experiments with $n = 477$ cells. **(c)** Time of the mother cell spent in the G2-phase under confinement. $N = 2$ experiments with $n = 50$ cells, unpaired t -test. **(d)** Growth of mother cell nuclear volume in the G2-phase under different levels of confinement. $N = 2$ experiments with $n = 39$ cells, Mann-Whitney test. **(e)** Scatter plot of the initial nuclear volume of mother cells at the entrance of the G2 phase, $N = 2$ experiments with $n = 41$ cells, unpaired t -test. **(f, g, h)** Quantification of the duration **(f)**, the relative nuclear growth **(g)** and the nuclear growth rate **(h)** of HT-29 cell expressing Fucci under confinement during the G1-phase and the S-G2-phase after the first cell division. $N = 2$ experiments with $n > 200$ cells, unpaired t -test for **(f, h)** and Mann-Whitney test for **(g)**. **(i)** Normalized nuclear volume decrease at 24 h of confinement and nuclear volume decrease after mitosis as a function of nuclear deformation and their respective linear fit.

Supplementary Figure 4

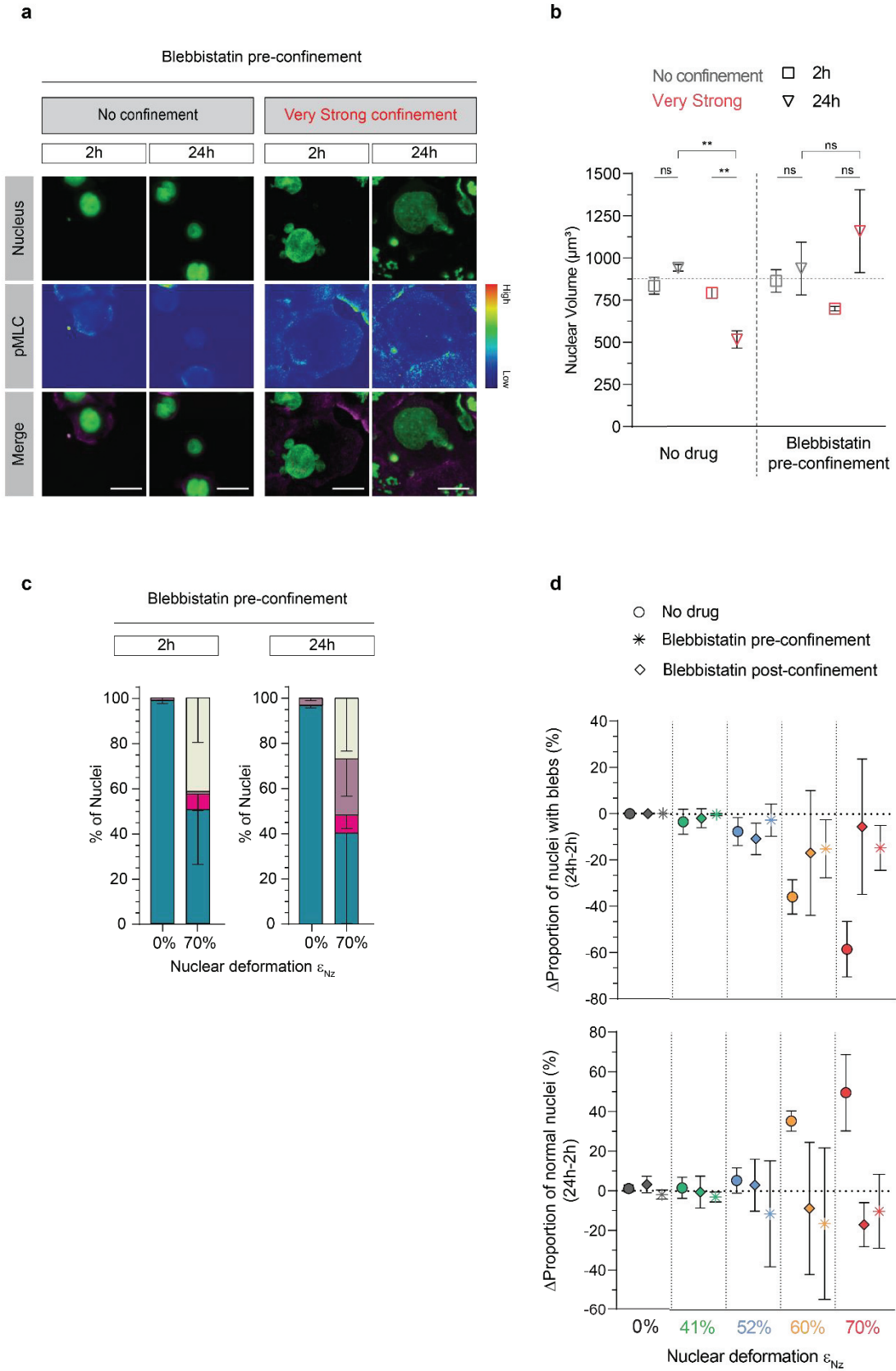


Figure 31: Supplementary Fig. 4

(a) Representative images of stained nuclei and phospho-Myosin Light Chain (p-MLC) with Blebbistatin – added before confinement – at 2 h and 24 h without confinement or under very strong confinement. *Scale bar = 20 μ m.* **(b)** Quantification of nuclear volume at 2 h and 24 h without drug or with Blebbistatin – added before confinement – without confinement or under very high confinement. *N = 3 experiments with n = 7,526 cells, mean \pm SEM, unpaired t-test (for no drug conditions) or Mann-Whitney test (for Blebbistatin conditions).* **(c)** Quantification of nuclei with blebs, dividing, apoptotic or normal without confinement or under very strong confinement at 2 h and 24 h, with Blebbistatin – added before confinement –. *N = 3 experiments with n = 7,526 cells.* **(d)** Difference in proportion of normal nuclei and nuclei with blebs between 2 h and 24 h under several conditions: without drug, with Blebbistatin added pre-confinement and with Blebbistatin added post-confinement. *N = 3 experiments with n > 10,000 cells.*

Supplementary Figure 5

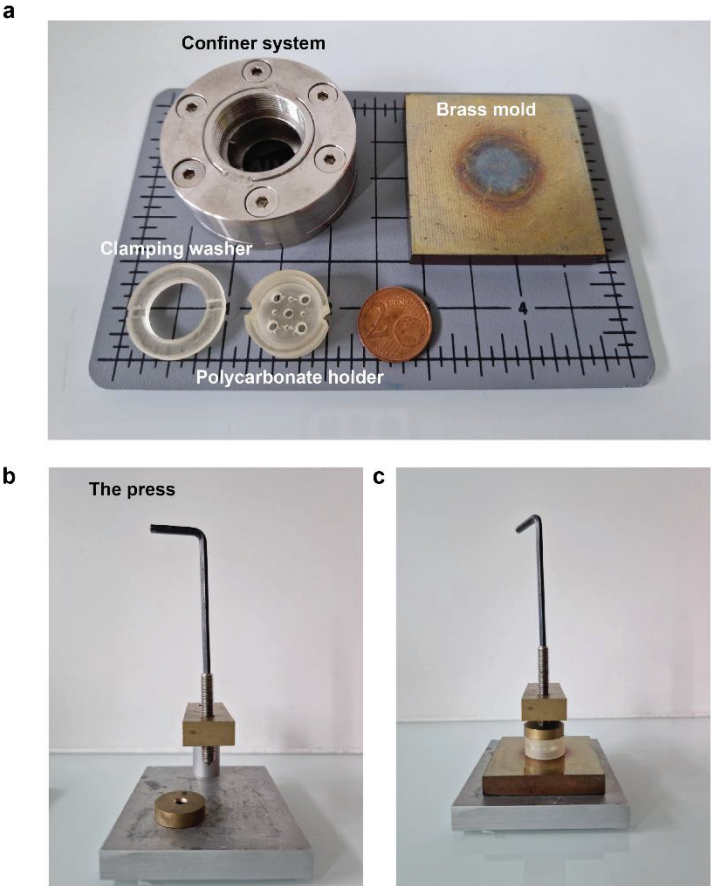


Figure 32: Supplementary Fig. 5

(a) Picture of the principal components of the confiner system and their name next to the brass mold.

(b) Picture of the press used to generate a uniform pressure during agarose molding. **(c)** Picture of the assembly process of agarose molding under press.

Supplementary Movies

Movie 1 - Example of abnormal divisions under very strong confinement

Movie 2 - Example of blebs disappearance after mitosis

Chapter 3

Long-term impact of 3D isotropic compression

« L'imprévisible est dans la nature même de l'entreprise scientifique. Si ce qu'on va trouver est vraiment nouveau, alors c'est par définition quelque chose d'inconnu à l'avance »

François Jacob

Content

ABSTRACT	129
INTRODUCTION.....	130
RESULTS	131
NUTRITIVE CULTURE CONDITIONS ARE CRUCIAL FOR CELL IDENTITY AND HIGHLIGHT CANCER CELLS PLASTICITY	131
GLUTAMINE STARVATION INDUCES METABOLIC STRESS	136
MECHANICAL STRESS DOES NOT INDUCE METABOLIC STRESS	139
ISOTROPIC COMPRESSION TRIGGERS DEDIFFERENTIATION OF COLORECTAL CANCER CELLS	141
SUPPLEMENTARY FIGURES.....	143
DISCUSSION AND PERSPECTIVES	147
MICROENVIRONMENT AFFECTS CELLULAR PLASTICITY	147
PUTATIVE MOLECULAR SIGNALING PATHWAYS INVOLVED IN THIS CSC-DRIVEN PLASTICITY.....	148
MECHANICAL STRESS MAY INCREASE CANCER CELL DRUG RESISTANCE AND TUMOR RELAPSE	149
TUMORS ARE AFFECTED BY SEVERAL TYPES OF MECHANICAL CONSTRAINTS.....	149
CONCLUSION	150
MATERIAL AND METHODS.....	151
CELL CULTURE	151
MULTICELLULAR TUMOR SPHEROIDS	152
AGAROSE MICROWELLS MICROFABRICATION	152
DEXTRAN OSMOTIC COMPRESSION	154
CONFOCAL FLUORESCENCE MICROSCOPY	154
LIVE-CELL IMAGING	154
RTqPCR.....	155
QUANTITATIVE IMAGE ANALYSIS.....	155
STATISTICS AND REPRODUCIBILITY OF EXPERIMENTS	156
REFERENCES	157

3D compression drives colorectal cancer cells toward stem-like phenotype independently of metabolic stress

Malèke Mouelhi^{1*}, Estelle Bastien¹, Stéphane Joly¹, Gaëtan Jardiné¹, Cédric Duret², Cédric Chaveroux², Charlotte Rivière^{1,3,4+*}, Sylvain Monnier^{1+*}

¹Univ Lyon, Université Claude Bernard Lyon 1, CNRS, Institut Lumière Matière, UMR 5306, 69622, Villeurbanne, France

²Centre de Recherche en Cancérologie de Lyon (CRCL), UMR INSERM 1052 CNRS 5286 - Centre Léon Bérard, France

³Institut Universitaire de France (IUF), France

⁴Institut Convergence PLAsCAN, Centre de Cancérologie de Lyon, INSERM U1052-CNRS UMR5286, Univ Lyon, Université Claude Bernard Lyon 1, Centre Léon Bérard, Lyon, France

*Senior author contributed equally to this work

*Corresponding authors

Abstract

During tumor progression, the tumor microenvironment evolves in response to pathological changes in the tissue and sustains tumor growth. Among these changes, increased stiffness of the extracellular matrix and the surrounding tissue alters cellular proliferation and metabolism, both of which have crucial consequences on therapy resistance. However, little is still known about this mechano-metabolic interplay in tumor progression and especially in the determination of cancer cell identity, at the origin of many treatments relapse. Here, we explore the influence of both glutamine starvation and compressive stress on HT-29 colorectal cancer spheroids. We find that nutritive culture conditions are crucial for cellular identity and that long-term glutamine starvation induces metabolic stress and dedifferentiation. We also observe that a compressive stress does not lead to metabolic stress but increases stemness marker in a glutamine-independent manner. Our results highlight the crucial role of mechanical constraints in inducing dedifferentiation of colorectal cancer cells in a 3D tumoral context. We anticipate our work to be a starting point to better understand the impact of mechanical environment on cancer cell identity and drug resistance.

Introduction

Colorectal cancer (CRC) is the third most common cancer worldwide according to the World Health Organization. In CRC, the crosstalk between malignant cells and the stromal part of the tumor plays a crucial role in the prognosis and the development of metastasis (Karlsson and Nyström, 2022). The stromal part of the tumor represents the tumor microenvironment and includes the non-malignant cells and an acellular part, called the extracellular matrix (ECM). The evolution of this microenvironment associated with tumor development induces changes in biochemical signals perceived by the cells but also changes in mechanical properties that influence the behavior of cancer cells, participating in tumor progression and therapy resistance (Madl and Heilshorn, 2018). Indeed, tumors are, in general, more rigid and generate and withstand mechanical stresses that can reach up to several kPa (Jain et al., 2014). These cancer cells are thus, subjected to different types of mechanical stresses that all have different implications and impacts depending on the tumor stage. These may include ECM remodeling, compressive stresses on the solid tumor, proliferation of cells in a confined environment (Nia et al., 2017), or shear stresses during metastatic cell escape (Butcher et al., 2009). Alleviating mechanical stress is now envisioned as an interesting therapeutic strategy (Sheridan, 2019). Mechanical stimuli could particularly affect a subpopulation of cancer cells sharing numerous properties with embryonic stem cells that are highly tumorigenic and thought to be responsible for tumor progression, resistance to therapies, and relapse (Paul et al., 2021). Indeed, these hierarchically organized cells called Cancer Stem Cells (CSC) have the ability to self-renew, differentiate into multiple lineages, and share common stem markers (Visvader and Lindeman, 2012). This subpopulation is highly plastic, as it has the capacity to change identity by undergoing a dedifferentiation process to adopt a new phenotype and new functions, and the tumor microenvironment can trigger the transition from CSC to non-CSC (ND et al., 2013). However, the contribution of the mechanical environment to the long-term fate of colorectal cancer cells remains poorly understood and the field is lacking *in-vitro* assays to assess the interplay between mechanobiology and CSCs in 3D in a more systematic manner (Roy Choudhury et al., 2019). On the other hand, there are also increasing evidence on the role of metabolic stresses on cancer cells phenotype, including their shift towards stem-like cells. Such metabolic stresses play a key role in cancer maintenance, metastasis formation, and resistance to therapy (Rinaldi et al., 2018).

To characterize the consequences of mechanical constraints on the tumor fate in an integrated manner, the challenge of this work was to mimic *in vitro*, on a 3D model tissue (HT-29 colorectal tumor spheroids), both the metabolic and physical constraints to which tumors are subjected *in vivo*. To this end, we combine metabolic and mechanical stresses using a recently published agarose-based microwell technique (Goodarzi et al., 2021; Riviere et al., 2018), to standardize and increase the production of tumor spheroids while controlling growth

conditions. As a proof-of-concept, metabolic stress was tuned by changing the concentration of glutamine, while the effect of mechanical stress was assessed using a dextran, a large polymer enabling the application of a mechano-osmotic stress on spheroids (Delarue et al., 2014; Montel et al., 2011). By combining quantitative measurements and real-time microscopy (timelapse), we show that the tumoral nutritive environment is of importance in the CSCs plasticity and fate with an increase of the Nanog stemness marker with a decrease in glutamine availability. Moreover, isotropic compression not only reduces spheroids growth over time but also triggers dedifferentiation of colorectal cancer cells, independently of glutamine starvation. The key interplay between the prolonged effect of nutrient and mechanical environment both influencing cancer cell identity has never been shown before. These changes are not without consequences and open new questions on the failure of current therapies to bring a complete cure to the largest number of colorectal cancer patients.

Results

Nutritive culture conditions are crucial for cell identity and highlight cancer cells plasticity

In order to characterize HT-29 cell line plasticity and the effect of culture medium, we cultured spheroids with either a classical rich medium or with a serum-free medium called “M11” (Relier et al., 2021, 2016), whose composition is detailed in Table 1. Spheroids were generated by self-aggregation of cells three days after cell seeding in agarose-based microwells (Figure 33a). First, spheroids growth was assessed using timelapse microscopy with the modified HT-29 cell line expressing Nanog-GFP. A similar growth curve was observed between spheroids grown in M11 and those grown in classical rich medium for the first 35 - 40 hours (Figure 34a, b). However, after 40h, spheroids grown in classical medium tend toward a plateau as opposed to M11 spheroids. Moreover, the density of fluorescence of Nanog is much higher for M11 cultured spheroids compared to classical rich medium (1.45 ± 0.07 compared to 1.2 ± 0.1 respectively, after 3 days, Figure 34b,c). In order to gain insights into the implications of such an increase of Nanog expression under M11 medium, we performed *in situ* immunostaining of spheroids grown for 3 days either in classical rich medium or in M11 medium. These experiments revealed a complete change in spheroids phenotype under M11. Indeed, phalloidin staining showed rounder cells, in a very loose tissue – probably due to the decrease of cell-cell adhesions – and the apparition of lumens within spheroids, similar to organoid-like structures (Figure 34d). These results corroborate live experiments as a diminution of spheroids circularity is observed approximatively at 35 - 40 h (Figure 34e). Intriguingly, this time matches the time where M11 spheroids start getting bigger than classical rich medium spheroids. That could be explained by the reduced tissue cohesion observed in Figure 34d. This increase in Nanog expression is also confirmed in 2D – using both RTqPCR and timelapse microscopy –

when a monolayer of HT-29 is cultured for 72h with M11 medium (Figure 35). Taken together, these results are in accordance with the fact that a serum-free medium enriched with growth factors favors the appearance and maintenance of a stem cell subpopulation during culturing and highlight the fact that nutritive culture conditions can set cellular identity.

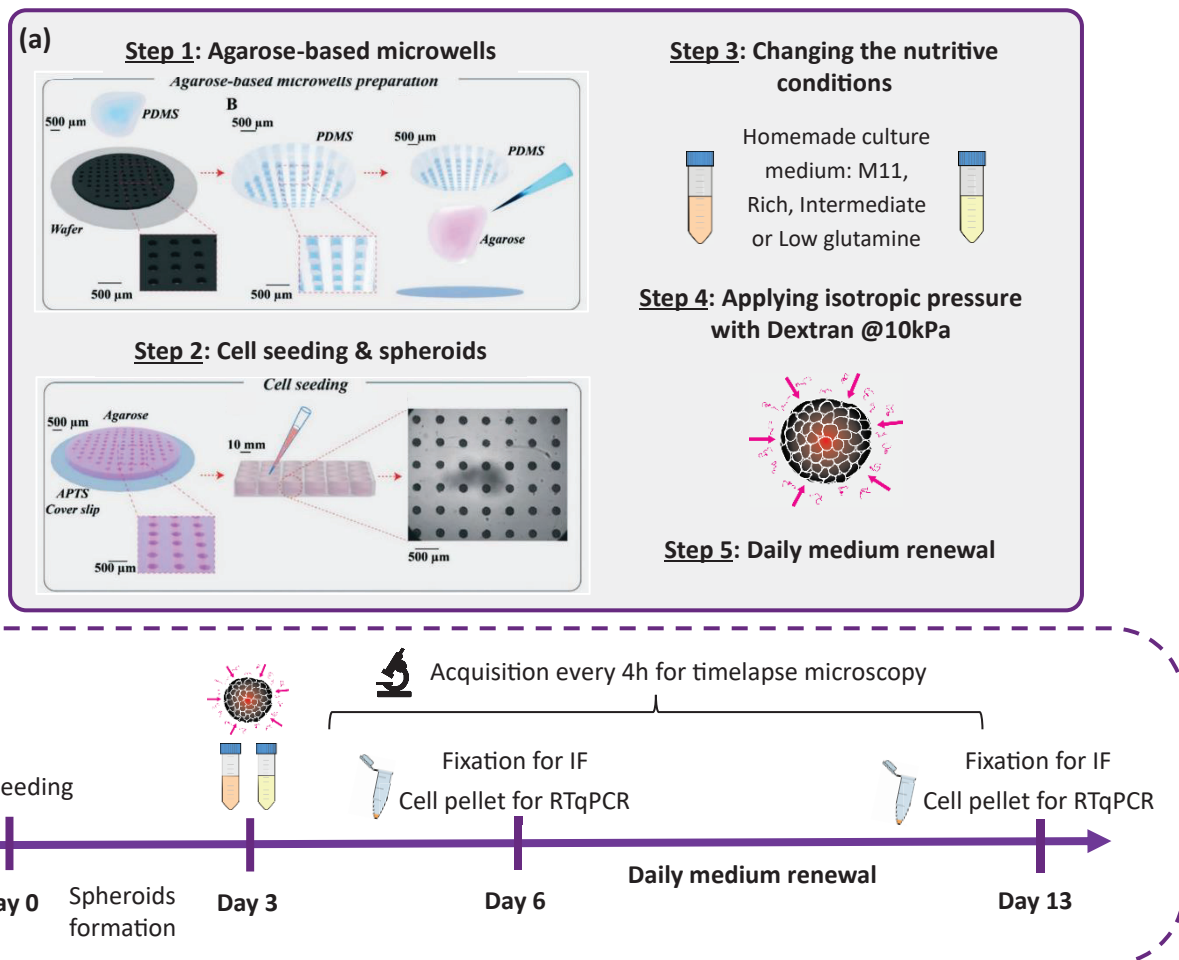


Figure 33: Experimental outlook and timeline.

(a) Description of the experimental procedure to generate in high-throughput 3D multicellular tumor spheroids (adapted from Goodarzi et al., 2021), and the following experimental steps to alter both metabolic (through changes in culture medium) and mechanical (via Dextran compression) environments. **(b)** Detailed experimental timeline from cell seeding to collecting samples.

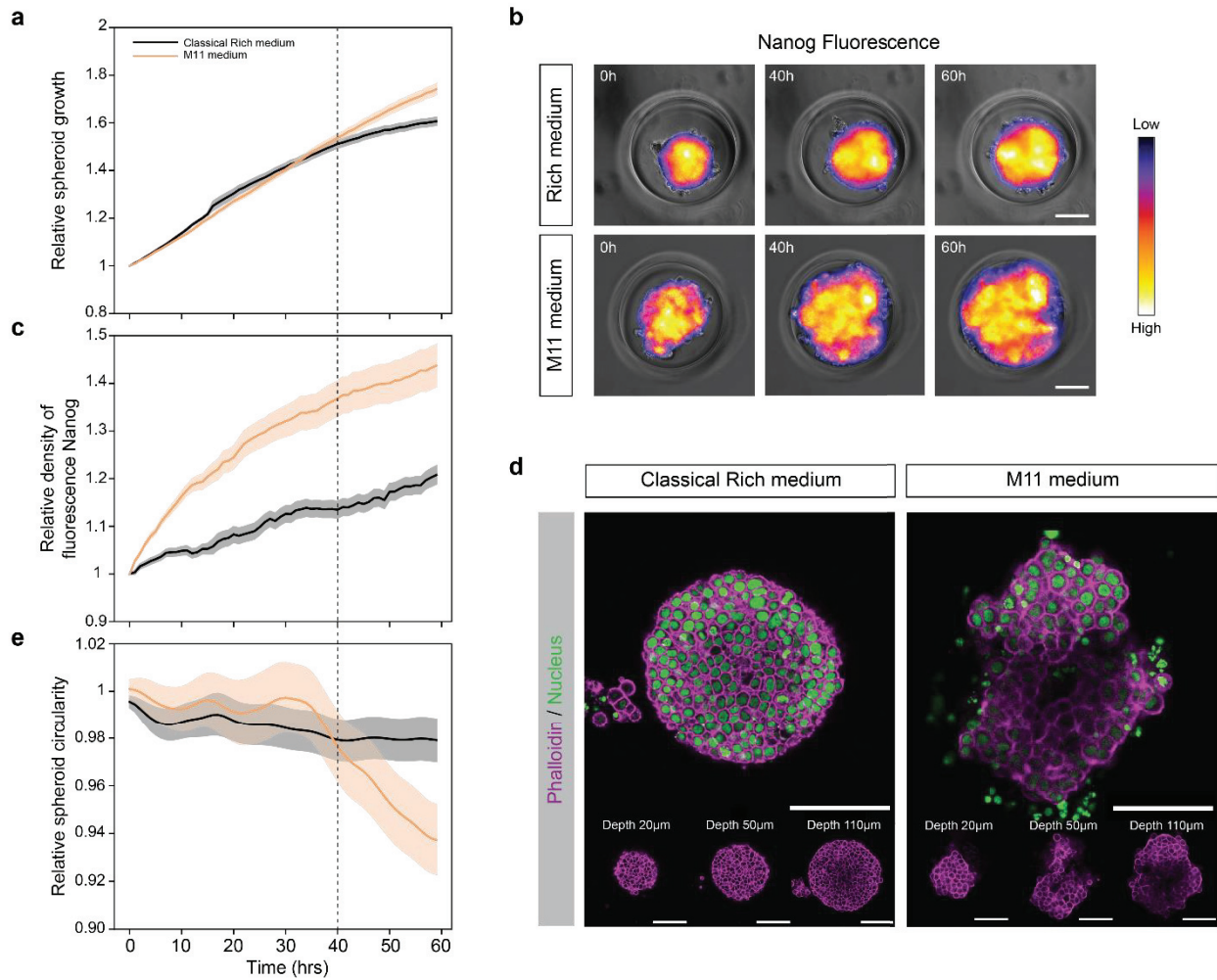


Figure 34: M11 medium modulates HT29 colorectal spheroids by resetting a new cellular identity.

(a) Quantification of spheroids growth over time under classical rich medium or M11, $N=2$ experiments. **(b)** Representative images of HT29-NanogGFP spheroids grown under classical rich medium or under M11, at different time. *Scale bar = 100 μ m*. **(c)** Quantification of the density of fluorescence of Nanog (intensity of fluorescence normalized by the size of the spheroid), under classical rich or M11 medium, $N=2$. **(d)** Confocal images of a spheroids grown under classical rich or M11 medium stained with NucGreen and Phalloidin. *Scale bar = 100 μ m*. **(e)** Evolution of spheroids circularity over time under classical rich or M11 medium, $N=2$.

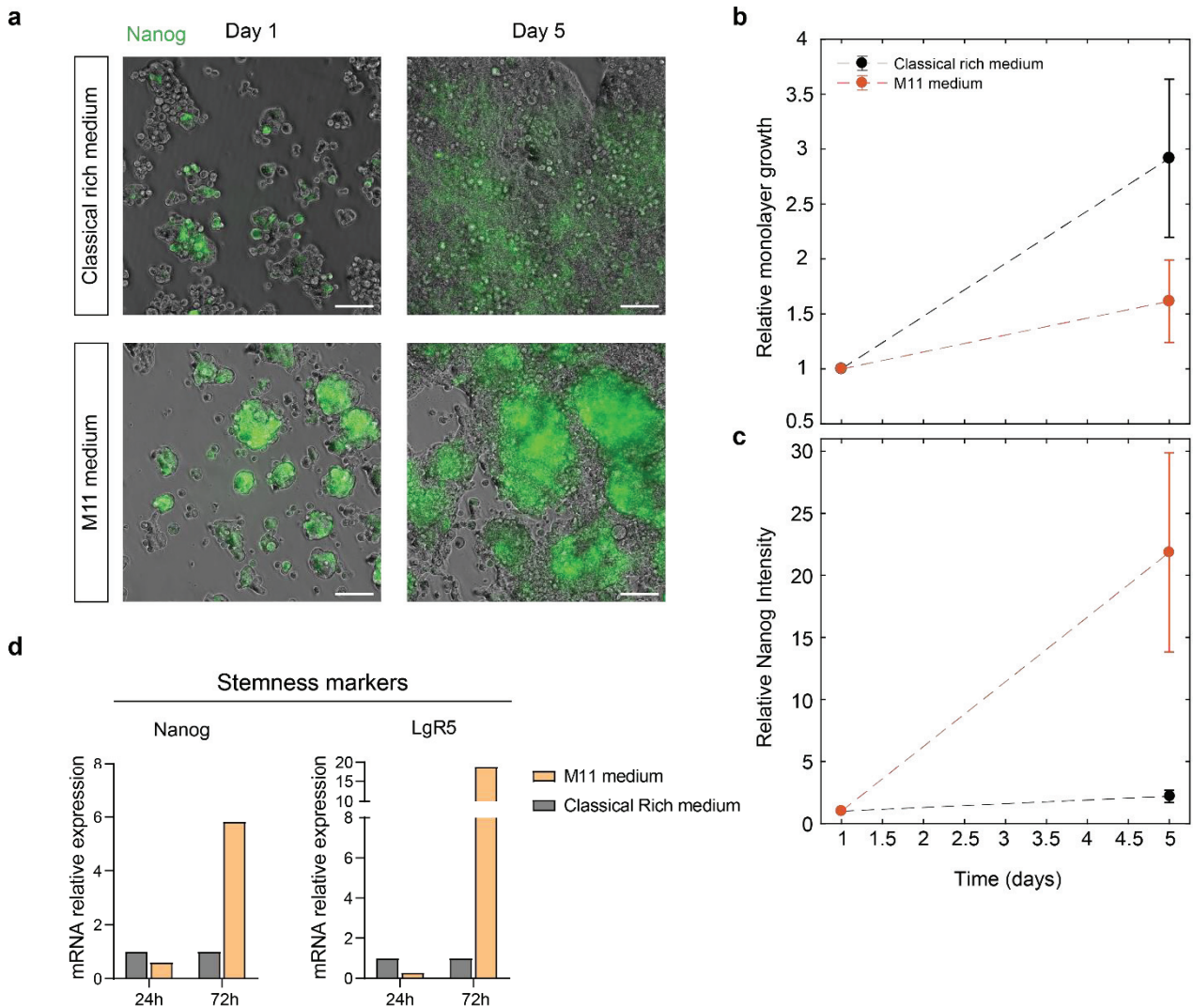


Figure 35: M11 medium has similar effect on 2D monolayer.

(a) Representative images of HT29 expressing Nanog-GFP monolayer grown under classical rich or M11 medium at 1 day and 5 days after seeding. *Scale bar = 100 μ m.* **(b)** Relative growth of HT29 monolayer grown under classical rich or M11 medium, $N=2$ experiments. **(c)** Relative Nanog fluorescence intensity of HT29 monolayer grown under classical rich or M11, $N=2$ experiments. **(d)** Level of mRNA expression of stemness makers genes (Nanog and LgR5) of HT29 monolayer grown either under classical rich medium or under M11, $N=1$ for now.

This prompted us to wonder if cancer cells keep the memory of their initial identity and if cellular plasticity can be controlled. For that, HT-29 cells have been cultured for several passages either in 2D, in classical adherent condition or in suspension (low attachment flask) with M11 medium. Then, when seeding, cells medium has been switched from classical rich medium to M11 or from M11 to classical rich medium. In parallel, single cells were seeded in agarose microwells as described in (Chambost et al., 2022, Figure 36 c) to assess cells ability to resist anoikis, a hallmark of CSC cells. Cell division, cell death and percentage of single cells that were able to make spheroids were assessed thanks to time-lapse imaging and machine learning automatic detection. Cells cultured in M11 and cells that passed from classical rich medium to M11 displayed a higher ability to make more spheroids (30%) compared to cells cultured in classical rich medium and cells that switched from M11 to classical rich medium (less than 10%, Figure 36a). These results confirm that serum-free condition promotes cells self-renewal capacities (Arab-Bafrani et al., 2016; Jäger et al., 2020), but especially their capacity to adapt quickly to their nutritive condition. It suggests that HT-29 cells are very plastic, and that they do not keep any memory of their previous state. Switching from classical rich medium to M11 medium seems to stimulate proliferation, as 60% of division happens 60 h after cell seeding (Figure 36b). Even if M11 and classical rich medium have the same amount of division, their dynamic over time is different and switching from M11 to classical rich medium seems to slow down cell division (only 10% division after 60 h, Figure 36b). Thus, taken together these results highlight the crucial role of nutritive culture condition in cell fate determination and plasticity.

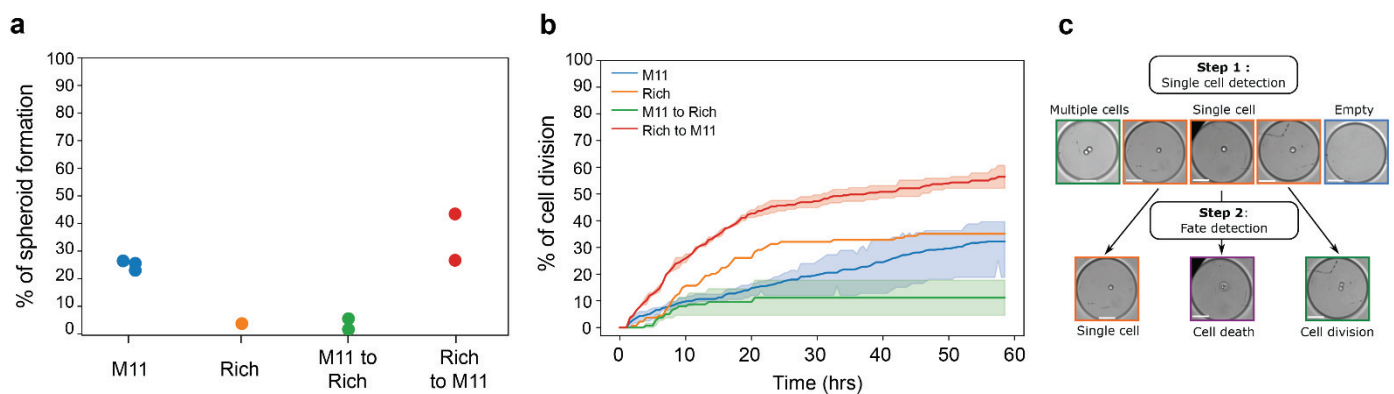


Figure 36: M11 medium favors spheroids formation in single cell assay.

(a) Percentage of formed spheroids after single cell assay under several medium conditions, ($N=1$). **(b)** Percentage of cell divisions over time for the same growing conditions ($N=1$). **(c)** Visual abstract of the single cell assay and its image analysis, from (Chambost et al., 2022).

Glutamine starvation induces metabolic stress

To reproduce the metabolic stress induced by the microenvironment that tumors undergo during their growth, tumor spheroids were cultivated under three conditions of medium with a decreasing concentration of the L-Glutamine amino acid. Glutamine is the most abundant amino acid in the blood and is a well-known nutrient involved in multiple aspects of cancer metabolism (Hensley et al., 2013). Glutamine intracellular signaling is essential for energy generation, redox homeostasis, and provides an important source of carbon, therefore promoting growth and cancer cell proliferation (Choi and Park, 2018; Windmueller and Spaeth, 1974). The gold standard concentration of this amino-acid is 2 mM for both laboratory-made or commercially available medium (Baer et al., 2010; Jäger et al., 2020; Liu et al., 2006). In this study, we called those medium “Rich”, “Intermediate” and “Low” because of their respective concentration of L-glutamine varying from [4mM] to [2mM] and [0.1mM] respectively (Table 1). Spheroids were formed for three days in classical rich culture medium, then, conditioned by each medium for 10 days with daily medium renewal (Figure 33) to ensure a constant level of nutrients. First, using RTqPCR, we studied the mRNA expression levels of several metabolic stress genes after 3 and 10 days of medium conditioning. Preliminary results demonstrated that 3 days of medium conditioning was not sufficient to change the metabolic response of HT-29 spheroids: mRNA expression of the three metabolic stress genes (BIP, TRB3, and Sestrin2) as well as the hypoxia gene EGLN3 remains unchanged (Figure 37a). However, after 10 days, we observed a gradual increase in metabolic stress due to L-Glutamine starvation. Indeed, mRNA expression of TRB3 gene (involved in ER-stress induced response) is multiplied by a factor of 4 for spheroids under low medium compared to rich (Figure 37b). Similarly, mRNA levels of Sestrin2 gene are also significantly increased for intermediate and low medium compared to rich (1.42 ± 0.2 for intermediate and 3.62 ± 1.4 for low, Figure 37b). It has been shown that Sestrin2 gene expression is involved in cancer cell glutamine intracellular signaling. Glutamine-deprived condition increases Sestrin2 expression to facilitate suppression of mTORC1 activity which regulates cell growth and proliferation (Byun et al., 2017). Hypoxia seems also impacted by glutamine starvation, highlighted by the significant decrease of EGLN3 expression in low condition compared to rich condition (Figure 37b). The dynamic of this changes was then assessed with timelapse microscopy, indicating that glutamine starvation impairs HT-29 spheroids growth in a gradually manner with the concentration of L-Glutamine (Figure 37c,d) since the third day for low medium and the fifth day for intermediate and rich medium.

Interestingly, these data also reveal a gradual increase of the stem transcription factor Nanog expression along with the glutamine starvation (Figure 37b) after 10 days of medium conditioning only. Indeed, Nanog mRNA expression is increased by a factor of 2.5 for intermediate and a factor of 4.2 for low glutamine medium while it remains unchanged after

three days. Moreover, this is corroborated in the timelapse experiments using the modified HT-29 cell line expressing Nanog-GFP. It seems that after 10 days of nutritive conditioning, the density of Nanog fluorescence is higher for spheroids grown in low medium rather than intermediate or rich (Figure 37d,e). These preliminary experiments suggest that at least 5 days of L-glutamine-starved medium would be necessary to generate substantial stress metabolic within HT-29 tumor spheroids and subsequently to induce the dedifferentiation of those colorectal cancer cells. Due to the heterogeneity of RTqPCR results, this assumption needs to be confirmed by additional experiments.

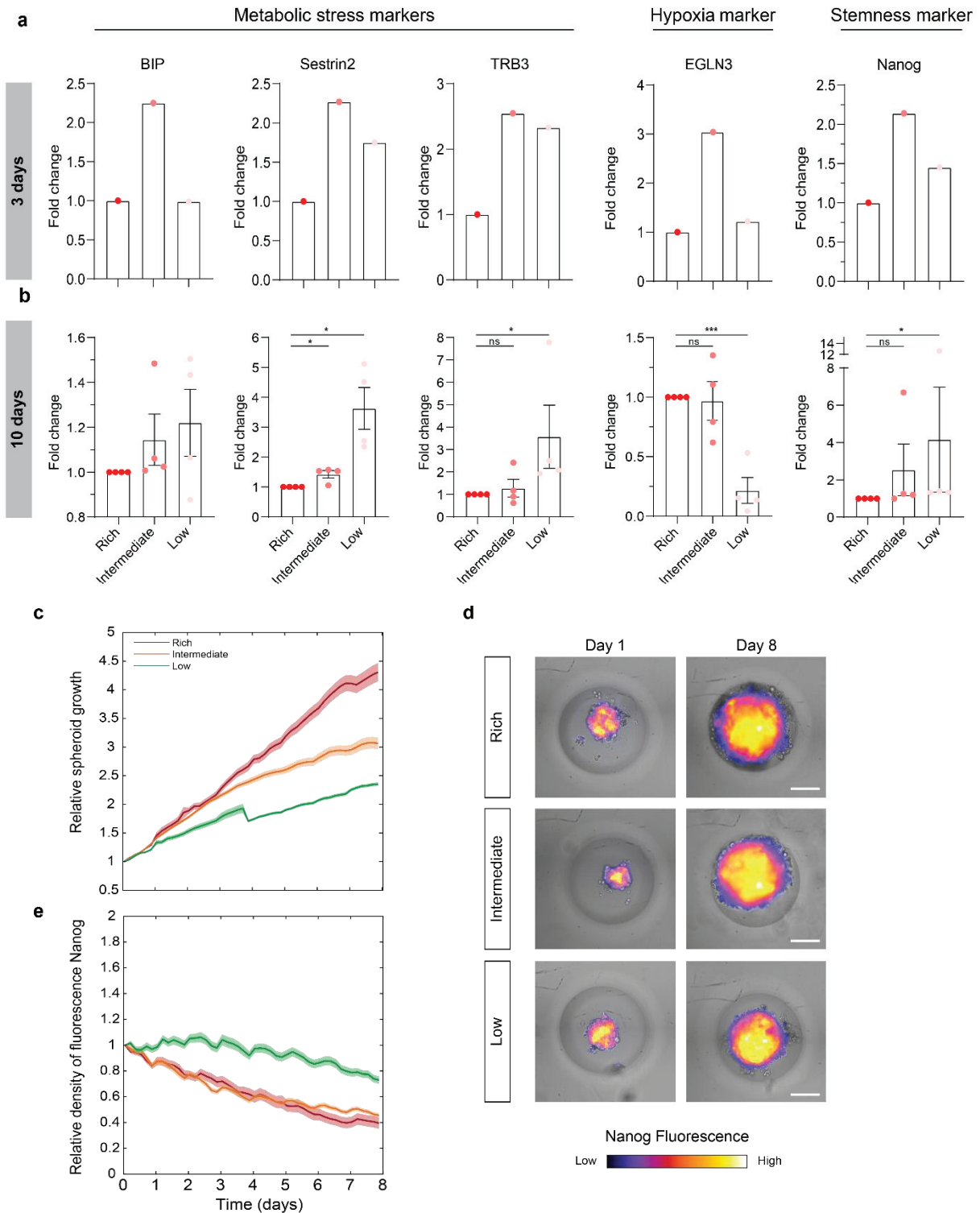


Figure 37: Short- and long-term impact of glutamine starvation on 3D spheroids. (a-b) Fold change mRNA expression of metabolic stress gene (BIP, Sestrin2, TRB3), hypoxia gene (EGLN3) and stemness gene (Nanog) of HT29 spheroids cultured for 3 (a) or 10 days (b) under rich, intermediate and low glutamine concentrations normalized by rich glutamine medium condition. $N=1$ for now (a) and $N=4$ experiments (b); Mann-Whitney test, *** $P < 0.001$, ** $P < 0.01$, * $P < 0.05$. (c) Quantification of spheroids growth over time under different glutamine concentrated medium. $N=2$ experiments. (d) Representative images of HT29-NanogGFP spheroids grown under low, intermediate or rich concentration of glutamine, at different times. Scale bar = 100 μm . (e) Quantification of the density of fluorescence of Nanog (intensity of fluorescence normalized by the size of the spheroid), under low, intermediate or rich concentration of glutamine. $N=2$ experiments.

Mechanical stress does not induce metabolic stress

Tumors are not only subjected to metabolic stress but also to an increased mechanical constraint during their growth. Therefore, we studied the effect of an applied mechanical stress of 10 kPa on the plasticity and dynamic of HT-29 spheroids. For that, in the same line of experiment that before (Figure 33), once spheroids are formed, a solution of dextran is added to the corresponding medium (rich, intermediate or low) to exert an isotropic mechanical compression, on HT-29 spheroids, from 1 to 10 kPa according to the dextran concentration. It has been shown that dextran compression impairs multicellular spheroids volume through the compression of ECM, the reduction of cell volume and the inhibition of cell proliferation (Delarue et al., 2014; Dolega et al., 2021; Monnier et al., 2016; Montel et al., 2012, 2011; Rizzuti et al., 2020). This previously published inhibition of cell proliferation could be explained by an increase in metabolic stress under compression and made us wonder about the mechano-metabolic interplay in tumor spheroids. We first hypothesized that an applied mechanical stress might promote cancer cell plasticity by increasing tumoral metabolic stress. Therefore, we assessed spheroids growth dynamic and genes expression changes after both medium conditioning and pressure application. Preliminary data showed that a 10kPa mechanical compression does not induce any metabolic stress after 3 days of glutamine starvation as mRNA expression levels of BIP, Sestrin 2 and TRB3 are not increased (Figure 38a). These results are for the moment preliminary (N=1 at day 3) and should be confirmed (experiments to reproduce these results are scheduled before my PhD defense). Interestingly, even after 10 days of 10 kPa pressure on HT-29 spheroids, we do not observe any cumulative effect of glutamine starvation and 10 kPa applied stress on the expression of metabolic stress genes (Figure 38b). Interestingly for spheroids grown under low glutamine medium, hypoxia gene EGLN3 mRNA levels are recovering basal levels when pressure is applied (Figure 38b), cancelling the initial effect of glutamine starvation on this hypoxia marker. More importantly, a 10 kPa mechanical stress impacts spheroids growth the same way whatever the medium condition, as there is no statistical difference of spheroids sizes between rich, intermediate and low medium under 10kPa after 10 days (Figure 38c), while medium alone were generating important differences of spheroids growth (Figure 37c).

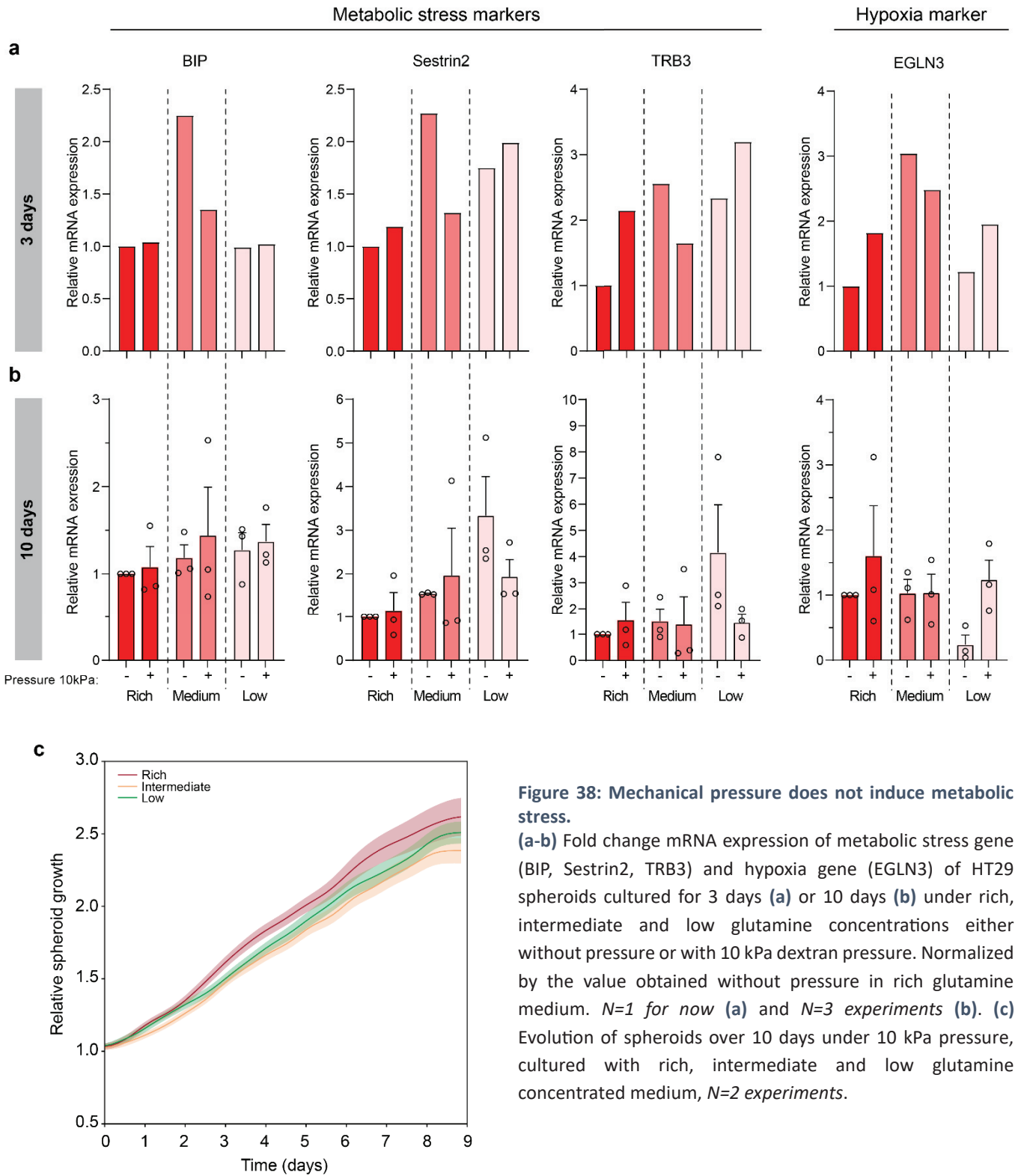


Figure 38: Mechanical pressure does not induce metabolic stress.

(a-b) Fold change mRNA expression of metabolic stress gene (BIP, Sestrin2, TRB3) and hypoxia gene (EGLN3) of HT29 spheroids cultured for 3 days (a) or 10 days (b) under rich, intermediate and low glutamine concentrations either without pressure or with 10 kPa dextran pressure. Normalized by the value obtained without pressure in rich glutamine medium. *N*=1 for now (a) and *N*=3 experiments (b). **(c)** Evolution of spheroids over 10 days under 10 kPa pressure, cultured with rich, intermediate and low glutamine concentrated medium, *N*=2 experiments.

Isotropic compression triggers dedifferentiation of colorectal cancer cells

Having shown that mechanical pressure does not induce metabolic stress neither after 3 nor 10 days of compression, we further examined the impact of such compression on cancer cells' identity. Preliminary data showed that 3 days of mechanical compression are sufficient to increase mRNA expression level of Nanog regardless of the glutamine starvation (Figure 39a). However, these results are for the moment preliminary (N=1 at day 3 for RTqPCR) and should be confirmed (experiments to reproduce these results are scheduled before my PhD defense). Spheroids growth and live Nanog expression were examined using HT-29 expressing Nanog-GFP and time-lapse imaging. While spheroids growth was increasingly impaired by the increase of the level of applied stress (1, 5, and 10 kPa), Nanog density of fluorescence gradually increased upon compression (Figure 39c). Subsequently, we wondered about the longer-term impact of mechanical compression on colorectal cancer cells stemness and looked at Nanog expression after 10 days, under a 10 kPa compression, and also observed a strong increase of mRNA level (increased by 1.9 for rich, by 4.4 for intermediate and by 2.5 for low, Figure 39b), independently of glutamine starvation since there is no cumulative effect between mechanical stress and glutamine starvation (Figure 41).

We further validated those results by looking at the live dynamic of Nanog-GFP for 10 days by time-lapse microscopy. Nanog fluorescence density abruptly increases under 10 kPa pressure over the first 3 days; regardless of the medium conditioning (Figure 40a,b). However, the curve dynamic under dextran is different according to the medium used: it considerably decreases after 3 days for rich medium, remains steady for intermediate medium, and slightly decreases for low medium. Therefore, these results show the important contribution of mechanical stress on the dedifferentiation of colorectal cancer cells, independently of glutamine starvation even if the mechanisms behind it remain elusive.

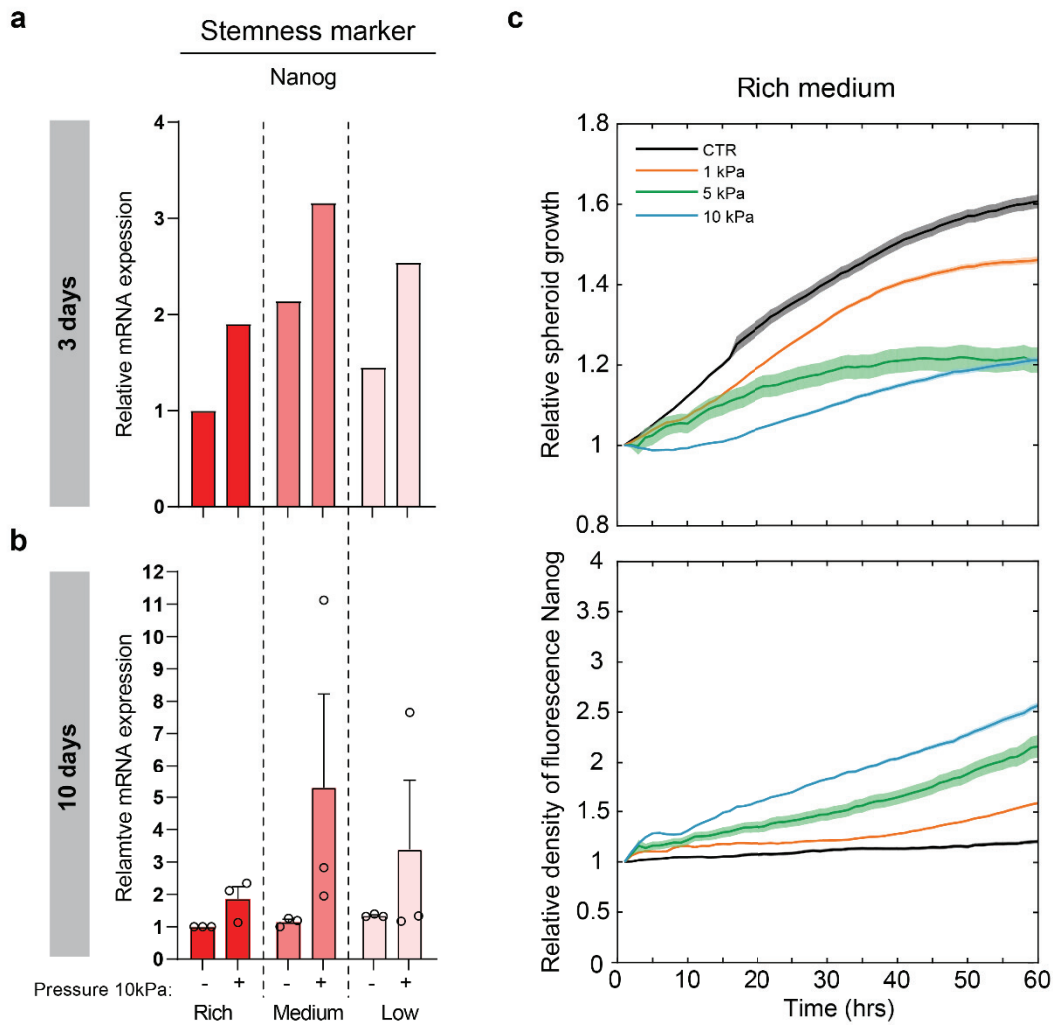


Figure 39: Mechanical compression increases stemness marker independently of glutamine starvation.

(a-b) Relative mRNA expression of the stem marker Nanog after 3 days **(a)** or 10 days **(b)** without pressure or under 10 kPa compression, cultured under rich, intermediate and low glutamine medium. Normalized by the value obtained without pressure in high glutamine medium. $N=1$ for now **(a)** and $N=3$ experiments **(b)**. **(c)** Evolution of spheroids growth and Nanog density of fluorescence over 3 days without any pressure (ctr) or under increasing pressure (1, 5, 10 kPa) for spheroids grown in rich glutamine medium, $N=2$ experiments.

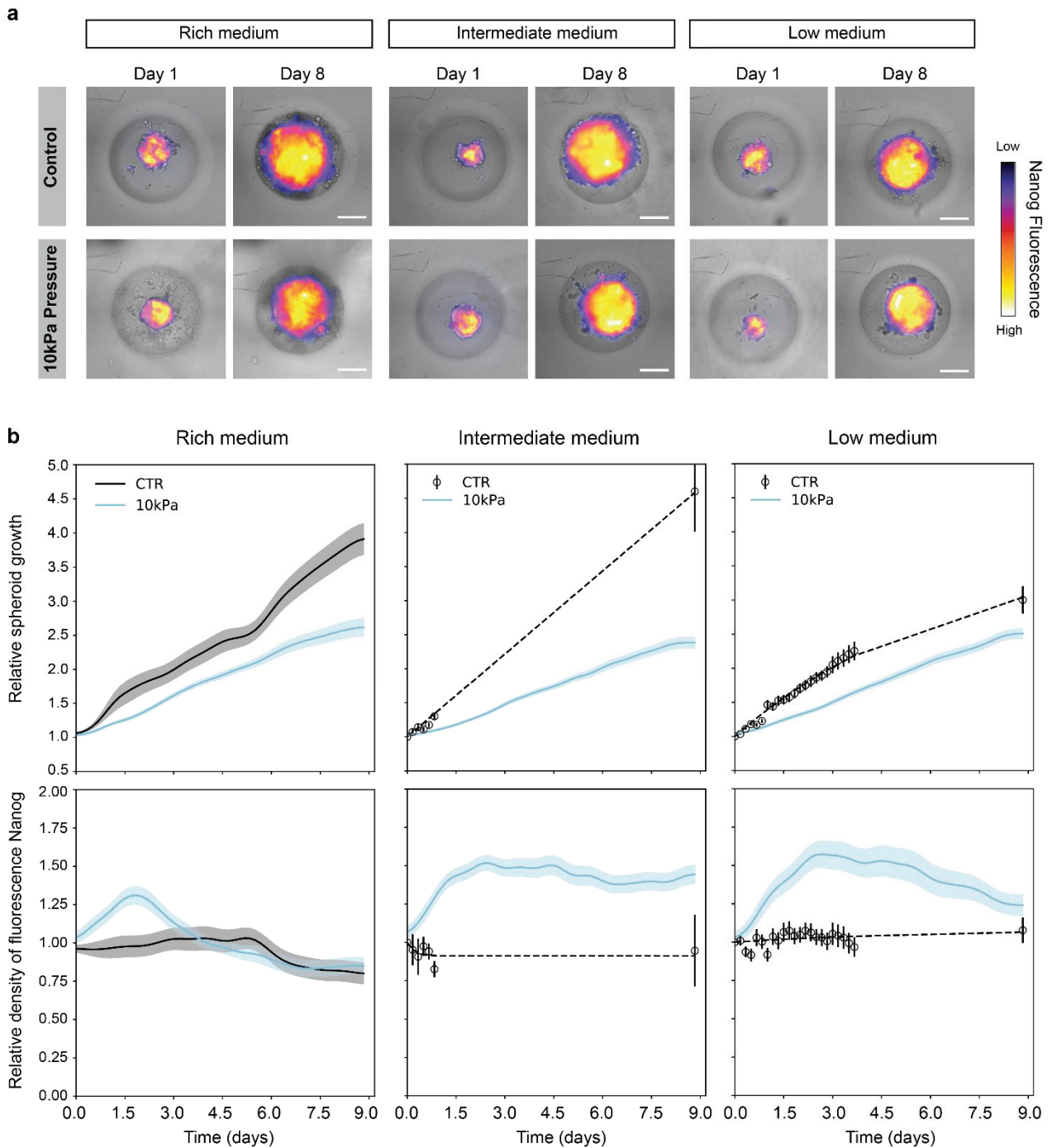


Figure 40: Isotropic compression dedifferentiate HT29 tumor spheroids.

(a) Representative images of HT29 expressing Nanog-GFP under rich, medium and low glutamine without pressure or under 10 kPa compression. Scale bar = 100 μ m. (b) Evolution of spheroids growth and Nanog density of fluorescence over 10 days without any pressure (ctr) or under 10 kPa pressure, cultured with rich, intermediate and low glutamine concentrated medium, $N=2$ experiments.

Supplementary Figures

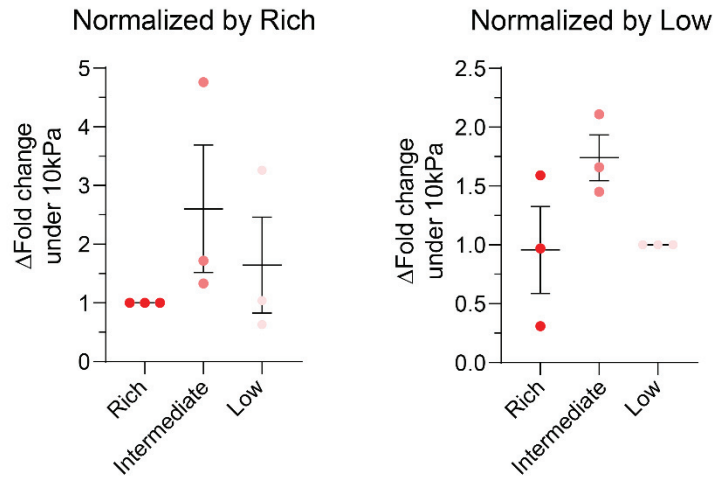


Figure 41: No cumulative effect of metabolic stress and mechanics on Nanog expression. Fold change difference of Nanog mRNA expression between 10kPa pressure and no pressure after 10 days, normalized either by rich glutamine medium or low glutamine medium, $N=3$ experiments.

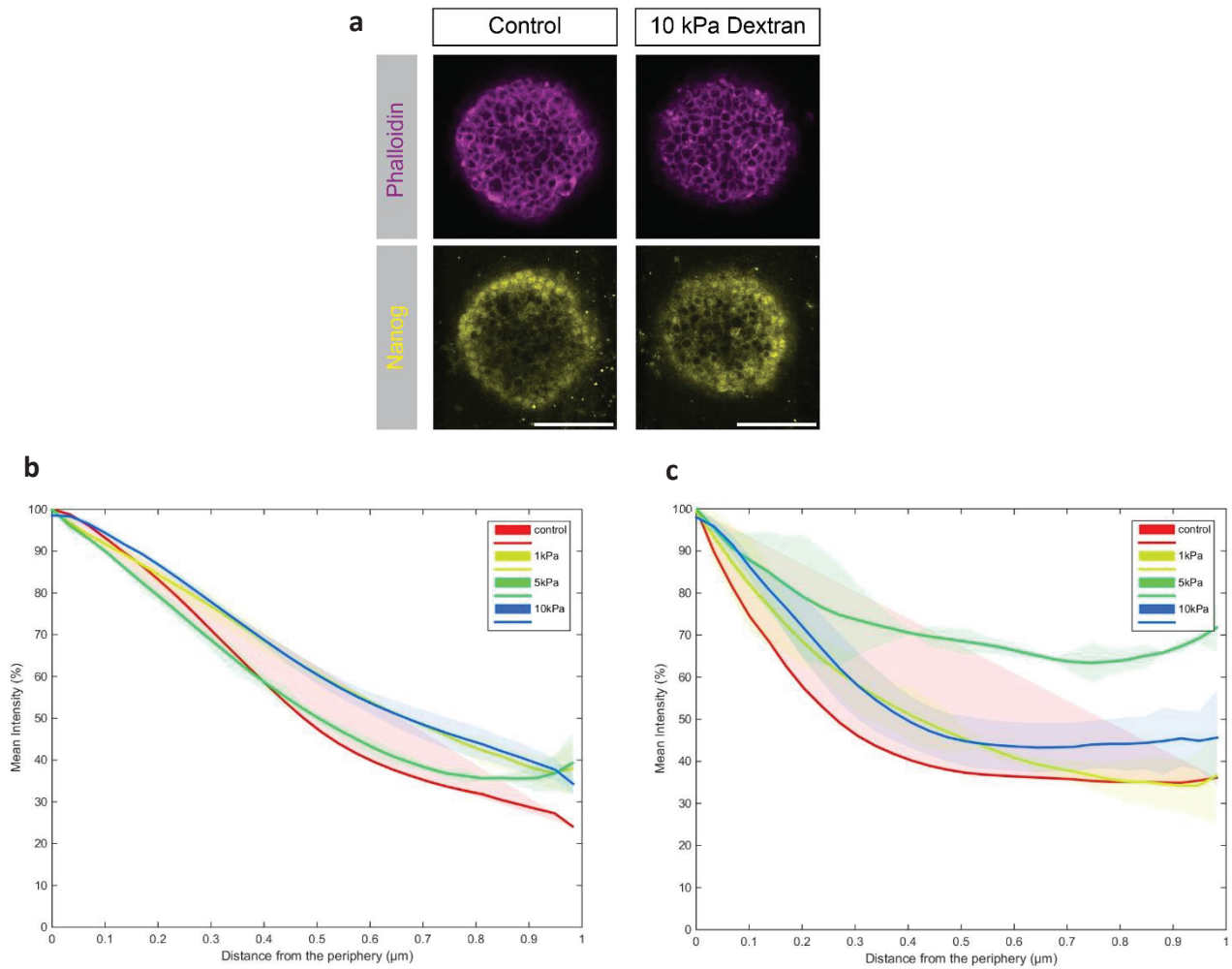


Figure 42: 3D spatial localization of Nanog protein within tumor spheroids.

(a) Representative images of HT29 spheroids slices stained with Nanog protein and phalloidin. *Scale bar = 100 μ m.*

(b-c) Phalloidin **(b)** and Nanog **(c)** mean intensity quantified radially from the surface to the center of spheroids under control or increasing mechanical compression (1, 5 or 10 kPa), *N=1 for now.*

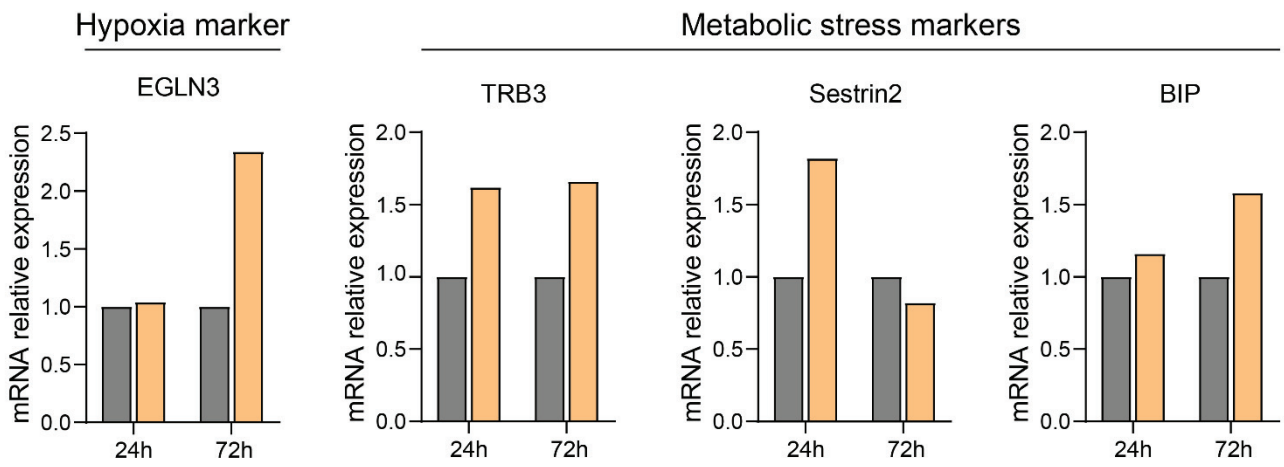


Figure 43: M11 effect on hypoxia and stress metabolic genes.

Level of mRNA expression of EGLN3 hypoxia gene and metabolic stress genes (TRB3, Sestrin2, BIP) of HT29 monolayer grown either under classical rich medium or under M11, *N=1 for now*.

Discussion and perspectives

Understanding how the biochemical and mechanical tumor microenvironment affect the plasticity driven CSC is of importance for understanding current cancer therapy failure and developing more effective treatment, that would eliminate cancer aggressiveness and relapse to therapy perpetuated by CSC. Using HT-29 spheroids grown in a standardized manner, we showed that the dynamic equilibrium between CSC and cancer cell is altered by both metabolic and mechanical cues. Indeed, serum-free medium and glutamine depleted medium increase Nanog expression, while glutamine starvation effectively reproduces intra-tumoral metabolic stress. We demonstrated that isotropic mechanical pressure induces a dedifferentiation of cancer cells towards a stem-like phenotype, independently of glutamine starvation and without generating additional metabolic stress.

Microenvironment affects cellular plasticity

Changes in cancer cell identity often occur in specific microenvironment niches. Such tumoral microenvironments have specific characteristics and are regulated by several factors: immune cells, cancer-associated fibroblast, ECM components, hypoxia, and pH (Lee et al., 2016). In particular, hypoxia affects the cancer cells stem state (Heddleston et al., 2010; Rainho et al., 2021). It has been shown for example, for brain cancer, that hypoxia dedifferentiates glioblastoma cells (Heddleston et al., 2009; Pistollato et al., 2010). The increase in hypoxia gene expression under mechanical compression observed in our low glutamine experiments restored the initial hypoxia phenotype before glutamine starvation. Therefore, we can wonder if the subsequent increase of Nanog expression in this condition is a combined effect of mechanics and hypoxia. Complementary experiments are necessary to be able to fully address this important point.

Further characterization is required to confirm the change in cell identity and the dedifferentiation of HT-29 spheroids. Indeed, it is necessary to analyze the expression of other stemness genes that have been described in colorectal cancer stem cells and called the core pluripotent transcription factors: Oct4, Sox2, C-myc, and Klf4 (Dotse and Bian, 2016; Gheytauchi et al., 2021). Moreover, a complete change of cellular identity should be accompanied by a decrease in differentiation markers, and an epithelial-to-mesenchymal transition (EMT). Indeed, EMT corresponds to the cellular process happening when an epithelial cell loses its adhesion with its neighboring cells and adopts a mesenchymal phenotype with an increased migration capacity (Mani et al., 2008). Thus, epithelial markers expression such as the intermediate filament Ck20 and cell-cell adhesion E-cadherin should decrease, to the benefit of mesenchymal markers such as vimentin, and N-cadherin (Dongre and Weinberg, 2019; Lytle et al., 2018). Herein, we evidenced an increase in Nanog transcription factor. Nanog expression upon this cellular reprogramming targeting genes of

Nanog transcriptional factor should also be impacted (Bak, Bax and Bcl-2). However, these findings may be somewhat limited by the only study of the transcription response. A reasonable question is the potential impact of both glutamine starvation and isotropic compression on translation and on the effective change on the resulting proteins. Therefore, the increase of Nanog protein, and in the same way all the genes studied here, must be verified by western blot and immunostaining. IF experiments have the advantages to be semi-quantitative and offer us information about subcellular localization of the protein and the preferred localization of the CSCs in 3D within the spheroids. Preliminary results obtained using confocal microscopy and *in-situ* clarification showed very few differences of Nanog protein staining as a function of distance from the periphery (Figure 42). Nevertheless, at that time, the clarification technique was not optimized, resulting in non-specific photons attenuation as a function of the distance from the periphery (exemplified in Figure 10b, with Phalloidin staining Intensity analysis). Besides, Nanog is a poorly expressed protein and could therefore generate more artefacts in IF in thick tissues. Optimizations of clarification protocols are required to obtain less photon attenuation and more interpretable data. For that, other clearing protocols as well as OCT inclusion together with physical slicing of the spheroids are currently developed in our team.

Moreover, CSC are dynamic and heterogeneous, thus cannot only be characterized with known stem/pluripotent markers. The gold standard method to characterize a CSC is an *in vivo* xenograft (Nassar and Blanpain, 2016) or a dynamic functional test *in vitro* (Chambost et al., 2022; Dotse and Bian, 2016). Hence, it would be interesting to evaluate the ability of a supposed single CSC to reform a complete spheroid (single cell assay) after 10 days of medium conditioning or after mechanical stress. Especially knowing the very fast plasticity following the change of environment showed in Figure 36. In parallel, the possible change in metastatic potential can be assessed with a spheroid migration assay on a collagen bed for example.

Putative molecular signaling pathways involved in this CSC-driven plasticity

We showed that adding dextran compression triggers HT-29 colorectal spheroids dedifferentiation by a purely mechanical effect. Thus, we can wonder through which mechanosensitive pathways this happens. It has been shown that Wnt/ β -catenin pathway is a pluripotency stemness signaling pathway as it's the main signaling pathway regulating self-renewal and proliferation of healthy intestinal epithelial (Chen et al., 2022), and their derivative colorectal carcinoma stem cells (Chen et al., 2020; Clevers, 2006). Moreover, most of the colorectal cancers carry the APC (tumor suppressor gene) mutation (among them, the HT-29 cell line used in this work (Zoetemelk et al., 2019)) that leads to an overactivation of the Wnt signaling pathway (Zanconato et al., 2016). Besides, several studies have highlighted the mechanosensitivity of this signaling pathway, as β -catenin itself can be regulated by mechanical cues (Totaro et al., 2018), or as the mechanosensitive transcription factors YAP/TAZ

are biochemical and transcriptional mediators of Wnt signaling. YAP/TAZ mediate the effects of Wnt pathway to promote proliferation and tumorigenesis of CSC (Diamantopoulou et al., 2017; Llado et al., 2015; Oudhoff et al., 2016). When Wnt pathway is “inactivated” YAP/TAZ and β -catenin are incorporated into the destruction complex for them to be sequestered in the cytoplasm and/or degraded. However, when Wnt signaling is “activated”, disassembly of this complex abolishes both β -catenin and YAP/TAZ cytosolic inhibition, triggering their nuclear accumulation and subsequent activation of targeted genes (Azzolin et al., 2014, 2012; Totaro et al., 2018). Loss of cell polarity, happening under inactivation of Hippo signaling and YAP/TAZ nuclear translocation, is a hallmark of cancer and an important feature of EMT associated with stemness characteristics. Consequently, YAP/TAZ are both inducers of EMT and downstream regulators of cancer stem cells attributes (Diepenbruck et al., 2014; Shao et al., 2014). Therefore, these mechanisms raise the possibility that mechanical regulation of YAP/TAZ and β -catenin are linked to other pluripotent transcription factors with β -catenin activation as final target (Lien and Fuchs, 2014). In this context, we performed preliminary immunostainings to identify the subcellular localization – thus, the potential activation – of YAP within compressed spheroids. The results are complicated to interpret due to the important photon attenuation with depth and other experiments are required and are planned before the PhD defense.

Mechanical stress may increase cancer cell drug resistance and tumor relapse

Increased mechanical compression during tumor growth is correlated with chemotherapy resistance. Using a pancreatic 3D spheroid model, Rizzuti et al (Rizzuti et al., 2020) have shown that this chemoresistance can be simply explained by the fact that compressive stress decreases cell proliferation, which in turn decreases the effect of chemotherapeutics targeting proliferating cells, such as gemcitabine. Such decrease in cell proliferation is consistent with the emergence of a CSC population that were revealed in our findings and could contribute to the drug resistance and therapy failure of colorectal spheroids upon mechanical stimulation. Therefore, targeting the CSC population is insufficient to cure cancer and we need a better understanding and precise identification of the mechanisms involved in this dedifferentiation that may occur after the elimination of the CSCs (Nassar and Blanpain, 2016).

In accordance with the present results, other studies have demonstrated the acquisition of stemness and chemoresistance properties after metabolic stress induced by conventional therapy (Kim, 2015). As glutamine metabolism contributes to cancer cell proliferation and adaptation to metabolic stress, several studies underline the idea of glutamine metabolism inhibition as a new therapeutic strategy (Baenke et al., 2016; Choi and Park, 2018).

Tumors are affected by several types of mechanical constraints

Despite these interesting results, the question of the type of applied mechanical constraint might be asked. Indeed, the physical properties of the tumor microenvironment are strongly

modified during tumor progression, with an increase in the stiffness of the ECM, changes in interstitial fluid pressure, and confinement stresses that are gradually increased when cells are proliferating in a spatially limited environment. Therefore, different experimental tools have been developed to apply *in vitro* such mechanical stresses on tumor spheroids. In our study, we decided to use a long-chain polymer called dextran (Montel et al., 2012) – too large to enter into the spheroids – integrated in the culture medium. It has already been shown that dextran induces a global pressure reproducing those experienced *in vivo* by compressing mainly the intercellular space (Dolega et al., 2021). However, as tumors are composed of cells embedded within ECM, the impact of mechanical stress can be direct on cells, or indirect by compressing the ECM and thus limiting cells access to nutrients. We demonstrated that the promotion of this stem state is a pure mechanical effect as mechano-osmotic pressure does not generate more metabolic stress. Moreover, the spheroids slowdown growth and cell proliferation inhibition under dextran compression might be at the origin of a dormant cell state within tumor spheroids. This hypothesis is supported by the induction of the cell cycle inhibitor p27 upon mechanical compression (Delarue et al., 2014) since Cyclin-Dependent Kinases such as p27 are known to be upregulated in non-proliferative cancer cells (Bragado et al., 2013; Sherr and Roberts, 1999). Such cancer dormancy could explain the absence of metabolic stress under mechanical compression.

In several other tools mechanical constraint of spheroids is built upon growth as tumor is proliferating in a confined environment. It is the case of alginate capsules (Alessandri et al., 2013), elastic matrix such as agarose (Rizzuti et al., 2020) or using PDMS groove (Desmaison et al., 2013). In future investigations, low-melting agarose matrix will most likely be used to determine whether the effect of growth-induced stress on spheroids growth and CSC population are similar to those demonstrated in this work with dextran.

Conclusion

To conclude, we have demonstrated in this chapter the plasticity of colorectal tumor spheroids, induced by the nutritive, metabolic, and physical microenvironment and promoting a stem-like state. This study calls for in-depth analysis of the signaling pathways involved in such dedifferentiation and the implication of this highly tumorigenic colorectal CSC-driven plasticity in therapy resistance and relapse.

Material and methods

Cell culture

HT-29 wild type colorectal adenocarcinoma cells were purchased from the ATCC (HT-29 HTB-38). The stable HT-29 cell line expressing GFP under Nanog promoter was a gift from Pannequin's team (IGF, Montpellier).

All cells were cultured in Dulbecco's modified Eagle's medium (DMEM - Glutamax, Gibco™) supplemented with 10% heat-inactivated fetal bovine serum (FBS; PanBiotech™), 100 units/100µg penicillin/streptomycin (Gibco™), called in this paper "classical rich medium". A second batch of HT-29-NanogGFP cell line was also cultivated in non-adherent conditions with the M11 medium, whose composition is described in Table 1 below.

Routinely, all HT-29 cell lines were grown in T-25 cell culture flasks and kept at 37°C and under 5% CO₂ environment. The culture medium was changed regularly, and cell passage was carried out at 70% confluency. Cell lines were tested for Mycoplasma and the tests were negative.

During the experiments, spheroids were incubated with different medium composition called "Rich", "Intermediate" and "Low" according to their respective concentration of L-Glutamine. A serum-free medium was also used and called "M11" medium. All medium compositions are presented in Table 1:

Table 1: Detailed medium composition

<u>RICH</u> <i>Commercially available</i>	<u>INTERMEDIATE</u> <i>Laboratory-made</i>	<u>LOW</u> <i>Laboratory-made</i>	<u>M11</u> <i>Commercially available</i>
DMEM – Glutamax Gibco™	DMEM w/o phenol red	DMEM w/o phenol red	DMEM F12 - Glutamax Gibco™
10% FBS heat- inactivated	10% SVF dialyzed	10% SVF dialyzed	
Pen/Strep 1%	Pen/Strep 1%	Pen/Strep 1%	Pen/Strep 1%
Glucose 4.5g/L	Glucose 2.88g/L	Glucose 2.88g/L	Glucose 3.15g/L (initial) + 0.6g/L (supplemented)
L-Glutamine 4mM	L-Glutamine 2mM	L-Glutamine 0.2mM	L-Glutamine 2.5mM
	Na Pyruvate 65µM	Na Pyruvate 65µM	Insuline 0.2% (0,02mg/mL)
	L-Proline 0.15mM	L-Proline 0.15mM	N2 1%
	L-Alanine 0.15mM	L-Alanine 0.15mM	H-EGF 20ng/mL
	L-Asparagine 0.34mM	L-Asparagine 0.2mM	FGF-2 10ng/mL
	L-Aspartic acid 0.15mM	L-Aspartic acid 0.15mM	
	L-Glutamic acid 0.15mM	L-Glutamic acid 0.15mM	

Multicellular tumor spheroids

HT-29 spheroids were formed in either 12 or 24-well plates containing in each well 202 agarose microwells of 300 μm in diameter (and 450 μm in depth), described below. After trypsinization and centrifugation, either 50 000 or 30 000 cells in 1.5 mL medium were seeded – in each well – respectively in a 12 or 24-well plate. Spheroids are formed after sedimentation in agarose microwells by cell self-aggregation. After 1 h, the plate was rinsed with fresh medium to remove cells that did not reach the bottom of the microwells. After 3 days, spheroids are ready for medium conditioning and/or isotropic compression.

Agarose microwells microfabrication

The microwell chip was designed using Autodesk® software and the master mold was created using the CNC Mini-Mill/GX on brass. The design chosen and used in this project is a chip containing 202 “U” shaped microwells of 300 μm diameter each surrounded by a wall (Figure 44) to prevent spheroids removal when the medium is renewed. A PDMS counter-mold is created and will be used for the final agarose molding. The PDMS (base and crosslinker mixed at 10:1 ratio) is cast on this brass chip and put under vacuum to eliminate bubbles and baked in an oven at 70° for 4 h. After rigidification, the PDMS mold is gently detached from the brass with isopropanol. With this method, several PDMS replica molds can be produced and each of them can be used multiple times.

Molding of free-standing microwells

At first, agarose molding needs a clean environment, thus it is necessary to clean with 70% ethanol the hot plate, tweezers, and glass coverslips. A solution of agarose diluted in distilled water (2% (w/v)) was prepared through autoclaving at 120 °C for 10 min, or 30s microwave (1000 W). The following steps, described hereby, are based on the protocol described in Goodarzi and al. (Goodarzi et al., 2021).

Protocol:

- Prewarm PDMS and tips on the hot plate at 90°C
- Put 130 μL of agarose on the PDMS mold
- Put a coverslip on top to spread the agarose drop with a uniform thickness
- Wait 5 min for gelling, then unmold the gel
- Put the gel in a 12- or 24-well plate
- Add PBS to keep the gel hydrated
- UV sterilization (24W lamp, 365 nm)
 - 30 min minimum without the plate lid
 - Change the PBS with sterile one under the hood
 - 30 min with the plate lid
- Parafilm and store at 4°C

- Culture medium needs to be added one day before seeding, and the plate incubated at 37°C to allow nutrient diffusion within each microwells.

Molding on APTS-functionalized coverslips

If microwells need to be fixed to the coverslips for time-lapse microscopy, coverslips functionalization is necessary. First, the 12- or 24-well plates need to be drilled (16mm hole and 12mm hole for 12- and 24- well plate respectively), to allow gluing of coverslips and gels. Drilled plates need to be cleaned with ethanol and sterilized 20 min under UV.

APTS treatment on glass coverslips protocol:

- Wash coverslips with ethanol and water
- Prepare a solution of :
 - 43.5 mL of distilled water
 - 12.5 μL of acetic acid 5mM
 - 435 μL of 3-APTS (Amino propyltriethosilane 99 % Acros™)1%
- Incubation 20 minutes under stirring at room temperature
- Rinse with water (3 times) + drying
- 15 minutes at 100 °C on a hot plate

APTS treatment on coverslips must be done the same day for better fixation of the agarose gels.

- Coverslips of 20 mm of diameter are used for a 12-well plate or 14 mm for a 24-well plate.
- Use those treated coverslips on the top of the PDMS mold during agarose molding.
- Glue the coverslips on the well plate (previously drilled) using the NOA glue (Norland Optical Adhesive NOA 81)
- UV sterilization (24W lamp, 365 nm)
 - 2 min on a closed plated (for the glue to polymerize)
 - Add sterile PBS under the hood
 - 40 min UV

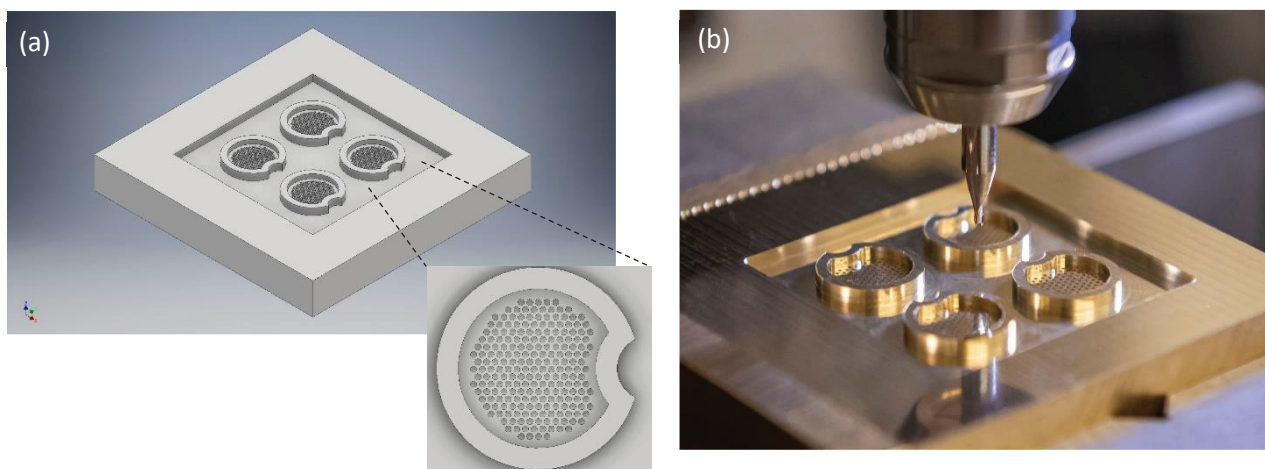


Figure 44: 300 μm diameter “U” shaped microwells mold.

(a) 3D design of the 300 μm diameter microwells mold with a zoom of one chip containing 202 “U” shaped microwells.

(b) Photo of the original brass mold micro-milled.

Dextran osmotic compression

Three days after seeding, when the MCTS are formed, Dextran (molecular mass 500 kDa; Sigma-Aldrich™) is added to the culture medium to exert mechanical stress at a concentration of 20 g/L to exert 1 kPa, 55 g/L to exert 5 kPa, and 80 g/L to exert 10 kPa. To facilitate solubilization of Dextran polymer in the medium, the solutions were placed at 37°C (Montel et al., 2012, 2011).

Immunostaining

Spheroids are fixed within the agarose microwells. For that, 4% PFA (Electron Microscopy Sciences™) was added and incubated for 20 min at RT. After incubation, samples were rinsed with PBS (2x20 min). The cells were permeabilized using 0.1% Triton X-100 (Acros Organics™) for 10 min at RT. After blocking for 1 h at RT with PBS - 5% BSA – 0.1% Tween20 (Sigma-Aldrich™) to inhibit non-specific binding of antibodies, cells were incubated overnight at 4°C with primary antibodies diluted in blocking solution. After 3x5min washes with PBS – 0.1% Tween20, samples were incubated with secondary antibodies for 2h at RT. The primary antibodies used are: Nanog (Sigma-Aldrich™ at 1/500); YAP (Cell signaling™ at 1/100). NucGreen™ Dead 488 (Invitrogen™, 1 drop per 3 ml in PBS); Alexa 546 Phalloidin (Invitrogen™ at 1/500); Alexa 555 Phalloidin (Invitrogen™ at 1/500) were also used. The secondary antibodies used are: Anti-Mouse 647 (Invitrogen™ at 1/500); anti-rabbit 647 (Invitrogen™ at 1/500), anti-rabbit 555 (Invitrogen™ at 1/500).

Clarification

After immunostaining, the spheroids are incubated overnight with a homemade clarification solution composed of PBS – 80% glycerol. Then, the agarose microwells containing the spheroids are punched with a 6 mm biopsy puncher, and inserted on top of a coverslip in adhesive spacers (Sunjinlab i-Spacer 4-0.5: 4 wells, 0.5mm of height and 7mm of diameter) with fresh clearing solution as mounting medium. Samples were, then, sealed with a microscope slide and nail varnish.

Confocal fluorescence microscopy

Fixed samples were visualized using a Leica SP5 confocal microscope with a 20x Dry objective (NA = 0.65) and a 25x Water (NA = 0.95) objective. Images were collected in sequential mode using averaging at a resolution of 1024x1024. Z-stacks of cells were acquired to image the whole spheroid (dz = 2 µm for each stack).

Live-cell imaging

HT-29 cell line expressing Nanog-GFP were observed with an inverted microscope Leica DMI8 using epifluorescence imaging. A time-lapse imaging was performed for 3 to 10 days in a controlled (CO₂, temperature and humidity) environment, using a 20x dry objective (NA =

0.65). A motorized x-y stage enabled the concomitant recording of up to 25 spheroids for each condition every 4 h.

RTqPCR

RNA extraction and cDNA synthesis

Spheroids for each condition were collected by turning upside-down the agarose microwells, enabling all spheroids to go out and be subsequently collected. Total RNAs were then extracted from spheroids using RNeasy Mini Kit (Qiagen®) according to the manufacturer's instructions. After measurement of RNA quantity and quality by a Spectrophotometer Micro-Volume EzDrop 1000 (BLUE-RAY BIOTECH®), cDNAs were synthesized with 500ng of total RNA using dNTP, DTT and random primers, RT-MMLV from Life Technologie™.

qPCR analysis

Real-time polymerase chain reaction (RT-qPCR) was performed using the SYBR Green Supermix from Biorad® with specific primers at a final concentration of [0.5µM] and 5µL of cDNA template on the LineGene 9600 Series from BIOER® real time PCR detection system with the following cycle conditions: 1 min at 95°C and 10 sec at 95°C, 30 sec at 60°C for 40 cycles. The relative expression values of target genes were quantified relative to HPRT, as the internal reference gene, by using the $2^{\Delta\Delta CT}$ method. Real-time PCR primers are listed in Table 2.

Table 2: qPCR primers

Genes group	Genes		Sequence 5' → 3'
Housekeeping	HPRT	Forward	TGACCTTGATTTATTTTGCATACC
		Reverse	CGAGCAAGACGTTTCAGTCCT
	RPS11	Forward	AGCAGCCGACCATCTTTC
		Reverse	ATAGCCTCCTTGGGTGTCTTG
Stemness	Lgr5	Forward	CCTGCTTGACTTTGAGGAAGACC
		Reverse	CCAGCCATCAAGCAGGTGTTCA
	Nanog	Forward	CTCCAACATCCTGAACCTCAGC
		Reverse	CGTCACACCATTGCTATTCTTCG
Metabolic stress	BIP	Forward	CTGTCCAGGCTGGTGTGCTCT
		Reverse	CTTGGTAGGCACCACTGTGTTC
	TRB3	Forward	TGGTACCCAGCTCCTCTACG
		Reverse	GACAAAGCGACACAGCTTGA
	SESN2	Forward	AGATGGAGAGCCGCTTTGAGCT
		Reverse	CCGATGAAGTCCTCATATCCG
Hypoxia	EGLN3	Forward	GAACAGGTTATGTTCCGCCACGTG
		Reverse	CCCTCTGGAAATATCCGCAGGA

Quantitative image analysis

Immunostained images were automatically analyzed using a homemade routine workflow using MATLAB® software, as described in (Goodarzi et al., 2021). Nuclei were segmented

directly in Matlab and the mask were used to determine subcellular localization of different protein from the periphery to the center of the spheroid.

Live movies were automatically analyzed using a homemade routine workflow using MATLAB® software. After spheroids segmentation, the area and mean intensity of fluorescence was measured directly in Matlab®. Density of fluorescence was calculated as the mean intensity of fluorescence normalized by the background intensity I_0 and by the size of the spheroids as follow:

$$D = \frac{(I - I_0)/I_0}{Volume}$$

Where volume is assimilated to a sphere and calculated as follow:

$$Volume = \frac{4}{3} \pi * \left(\frac{Area}{\pi} \right)^{3/2}$$

Statistics and reproducibility of experiments

Statistical data were expressed as mean \pm standard deviation unless mentioned otherwise. Sample size (n) and the number of repetitions (N) are specified in the text of the paper or figure legends. The statistical significance between experimental conditions was determined by a two-tailed unpaired t-test, Welch's test, or Mann-Whitney test after confirming that the data met appropriate assumptions (normality distribution, homogeneous variance, and independent sampling). All data were analyzed with GraphPad Prism 8.0. (San Diego, CA, USA). **** P<0.0001, *** P<0.001, ** P<0.01, * P<0.05.

References

- Alessandri, K., Sarangi, B.R., Gurchenkov, V.V., Sinha, B., Kießling, T.R., Fetler, L., Rico, F., Scheuring, S., Lamaze, C., Simon, A., Geraldo, S., Vignjevic, D., Doméjean, H., Rolland, L., Funfak, A., Bibette, J., Bremond, N., Nassoy, P., 2013. Cellular capsules as a tool for multicellular spheroid production and for investigating the mechanics of tumor progression in vitro. *Proc. Natl. Acad. Sci. U. S. A.* 110, 14843–8. <https://doi.org/10.1073/pnas.1309482110>
- Arab-Bafrani, Z., Shahbazi-Gahrouei, D., Abbasian, M., Saberi, A., Fesharaki, M., Hejazi, S.H., Manshaee, S., 2016. Culturing in serum-free culture medium on collagen type-I-coated plate increases expression of CD133 and retains original phenotype of HT-29 cancer stem cell. *Adv. Biomed. Res.* 5, 59. <https://doi.org/10.4103/2277-9175.179181>
- Azzolin, L., Panciera, T., Soligo, S., Enzo, E., Bicciato, S., Dupont, S., Bresolin, S., Frasson, C., Basso, G., Guzzardo, V., Fassina, A., Cordenonsi, M., Piccolo, S., 2014. YAP/TAZ incorporation in the β -catenin destruction complex orchestrates the Wnt response. *Cell* 158, 157–170. <https://doi.org/10.1016/j.cell.2014.06.013>
- Azzolin, L., Zanconato, F., Bresolin, S., Forcato, M., Basso, G., Bicciato, S., Cordenonsi, M., Piccolo, S., 2012. Role of TAZ as mediator of Wnt signaling. *Cell* 151, 1443–1456. <https://doi.org/10.1016/j.cell.2012.11.027>
- Baenke, F., Chaneton, B., Smith, M., Van Den Broek, N., Hogan, K., Tang, H., Viros, A., Martin, M., Galbraith, L., Girotti, M.R., Dhomen, N., Gottlieb, E., Marais, R., 2016. Resistance to BRAF inhibitors induces glutamine dependency in melanoma cells. *Mol. Oncol.* 10, 73–84. <https://doi.org/10.1016/j.molonc.2015.08.003>
- Baer, P.C., Griesche, N., Luttmann, W., Schubert, R., Luttmann, A., Geiger, H., 2010. Human adipose-derived mesenchymal stem cells in vitro: evaluation of an optimal expansion medium preserving stemness. *Cytotherapy* 12, 96–106. <https://doi.org/10.3109/14653240903377045>
- Bragado, P., Estrada, Y., Parikh, F., Krause, S., Capobianco, C., Farina, H.G., Schewe, D.M., Aguirre-Ghiso, J.A., 2013. TGF- β 2 dictates disseminated tumour cell fate in target organs through TGF- β -RIII and p38 α / β signalling. *Nat. Cell Biol.* 15, 1351–1361. <https://doi.org/10.1038/ncb2861>
- Butcher, D.T., Alliston, T., Weaver, V.M., 2009. A tense situation: Forcing tumour progression. *Nat. Rev. Cancer* 9, 108–122. <https://doi.org/10.1038/nrc2544>
- Byun, J.-K., Choi, Y.-K., Kim, J.-H., Jeong, J.Y., Jeon, H.-J., Kim, M.-K., Hwang, I., Lee, S.-Y., Lee, Y.M., Lee, I.-K., Park, K.-G., 2017. A Positive Feedback Loop between Sestrin2 and mTORC2 Is Required for the Survival of Glutamine-Depleted Lung Cancer Cells. *Cell Rep.* 20, 586–599. <https://doi.org/10.1016/j.celrep.2017.06.066>
- Chambost, A.J., Berabez, N., Cochet-Escartin, O., Ducray, F., Gabut, M., Isaac, C., Martel, S., Idbaih, A., Rousseau, D., Meyronet, D., Monnier, S., 2022. Machine learning-based detection of label-free cancer stem-like cell fate. *Sci. Rep.* 12, 19066. <https://doi.org/10.1038/s41598-022-21822-z>
- Chen, G., Guo, Y., Li, C., Li, S., Wan, X., 2020. Small Molecules that Promote Self-Renewal of Stem Cells and Somatic Cell Reprogramming. *Stem Cell Rev. Rep.* 16, 511–523. <https://doi.org/10.1007/s12015-020-09965-w>

- Chen, G., Yin, S., Zeng, H., Li, H., Wan, X., 2022. Regulation of Embryonic Stem Cell Self-Renewal. *Life* 12, 1151. <https://doi.org/10.3390/life12081151>
- Choi, Y.-K., Park, K.-G., 2018. Targeting Glutamine Metabolism for Cancer Treatment. *Biomol. Ther.* 26, 19–28. <https://doi.org/10.4062/biomolther.2017.178>
- Clevers, H., 2006. Wnt/ β -Catenin Signaling in Development and Disease. *Cell* 127, 469–480. <https://doi.org/10.1016/j.cell.2006.10.018>
- Delarue, M., Montel, F., Vignjevic, D., Prost, J., Joanny, J.F., Cappello, G., 2014. Compressive stress inhibits proliferation in tumor spheroids through a volume limitation. *Biophys. J.* 107, 1821–1828. <https://doi.org/10.1016/j.bpj.2014.08.031>
- Desmaison, A., Frongia, C., Grenier, K., Ducommun, B., Lobjois, V., 2013. Mechanical Stress Impairs Mitosis Progression in Multi-Cellular Tumor Spheroids. *PLOS ONE* 8, e80447. <https://doi.org/10.1371/journal.pone.0080447>
- Diamantopoulou, Z., White, G., Fadlullah, M.Z.H., Dreger, M., Pickering, K., Maltas, J., Ashton, G., MacLeod, R., Baillie, G.S., Kouskoff, V., Lacaud, G., Murray, G.I., Sansom, O.J., Hurlstone, A.F.L., Malliri, A., 2017. TIAM1 Antagonizes TAZ/YAP Both in the Destruction Complex in the Cytoplasm and in the Nucleus to Inhibit Invasion of Intestinal Epithelial Cells. *Cancer Cell* 31, 621–634.e6. <https://doi.org/10.1016/j.ccell.2017.03.007>
- Diepenbruck, M., Waldmeier, L., Ivanek, R., Berninger, P., Arnold, P., van Nimwegen, E., Christofori, G., 2014. Tead2 expression levels control the subcellular distribution of Yap and Taz, zyxin expression and epithelial-mesenchymal transition. *J. Cell Sci.* 127, 1523–1536. <https://doi.org/10.1242/jcs.139865>
- Dolega, M.E., Monnier, S., Brunel, B., Joanny, J.F., Recho, P., Cappello, G., 2021. Extra-cellular matrix in multicellular aggregates acts as a pressure sensor controlling cell proliferation and motility. *eLife* 10. <https://doi.org/10.7554/ELIFE.63258>
- Dotse, E., Bian, Y., 2016. Isolation of colorectal cancer stem-like cells. *Cytotechnology* 68, 609–619. <https://doi.org/10.1007/s10616-014-9806-0>
- Gheytauchi, E., Naseri, M., Karimi-Busheri, F., Atyabi, F., Mirsharif, E.S., Bozorgmehr, M., Ghods, R., Madjd, Z., 2021. Morphological and molecular characteristics of spheroid formation in HT-29 and Caco-2 colorectal cancer cell lines. *Cancer Cell Int.* 21, 1–16. <https://doi.org/10.1186/s12935-021-01898-9>
- Goodarzi, S., Prunet, A., Rossetti, F., Bort, G., Tillement, O., Porcel, E., Lacombe, S., Wu, T.-D., Guerquin-Kern, J.-L., Delanoë-Ayari, H., Lux, F., Rivière, C., 2021. Quantifying nanotherapeutic penetration using a hydrogel-based microsystem as a new 3D in vitro platform. *Lab. Chip* 21, 2495–2510. <https://doi.org/10.1039/d1lc00192b>
- Heddleston, J.M., Li, Z., Lathia, J.D., Bao, S., Hjelmeland, A.B., Rich, J.N., 2010. Hypoxia inducible factors in cancer stem cells. *Br. J. Cancer* 102, 789–795. <https://doi.org/10.1038/sj.bjc.6605551>
- Heddleston, J.M., Li, Z., McLendon, R.E., Hjelmeland, A.B., Rich, J.N., 2009. The hypoxic microenvironment maintains glioblastoma stem cells and promotes reprogramming towards a cancer stem cell phenotype. *Cell Cycle Georget. Tex* 8, 3274–3284. <https://doi.org/10.4161/cc.8.20.9701>

- Hensley, C.T., Wasti, A.T., DeBerardinis, R.J., 2013. Glutamine and cancer: cell biology, physiology, and clinical opportunities. *J. Clin. Invest.* 123, 3678–3684. <https://doi.org/10.1172/JCI69600>
- Jäger, A., Heim, N., Kramer, F.J., Setiawan, M., Peitz, M., Konermann, A., 2020. A novel serum-free medium for the isolation, expansion and maintenance of stemness and tissue-specific markers of primary human periodontal ligament cells. *Ann. Anat. - Anat. Anz.* 231, 151517. <https://doi.org/10.1016/j.aanat.2020.151517>
- Jain, R.K., Martin, J.D., Stylianopoulos, T., 2014. The role of mechanical forces in tumor growth and therapy. *Annu. Rev. Biomed. Eng.* 16, 321–46. <https://doi.org/10.1146/annurev-bioeng-071813-105259>
- Karlsson, S., Nyström, H., 2022. The extracellular matrix in colorectal cancer and its metastatic settling – Alterations and biological implications. *Crit. Rev. Oncol. Hematol.* 175, 103712. <https://doi.org/10.1016/j.critrevonc.2022.103712>
- Kim, S.-Y., 2015. Cancer metabolism: targeting cancer universality. *Arch. Pharm. Res.* 38, 299–301. <https://doi.org/10.1007/s12272-015-0551-5>
- Lee, G., Hall, R.R., Ahmed, A.U., Ahmed, A.U., 2016. Cancer Stem Cells: Cellular Plasticity, Niche, and its Clinical Relevance. *J. Stem Cell Res. Ther.* 6. <https://doi.org/10.4172/2157-7633.1000363>
- Lien, W.-H., Fuchs, E., 2014. Wnt some lose some: transcriptional governance of stem cells by Wnt/ β -catenin signaling. *Genes Dev.* 28, 1517–1532. <https://doi.org/10.1101/gad.244772.114>
- Liu, Y., Song, Z., Zhao, Y., Qin, H., Cai, J., Zhang, H., Yu, T., Jiang, S., Wang, G., Ding, M., Deng, H., 2006. A novel chemical-defined medium with bFGF and N2B27 supplements supports undifferentiated growth in human embryonic stem cells. *Biochem. Biophys. Res. Commun.* 346, 131–139. <https://doi.org/10.1016/j.bbrc.2006.05.086>
- Llado, V., Nakanishi, Y., Duran, A., Reina-Campos, M., Shelton, P.M., Linares, J.F., Yajima, T., Campos, A., Aza-Blanc, P., Leitges, M., Diaz-Meco, M.T., Moscat, J., 2015. Repression of Intestinal Stem Cell Function and Tumorigenesis through Direct Phosphorylation of β -Catenin and Yap by PKC ζ . *Cell Rep.* 10, 740–754. <https://doi.org/10.1016/j.celrep.2015.01.007>
- Madl, C.M., Heilshorn, S.C., 2018. Engineering Hydrogel Microenvironments to Recapitulate the Stem Cell Niche. *Annu. Rev. Biomed. Eng.* 20, 21–47. <https://doi.org/10.1146/annurev-bioeng-062117-120954>
- Mani, S.A., Guo, W., Liao, M.-J., Eaton, E.N., Ayyanan, A., Zhou, A.Y., Brooks, M., Reinhard, F., Zhang, C.C., Shipitsin, M., Campbell, L.L., Polyak, K., Brisken, C., Yang, J., Weinberg, R.A., 2008. The epithelial-mesenchymal transition generates cells with properties of stem cells. *Cell* 133, 704–715. <https://doi.org/10.1016/j.cell.2008.03.027>
- Monnier, S., Delarue, M., Brunel, B., Dolega, M.E., Delon, A., Cappello, G., 2016. Effect of an osmotic stress on multicellular aggregates. *Methods* 94, 114–119. <https://doi.org/10.1016/j.ymeth.2015.07.009>
- Montel, F., Delarue, M., Elgeti, J., Malaquin, L., Basan, M., Risler, T., Cabane, B., Vignjevic, D., Prost, J., Cappello, G., Joanny, J.F., 2011. Stress clamp experiments on multicellular tumor spheroids. *Phys. Rev. Lett.* 107, 1–4. <https://doi.org/10.1103/PhysRevLett.107.188102>

- Montel, F., Delarue, M., Elgeti, J., Vignjevic, D., Cappello, G., Prost, J., 2012. Isotropic stress reduces cell proliferation in tumor spheroids. *New J. Phys.* 14, 055008. <https://doi.org/10.1088/1367-2630/14/5/055008>
- Nassar, D., Blanpain, C., 2016. Cancer Stem Cells: Basic Concepts and Therapeutic Implications. *Annu. Rev. Pathol.* 11, 47–76. <https://doi.org/10.1146/annurev-pathol-012615-044438>
- ND, M., RA, W., CL, C., 2013. Cell plasticity and heterogeneity in cancer. *Clin. Chem.* 59, 168–179. <https://doi.org/10.1373/CLINCHEM.2012.184655>
- Nia, H.T., Liu, H., Seano, G., Datta, M., Jones, D., Rahbari, N., Incio, J., Chauhan, V.P., Jung, K., Martin, J.D., Askoxylakis, V., Padera, T.P., Fukumura, D., Boucher, Y., Hornicek, F.J., Grodzinsky, A.J., Baish, J.W., Munn, L.L., Jain, R.K., 2017. Solid stress and elastic energy as measures of tumour mechanopathology. *Nat. Biomed. Eng.* 1, 1–11. <https://doi.org/10.1038/s41551-016-0004>
- Oudhoff, M.J., Braam, M.J.S., Freeman, S.A., Wong, D., Rattray, D.G., Wang, J., Antignano, F., Snyder, K., Refaeli, I., Hughes, M.R., McNagny, K.M., Gold, M.R., Arrowsmith, C.H., Sato, T., Rossi, F.M.V., Tatlock, J.H., Owen, D.R., Brown, P.J., Zaph, C., 2016. SETD7 Controls Intestinal Regeneration and Tumorigenesis by Regulating Wnt/ β -Catenin and Hippo/YAP Signaling. *Dev. Cell* 37, 47–57. <https://doi.org/10.1016/j.devcel.2016.03.002>
- Paul, R., Dorsey, J.F., Fan, Y., 2021. Cell plasticity, senescence, and quiescence in cancer stem cells: Biological and therapeutic implications. *Pharmacol. Ther.* 107985. <https://doi.org/10.1016/j.pharmthera.2021.107985>
- Pistollato, F., Abbadì, S., Rampazzo, E., Persano, L., Della Puppa, A., Frasson, C., Sarto, E., Scienza, R., D'avella, D., Basso, G., 2010. Intratumoral hypoxic gradient drives stem cells distribution and MGMT expression in glioblastoma. *Stem Cells Dayt. Ohio* 28, 851–862. <https://doi.org/10.1002/stem.415>
- Rainho, M. de A., Mencialha, A.L., Thole, A.A., 2021. Hypoxia effects on cancer stem cell phenotype in colorectal cancer: a mini-review. *Mol. Biol. Rep.* 48, 7527–7535. <https://doi.org/10.1007/s11033-021-06809-9>
- Relier, S., Ripoll, J., Guillorit, H., Amalric, A., Achour, C., Boissière, F., Vialaret, J., Attina, A., Debart, F., Choquet, A., Macari, F., Marchand, V., Motorin, Y., Samalin, E., Vasseur, J.-J., Pannequin, J., Aguilo, F., Lopez-Crapez, E., Hirtz, C., Rivals, E., Bastide, A., David, A., 2021. FTO-mediated cytoplasmic m6Am demethylation adjusts stem-like properties in colorectal cancer cell. *Nat. Commun.* 12, 1716. <https://doi.org/10.1038/s41467-021-21758-4>
- Relier, S., Yazdani, L., Ayad, O., Choquet, A., Bourgaux, J.-F., Prudhomme, M., Pannequin, J., Macari, F., David, A., 2016. Antibiotics inhibit sphere-forming ability in suspension culture. *Cancer Cell Int.* 16, 6. <https://doi.org/10.1186/s12935-016-0277-6>
- Rinaldi, G., Rossi, M., Fendt, S.-M., 2018. Metabolic interactions in cancer: cellular metabolism at the interface between the microenvironment, the cancer cell phenotype and the epigenetic landscape. *WIREs Syst. Biol. Med.* 10, e1397. <https://doi.org/10.1002/wsbm.1397>
- Riviere, C., Prunet, A., Fuoco, L., Delanoë-Ayari, H., 2018. Plaque de Micropuits En Hydrogel Biocompatible (Biocompatible Hydrogel Microwell Plate) FR3079524A1.
- Rizzuti, I.F., Mascheroni, P., Arcucci, S., Ben-Mériem, Z., Prunet, A., Barentin, C., Rivière, C., Delanoë-Ayari, H., Hatzikirou, H., Guillermet-Guibert, J., Delarue, M., 2020. Mechanical Control of Cell

- Proliferation Increases Resistance to Chemotherapeutic Agents. *Phys. Rev. Lett.* 125, 128103. <https://doi.org/10.1103/PhysRevLett.125.128103>
- Roy Choudhury, A., Gupta, S., Chaturvedi, P.K., Kumar, N., Pandey, D., 2019. Mechanobiology of Cancer Stem Cells and Their Niche. *Cancer Microenviron.* 12, 17–27. <https://doi.org/10.1007/s12307-019-00222-4>
- Shao, D.D., Xue, W., Krall, E.B., Bhutkar, A., Piccioni, F., Wang, X., Schinzel, A.C., Sood, S., Rosenbluh, J., Kim, J.W., Zwang, Y., Roberts, T.M., Root, D.E., Jacks, T., Hahn, W.C., 2014. KRAS and YAP1 Converge to Regulate EMT and Tumor Survival. *Cell* 158, 171–184. <https://doi.org/10.1016/j.cell.2014.06.004>
- Sheridan, C., 2019. Pancreatic cancer provides testbed for first mechanotherapeutics. *Nat. Biotechnol.* 37, 829–831. <https://doi.org/10.1038/d41587-019-00019-2>
- Sherr, C.J., Roberts, J.M., 1999. CDK inhibitors: positive and negative regulators of G1-phase progression. *Genes Dev.* 13, 1501–1512.
- Totaro, A., Panciera, T., Piccolo, S., 2018. YAP/TAZ upstream signals and downstream responses. *Nat. Cell Biol.* 20, 888–899. <https://doi.org/10.1038/s41556-018-0142-z>
- Visvader, J.E., Lindeman, G.J., 2012. Cancer stem cells: current status and evolving complexities. *Cell Stem Cell* 10, 717–28. <https://doi.org/10.1016/j.stem.2012.05.007>
- Windmueller, H.G., Spaeth, A.E., 1974. Uptake and Metabolism of Plasma Glutamine by the Small Intestine. *J. Biol. Chem.* 249, 5070–5079. [https://doi.org/10.1016/S0021-9258\(19\)42329-6](https://doi.org/10.1016/S0021-9258(19)42329-6)
- Zanconato, F., Cordenonsi, M., Piccolo, S., 2016. YAP/TAZ at the Roots of Cancer. *Cancer Cell* 29, 783–803. <https://doi.org/10.1016/j.ccell.2016.05.005>
- Zoetemelk, M., Rausch, M., Colin, D.J., Dormond, O., Nowak-Sliwinska, P., 2019. Short-term 3D culture systems of various complexity for treatment optimization of colorectal carcinoma. *Sci. Rep.* 9, 7103. <https://doi.org/10.1038/s41598-019-42836-0>

Chapter 4

General Discussion and Perspectives

« La connaissance scientifique possède en quelque sorte des propriétés fractales : nous avons beau accroître notre savoir, le reste – si infime soit-il – sera toujours si infiniment complexe que l'ensemble de départ »

Isaac Asimov

Content

LONG-TERM CANCER CELL NUCLEAR ADAPTATION TO IMPOSED DEFORMATION	165
IN DEPTH-UNDERSTANDING OF THE MECHANISMS AND MOLECULAR PATHWAY(S) INVOLVED IN SUCH NUCLEAR ADAPTATION	165
IN DEPTH-ANALYSIS OF THE CONSEQUENCES OF SUCH NUCLEAR ADAPTATION FOR CANCER RELAPSE AND RESISTANCE TO TREATMENT	171
CANCER CELL IDENTITY CHANGE UNDER LONG-TERM MECHANICAL CONSTRAINTS.....	172
REFERENCES	174

Long-term cancer cell nuclear adaptation to imposed deformation

The design and development of the soft confiner allowed filling the gap of in vitro assays to evaluate the long-term impact of applied strain. This device enables to impose a precise uniaxial confinement on cells for several days using agarose hydrogel to passively renew the medium in which cells grow during such a long period. In this work, we have demonstrated that cells nuclei can adapt to strong deformation as they go through division. The regulation of nuclear volume and tension is an active process requiring the contractility machinery and mediated by mitosis to reach a new homeostasis state. We have shown that this global regulation is defined by the apparent total surface of the nuclear envelope. These interesting results raise new questions about such fundamental regulation that would be interesting to analyze deeper. The results obtained in this part of my PhD now calls for (1) an in-depth knowledge of the molecular pathway(s) involved in such volume adaptation, and (2) an understanding of the implications of such adaptation for cancer relapse and treatment resistance.

[In depth-understanding of the mechanisms and molecular pathway\(s\) involved in such nuclear adaptation](#)

What are the underlying mechanosensitive pathways involved?

Many different mechanosensitive pathways could be implied in such volume adaptation. We could think of the stretched-activated Piezo channels at the cell membrane, or the role of focal adhesions and integrins in mediating mechanical signals to the nucleus through the cytoskeleton and LINC complex. This can lead to the activation of several signaling pathways such as Wnt, MAPK/ERK, PI3K/AKT and other mechanosensitive transcription factors like YAP/TAZ. B-catenin/Wnt signaling can also be activated by changes in cell-cell adhesion. It is possible to modulate cell adhesion and therefore the nuclear prestress by changing coating of the coverslip to impair integrins to nucleus mechanotransduction and study its impact on nuclear adaptation to confinement.

Staining of the YAP transcription factor under several levels of confinement was performed and testifies of the complexity of the mechanisms involved in long time scale range. Indeed, preliminary data show an important heterogeneity of YAP subcellular localization both in time and according to the level of imposed deformation (Figure 45a). Although it has not been quantified yet, it seems that after 2 h, YAP nuclear localization is increased with an increase in confinement. Interestingly, this nuclear localisation seems lost after 24h which corresponds to the release of the NE tension.

Intriguingly, after 2 h and under very strong confinement, YAP is preferentially localized within nuclear blebs (Figure 45b) although no nuclear pores nor LINC complexes are found at this

portion of the nuclear membrane (Davidson et al., 2014; Denais et al., 2016; Raab et al., 2016; Srivastava et al., 2021). A reasonable explanation of this intriguing YAP localization could be a consequence of the heterochromatin decondensation following the unfolding of the nuclear envelope. Subsequently, activated genes might be regulated by YAP transcription factor. Moreover, it has been shown that mechanical forces imposed on the nucleus facilitate the nuclear accumulation of diverse transcription factors (Dantas et al., 2022; Lombardi and Lammerding, 2011).

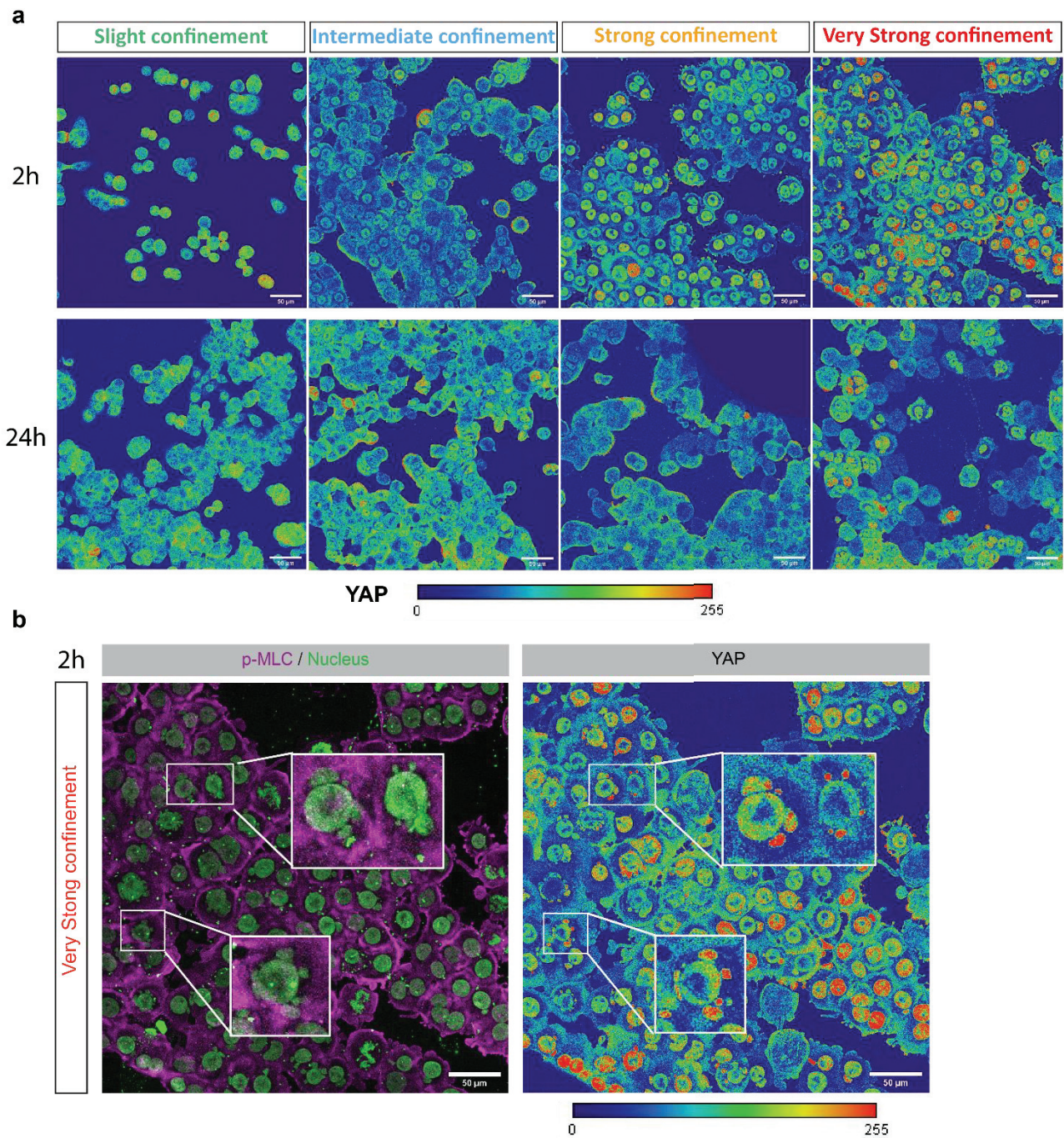


Figure 45: Representative images of stained YAP in HT-29 cells under confinement.

(a) Representative images of stained YAP under several levels of confinement at 2 h and 24 h. *Scale bar = 50 μ m.* **(b)** Representative images of stained nuclei, p-MLC and YAP with zoomed blebbing nuclei under very strong confinement at 2 h. *Scale bar = 50 μ m.*

Are other cellular signaling activated under this prolonged imposed deformation?

We have shown the absence of long-term nuclear volume and tension adaptation with blebbistatin and therefore the necessity of the contractility machinery for this global nuclear adaptation. Moreover, as shown in Lomakin et al., 2020, confinement increases nuclear tension which triggers cPLA2 activation, and calcium release. To test if this long-term nuclear adaptation is calcium-dependent, the release of calcium ions from internal stores was blocked using BAPTA-AM combined with 2APB. We evidenced an absence of nuclear area regulation under strong confinement at 24 h (Figure 46b). The dependency on cPLA2 activity was also tested by interfering with cPLA2 activity with AACOCF3 drug. No long-term nuclear volume adaptation was observed under strong confinement (Figure 46c), confirming the essential role of both intracellular calcium and cPLA2 activation in long-term nuclear volume adaptation. These very interesting results were obtained by Morgane Roinard, a current intern in the team. However, the impact of these drugs on nuclear envelope folding and tension is still under investigation. We can also wonder about the role of other cytoskeleton proteins on nuclear volume and tension adaptation. Vimentin intermediate filaments in particular raised our attention as it has been shown to form a protective cage around the nucleus under confinement (Patteson et al., 2019). Therefore, preliminary experiments of stained vimentin under several levels of confinement were performed, indicating a potential regulation of vimentin as well after 24 h of confinement (Figure 47).

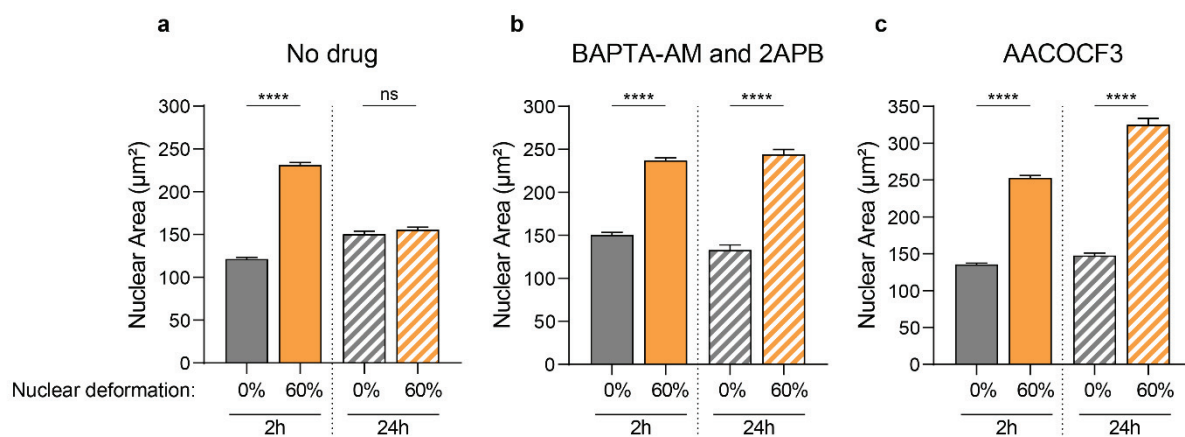


Figure 46: Nuclear Area adaptation is altered under contractility linked drugs.

(a) Nuclear projected area adaptation at 24h under strong confinement. $N=3$ experiments with $n=3484$ cells, mean \pm SEM, Welch's t test. (b) Nuclear projected area quantification under calcium inhibition drugs BAPTA-AM and 2APB at 2 h and 24 h without confinement or under strong confinement. $N=3$ experiments with $n=2597$ cells, mean \pm SEM, Welch's t test. (c) Nuclear projected area quantification under cPLA2 drug AACOCF3 at 2 h and 24 h without confinement or under strong confinement. $N=3$ experiments with $n=4177$ cells, mean \pm SEM, Welch's t test. **** $P<0.0001$. Results were obtained by Morgane Roinard, current M2 intern.

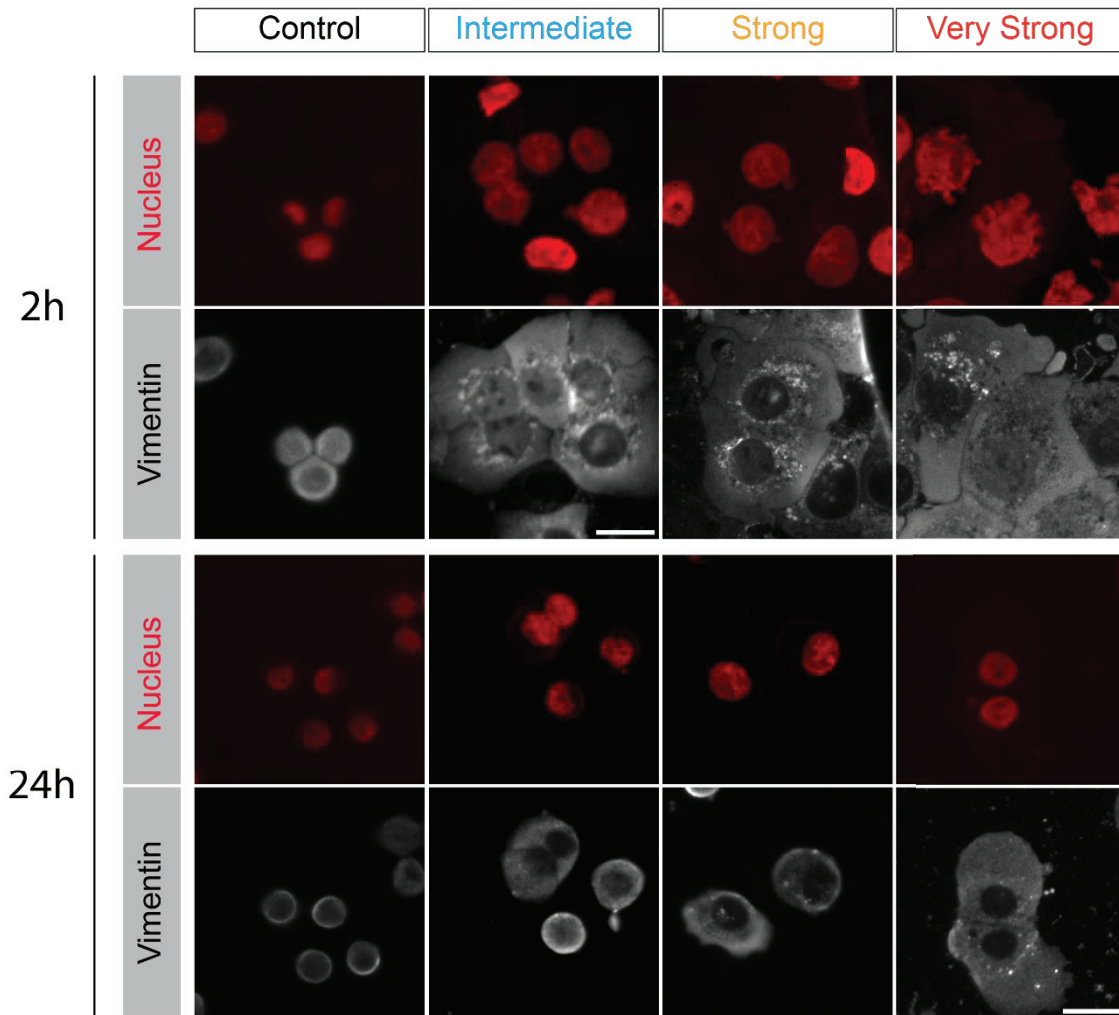


Figure 47: Representative images of stained vimentin in HT-29 cells under different levels of confinement. Stained nuclei and vimentin after 2 h and 24 h of confinement. *Scale bar = 20 μ m.*

What about the whole cell?

An important question to raise is if the whole cell follows the same nuclear volume regulation in order to keep a nuclear to cell volume ratio constant as cytoplasmic and nuclear volume are normally tightly coupled. However, it has recently been shown that substantial increase of nuclear envelope tension leads to uncoupling of nucleo-cytoplasmic volume coupling due to a higher nuclear import (Andreu et al., 2022; Pennacchio et al., 2022). Several methods compatible with our soft confiner system could be used to obtain precisely the cell volume like Fluorescence Exclusion Microscopy, or membrane markers staining.

How confinement influences migratory properties and invasion capacities of cancer cells?

Confinement-triggered cPLA2 activation and calcium release provoke downstream actomyosin contractility that results in increased cell migratory capacity (Lomakin et al., 2020; Venturini et al., 2020). This increased migratory behavior was also observed with our HT-29 epithelial cell

line under strong deformation which corresponds to the same confinement threshold showed in Lomakin et al., (5 μm confinement). Moreover, this behavior is even more striking during mitosis, triggered by the nuclear envelope breakdown, as polar plot tracks are more spread under strong confinement compared to control (Figure 48). One hypothesis is the release of intranuclear pressure within the cytoplasm triggering a burst of pressure and the rapid actin cortical flow in the front of plasma membrane leader bleb-based migration (Bergert et al., 2015; García-Arcos et al., 2022; Logue et al., 2015).

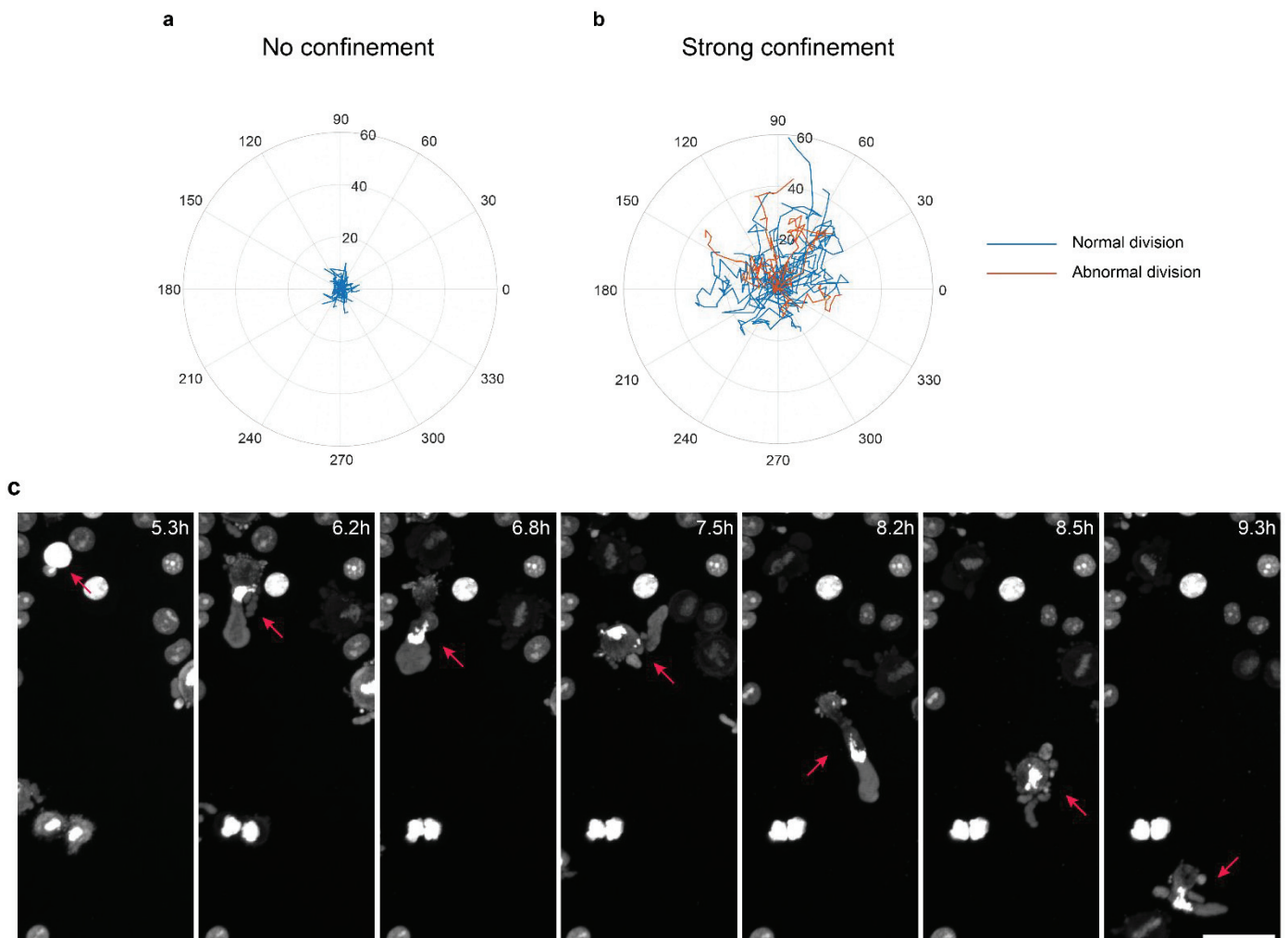


Figure 48: Nuclei displacement during mitosis.

Polar plot of nuclei displacement during mitosis (from nuclear envelope breakdown to cytokinesis) without confinement (a) or under strong confinement (b). (c) Timelapse images NLS-RFP and histone-stained nuclei under strong confinement. Red arrows show the displacement of a nuclei during mitosis under strong confinement. Scale bar = 50 μm .

What is the influence of agarose stiffness on long-term nuclear adaptation?

We can hypothesize that a reduced stiffness will allow the cells to deform the above agarose gel, therefore being less sensitive to the imposed deformation. A reduced stiffness could also

lead to classical round mitosis (Lancaster et al., 2013) preventing the long-term nuclear adaptation that we evidenced. To change agarose gel stiffness, two possibilities are available: either a change in standard agarose concentration or using low melting point agarose.

How will a release of confinement affect nucleus size after it has reached a new volume and tension homeostasis?

The removal of the imposed deformation should not have the same effect if it is done before or after the first mitosis. Before mitosis, confinement removal should release nuclear tension, and the nuclear state should return as before the applied deformation.

However, if the confinement is removed after the first mitosis, nuclear regulation would have already happened resulting in a smaller nucleus with an untensed nuclear envelope. We can thus wonder if the nucleus will then swell to its original size pre-confinement or keep its smaller post-regulated one. Driven by the fact that the nuclear apparent surface sets the nuclear volume, one major hypothesis that could explain our geometrical model is that nuclear envelope reforms at the “metaphasic plaque” which is not spherical. Following that hypothesis, if the confinement is removed after the first mitosis, nuclei would keep their smaller size until the second division where they should go back to their original (pre-confinement) size instead of reaching a homeostasis. Therefore, testing this hypothesis would provide revealing information on the mechanisms involved in nuclear volume regulation arising during mitosis.

Is prolonged confinement affecting other colorectal cancer cell lines in the same way?

We can wonder if this global long-term nuclear adaptation is a ubiquitous cancerous phenomenon and if the stage of invasiveness, as well as nuclear structure composition could modify this regulation. Preliminary experiments were performed by Alexis Saffon, a previous intern in the team, on HCT-116 colorectal cell line. HCT-116 is a more invasive cell line, but with no p53 mutation, is MSI, and has a different nuclear structure composition (with larger amount of lamin B2). Preliminary results shown in Figure 49 are difficult to interpret but seem to indicate no nuclear regulation at 24 h under strong confinement for HCT-116 cells. Despite higher levels of B-type lamins in HCT-116 nuclear envelope – which increases nuclear envelope elasticity (Wintner et al., 2020) –, nuclei with blebs are still observed under strong confinement (Figure 49c). Moreover, the presence of both lamin B2, essential for mitotic spindle formation (Kuga et al., 2014), and unmutated p53 could alter confined mitosis explaining this absence of long-term global nuclear regulation. To test whether the structural composition of the nuclear envelope or the genetical status of cancer cells explains the mitosis-mediated nuclear adaptation to confinement is the use of HCT-116 p53^{-/-} cell line, that can be provided by our

collaborators (Cédric Chaveroux from the CRCL). In addition, the MSI status of HCT-116 cell line will more likely not regulate confinement induced DNA-damages at 24 h of confinement.

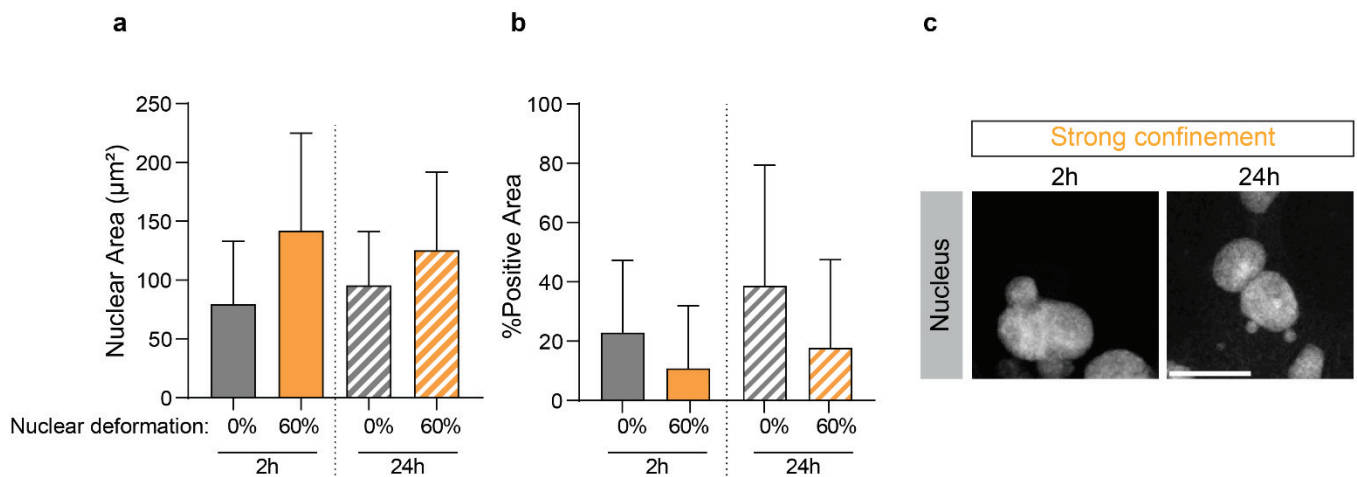


Figure 49: HCT-116 cell lines nuclear readouts under strong confinement.

(a) Quantification of nuclear projected area of HCT-116 under strong confinement at 2 h or 24 h ($N=1$). (b) Quantification of the positive area of the nuclear envelope (lamin A/C) which represents the folded nuclear envelope ($N=1$). (c) Representative images of HCT-116 nuclei at 2 h and 24 h under strong confinement. Scale bar = 20 μm . Results were obtained by Alexis Saffon, a former intern.

In depth-analysis of the consequences of such nuclear adaptation for cancer relapse and resistance to treatment

How this regulation affects transcription activity and protein expression?

Evidence have shown that lamins have a role in the regulation of transcription, replication, and genome stability (Mattout-Drubezki and Gruenbaum, 2003; Patil and Sengupta, 2021) and are also implicated in DNA repair pathways. Moreover, chromatin organization and condensation are linked to gene expression. Thus, the long-term adaptation of the nuclear envelope that we evidenced might be linked to downstream changes in cell transcriptome and proteome, helping the cell to reach a new homeostatic state under confinement.

What are the consequences of such long-term adaptation to mechanical constraints on therapy resistance? How can we play on that to favor drug response?

Long-term nuclear global adaptation to confinement, together with repair of DNA damage, both correlated with cell-cycle re-entry could prevent the efficacy of anti-cancerous drugs as most of them affect cell proliferation and cell cycle. Therefore, long term confinement experiments under 5-FU chemotherapy (which is the reference treatment for colorectal cancer) are planned to investigate the therapeutic impact of such nuclear adaptation to imposed deformation.

Cancer cell identity change under long-term mechanical constraints

In the third chapter, we have demonstrated in a standardized and controlled manner the importance of both nutritive and mechanical environments on cancer cells identity in a 3D model tissue (tumor spheroids). Indeed, culture medium conditions highly influence cancer cells' fate, modifying their compactness and differentiation state, hence strengthening tumor heterogeneity. Moreover, tumor dynamics analysis highlights the formation of cancer stem-like cells under mechanical stress, through the dedifferentiation of committed cells. These results open new questions on the impact of nutrients and mechanical environment, both influencing the phenotype and gene expression of colorectal spheroids.

What are the effects of isotropic compression on the ECM/non-cellular structure?

Mechanical compression not only impacts cancer cells but has an overall impact on the surrounding ECM structure. Therefore, the impact of mechanical stress can be direct on cells, or indirect by compressing the ECM and thus limiting cell's access to nutrients or diverse molecules such as cytokines. Studying the diffusion properties within the 3D tumor spheroids under mechanical constraint is of importance for better understanding the impact of physico-chemical gradient in cancer development or drug accessibility. Moreover, the spatial distribution of stress could be heterogenous as well, with a tension at the surface of the tumor spheroid different from the inner cell compression. Assessing this spatial distribution of effective mechanical stress on cancer cells' fate might give us information on the heterogeneity of cell identity within a tumor and might be linked to cellular volume and crowding spatially distributed shown by Han et al., 2019 in breast cancer. This is notably the topic of the thesis of G. Jardiné.

What are the consequences at the unicellular level of such functional and phenotypic regulation?

It could be interesting to investigate the target genes impacted by these functional and phenotypic regulations. Indeed, cell size, cell crowding as well as cell cycle progression could be altered by both metabolic and mechanical stress. In the team, these parameters are currently under investigation by the current PhD work of G. Jardiné.

How tumor heterogeneity impacts cancer treatment and contributes to therapy resistance?

Tumor heterogeneity is a hallmark of cancer and, as described in this manuscript, highly contributes to therapy resistance. Therefore, understanding to which extent environment-driven plasticity affects cancer cell identity is crucial for patient prognosis and personalized therapy. For that, quantification of both the spatial distribution of cancer stem cells within a tumor spheroid and the proportion of dedifferentiated cells is needed. Spheroids immunostainings experiments for CSC makers are planned before my PhD defense. Moreover, it could be interesting to treat colorectal tumor spheroids with 5-FU (colorectal reference

chemotherapy) under metabolic or mechanical stress or both to test whether tumor microenvironmental changes affect drug response.

Is this new tumoral identity under glutamine starvation and/or mechanical compression changing the invasiveness of cancer cells?

The stem-like phenotype observed in colorectal cancer cells under both glutamine starvation and mechanical compression could also affect cancer cells' tumorigenicity. To study the change in cancer cell invasiveness properties, an invasion assay can be performed. For that, spheroids can be seeded on a collagen bed and the speed of their spreading can be analyzed as well as the branching size. These experiments could be performed after the application of metabolic or mechanical stress on spheroids. It could be an interesting functional experiment to assess the effective changes of cancer cells' identity.

Will a more complex model of tumor spheroid also regulate its phenotype and identity under mechanical stress?

As we have shown in this work, it is crucial to take into account the tumor microenvironment when studying cancer development and progression, however our system remains simple as none of the stromal cellular environment was considered in our experiments. Indeed, parameters such as cell cohesion or ECM composition could be altered by CAFs. Immune cells could also alter tumor progression by secreting numerous factors, while vascular components could toggle the tumoral chemical gradient. Our tumor spheroid model is avascular and relatively small which has the advantage to generate no necrotic core. It would be interesting now to complexify the model to better recapitulate the complexity of *in vivo* tumors, by doing experiments with larger spheroids, including co-culture of CAFs, or including ECM for example.

What about other tumorigenicity colorectal cancer cell lines?

As in the 2D experiments, it could be interesting to reproduce those experiments with HCT-116 cell line which has a higher metastatic potential than HT-29, a different genomic instability, but no p53 mutation and a structural difference in terms of cell-cell cohesion and matrix production. Especially as 2D preliminary data shows differences between HT-29 and HCT-116 cell lines (Figure 49).

References

- Andreu, I., Granero-Moya, I., Chahare, N.R., Clein, K., Molina-Jordán, M., Beedle, A.E.M., Elosegui-Artola, A., Abenza, J.F., Rossetti, L., Trepas, X., Raveh, B., Roca-Cusachs, P., 2022. Mechanical force application to the nucleus regulates nucleocytoplasmic transport. *Nat. Cell Biol.* 24, 896–905. <https://doi.org/10.1038/s41556-022-00927-7>
- Bergert, M., Erzberger, A., Desai, R.A., Aspalter, I.M., Oates, A.C., Charras, G., Salbreux, G., Paluch, E.K., 2015. Force transmission during adhesion-independent migration. *Nat. Cell Biol.* 17, 524–529. <https://doi.org/10.1038/ncb3134>
- Dantas, M., Oliveira, A., Aguiar, P., Maiato, H., Ferreira, J.G., 2022. Nuclear tension controls mitotic entry by regulating cyclin B1 nuclear translocation. *J. Cell Biol.* 221, e202205051. <https://doi.org/10.1083/jcb.202205051>
- Davidson, P.M., Denais, C., Bakshi, M.C., Lammerding, J., 2014. Nuclear deformability constitutes a rate-limiting step during cell migration in 3-D environments. *Cell. Mol. Bioeng.* 7, 293–306. <https://doi.org/10.1007/s12195-014-0342-y>
- Denais, C.M., Gilbert, R.M., Isermann, P., McGregor, A.L., Te Lindert, M., Weigelin, B., Davidson, P.M., Friedl, P., Wolf, K., Lammerding, J., 2016. Nuclear envelope rupture and repair during cancer cell migration. *Science* 352, 353–358. <https://doi.org/10.1126/science.aad7297>
- García-Arcos, J.M., Ziegler, J., Grigolon, S., Reymond, L., Shajepal, G., Cattin, C.J., Lomakin, A., Müller, D., Ruprecht, V., Wieser, S., Voituriez, R., Piel, M., 2022. Advected percolation in the actomyosin cortex drives amoeboid cell motility. <https://doi.org/10.1101/2022.07.14.500109>
- Han, Y.L., Pegoraro, A.F., Li, H., Li, K., Yuan, Y., Xu, G., Gu, Z., Sun, J., Hao, Y., Gupta, S.K., Li, Y., Tang, W., Kang, H., Teng, L., Fredberg, J.J., Guo, M., 2019. Cell swelling, softening and invasion in a three-dimensional breast cancer model. *Nat. Phys.* <https://doi.org/10.1038/s41567-019-0680-8>
- Kuga, T., Nie, H., Kazami, T., Satoh, M., Matsushita, K., Nomura, F., Maeshima, K., Nakayama, Y., Tomonaga, T., 2014. Lamin B2 prevents chromosome instability by ensuring proper mitotic chromosome segregation. *Oncogenesis* 3, e94. <https://doi.org/10.1038/oncsis.2014.6>
- Lancaster, O.M., LeBerre, M., Dimitracopoulos, A., Bonazzi, D., Zlotek-Zlotkiewicz, E., Picone, R., Duke, T., Piel, M., Baum, B., 2013. Mitotic Rounding Alters Cell Geometry to Ensure Efficient Bipolar Spindle Formation. *Dev. Cell* 25, 270–283. <https://doi.org/10.1016/j.devcel.2013.03.014>
- Logue, J.S., Cartagena-Rivera, A.X., Baird, M.A., Davidson, M.W., Chadwick, R.S., Waterman, C.M., 2015. Erk regulation of actin capping and bundling by Eps8 promotes cortex

- tension and leader bleb-based migration. *eLife* 4, e08314. <https://doi.org/10.7554/eLife.08314>
- Lomakin, A.J., Cattin, C.J., Garcia-Arcos, J.M., Zhitnyak, I.Y., Driscoll, M.K., Welf, E.S., Petrie, R.J., Lennon-Duménil, A.M., Müller, D.J., 2020. The nucleus acts as a ruler tailoring cell responses to spatial constraints. *Science* 370, eaba2894. <https://doi.org/10.1101/863514>
- Lombardi, M.L., Lammerding, J., 2011. Keeping the LINC: the importance of nucleocytoplasmic coupling in intracellular force transmission and cellular function. *Biochem. Soc. Trans.* 39, 1729–1734. <https://doi.org/10.1042/BST20110686>
- Mattout-Drubezki, A., Gruenbaum, Y., 2003. Dynamic interactions of nuclear lamina proteins with chromatin and transcriptional machinery. *Cell. Mol. Life Sci. CMLS* 60, 2053–2063. <https://doi.org/10.1007/s00018-003-3038-3>
- Patil, S., Sengupta, K., 2021. Role of A- and B-type lamins in nuclear structure–function relationships. *Biol. Cell* 113, 295–310. <https://doi.org/10.1111/boc.202000160>
- Patteson, A.E., Vahabikashi, A., Pogoda, K., Adam, S.A., Mandal, K., Kittisopikul, M., Sivagurunathan, S., Goldman, A., Goldman, R.D., Janmey, P.A., 2019. Vimentin protects cells against nuclear rupture and DNA damage during migration. *J. Cell Biol.* 218, 4079–4092. <https://doi.org/10.1083/jcb.201902046>
- Pennacchio, F.A., Poli, A., Pramotton, F.M., Lavore, S., Rancati, I., Cinquanta, M., Vorselen, D., Prina, E., Romano, O.M., Ferrari, A., Piel, M., Lagomarsino, M.C., Maiuri, P., 2022. Force-biased nuclear import sets nuclear-cytoplasmic volumetric coupling by osmosis. <https://doi.org/10.1101/2022.06.07.494975>
- Raab, M., Gentili, M., de Belly, H., Thiam, H.R., Vargas, P., Jimenez, A.J., Lautenschlaeger, F., Voituriez, R., Lennon-Duménil, A.M., Manel, N., Piel, M., 2016. ESCRT III repairs nuclear envelope ruptures during cell migration to limit DNA damage and cell death. *Science* 352, 359–362. <https://doi.org/10.1126/science.aad7611>
- Srivastava, N., Nader, G.P. de F., Williard, A., Rollin, R., Cuvelier, D., Lomakin, A., Piel, M., 2021. Nuclear fragility, blaming the blebs. *Curr. Opin. Cell Biol., Cell Nucleus* 70, 100–108. <https://doi.org/10.1016/j.ceb.2021.01.007>
- Venturini, V., Pezzano, F., Català Castro, F., Häkkinen, H.-M., Jiménez-Delgado, S., Colomer-Rosell, M., Marro, M., Tolosa-Ramon, Q., Paz-López, S., Valverde, M.A., Weghuber, J., Loza-Alvarez, P., Krieg, M., Wieser, S., Ruprecht, V., 2020. The nucleus measures shape changes for cellular proprioception to control dynamic cell behavior. *Science* 370, eaba2644. <https://doi.org/10.1126/science.aba2644>
- Wintner, O., Hirsch-Attas, N., Schlossberg, M., Brofman, F., Friedman, R., Kupervaser, M., Kitsberg, D., Buxboim, A., 2020. A Unified Linear Viscoelastic Model of the Cell Nucleus Defines the Mechanical Contributions of Lamins and Chromatin. *Adv. Sci.* 7, 1901222. <https://doi.org/10.1002/advs.201901222>

General Conclusion

Mechanical constraints that cancer cells undergo during tumor progression are various and depend on their development stage. In addition, mechanical stimulation of cells depends on their position within the tumor. This variation influences both their proliferation and migration but also their phenotype and tumorigenicity. Thus, it is important to be able to characterize their biophysical properties under different mechanical stress conditions, in a reproductive and standardized environment mimicking *in vivo* growth conditions.

The work presented in this manuscript focused on the uniaxial confinement that cells are subjected during metastatic cell escape and on the 3D isotropic stress that the main core of the tumor withstands during tumor expansion. We have demonstrated the key role of division in the adaptation of cancer cells to prolonged mechanical stress and the mechanically-driven dedifferentiation of cancer cells in tumor spheroids that have never been shown before. These changes are not without consequences and could explain the failure of current therapies to bring a complete cure to the greatest number of cancer patients.

These studies, at the interface between the fields of physics and cancer biology, required the use of various techniques ranging from cell culture to molecular biology techniques, including imaging and microfabrication techniques as well as the development of several analysis tools for complex and heavy data. It allowed to enrich the scientific knowledge of the two developed approaches, which benefits both the biophysical and cancer biology communities.

To conclude, the results of my PhD brought innovations from a technological, scientific and medical point of view. Indeed, these results allow us to validate new types of reliable *in vitro* assays to analyze in a robust and systematic way the effect of mechanics on the response of cancer cells. Indeed, the high statistics obtained give access to essential information at both the population and single-cell levels. My thesis work will thus help to better understand the interactions between mechanical and metabolic stress, cellular plasticity and adaptation as well as cell resistance to treatments. These results represent a key step to further evaluate quantitatively the predictive value of our approach, by analyzing cells from patients before and after treatment, with and without relapse.

Glossary

Force is a push or pull on an object. It has a magnitude and a direction, making it a vectoral quantity. It is measured in newtons (N) and represented by the symbol F.

Mechanical stress is a force applied per unit area ($\text{N}\cdot\text{m}^{-2}$). There are two types: normal stress (tension and compression), and shear stress.

Tensile stress or **tension** is a stress applied perpendicular to the object. Tensile is related to stretching in contrasts with compressive.

Compressive stress or **compression** is also a stress applied perpendicular to the object, but results in compaction.

Shear stress occurs when two forces act parallel to the area of the object.

Strain is the extent of deformation of an object under a force, usually the change in length divided by the original length.

Stiffness is the extent of resistance of an object to deformation by applied forces and is measured as various moduli including Young's, shear and bulk, which apply to different types of deformation and measured in Pascal (Pa). The stiffer an object, the more difficult it is to deform it when subjected to a given force.

Tumor solid stress are the forces that results from and contained in the solid state of the tumor, including ECM, cancer and stroma cells.

Tumor fluid pressure is the pressure that results from the liquid phase of the tumor, mainly the interstitial fluid that surrounds cells. Fluid pressure has both hydrostatic and osmotic components.

Osmotic pressure is the pressure difference needed to stop the flow of solvent across a semipermeable membrane.

Elasticity is the ability of a deformed object to return to its original shape after removal of the force. The modulus of elasticity is defined as the ratio of stress to strain. Young's modulus (E) describes the elasticity of an object subjected to tensile and compression stress. Shear modulus (G) describes the elasticity of an object subjected to shear stress.

Viscoelasticity is the property of materials that possess both elastic and viscous properties when deformed. The strain of viscous materials is time-dependent, while strain of elastic materials is time-independent.

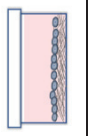
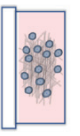
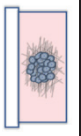
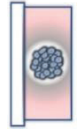
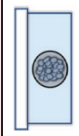


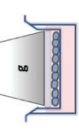

| Appendices

« Dans la vie rien n'est à craindre, tout est à comprendre »

Marie Curie

Appendix 1: Table summarizing the different types of experimental methods to apply mechanical constraints on cells

Adapted from (Kalli and Stylianopoulos, 2018)

	Experimental Setup		Cancer Model	Method	Biological outcomes	References
ECM Stiffness	2D substrate	Cell monolayer 	Glioblastoma Normal portal fibroblast Fibrosarcoma, CAFs Breast and pancreatic cancer	Polyacrylamide gels + coating (fibronectin, collagen etc)	Mechanotransduction Cell migration, Traction forces Cytoskeleton contractility Gene expression, Cell shape	(Elosegui-Artola et al., 2017; Friedland et al., 2009; Li et al., 2007; Panciera et al., 2020; Ulrich et al., 2009; Zhang et al., 2016)
		Single cells 	Breast cancer Glioma Prostate cancer	Collagen matrix Matrigel	Mechanotransduction Cell migration and invasion Gene expression, Cell shape	(Kaufman et al., 2005; Kraning-Rush and Reinhart-King, 2012; Paszek et al., 2005; Pedersen and Swartz, 2005; Zaman et al., 2006)
	3D matrix	Tumor spheroids 	Breast cancer Pancreatic cancer Normal fibroblasts and CAFs	Collagen matrix Matrigel	Proliferation Cell invasion Gene expression	(Gkretsi et al., 2017; Levental et al., 2009; Panciera et al., 2020; Zhang et al., 2016)
		In matrix 	Breast cancer Pancreatic adenocarcinoma Human and mouse colon adenocarcinoma Mouse sarcoma cells	Dextran compression Agarose embedding	Tumor morphology Tumor growth Cell proliferation Effect of treatment Estimation of solid stress	(Cheng et al., 2009; Delarue et al., 2014b, 2014a; Dolega et al., 2021; Helmlinger et al., 1997; Monnier et al., 2016; Montel et al., 2012; Rizzuti et al., 2020)
	Tumor spheroids	In capsules 	Mouse colon carcinoma	Alginate capsules	Tumor growth Cell migration	(Alessandri et al., 2013)
		In PDMS 	Colorectal cancer Pancreatic adenocarcinoma	PDMS groove PDMS chambers	Tumor growth Effect on mitosis	(Desmaison et al., 2018, 2013; Meriem et al., 2023)
Solid Stress	Tumors	In vivo/In situ 	Melanoma, glioblastoma, fibrosarcoma Breast and colorectal cancer	Tumor excision	Link between solid stress and tumor/tissue stiffness Impact on drug delivery	(Fernández-Sánchez et al., 2015; Nia et al., 2017; Panciera et al., 2020; Stylianopoulos et al., 2012)
		Compressed monolayer 	Bone osteosarcoma Breast cancer Colorectal cancer Normal pancreatic fibroblast Renal carcinoma	PDMS Piston Agarose Cushion Agarose soft confiner	Cell migration and invasion Gene expression EMT Effect of treatment	(Chen et al., 2017; Cheng et al., 2009; Kalli et al., 2018; Mitsui et al., 2006; Tse et al., 2012)
Isolated cells	Compressed cells in matrix 	Breast cancer Brain cancer Mouse colon carcinoma	Matrigel + Confiners	Gene expression Cell morphology	(Demou, 2010; Dolega et al., 2021)	

References

- Alessandri, K., Sarangi, B.R., Gurchenkov, V.V., Sinha, B., Kießling, T.R., Fetler, L., Rico, F., Scheuring, S., Lamaze, C., Simon, A., Geraldo, S., Vignjevic, D., Doméjean, H., Rolland, L., Funfak, A., Bibette, J., Bremond, N., Nassoy, P., 2013. Cellular capsules as a tool for multicellular spheroid production and for investigating the mechanics of tumor progression in vitro. *Proc. Natl. Acad. Sci. U. S. A.* 110, 14843–8. <https://doi.org/10.1073/pnas.1309482110>
- Chen, Q., Yang, D., Zong, H., Zhu, L., Wang, L., Wang, X., Zhu, X., Song, X., Wang, J., 2017. Growth-induced stress enhances epithelial-mesenchymal transition induced by IL-6 in clear cell renal cell carcinoma via the Akt/GSK-3 β / β -catenin signaling pathway. *Oncogenesis* 6, e375–e375. <https://doi.org/10.1038/oncsis.2017.74>
- Cheng, G., Tse, J., Jain, R.K., Munn, L.L., 2009. Micro-Environmental Mechanical Stress Controls Tumor Spheroid Size and Morphology by Suppressing Proliferation and Inducing Apoptosis in Cancer Cells. *PLOS ONE* 4, e4632. <https://doi.org/10.1371/journal.pone.0004632>
- Delarue, M., Joanny, J.-F., Jülicher, F., Prost, J., 2014a. Stress distributions and cell flows in a growing cell aggregate. *Interface Focus* 4, 20140033. <https://doi.org/10.1098/rsfs.2014.0033>
- Delarue, M., Montel, F., Vignjevic, D., Prost, J., Joanny, J.F., Cappello, G., 2014b. Compressive stress inhibits proliferation in tumor spheroids through a volume limitation. *Biophys. J.* 107, 1821–1828. <https://doi.org/10.1016/j.bpj.2014.08.031>
- Demou, Z.N., 2010. Gene Expression Profiles in 3D Tumor Analogs Indicate Compressive Strain Differentially Enhances Metastatic Potential. *Ann. Biomed. Eng.* 38, 3509–3520. <https://doi.org/10.1007/s10439-010-0097-0>
- Desmason, A., Frongia, C., Grenier, K., Ducommun, B., Lobjois, V., 2013. Mechanical Stress Impairs Mitosis Progression in Multi-Cellular Tumor Spheroids. *PLOS ONE* 8, e80447. <https://doi.org/10.1371/journal.pone.0080447>
- Desmason, A., Guillaume, L., Triclin, S., Weiss, P., Ducommun, B., Lobjois, V., 2018. Impact of physical confinement on nuclei geometry and cell division dynamics in 3D spheroids. *Sci. Rep.* 8, 1–8. <https://doi.org/10.1038/s41598-018-27060-6>
- Dolega, M.E., Monnier, S., Brunel, B., Joanny, J.F., Recho, P., Cappello, G., 2021. Extra-cellular matrix in multicellular aggregates acts as a pressure sensor controlling cell proliferation and motility. *eLife* 10. <https://doi.org/10.7554/ELIFE.63258>
- Elosegui-Artola, A., Andreu, I., Beedle, A.E.M., Lezamiz, A., Uroz, M., Kosmalska, A.J., Oria, R., Kechagia, J.Z., Rico-Lastres, P., Le Roux, A.L., Shanahan, C.M., Trepas, X., Navajas, D., Garcia-Manyès, S., Roca-Cusachs, P., 2017. Force Triggers YAP Nuclear Entry by Regulating Transport across Nuclear Pores. *Cell* 171, 1397–1410.e14. <https://doi.org/10.1016/j.cell.2017.10.008>
- Fernández-Sánchez, M.E., Barbier, S., Whitehead, J., Béalle, G., Michel, A., Latorre-Ossa, H., Rey, C., Fouassier, L., Claperon, A., Brullé, L., Girard, E., Servant, N., Rio-Frio, T., Marie, H., Lesieur, S., Housset, C., Gennisson, J.-L., Tanter, M., Ménager, C., Fre, S., Robine, S., Farge, E., 2015. Mechanical induction of the tumorigenic β -catenin pathway by tumour growth pressure. *Nature* 523, 92–95. <https://doi.org/10.1038/nature14329>
- Friedland, J.C., Lee, M.H., Boettiger, D., 2009. Mechanically Activated Integrin Switch Controls α 5 β 1 Function. *Science* 323, 642–644. <https://doi.org/10.1126/science.1168441>

- Gkretsi, V., Stylianou, A., Louca, M., Stylianopoulos, T., 2017. Identification of Ras suppressor-1 (RSU-1) as a potential breast cancer metastasis biomarker using a three-dimensional in vitro approach. *Oncotarget* 8, 27364–27379. <https://doi.org/10.18632/oncotarget.16062>
- Helmlinger, G., Netti, P.A., Lichtenbeld, H.C., Melder, R.J., Jain, R.K., 1997. Solid stress inhibits the growth of multicellular tumor spheroids. *Nat. Biotechnol.* 15, 778–783. <https://doi.org/10.1038/nbt0897-778>
- Kalli, M., Papageorgis, P., Gkretsi, V., Stylianopoulos, T., 2018. Solid Stress Facilitates Fibroblasts Activation to Promote Pancreatic Cancer Cell Migration. *Ann. Biomed. Eng.* 46, 657–669. <https://doi.org/10.1007/s10439-018-1997-7>
- Kalli, M., Stylianopoulos, T., 2018. Defining the role of solid stress and matrix stiffness in cancer cell proliferation and metastasis. *Front. Oncol.* 8. <https://doi.org/10.3389/fonc.2018.00055>
- Kaufman, L.J., Brangwynne, C.P., Kasza, K.E., Filippidi, E., Gordon, V.D., Deisboeck, T.S., Weitz, D.A., 2005. Glioma Expansion in Collagen I Matrices: Analyzing Collagen Concentration-Dependent Growth and Motility Patterns. *Biophys. J.* 89, 635–650. <https://doi.org/10.1529/biophysj.105.061994>
- Kraning-Rush, C.M., Reinhart-King, C.A., 2012. Controlling matrix stiffness and topography for the study of tumor cell migration. *Cell Adhes. Migr.* 6, 274–279. <https://doi.org/10.4161/cam.21076>
- Levental, K.R., Yu, H., Kass, L., Lakins, J.N., Egeblad, M., Erler, J.T., Fong, S.F.T., Csiszar, K., Giaccia, A., Weninger, W., Yamauchi, M., Gasser, D.L., Weaver, V.M., 2009. Matrix Crosslinking Forces Tumor Progression by Enhancing Integrin Signaling. *Cell* 139, 891–906. <https://doi.org/10.1016/j.cell.2009.10.027>
- Li, Z., Dranoff, J.A., Chan, E.P., Uemura, M., Sévigny, J., Wells, R.G., 2007. Transforming growth factor- β and substrate stiffness regulate portal fibroblast activation in culture. *Hepatology* 46, 1246–1256. <https://doi.org/10.1002/hep.21792>
- Meriem, Z.B., Mateo, T., Faccini, J., Denais, C., Dusfour-Castan, R., Guynet, C., Merle, T., Suzanne, M., Di-Luoffo, M., Guillermet-Guibert, J., Alric, B., Landiech, S., Malaquin, L., Mesnilgrete, F., Laborde, A., Mazenq, L., Courson, R., Delarue, M., 2023. An easy-to-use microfluidic mechano-chemostat for tissues and organisms reveals that confined growth is accompanied with increased macromolecular crowding. <https://doi.org/10.1101/2023.03.29.534752>
- Mitsui, N., Suzuki, N., Koyama, Y., Yanagisawa, M., Otsuka, K., Shimizu, N., Maeno, M., 2006. Effect of compressive force on the expression of MMPs, PAs, and their inhibitors in osteoblastic Saos-2 cells. *Life Sci.* 79, 575–583. <https://doi.org/10.1016/j.lfs.2006.01.040>
- Monnier, S., Delarue, M., Brunel, B., Dolega, M.E., Delon, A., Cappello, G., 2016. Effect of an osmotic stress on multicellular aggregates. *Methods* 94, 114–119. <https://doi.org/10.1016/j.ymeth.2015.07.009>
- Montel, F., Delarue, M., Elgeti, J., Vignjevic, D., Cappello, G., Prost, J., 2012. Isotropic stress reduces cell proliferation in tumor spheroids. *New J. Phys.* 14, 055008. <https://doi.org/10.1088/1367-2630/14/5/055008>
- Nia, H.T., Liu, H., Seano, G., Datta, M., Jones, D., Rahbari, N., Incio, J., Chauhan, V.P., Jung, K., Martin, J.D., Askoxylakis, V., Padera, T.P., Fukumura, D., Boucher, Y., Hornicek, F.J., Grodzinsky, A.J.,

- Baish, J.W., Munn, L.L., Jain, R.K., 2017. Solid stress and elastic energy as measures of tumour mechanopathology. *Nat. Biomed. Eng.* 1, 1–11. <https://doi.org/10.1038/s41551-016-0004>
- Pancierera, T., Citron, A., Di Biagio, D., Battilana, G., Gandin, A., Giulitti, S., Forcato, M., Bicciato, S., Panzetta, V., Fusco, S., Azzolin, L., Totaro, A., Dei Tos, A.P., Fassan, M., Vindigni, V., Bassetto, F., Rosato, A., Brusatin, G., Cordenonsi, M., Piccolo, S., 2020. Reprogramming normal cells into tumour precursors requires ECM stiffness and oncogene-mediated changes of cell mechanical properties. *Nat. Mater.* 1–10. <https://doi.org/10.1038/s41563-020-0615-x>
- Paszek, M.J., Zahir, N., Johnson, K.R., Lakins, J.N., Rozenberg, G.I., Gefen, A., Reinhart-King, C.A., Margulies, S.S., Dembo, M., Boettiger, D., Hammer, D.A., Weaver, V.M., 2005. Tensional homeostasis and the malignant phenotype. *Cancer Cell* 8, 241–254. <https://doi.org/10.1016/j.ccr.2005.08.010>
- Pedersen, J.A., Swartz, M.A., 2005. Mechanobiology in the Third Dimension. *Ann. Biomed. Eng.* 33, 1469–1490. <https://doi.org/10.1007/s10439-005-8159-4>
- Rizzuti, I.F., Mascheroni, P., Arcucci, S., Ben-Mériem, Z., Prunet, A., Barentin, C., Rivière, C., Delanoë-Ayari, H., Hatzikirou, H., Guillermet-Guibert, J., Delarue, M., 2020. Mechanical Control of Cell Proliferation Increases Resistance to Chemotherapeutic Agents. *Phys. Rev. Lett.* 125, 128103. <https://doi.org/10.1103/PhysRevLett.125.128103>
- Stylianopoulos, T., Martin, J.D., Chauhan, V.P., Jain, S.R., Diop-Frimpong, B., Bardeesy, N., Smith, B.L., Ferrone, C.R., Hornicek, F.J., Boucher, Y., Munn, L.L., Jain, R.K., 2012. Causes, consequences, and remedies for growth-induced solid stress in murine and human tumors. *Proc. Natl. Acad. Sci. U. S. A.* 109, 15101–8. <https://doi.org/10.1073/pnas.1213353109>
- Tse, J.M., Cheng, G., Tyrrell, J.A., Wilcox-Adelman, S.A., Boucher, Y., Jain, R.K., Munn, L.L., 2012. Mechanical compression drives cancer cells toward invasive phenotype. *Proc. Natl. Acad. Sci.* 109, 911–916. <https://doi.org/10.1073/pnas.1118910109>
- Ulrich, T.A., de Juan Pardo, E.M., Kumar, S., 2009. The Mechanical Rigidity of the Extracellular Matrix Regulates the Structure, Motility, and Proliferation of Glioma Cells. *Cancer Res.* 69, 4167–4174. <https://doi.org/10.1158/0008-5472.CAN-08-4859>
- Zaman, M.H., Trapani, L.M., Sieminski, A.L., MacKellar, D., Gong, H., Kamm, R.D., Wells, A., Lauffenburger, D.A., Matsudaira, P., 2006. Migration of tumor cells in 3D matrices is governed by matrix stiffness along with cell-matrix adhesion and proteolysis. *Proc. Natl. Acad. Sci.* 103, 10889–10894. <https://doi.org/10.1073/pnas.0604460103>
- Zhang, K., Grither, W.R., Van Hove, S., Biswas, H., Ponik, S.M., Eliceiri, K.W., Keely, P.J., Longmore, G.D., 2016. Mechanical signals regulate and activate SNAIL1 protein to control the fibrogenic response of cancer-associated fibroblasts. *J. Cell Sci.* 129, 1989–2002. <https://doi.org/10.1242/jcs.180539>



Probing molecular crowding in compressed tissues with Brillouin light scattering

Guqi Yan ^a, Sylvain Monnier ^a, Malèke Mouelhi ^a, and Thomas Dehoux ^{a,1}

^aInstitut Lumière Matière, UMR5306, Université Lyon 1-CNRS, Université de Lyon, 69622 Villeurbanne, France

Edited by David Weitz, Department of Physics, Division of Engineering and Applied Science, Harvard University, Cambridge, MA; received July 27, 2021
accepted December 13, 2021

1;

Volume regulation is key in maintaining important tissue functions, such as growth or healing. This is achieved by modulation of **active contractility as well as water efflux that changes molecular crowding** within individual cells. Local sensors have been developed to monitor stresses or forces in model tissues, but these **approaches do not capture the contribution of liquid flows** to volume regulation. Here, we use a tool based on Brillouin light scattering (BLS) that uses the interaction of a laser light with **inherent picosecond timescale density fluctuations in the sample**. To investigate volume variations, we induced osmotic perturbations with a polysaccharide osmolyte, Dextran (Dx), and compress cells locally within multicellular spheroids (MCSs). During osmotic compressions, we observe an increase in the BLS frequency shift **that reflects local variations in the compressibility**. To elucidate these data, we propose a model based on a mixing law that describes the increase of molecular crowding upon reduction of the **intracellular fluids**. **Comparison with the data suggests a nonlinear increase of the compressibility** due to the dense crowding that induces hydrodynamic interactions between the cellular polymers.

Brillouin light scattering | cellular crowding | spheroid

Volume regulation is key in maintaining important tissue functions, such as embryogenesis or wound healing (1). Perturbation of volume homeostasis, by external forces applied to the tissue or abnormal regulation, has also been associated with the development of degenerative diseases, such as cancer (2). Coordinated modulation of active contractility, membrane tension, and cell–cell and cell–extracellular matrix junctions are known to drive cell shape and volume. For this reason, a large body of research has been devoted to the implementation of local sensors to monitor stresses or forces in model tissues during hyperosmotic shocks (3, 4). Such approaches focus on stiffness regulation, but they cannot capture the role of water efflux that changes molecular crowding within individual cells and can impact cell fate (5) and induce cytoplasm phase separation (6) or colloidal glass-like transition (7).

In recent years, a new quantitative microscopy based on Brillouin light scattering (BLS) has been proposed that uses the interaction of a laser light with picosecond timescale density fluctuations in the sample (8). BLS has been successfully used for mechanical phenotyping and imaging with a contrast based on the stiffness (9), but its relevance from a physiological standpoint remains debated due to the ultrashort timescales involved. Since the probing mechanism involves coupling of photons to longitudinal phonons, variations in the scattering spectra can be interpreted as the response of the sample to an infinitesimal uniaxial compression and formally described by the longitudinal modulus M . In an idealized two-phase biological sample, variations of M would be driven in part by the polymer meshwork but also—and this feature separates BLS from classical microrheology approaches—by the compressibility and the dynamics of the liquid phase (10).

Usually discarded, this unique feature was used to interrogate the liquid-to-solid transition in stress granules related to amyotrophic lateral sclerosis diseases (11). However, an investigation

of hydrogels also recently suggested that water content should play an important role in the response in biological materials (12). In tissues, the respective contributions of the stiffness of the elastic network and of the liquid phase remain unclear. To elucidate this question and investigate its implication in volume control, we induced osmotic perturbations in order to compress isotropically multicellular tissues. We demonstrate that volume changes due to water efflux at the cellular level dominate the BLS response. Comparison of the data with a model based on a mixing law suggests that the increase of molecular crowding upon reduction of the intracellular fluids leads to a nonlinear acoustic behavior due to hydrodynamic interactions within the cells.

Results

Volume Control in Multicellular Spheroids with Osmotic Shocks. To investigate volume regulation in three-dimensional (3D) clusters, we engineered multicellular spheroids (MCSs) from the spontaneous aggregation of the colorectal carcinoma cell line HCT116. In contrast to single-cell experiments, such a model allows for the analysis of the volume regulation by both intracellular spaces and intercellular spaces (ICs). One of the difficulties of analyzing volume changes in mammalian cells is that compression can be followed by a regulatory volume increase driven by ion channels and pumps (13). To circumvent this difficulty, we imposed isotropic osmotic compressions using solutions containing Dextran (Dx) molecules that do not lead to regulatory volume increase (SI Appendix, Fig. S2) (14).

Dx is a type of biocompatible glucose polymer that generates osmotic pressures depending on its molecular weight and

Significance

Volume regulation is key in maintaining important tissue functions, such as growth or healing. In this process, the role of **efflux of cellular fluids is difficult to capture due to the lack of apt technologies**. Here, we use a tool based on Brillouin light scattering (BLS) that uses the interaction of a laser light **with inherent picosecond timescale density fluctuations in the sample**. We induced gradual volume decrease in multicellular spheroids using osmotic perturbations. BLS revealed a **nonlinear increase of the tissue compressibility** due to the subsequent increased biopolymer crowding within the cells. Our **findings should inspire research regarding volume regulation and cellular crowding in tissues and stimulate the emergence of models for cell mechanics at short timescales**.

Author contributions: T.D. and S.M. designed research; G.Y., S.M., and M.M. performed research; G.Y., S.M., and T.D. analyzed data; and G.Y., S.M., and T.D. wrote the paper.

The authors declare no competing interest.

This article is a PNAS Direct Submission.

This article is distributed under [Creative Commons Attribution-NonCommercial-NoDerivatives License 4.0 \(CC BY-NC-ND\)](https://creativecommons.org/licenses/by-nc-nd/4.0/).

¹To whom correspondence may be addressed. Email: thomas.dehoux@univ-lyon1.fr.

This article contains supporting information online at <https://www.pnas.org/lookup/suppl/doi:10.1073/pnas.2113614119/-/DCSupplemental>.

Published January 19, 2022.

concentration. We take advantage of the selective compression method described in ref. 15. Briefly, 6-kDa Dx molecules can diffuse throughout the ICS and thus, only apply a local osmotic pressure to the cell within the MCS. This mechanism of compression is sketched in Fig. 1 A.

As an illustration of the impact of osmotic compression by Dx on the structure of MCS, we placed MCS in between two plates separated by $\approx 70 \mu\text{m}$ and labeled the ICS with a fluorescent dye (tissue confiner is discussed in Materials and Method); the reduced thickness of the sample allows two-photon microscopy in a two-dimensional (2D)-like configuration. Fig. 1 B shows the images obtained before and after the shock with 6 kDa Dx. The two-photon images clearly show a reduction of both the MCS and cell volumes, consistent with the literature (15). To quantify this observation, we plot the MCS volume determined from the white light images recorded on the BLS microscope during the shocks in Fig. 1 C ($n = 40, N = 2$) (SI Appendix, Note 1). We observe a linear dependence of the normalized MCS volume change with increasing Dx concentration c_d ,

$$\Delta V_c / V_c = (V_c^0 - V_c) / V_c = c_d / \gamma, \quad [1]$$

with V_c^0 the initial volume and $\gamma = 0.77$ obtained from the best fit to the data.

To quantify the contribution of cell compression to this volume reduction, we measured the volume variation in single cells during shocks for different Dx concentrations using the fluorescence exclusion microscopy (FXm) (Materials and Method). Briefly, HCT116 cells were suspended in a medium supplemented with a fluorescent dye that does not cross the cell membrane, and they were inserted in a microfluidic chamber with a fixed height. Fluorescence is excluded from the cells, leading to a decrease in total fluorescence, proportional to cell volume (16). Images obtained in epifluorescence microscopy with a large depth of field allow for integrating intensity over the whole chamber height ($\approx 20 \mu\text{m}$). This signal is integrated over the cell-projected area to calculate cell volume (17). Here, we also observe a linear dependence of the normalized increment in cell volume with increasing Dx concentration. Using Eq. 1 to fit these data yields $\gamma = 0.68$. This γ value is close to that found from the MCS volume, demonstrating that cell compression is the main source of volume variation during osmotic compressions with small Dx molecules.

Brillouin Spectroscopy Reveals Cell Compression. To implement Brillouin spectroscopy with a high throughput, we engineered patterns of hundreds of agarose-based microwells (Materials and

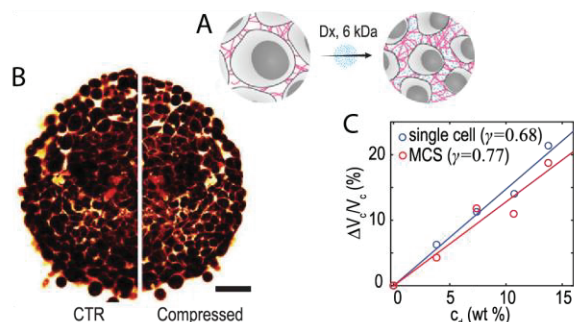


Fig. 1. (A) Schematic representation of the isotropic osmotic compression by Dx. (B) Two-photon images of MCS captured before and after shocks with 6 kDa Dx. (Scale bar: $100 \mu\text{m}$.) (C) Variation of single-cell volume vs. Dx concentration measured by FXm on single cells (blue markers and line fit) and determined from MCS volume variations (red markers and line fit) (SI Appendix, Note 1).

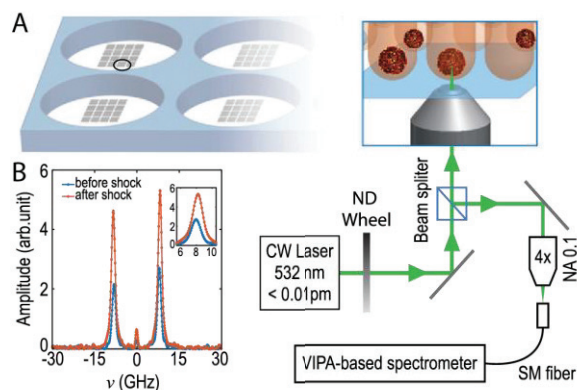


Fig. 2. (A) Schematic of microstructured wells for MCS; the virtually imaged phase array (VIPA)-based Brillouin spectrometer is coupled with a microscope. (B) Typical spectrum obtained at the center of an MCS before and after the shock. (Inset) Zoomed-in view of the anti-Stokes shift. SM, single mode. NA, numerical aperture; ND, neutral density; CW, continuous wave.

Methods), each of them containing one MCS, as is sketched in Fig. 2 A. Such a custom-made plate is placed in an inverted microscope equipped with an environmental chamber. We focus a laser beam at the center of the MCS and collect the backscattered light with a $20\times$ objective lens that gives a scattering volume of $\approx 5 \times 17 \mu\text{m}$. We analyze the spectrum of the backscattered light using a virtually imaged phase array (VIPA)-based spectrometer (18). We show in Fig. 2 B the typical spectra obtained before and after shocks. We plot the BLS frequency shift ν as a function of time in Fig. 3 A ($n = 40, N = 2$) during shocks with Dx molecules at 160 g/L. We observe a significant increase of the BLS shift ν after the shock that stabilizes after ≈ 30 min.

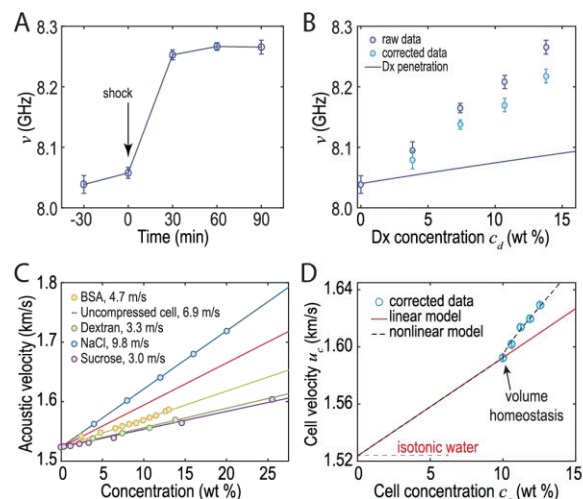


Fig. 3. (A) BLS frequency shift during osmotic compressions vs. time after shock for Dx solutions at 160 g/L. (B) Brillouin shift before (dark blue; raw data) and after subtraction (light blue) of the contribution of the penetration of small Dx molecules vs. Dx concentration. The solid line indicates the sole contribution of Dx penetration. (C) Velocity increment measured for different solutions (results for NaCl are from ref. 18). (D) Sound velocity in cells u_c vs. cell concentration (blue markers; corrected to remove the contribution of Dx penetration as in B). Black lines show the predictions by the linear (solid) and nonlinear (dashed) models. BSA, bovine serum albumin.

Although a similar increase in v has been observed on single cells (8), its origin remains debated. Assuming that the refractive index and mass density are not significantly affected by the osmotic conditions, it was initially proposed that such an increase was due to structural changes (8). Recent studies, however, suggested that water content—or volume—should also play an important role (12). In order to clarify this possible contribution in MCS, we imposed osmotic compressions at increasing pressures p using solutions containing increasing concentrations of Dx. We first plot in Fig. 3 B the BLS shift v_{small} vs. osmolyte concentration c_d . We observe a largely linear increase in v_{small} , but this variation also includes an artifactual increase due to the replacement of the intercellular fluids by Dx solutions with a higher refractive index, sound velocity, and mass density. In order to isolate the contribution of cell compression, we correct for this effect using a mixing law model.

We describe the MCS as the spatial average of cellular and intercellular compartments with a volume fraction of cells $\phi = 0.9$ (15). The ICS is initially considered to behave as an isotonic solution (1% sodium chloride) but is replaced by the small Dx molecules that can penetrate into the ICS. Since the Brillouin shift v depends on the refractive index n , mass density ρ , and longitudinal modulus M (or equivalently, sound velocity $u = \sqrt{M/\rho}$), it is necessary to define these quantities for the ICS. We consider the variations in refractive index $\Delta n_i = \alpha \Delta c_d$ and mass density $\Delta \rho_i = \xi \Delta c_d$, with classical values $\alpha = 0.0019$ and $\xi = 3.75 \text{ kg/m}^3$ found in the literature (19, 20). We determined the velocity increment, $\Delta u_i = \beta_i \Delta c_d$, from the frequency shift measured in Dx solutions of relevant concentrations and found $\beta_i = 2.5 \text{ m/s}$ at 37°C . To validate this result, we compared it with several reference solutions (sucrose, NaCl, and bovine serum albumin) (Fig. 3 C). As expected, the value for Dx is close to that of sucrose. From these values, we evaluate the average u , ρ , and n values for the MCS using standard mixing laws (Materials and Methods) and determine the artifactual frequency increase, v_{artefact} , due to the penetration of the Dx molecules. We plot the corrected frequency, $v_{\text{corr}} = v - v_{\text{artefact}}$, in Fig. 3 B as well as the prediction for v_{artefact} (Fig. 3 B, solid line). We observe a smaller corrected frequency shift that represents the sole contribution of the compressed cells.

Modeling a Crowding-Induced Nonlinear Acoustic Behavior. One may postulate that the increase in v arises from the increased solute concentration within the compressed cells. To integrate cell volume in a predictive model for tissue compression, we refine our previous description and model the cells as a dilute suspension of proteins and ions with an initial concentration $c_c^0 = 10 \text{ wt } \%$, as measured on a similar cell line (17, 21). During the osmotic shock, we assume a constant dry mass, so the decrease in cell volume ΔV_c is accompanied by an increase in the concentration $\Delta c_c = c_c^0 \Delta V_c / (V_c - \Delta V_c)$ within the cells. Since we have measured the normalized increment in cell volume $\Delta V_c / V_c$ (Eq. 1 and Fig. 1 C), we can simply write

$$\Delta c_c = c_c^0 \frac{c_d}{\gamma - c_d} \quad [2]$$

Since α and ξ are largely independent of the type of molecule (19, 20), we can express the increase in refractive index $\Delta n_c = \alpha \Delta c_c$ and mass density $\rho_c = \xi \Delta c_c$, as we did for the ICS. However, because there is a greater dependence of the velocity increment, as exemplified by the values measured in several biorelevant fluids (Fig. 3 C), we need to determine the velocity increment in cells, Δu_c .

As observed in Fig. 3 C, the velocity increment in dilute polymer solutions is near linear as can be approximated by Wood's formula based on the additivity of compressibilities (22). As a first approach, we thus use

$$\Delta u_c / \Delta c_c = \beta_c^0 \quad [3]$$

and we determine β_c^0 by fitting the frequency shift before the shock ($\Delta c_c = 0$). We find a velocity increment, $\beta_c^0 = 6.9 \text{ m/s}$, that lies in between solutions of proteins (e.g., bovine serum albumin [BSA]) and ions (e.g., NaCl), providing a plausible value for cells within a tissue (the red line in Fig. 3 C). Implementing this modeling of the cells in the model based on the spatial average of cellular and intercellular compartments we described previously, we predict the frequency shift resulting from cell compression. For ease of comparison of the modeling with the data, we convert Dx concentration to cell concentration using Eq. 2. We then convert v to a cell velocity using the mixing laws for the refractive index and velocity (SI Appendix, Note 2). We plot u_c vs. c_c in Fig. 3 D (markers) and compare with the prediction (Fig. 3 D, solid line). We observe a cell velocity of $\approx 1,594 \text{ m/s}$ before the shock, in good agreement with values obtained for single cells by acoustic microscopy at similar frequencies (23–25). Interestingly, we see that we cannot describe the full frequency shift, clarifying that a phenomenon additional to the variation in cell volume is at work.

To investigate a possible contribution of a structural change due to cytoskeleton remodeling, we inhibit actin polymerization with cytochalasin D (cytoD) (Materials and Methods). We plot the BLS frequency shift v mock treated with dimethyl sulfoxide (DMSO) and treated with cytoD in Fig. 4 A ($n = 40$, $N = 2$). We observe a significant decrease of the BLS shift v after actin depolymerization ($P < 0.0001$), as has been observed at the single-cell scale (8). We also determined the MCS volume from the projected area in bright-field imaging. We observed a significant increase in volume ($\approx 25 \%$, leading to negative ΔV values) upon actin depolymerization ($n = 8$, $P < 0.0001$) (Fig. 4B). This volume increase most probably arises from an increase of the ICS since actin depolymerization with cytoD does not affect cellular volume, as is sketched in Fig. 4 C (26). We plot in Fig. 4 D the prediction from the model we presented earlier (Fig. 4 D, plain line) and the cytoD/DMSO data points. We see that such an increase in MCS volume can entirely explain the observed decrease in v . This result indicates that a possible cytoskeleton remodeling has negligible influence on the frequency shift.

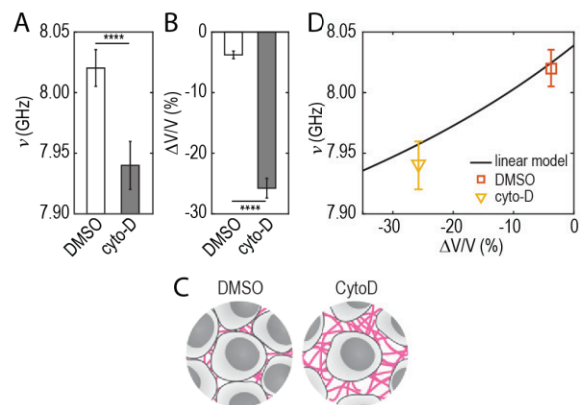


Fig. 4. (A) Frequency shift and (B) normalized volume measured in the agarose microwells measured on MCS treated with DMSO or cytoD. $**** P < 0.0001$, unpaired two-tailed t test. (C) Schematic representation of the compression by cytoD. (D) Frequency shift predicted by the linear model (solid line) vs. volume change of MCS treated with DMSO (square) and cytoD (triangle).

Increase of sound velocity with increasing solute concentration can be well described by the volume average of the compressibilities in colloidal suspensions (27) or emulsions (28). In biological solutions containing polymers and ions, however, intermolecular interactions (e.g., hydrogen bonds or dipole interactions) can lead to correlation of volume fluctuation of adjacent molecules, often resulting in a deviation from such classical description (29). For this reason, a power law is usually preferred:

$$\Delta u_c / \Delta c_c = \beta_c^0 + \beta_c^1 (\Delta c_c - c_c^0)^\tau, \quad [4]$$

where $\beta_c^1 = 9.1 \text{ m/s}$ is determined by the best fit to the data and $\tau = 0.5$ as is used in electrolytic solutions (30). We observe excellent agreement in Fig. 3D (dashed line). This comparison strongly suggests that the observed increase in v arises from a nonlinear acoustic behavior due to the increased crowding within the cells inside the MCS.

Discussion

In conclusion, we have shown that BLS can monitor locally—without any label—the impact of tissue compression. This methodology is a powerful noncontact, label-free, and high-throughput alternative to microinjected stress sensors (3, 4) and opens up possibilities to investigate the role of cell volume during various cellular events (17) at the tissue scale and down to the single-cell scale. It should also find applications for the investigation of focal pressure in small animals during development (31). Constant improving of spectrometers, both in terms of sensitivity and speed, and implementation of BLS-compatible endoscopes and adaptive optics should also allow medical translation in the near future.

The velocity increment in cells, $\beta_c = 6.9 \text{ m/s}$, is three orders of magnitude larger than the refractive index increment, $\alpha = 0.0019$. BLS is therefore exquisitely sensitive to changes in the sound velocity with changes in cell volume (or solute concentration within them). We have observed a clear deviation of the data from the classical mixing law model based on the volume average of the compressibilities. We have proposed a model that accounts for a nonlinear increase of the sound velocity with decreasing cell volume.

This simple empirical approach captures the main features of our data and suggests that the dense crowding in the cells induces correlated fluctuations of the cellular polymers. Similar observations have been made in hydrogels, where the emergence of such nonlinear acoustic behavior has been attributed to a stiffening of the elastic frame composed by the intercellular components (32). The exact nature of such interactions requires more in-depth exploration of the complexity of multicellular systems and the development of more refined theoretical acoustic descriptions. In particular, it seems important to investigate the possible effect of active volume regulations that might occur at short timescales with different osmolytes and for an extended range of volumes.

Such sensitivity of the sound velocity has been used to probe protein transitions (33), binding events (34), or hydration (35) at the macroscale using ultrasonic frequencies. The ability of BLS to produce such data at hypersonic frequencies at the single-cell scale should allow for investigating structural arrests or phase separations during protein condensation. We also anticipate that our results should stimulate the emergence of models for cell mechanics at short timescales and expand the range of application of BLS to the life sciences.

Materials and Methods

Cell Culture and Reagents. HCT116 colorectal carcinoma (CCL-247) adenocarcinoma cell lines were purchased from the American Type Culture Collection. Cells were cultured in Dulbecco's Modified Eagle Medium (DMEM) supplemented with 10% fetal bovine serum (FBS; PAN Biotech), $1 \times$ penicillin/streptomycin (P/S), and glutamax (Life Technologies) at 37°C under a

$5\% \text{ CO}_2$ atmosphere. All cells were used at low passage numbers, subconfluent cultured, and plated at 10^4 cells per cm^2 . MCSs for BLS imaging were obtained by seeding the cells onto the homemade agarose microwells and grown for 4 to 5 d in culture medium.

FXm for Single-Cell Volume Measurements. Cell volumes were obtained using FXm as detailed in refs. 16 and 17. Briefly, cells were incubated in polydimethylsiloxane (PDMS) with medium supplemented with a fluorescent dye coupled to small (10-kDa) Dx molecules to prevent entry into cells. Fluorescence is thus excluded by the cells, and volume is obtained by integrating the fluorescence intensity over the cell. Chips for volume measurements of single cells were made by pouring a mixture (1:10) of PDMS elastomer and curing agent (Sylgard 184) onto a brass master and cured at 80°C for at least of 2 h. Inlets and outlets were created with a 3-mm biopsy puncher. Chips were prepared a few days ahead of the experiment, bonded with oxygen plasma for 30 s, warmed up at 80°C for 3 min, incubated with Poly-L-lysine (Sigma) for 30 min to 1 h, washed first with phosphate-buffered saline (PBS) then washed with dH_2O , dried, and stored sealed with a paraffin film. The chips can be stored up to 10 d. The chambers were washed with PBS before cell injection.

Imaging started within 10 min after cell injection in order to prevent adhesion and thus, cells response to the shear stress generated by medium exchange. Acquisition was performed at 37°C in CO_2 independent medium (Life Technologies) supplemented with 1 g/L Alexa647 Dx (10 kDa; Thermo Fischer Scientific) on an epifluorescence microscope (Leica DMi8) with a $10\times$ objective (numerical aperture (NA) 0.3).

Tissue Confiner Experiments. Spheroids were harvested 4 or 5 d after cell seeding and injected in the 2D confiner microsystem using an MFCS pressure controller (Fluigent). Spheroids rested from 2 to 5 h to relax in the microsystem at 37°C in CO_2 independent medium. Before two-photon imaging, medium supplemented with 2 g/L fluorescein isothiocyanate-Dx (10 kDa; Sigma Aldrich) was injected to label the ICS. Medium exchange was performed manually using large inlets ($> 1 \text{ mm}$) during two-photon acquisition. Images were recorded at 37°C on a Nikon C1 two-photon microscope coupled with a femtosecond laser at 780 nm with a $40\times$ water-immersion objective (NA 1.10).

The chip was made by pouring PDMS elastomere and curing agent (1:10) on a mold and cured for at least 2 h. Molds were made using the classical photolithography technique. Chips were bonded to glass coverslips with 30 s oxygen plasma. Immediately after bonding, a solution of PLL-g-PEG (SuSoS) at 1 g/L was injected and incubated for 30 min in humid atmosphere to prevent cell surface adhesion during the experiment. The chips were washed with dH_2O , dried, and sealed with a paraffin film. They can be stored up to 1 wk and washed with PBS prior to spheroid injection.

Agarose Microwells Molding. A solution of 4% (wt/vol) agarose (Sigma Aldrich) in distilled water was prepared by autoclaving at 120°C for 15 min. The agarose solution was deposited on the prewarmed PDMS molds (placed on a hot plate at 78°C for standard agarose) and covered with silanized coverslips. Then, the mold and coverslip were removed from the hot plate and left to jellify at reach room temperature for 10 min. PDMS molds were removed, and the coverslips with the agarose microwells were glued to homemade bottomless six-well plates using biocompatible Norland optical adhesives (NOA81; Norland Products).

Molds Fabrication. For the agarose microwells and FXm experiments, master molds were fabricated on brass substrate with a micromilling machine (MiniMill3; Minitech) using a flat or ball-nose milling cutter (Dixi Poly-tool). Height profiles and surface roughness were measured with a vertical scanning interferometric profilometer (Bruker). The 3D mold design and tool paths were generated using Autodesk Inventor Professional software (Autodesk).

Molds for spheroid confinement were made with classical soft lithography techniques. PDMS molds for agarose molding are counter molds obtained from brass master molds.

Osmotic Compressions. We induced osmotic perturbations with a polysaccharide osmolyte, Dx (6 kDa), at different concentrations (40, 80, 120, and 160 g/L). The solutions were prepared by diluting Dx powder from *Leuconostoc mesenteroides* (Sigma Aldrich) into CO_2 independent imaging medium (DMEM supplemented with glutamax, 10% FBS, $1 \times$ P/S, and 20 mM hydroxyethyl piperazineethanesulfonic acid; Life Technologies). Culture medium was replaced by imaging medium for at least 10 min to equilibrate before adding the compression solutions. For easier comparison, the concentrations are expressed in units of solute concentrations to [weight percentage]. For BLS imaging, we changed the culture medium by fresh

culture 30 min before the shock and verified that the BLS frequency shift was not changing upon renewing culture medium.

Brillouin Spectroscopy. BLS is an inelastic process (36) arising with creation (Stokes process) or annihilation (anti-Stokes process) of acoustic phonons in the medium. The resulting spectra consist of peaks shifted by frequencies $\pm v$ (the + and - signs correspond to the anti-Stokes and Stokes contributions, respectively) relative to the frequency of the incident laser light (Fig. 2 shows a typical spectrum). The Brillouin frequency shift, v , is defined by the following relations (37):

$$v = 2n u / \lambda, \quad (5)$$

where n is the refractive index, $u = \sqrt{M/\rho}$ is the acoustic velocity (with M the elastic modulus and ρ the density), and λ the laser wavelength (18). We used a 532-nm single-mode continuous wave laser with a spectral line width < 0.01 pm (Spectra-Physics Excelsior-532; 15 mW measured at the sample). The laser is coupled to an inverted life science microscope (Nikon Eclipse Ti2-U) to focus and collect the backscattered light with the same objective lens ($20\times$, NA 0.35). We chose a lens with a low numerical aperture to avoid broadening of the Brillouin spectrum (38). The direction of the output beam is collected by an objective lens ($4\times$, NA 0.10) into a single-mode fiber (1 m, 400 to 680 nm, core diameter $3\ \mu\text{m}$) connected to a Brillouin spectrometer as

shown in Fig. 2. The VIPA-based spectrometer (Light Machinery; Hyperfine HF-8999-532) is based on a 3.37-mm-thick VIPA etalon (30 GHz, 500 to 600 nm) and is equipped with two double-pass air-spaced etalons to increase the contrast to about 120 dB. The fiber is directly connected to the built-in connector of the spectrometer. The free spectral range of the VIPA used in our work is 30 GHz, corresponding to a sampling interval of 0.11 GHz. To ensure perfect control of the sample, the microscope is enclosed in an environmental chamber to maintain a constant temperature (37°C) and 5% CO_2 level. For the BLS measurements of MCS under osmotic shocks, we changed the culture medium at time $t = 0$ min and then added the Dx solutions after measurements of time $t = 30$ min. For each condition, we probed 20 MCS.

Data Availability. Raw data and associated treatments have been deposited in Zenodo (DOI: 10.5281/zenodo.5773601) (39).

ACKNOWLEDGMENTS. This work was partly supported by Agence Nationale de la Recherche Grant ANR-17-CE11-0010-01, by the Instituts Thématiques Multiorganismes Cancer AVIESAN (Alliance Nationale pour les Sciences de la Vie et de la Santé/National Alliance for Life Sciences & Health) within the framework of the Cancer Plan, and by the CNRS through the Mission pour les Initiatives Transverses et Interdisciplinaires interdisciplinary programs.

- H. Jiang, S. X. Sun, Cellular pressure and volume regulation and implications for cell mechanics. *Biophys. J.* 105, 609–619 (2013).
- Y. L. Han et al., Cell swelling, softening and invasion in a three-dimensional breast cancer model. *Nat. Phys.* 16, 101–108 (2020).
- O. Campas et al., Quantifying cell-generated mechanical forces within living embryonic tissues. *Nat. Meth.* 11, 183–189 (2014).
- M. E. Dolega et al., Cell-like pressure sensors reveal increase of mechanical stress towards the core of multicellular spheroids under compression. *Nat. Commun.* 8, 14056 (2017).
- M. Guo et al., Cell volume change through water efflux impacts cell stiffness and stem cell fate. *Proc. Natl. Acad. Sci.* 114, E8618–E8627 (2017).
- M. Delarue et al., mtorc1 controls phase separation and the biophysical properties of the cytoplasm by tuning crowding. *Cell* 174, 338–349.e20 (2018).
- E. H. Zhou et al., Universal behavior of the osmotically compressed cell and its analogy to the colloidal glass transition. *Proc. Natl. Acad. Sci.* 106, 10632–10637 (2009).
- G. Scarcelli et al., Noncontact three-dimensional mapping of intracellular hydro-mechanical properties by Brillouin microscopy. *Nat. Meth.* 12, 1132–1134 (2015).
- R. Prevedel, A. Diz-Muñoz, G. Ruocco, G. Antonacci, Brillouin microscopy: An emerging tool for mechanobiology. *Nat. Meth.* 16, 969–977 (2019).
- F. Palombo, D. Fioretto, Brillouin light scattering: Applications in biomedical sciences. *Chem. Rev.* 119, 7833–7847 (2019).
- G. Antonacci, V. de Turris, A. Rosa, G. Ruocco, Background-deflection Brillouin microscopy reveals altered biomechanics of intracellular stress granules by ALS protein fus. *Commun. Biol.* 1, 139 (2018).
- P.-J. Wu et al., Water content, not stiffness, dominates Brillouin spectroscopy measurements in hydrated materials. *Nat. Meth.* 15, 561–562 (2018).
- B. D. Hoffman, J. C. Crocker, Cell mechanics: Dissecting the physical responses of cells to force. *Annu. Rev. Biomed. Eng.* 11, 259–288 (2009).
- S. Monnier et al., Effect of an osmotic stress on multicellular aggregates. *Methods* 94, 114–119 (2015).
- M. E. Dolega, Extracellular matrix in multicellular aggregates acts as a pressure sensor controlling cell proliferation and motility. *eLife* 10, e63258 (2021).
- C. Cadart et al., Fluorescence exclusion measurement of volume in live cells. *Meth. Cell Biol.* 139, 103–120 (2017).
- E. Zlotek-Zlotkiewicz, S. Monnier, G. Cappello, M. Le Berre, M. Piel, Optical volume and mass measurements show that mammalian cells swell during mitosis. *J. Cell Biol.* 211, 765–774 (2015).
- G. Yan, A. Bazir, J. Margueritat, T. Dehoux, Evaluation of commercial virtually imaged phase array and Fabry-Pérot based Brillouin spectrometers for applications to biology. *Biomed. Opt. Express* 11, 6933–6944 (2020).
- R. Barer, S. Tkaczyk, Refractive index of concentrated protein solutions. *Nature* 173, 821–822 (1954).
- N. Akashi, J.-I. Kushibiki, F. Dunn, Measurements of acoustic properties of aqueous dextran solutions in the VHF/UHF range. *Ultrasonics* 38, 915–919 (2000).
- C. Roffay et al., Quantitative coupling of cell volume and membrane tension during osmotic shocks. *bioRxiv* [Preprint] (2021). <https://doi.org/10.1101/2021.01.22.427801> (Accessed 30 August 2021).
- J. G. Berryman, Analysis of ultrasonic velocities in hydrocarbon mixtures. *J. Acoust. Soc. Am.* 93, 2666–2668 (1993).
- E. C. Weiss, P. Anastasiadis, G. Pilarczyk, R. M. Lerner, P. V. Zinin, Mechanical properties of single cells by high-frequency time-resolved acoustic microscopy. *IEEE Trans. Ultrason. Ferroelectr. Freq. Control.* 54, 2257–2271 (2007).
- E. M. Strohm and M. C. Kolios, “Measuring the mechanical properties of cells using acoustic microscopy,” 2009 Annual International Conference of the IEEE Engineering in Medicine and Biology Society, 2009, pp. 6042–6045.
- A. Kinoshita et al., Evaluation of acoustic properties of the live human smooth-muscle cell using scanning acoustic microscopy. *Ultras. Med. Biol.* 24, 1397–1405 (1998).
- L. Venkova et al., A mechano-osmotic feedback couples cell volume to the rate of cell deformation. *bioRxiv* [Preprint] (2021). <https://doi.org/10.1101/2021.06.08.447538> (Accessed 30 August 2021).
- R. E. Challis, M. J. W. Povey, M. L. Mather, A. K. Holmes, Ultrasound techniques for characterizing colloidal dispersions. *Rep. Prog. Phys.* 68, 1541–1637 (2005).
- L. Ye et al., Dynamic rigidity percolation in inverted micelles. *Phys. Rev. Lett.* 63, 263–266 (1989).
- H. Pfeiffer, K. Heremans, The sound velocity in ideal liquid mixtures from thermal volume fluctuations. *ChemPhysChem.* 6, 697–705 (2005).
- S. Barnartt, The velocity of sound in electrolytic solutions. *J. Chem. Phys.* 20, 278–279 (1952).
- I. Remer, R. Shaashoua, N. Shemesh, A. Ben-Zvi, A. Bilencu, High-sensitivity and high-specificity biomechanical imaging by stimulated Brillouin scattering microscopy. *Nat. Meth.* 17, 913–916 (2020).
- T. J. C. Hosea, S. C. Ng, Elastodynamics of PVA hydrogels as studied by Brillouin spectroscopy. *Chem. Phys.* 103, 345–352 (1986).
- N. Taulier, T. V. Chalikian, Compressibility of protein transitions. *Biochim. Biophys. Acta* 1595, 48–70 (2002).
- T. V. Chalikian, G. E. Plum, A. P. Sarvazyan, K. J. Breslauer, Influence of drug binding on dna hydration: Acoustic and densimetric characterizations of netropsin binding to the poly(dadt).cntdot.poly(dadt) and poly(da).cntdot.poly(dt) duplexes and the poly(dt).cntdot.poly(da).cntdot.poly(dt) triplex at 25 degrees C. *Biochemistry* 33, 8629–8640 (1994).
- T. V. Chalikian, A. P. Sarvazyan, K. J. Breslauer, Hydration and partial compressibility of biological compounds. *Biophys. Chem.* 51, 89–109 (1994).
- L. Brillouin, Diffusion de la lumière et des rayons X par un corps transparent homogène, influence de l’agitation thermique. *Ann. Phys.* 17, 88–122 (1922).
- J. M. Vaughan, J. T. Randall, Brillouin scattering, density and elastic properties of the lens and cornea of the eye. *Nature* 284, 489–491 (1980).
- J. Margueritat et al., High-frequency mechanical properties of tumors measured by Brillouin light scattering. *Phys. Rev. Lett.* 122, 018101 (2019).
- G. Yan, S. Monnier, M. Mouelhi, T. Dehoux, Probing molecular crowding in compressed tissues with Brillouin light scattering. *Zenodo*. <https://doi.org/10.5281/zenodo.5773601>. Deposited 13 December 2021.

